Dawson City Landscape Hazards

Geoscience Mapping for Climate Change Adaptation Planning

Northern Climate ExChange
YUKON RESEARCH CENTRE · Yukon College

Front cover photograph: Aerial view of Dawson City, Yukon, looking southwest towards the Yukon River.
Photo credit: archbould.com

LEAD AUTHORS

Bronwyn Benkert	Northern Climate ExChange, Yukon Research Centre, Yukon College
Kristen Kennedy	Yukon Geological Survey, Government of Yukon
Daniel Fortier	Université de Montréal
Antoni Lewkowicz	University of Ottawa

CONTRIBUTING AUTHORS

Louis-Philippe Roy	Northern Climate ExChange, Yukon Research Centre, Yukon College
Katerine Grandmont	Université de Montréal
Isabelle de Grandpré	Université de Montréal
Sarah Laxton	Yukon Geological Survey, Government of Yukon
Karen McKenna	Yukon Geological Survey, Government of Yukon
Kelly Moote	Northern Climate Exchange, Yukon Research Centre, Yukon College

TECHNICAL ADVISORS

Jeff Bond	Yukon Geological Survey, Government of Yukon
Lacia Kinnear	Northern Climate ExChange, Yukon Research Centre, Yukon College

TECHNICAL EDITING AND PRODUCTION	Leyla Weston, private consultant, Whitehorse, Yukon

Table of Contents

INTRODUCTION

Climate change is a significant challenge for northern communities, where the impacts of a warming climate are already having considerable effects (Huntington and Weller, 2005). Many people living in small, isolated communities in northern Yukon are concerned about climate-related risks in their regions. Because adverse impacts are a reality, it is important to implement measures to reduce or moderate the negative effects of climate change – in other words, to implement climate change adaptation strategies.

CLIMATE CHANGE ADAPTATION PLANNING

Community-based adaptation planning aims to incorporate the potential impacts of climate change into decision-making for community development. For example, the design of a new building that is resilient to permafrost thaw, or the selection of future development zones away from areas that may be prone to flooding during the spring melt, are both decisions rooted in adaptation planning. Ultimately, adaptation planning anticipates future scenarios, reduces risk, increases resilience, and may even seek to reap the benefits of certain aspects of climate change.

In order to better prepare our communities to incorporate adaptation planning in the decision-making process, we must first identify the risks of, or vulnerabilities to, climate change, and then mitigate or reduce these risks so that we may adapt in a safe, sustainable manner.

Hazards maps help identify potential future risks associated with natural phenomena such as permafrost thaw, landslides and flooding. In order to adequately measure the potential risks associated with climate change, it is critical to gather scientific baseline data. These data, in conjunction with complementary research and future climate projections, strive to reduce vulnerability by increasing our knowledge base; this in turn will increase a community's adaptive capacity to climate change.

WHAT ARE HAZARDS MAPS?

A hazards map is a map that delineates or highlights areas on the land that are affected by, or are vulnerable to, a particular hazard. For example, in northern latitudes such as Yukon, thawing permafrost can be a significant climate change-related hazard. Flooding is another common hazard faced by Yukon communities, which may or may not be directly related to thawing permafrost. Hazards maps illustrate the risk associated with these and other hazards (ranked by risk severity), and are represented graphically in stoplight colours.

Hazards maps integrate complex environmental data into an easy-to-interpret, user-friendly tool for decision-making. The maps are created on a community-by-community basis and combine information about current and future landscape and climate conditions in order to rank the risk related to environmental change. As a result, they are tailored to each community's unique environment.

HAZARDS MAPS AND DECISION-MAKING

Hazard mapping, in conjunction with risk assessment, forms the basis of the risk management decision-making process by providing a community with baseline information that is necessary to understanding what risks may exist. One of the main objectives of the risk management process is to determine "what risks potentially interfere with the community's ability to meet the goals and objectives defining the community's vision for the future" (Noson, 2002). In this case, hazards maps help address a community's goal of incorporating climate change adaptation planning into its approaches to decision making and community development.

The series of landscape hazards maps produced by Northern Climate ExChange (NCE) and its partners are prepared as guides; that is, they act as one of the first steps in community planning and development. They identify areas where there is low risk of hazards exposure, as well as areas requiring more advanced and detailed scientific and engineering studies, should development be desired. Because hazards maps depict risk using stoplight colours, they are accessible and easy to interpret; in addition to community planning, hazards maps are useful educational tools illustrating local environmental conditions. They may also be used by scientists studying hazard phenomena (Noson, 2002), or could be revisited several years in the future to assess landscape change over time.

While hazards maps are tailored to local conditions and provide more detail than most other existing map products, it is important to note that they do not capture fine-scale variability within a site. For example, a slope underlain by permafrost may be more susceptible to thaw slumps in some areas compared to others because of small-scale variations in ice content of the soil or morphology of the slope. However, the entire slope may be classified as moderate risk to encompass the highest possible degree of vulnerability. Because of this, it is important to recognize the limitations of hazards maps – they provide an initial guide to local conditions, but detailed site studies (e.g., geotechnical or engineering studies) will still be required.

HOW HAZARDS MAPS ARE CREATED

There are many different approaches to creating hazards maps. Different mapping projects from different jurisdictions around Canada's North, and globally, will incorporate different hazards elements and types of data. For this project, we developed an approach that incorporates local community concerns and infrastructure, disturbance history, permafrost distribution and characteristics, surficial geology conditions, hydrology, and projections of future climate. Approaches for each stage are briefly described below. Detailed descriptions of each approach, including equipment used, lab analyses conducted, and data processing specifics are included in Appendix A.

COMMUNITY CONSULTATION

Support from local community governments and First Nations is sought for each hazards mapping project when project funding proposals are developed. Upon project commencement, community consultations, meetings and interviews are held with members of the public and local decision-makers to identify areas of concern and sites for potential future development. These areas of interest then become case-study sites as part of the hazards project. Where local capacity exists, a community project liaison is hired to serve as a link between the research team and the community.

DISTURBANCE HISTORY

The research team gathers information about natural and human-caused disturbances that may affect current landscape conditions. For example, forest fires change vegetation cover and affect active layer thickness, while regulating and re-routing waterways or clearing land for development can affect local hydrology and permafrost conditions (De Grandpré et al., 2012). Old disturbances help explain why current landscape dynamics operate as they do, while newer disturbances offer insight into potential future landscape evolution.

SURFICIAL GEOLOGY CHARACTERIZATION

Surficial geology is the study of the unconsolidated material (i.e., the surficial material that overlies bedrock) on the Earth's surface, including all sediments and soils. Surficial geology mapping

involves a combination of aerial photograph interpretation and fieldwork. Surficial geology maps provide information on the physical properties and characteristics of the surface sediments, the morphology (shape) of the landforms produced, and the genesis or origin of the landforms. In the process of mapping the surficial geology, the distribution of permafrost is also captured, making these maps an essential part of the hazards assessment process. The surficial geology maps become the basis for the final hazards maps produced through each project.

PERMAFROST DISTRIBUTION AND CHARACTERISTICS

Permafrost is defined as ground (including rock, unconsolidated sediments and organic material) that remains at or below 0°C for a minimum of two consecutive years (Brown et al., 1997). For this project, the research team studied both the distribution and characteristics of permafrost as part of the hazards map development.

Permafrost distribution is studied via the application of two geophysical surveys: 1) ground-penetrating radar (GPR), and 2) electrical resistivity tomography (ERT). Ground-penetrating radar uses electromagnetic radiation to send a tiny pulse of energy into the ground, and then measures the speed and strength of that pulse's reflection back to the instrument. It produces an image that delineates boundaries created by changes in soil characteristics (for example, the presence of frozen ground or stratigraphic layers). Electrical resistivity tomography is another type of non-invasive geophysical survey that measures the changes in the ability of the ground to conduct electricity along a transect. ERT profiling has been used extensively to investigate mountain permafrost in Europe (e.g., Kneisel et al., 2000, 2008; Hauck et al., 2004; Hilbich et al., 2008, 2009) and is growing in importance in North America as a technique for permafrost investigations in mountains and elsewhere (e.g., Lewkowicz et al., 2011). An electrical resistivity survey produces a two-dimensional image of the subsurface which can be used to identify frozen (high resistivity) versus unfrozen (low resistivity) surface materials or soils, and can therefore be used to map permafrost distribution along a transect.

Permafrost characteristics are studied by extracting cores of permafrost from the ground and conducting a series of laboratory analyses on subsections of these cores. These analyses provide information about grain size, porosity, ice volume, and settlement potential, among other properties. These characteristics affect how different materials and soils will behave if permafrost thaws, and are also useful in verifying interpretations of the geophysical techniques described above.

HYDROLOGICAL CHARACTERIZATION

The study of the movement and distribution of water is critical in understanding responses to climate change. Having baseline knowledge of the hydrologic regime in an area is essential in defining potential future hazards that are related to climate change. To incorporate hydrological conditions and risk into hazards maps, data about river discharge, lake level and the groundwater table are gathered from monitoring stations. Flood histories are also compiled from existing records and anecdotal evidence. Historical patterns are analyzed, and current conditions are assessed on the context of projected future changes in climate.

PROJECTIONS OF FUTURE ENVIRONMENTAL CONDITIONS

An important component of the hazards mapping projects involves projections of future environmental conditions. They represent an important aspect of adaptation planning, which by definition requires a future focus; thus incorporating future-oriented data is a key element of the development of hazards maps.

The future environmental conditions modelled through this project are completed through permafrost probability projections and climate projections. Models of permafrost probability are developed using data from a series of meteorological and permafrost monitoring stations established by research partners throughout the territory. These models build on existing knowledge of permafrost distribution to depict future changes in permafrost under different scenarios of annual air temperature increase as a result of climate change.

Climate projections for each community are developed by using a variety of Global Climate Models (GCMs) in combination with discrete scenarios, in order to make a range of projections for numerous climate variables (e.g., temperature and precipitation) on a local scale. Hazards projects typically incorporate a range of scenarios (reflecting escalating degrees of climate change) at several points in the future (e.g., 2020, 2050 and 2080).

HAZARD RANKING

Hazard mapping applies a variety of scientific data in order to arrive at a hazard risk ranking. The combination of surficial material type (glacial deposits and soils), landform shape and slope, permafrost nature and distribution, hydrological conditions, and the present climate regime are used to rank hazard risk. For easy interpretation, a stop-light colour coding system is applied to each risk ranking.

The hazards ranking is tailored to suit the conditions in each of the communities mapped. For example, in communities where permafrost presence or absence largely determines risk, three risk categories are sufficient. In environments with more complex landscape conditions (e.g., where permafrost conditions are more nuanced), a fourth risk category is introduced. Tailoring risk ranking to community conditions makes hazards maps relevant and reflective of the local landscape. The hazards risk ranking matrix used in this project is discussed in more detail in the section *"Integrating risk in a landscape hazards map for the Dawson region"*, p. 80 of this report.

LIMITATIONS AND UNCERTAINTY

It is very important to note that this report is prepared as a guide for planning. It should not be used as the basis for final site selection for development, and it does not replace geotechnical and/or engineering assessments completed on a site level. Rather, it should be treated as a tool for use in identifying areas of interest with regards to future large-scale land use planning, which will then undergo subsequent site-specific investigations (which may include geotechnical or engineering assessments).

It is also important to note that the classification scheme applied here does contain a level of uncertainty. Because of the scale at which the study area was mapped, and the duration of the field program for this project, researchers were unable to visit all the areas within the map boundary. Therefore, results have been extrapolated beyond areas visited by researchers. While we have developed a model that integrates the geoscience data the research team has collected to make the most informed assessment of hazard risk for the study area, this approach does introduce some uncertainty that users of the hazard risk maps should be aware of.

Finally, it is important to note that in some cases, a polygon may contain areas of both higher and lower risk. In such cases, we have taken a precautionary approach and applied a category of higher risk where we were not confident in lower categories. This is another reason why the hazards map should serve only as an initial guide for planning purposes, and should not replace site-specific investigations – the landscape within each polygon will vary naturally.

THE DAWSON CITY REGION

Dawson City (64.35°N, 139.39°W) is located in northwestern Yukon at the confluence of the Klondike and Yukon rivers (Figure 1). The community is located 530 km north of Whitehorse along the Klondike Highway. During the summer months, Dawson City can be accessed from the north by the Top of World Highway, via Tok, Alaska.
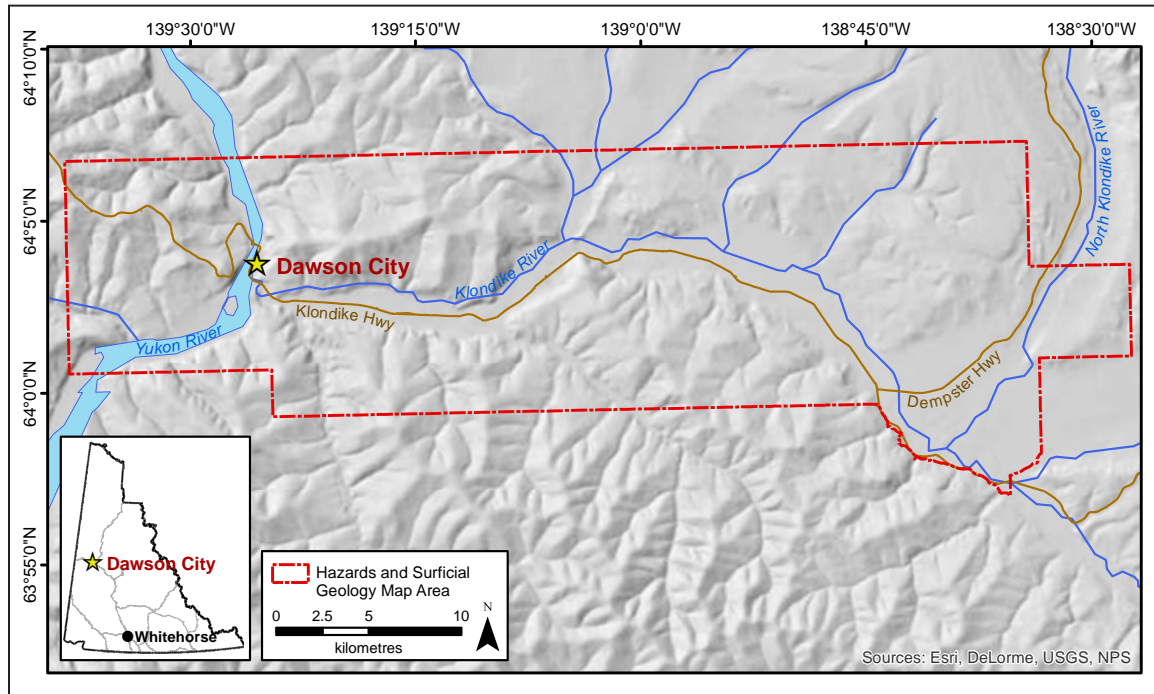
Figure 1. Location of study area, illustrating the surficial geology and hazards map footprints.

Dawson City is situated within the Traditional Territory of the Tr'ondëk Hwëch'in. The Tr'ondëk Hwëch'in comprise a diverse mix of families descended from Gwich'in, Northern Tutchone and other language groups. They have been a self-governing First Nation since 1998 and have approximately 1,100 members (Tr'ondëk Hwëch'in, 2014).

Dawson City is the heart of the world-famous Klondike Gold Rush. Prior to August 17, 1896, the date when George Carmack, Dawson Charlie and Skookum Jim discovered gold on Rabbit Creek, approximately 1,000 people were living in Yukon. By July of the following year, news of the gold discoveries had reached the outside world causing miners from San Francisco and Seattle to undertake the treacherous trip to the Klondike. Shops, theatres, saloons, casinos and dance halls were quickly established to serve the miners and a thriving, bustling city of nearly 25,000 people had been established by 1898 (Yukon Community Profiles, 2014). During this time, Dawson City was the largest city in Canada west of Winnipeg. Although most participants in the gold rush did not strike it rich, it is estimated that $29 million in gold was hand-mined around Dawson City between 1896 and 1899. Three years later, the Gold Rush had ended and many had moved on. Today, Dawson City is the second largest community in Yukon.

Throughout the 20th century, the mining industry has continued to play a prominent role in the local economy of Dawson City. Today, this industry is characterized by seasonal placer mining and hardrock mining, as well as exploration activities (NCE, 2011). However, based on the community's colourful past and historical importance, Dawson's primary economic activity is tourism (Yukon

Community Profiles, 2014). It is mainly a seasonal industry, peaking in the summer months, when tourists are able to enjoy key attractions including traditional dirt roads and boardwalks, renovated heritage buildings, historic placer mining dredges, gold panning opportunities, and gambling halls and bars. During the winter months, attractions include the Yukon Quest – a dog sled race between Fairbanks, Alaska and Whitehorse, Yukon – as well as viewing of the northern lights (aurora borealis). Other employment opportunities available in Dawson City, albeit limited, include jobs with the Tr'ondëk Hwëch'in, City of Dawson, Yukon government, and community organizations (Yukon Community Profiles, 2014).

Dawson City has a wide variety of services and amenities including a library, school, bank, service stations, a post office, a seasonal swimming pool, an ice arena, curling rink, fitness centre, community gardens, as well as grocery stores, hardware stores, clothing stores, book stores and restaurants. There is also a 24-hour Ambulance Service, an RCMP detachment, a fire department and a hospital (Yukon Community Profiles, 2014). The Tr'odëk Hätr'unohtän Zho (Klondike Learning House) campus of Yukon College is also located in Dawson City, as well as the Yukon School of Visual Arts (SOVA), which is an accredited art college that is a joint venture between the Dawson City Arts Society, Tr'ondëk Hwëch'in First Nation and Yukon College.

In 2011, there were 1,319 people living in Dawson City (Yukon Community Profiles, 2014). The population remained almost the same from the 2006 to 2011 census; however, numbers increase significantly during the summer months due to seasonal work opportunities (Yukon Community Profiles, 2014).

Approximately 30% of residents are identified as Aboriginal, 12.5% as French-Canadian and 36% as European (Yukon Community Profiles, 2014). In 2011, there were 680 occupied private dwellings in Dawson City (YBS, 2014). In 2013, the median value of a single-family dwelling was $209,212 (Yukon Community Profiles, 2014).

PHYSIOGRAPHY

Dawson City is located on the floodplain of the Yukon and Klondike rivers, close to the boundary of two distinct ecological zones: 1) the boundary of the discontinuous/continuous permafrost zones, and 2) the boundary of the taiga/boreal ecozones (NCE, 2011). Dawson City is located within the Klondike Plateau Ecoregion (Smith et al., 2004), which is a Tertiary-aged upland that has undergone variable uplift and stream dissection, resulting in rounded summits and ridges, and deep, V-shaped valleys (McKillop et al., 2013). These valleys, characteristic of an area that has not been glaciated in the recent past, distinguish the Klondike Plateau from adjacent ecoregions.

The Dawson Range, which trends northwest-southeast between the Yukon River to the north and the Nisling River to the south, is the most prominent feature within the plateau. Its higher and more rugged terrain reflects enhanced erosion following locally, greater uplift. Most valley sides exhibit convex profiles, whereas concave terrain is restricted to localized bench or gully features, and valley bottoms filled with material derived from upslope erosion (McKillop et al., 2013). Apex Mountain, at 2026 m above sea level (a.s.l.), is the highest peak in the Dawson Range and in the ecoregion (Smith et al., 2004). Most ridges are 1200 to 1700 m a.s.l. The lowest point in the ecoregion is less than 300 m a.s.l., where the Yukon River flows into Alaska, downstream from Dawson City. Local relief ranges from 450 m to 700 m.

As described by McKillop et al. (2013):

> "Several major rivers have incised deeply into the plateau surface. The Donjek River flows into the White River, which enters the Yukon River just upstream of its confluence with the Stewart River. Other rivers include the Nisling, Klotassin,

Ladue, Sixty Mile, Indian, and Fortymile rivers. Some valley reaches of the rivers and major tributaries are more entrenched than others, depending on their proximity to the Yukon River. Reaches in close proximity to the Yukon River commonly contain stream-cut bedrock terraces along one or both sides of the valley, most likely formed by accelerated degradation (down-cutting) initiated by the reversal of the Yukon River from a south to north-flowing drainage during the late Pliocene to early Pleistocene. Some headwater tributaries also exhibit anomalously steep toe slopes that may correspond to this base level change. The scarcity of lakes is attributed to the dominantly fluvial origin of the landscape and the absence of glacial scouring."
(Page 5)

The only significant lakes in the Klondike Plateau Ecoregion are in the southeast corner in the glaciated Wellesley Depression (Smith et al., 2004). The largest of these is Wellesley Lake.

VEGETATION

Vegetation is determined by elevation, topography and microclimate. The vegetation of this ecoregion comprises ecosystems ranging from boreal forest and wetlands in valleys, to alpine tundra on ridge crests (McKillop et al., 2013). Treeline is close to 1000 m a.s.l. in the northern part of the ecoregion and around 1200 m a.s.l. in the south. Below treeline, the pattern of vegetation is closely linked to aspect and distribution of permafrost, due to different thermal and moisture tolerances of different species (McKillop et al., 2013). Stunted black spruce woodlands on cold, north-facing sites contrast with mixed forests on warm, south-facing slopes.

Below treeline, black and white spruce forests dominate the ecoregion in both pure and mixed stands. Other common tree species include balsam poplar, paper birch, trembling aspen, willow, and water birch; these are mid-successional communities that will gradually become conifer stands in time. The understory typically comprises ground shrubs, diverse forbs, and feathermoss. Since this ecoregion includes the area with the highest frequency of lightning strikes in Yukon, it is common to find young, mixed forests. On south-facing slopes, surface organics are thin or absent, removed by fire, and are commonly mixed with charcoal. Many forests are a mosaic of seral stands predominating over mature stands. Following a forest fire, mixtures of Alaska birch and trembling aspen are the first to recolonize the slopes.

In riparian zones, vegetation patterns reflect the frequency of flooding and presence of permafrost (McKillop et al., 2013). On stable fluvial terraces alongside meandering streams, white spruce and feathermoss communities are common, and permafrost may be absent or occur at depth. In areas of more recent flooding, balsam poplar (*Populus balsamifera*) mixed with white spruce is common and permafrost is generally absent. Willow, alder (*Alnus spp.*), and balsam poplar dominate riparian areas subject to frequent flooding.

CONTEMPORARY CLIMATE

Dawson is located in the Central Yukon Basin (Wahl et al., 1987). The St. Elias Mountains and the region's distance from the Gulf of Alaska influences its climate, making it climatically different from areas to the south. Temperatures are highly variable – summers can be extremely warm, while winters can have long, very cold periods. The record-low temperature for continental North America was recorded in this climate zone at Snag, Yukon (-62.8°C on February 3, 1947). Precipitation is moderate, winds tend to be light, and storm centres commonly skirt this region, especially in winter (Wahl et al., 1987).

Based on 30-year (1981-2010) climate normal data collected from the Dawson Airport meteorological monitoring station (the closest station with a long-term monitoring record; 64°02' N, 139°07' W),

average January and July temperatures are -26.0°C and 15.7°C, respectively (Environment Canada, 2014a). Average annual precipitation is 324.4 mm, and of this, approximately one-third falls as snow during the winter season (Environment Canada, 2014a). Month-by-month climate normal temperature and precipitation data are summarized in Figure 2.
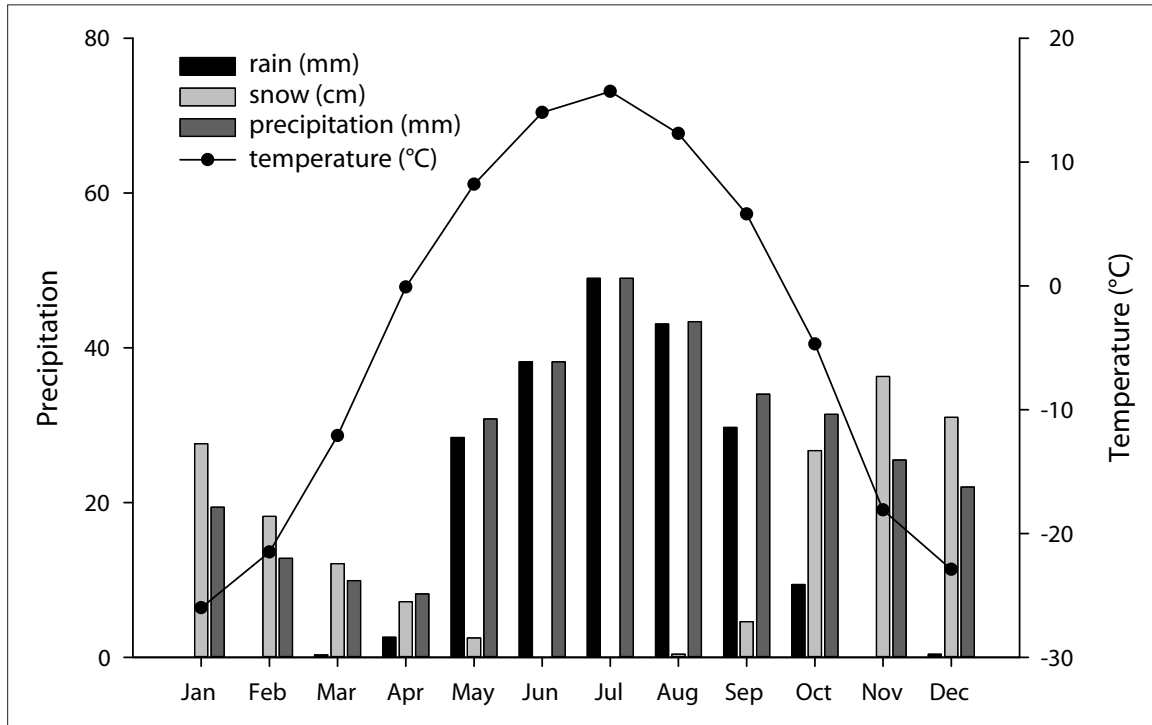
Figure 2. Climate normal (1981-2010) temperature and precipitation data for the Dawson City Airport meteorological monitoring station (Environment Canada, 2014a). To calculate total precipitation in millimetres, snowfall was converted to snow water equivalent and summed with rainfall.

PAST CLIMATE TRENDS

Environment Canada produces regional summaries of climate and precipitation data that provide a generalization of climate trends by integrating instrumental data from several stations (Environment Canada, 2014b). For this region, Environment Canada amalgamates data from northern British Columbia and Yukon stations, which has allowed them to develop a record of regional climate trends that spans the past 65 years. Data indicate that between ~1950 and 1975, the regional climate was generally cooler and drier than normal (based on 1961-1990 climate conditions), while between ~1975 and 2013, the climate was generally warmer and wetter than normal (Figure 3).

To examine past climate trends, historical temperature and precipitation data records from the Dawson Airport meteorological monitoring station were examined. Relatively complete records of temperature and precipitation date back to about 1900, making this one of the longest historical climate records for the territory. The data were amalgamated by season for simplicity, and linear regressions were superimposed on seasonal data records, to provide a basis for identifying potential trends in temperature and precipitation over the period of record. Temperature records are shown in Figure 4, while precipitation records are shown in Figure 5.
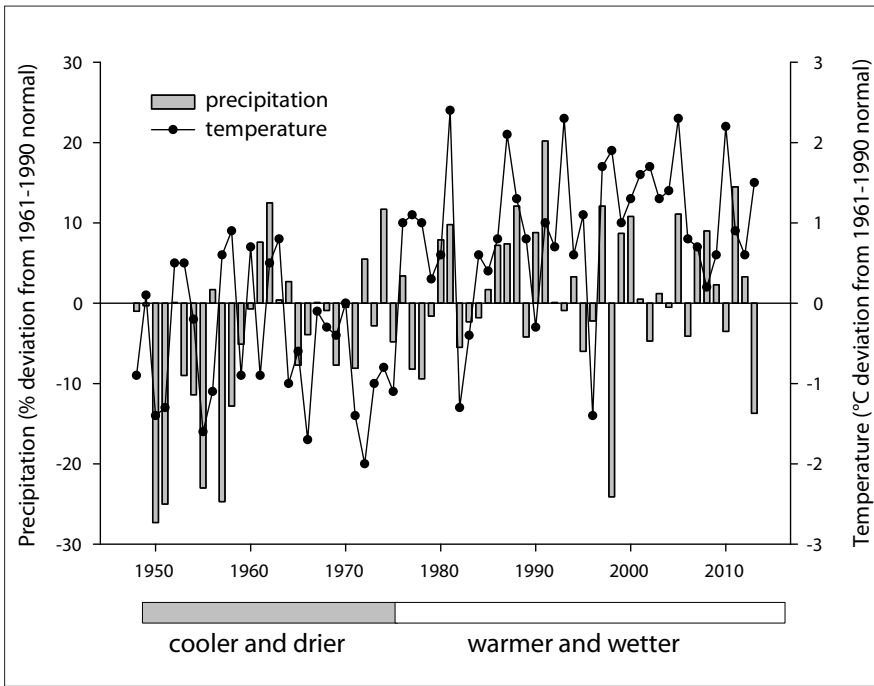
Figure 3. *Regional climate trends for northern British Columbia and Yukon, developed using data amalgamated by Environment Canada (2014b). Data has been normalized to indicate deviation from 1961-1990 climate normal conditions. Negative values indicate precipitation amounts and temperatures below normal for the 1961-1990 period, while positive values indicate exceedance of normal conditions.*
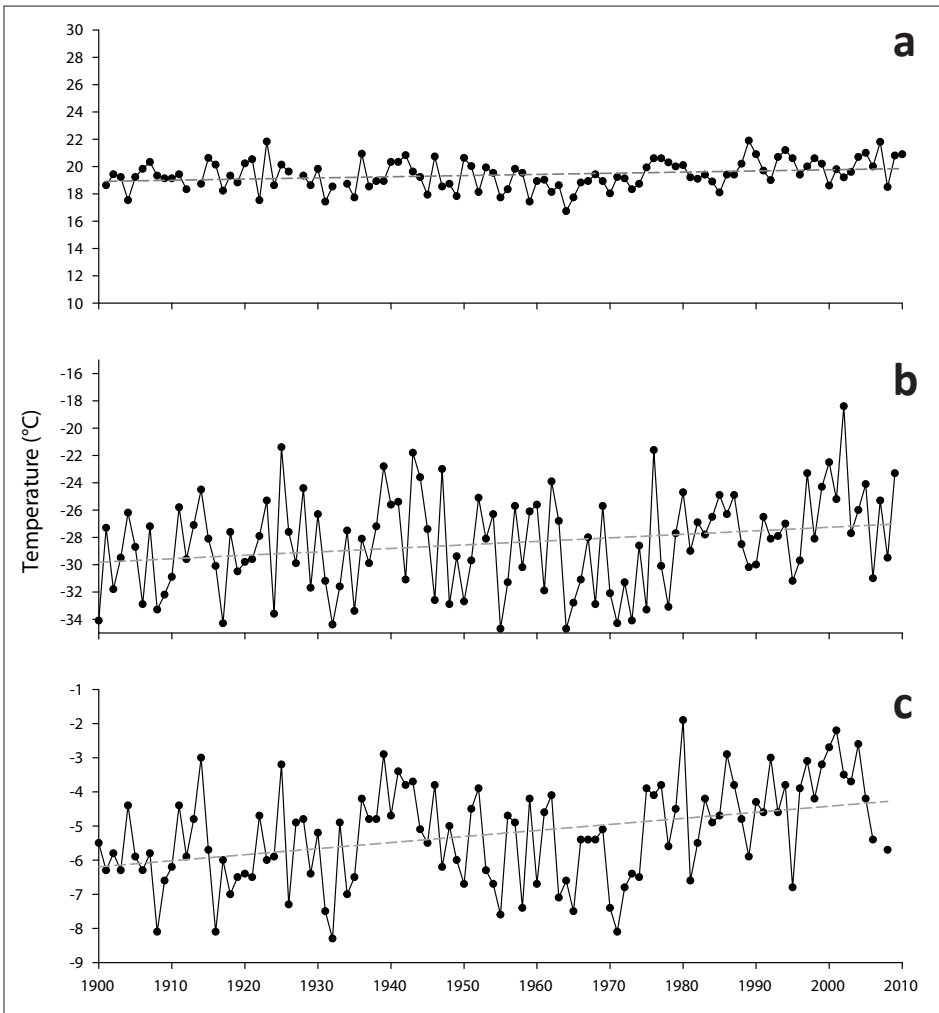
Figure 4. *Historical temperature data from Dawson City, based on data amalgamated by Purves (2010), illustrating (a) summer, (b) winter and (c) annual average temperature. The dashed grey line represents a linear regression through the dataset.*

9
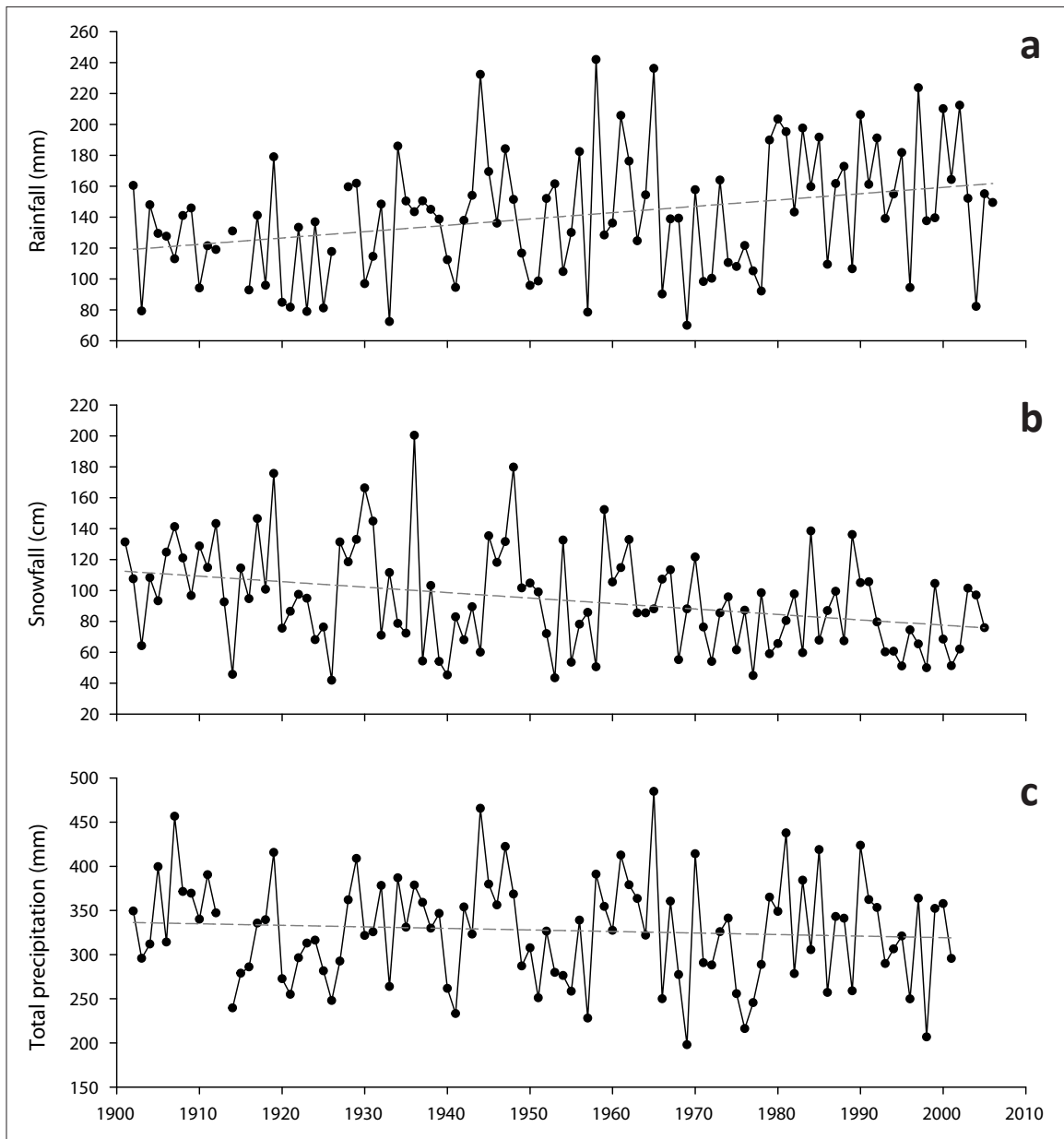
Figure 5. Historical temperature data from Dawson City, based on data amalgamated by Purves (2010), illustrating (a) summer, (b) winter and (c) annual average precipitation. To calculate mean annual precipitation in millimetres, winter precipitation was converted to snow water equivalent and summed with rainfall. The dashed grey line represents a linear regression through the dataset.

The greatest range in seasonal temperature variability occurred in the winter, with a 16.3°C difference in the highest and lowest recorded temperatures over the period of record. In contrast, summer temperature variability was much lower (5.2°C). Variability in mean annual temperatures over the period of record was 6.4°C. Regression lines suggest winter temperatures are increasing more rapidly than summer temperatures over the period of record, which is consistent with modelling that predicts climate change-induced temperature increases will be greatest in winter (Warren and Lemmen, 2014). Summer temperatures also appear to be increasing slightly over the period of record. Precipitation records also indicate long-term changes in rainfall and snowfall

THE DAWSON CITY REGION

amounts. While trend lines superimposed on both records do indicate long-term changes in both parameters, it is important to note that both datasets contain a great deal of annual variability throughout. For example, rainfall amounts range from 70 mm to 242 mm during the period of record, while snowfall amounts range from 42 cm to 200 cm. Despite the annual variability, overall trends in total annual rainfall appear to be increasing, while total annual snowfall appear to be decreasing; this is consistent with warmer winters and increasing mean annual air temperatures (see Figure 4).

HYDROLOGY

Surface water

The subwatershed of the Dawson region forms part of the Yukon River watershed, which covers 260 000 km^2 or 54% of Yukon Territory (Smith et al., 2004). The area is situated in the Interior Hydrologic Region of the Territory. First and second-order streams in the region are generally steep and relatively short, producing rapid, flashy streamflow responses during the spring melt. Peaks in spring streamflow are in response to snowmelt and are usually achieved in June, although summer rainfall can sustain high flows or produce secondary peaks later in the season. Low flows are typically exhibited just prior to the spring breakup, whereby discharge is maintained primarily by groundwater contributions (Janowicz, 2008). In the Klondike Plateau subregion, in which Dawson City is located, mean annual runoff is moderately low, ranging from 85 mm to 293 mm (average 175 mm; Smith et al., 2004).

Dawson City is situated at the confluence of the Klondike and Yukon rivers (see Figure 1). Dawson City is within the floodplain of the Yukon River; however, the floodplain is not considered active, as a dike was constructed to protect the community from flooding by the river. Reports indicate that, prior to the dike construction, Dawson was one of the most flood-affected settlements in Yukon, with at least a dozen flood events since the community's establishment in 1897 (NCE, 2011). Flooding in the area can result from ice jams during spring break-up, open water floods due to snowmelt pulses and rain events, and wash-outs that result from heavy rain during the summer and fall seasons.

Ice jam floods have been identified as a notable hazard for the region, given the potential for rapid increases in water level upstream of the jam during its formation and lifespan. In the Dawson region, ice jams typically form downstream from the community, making the town vulnerable to backwater flooding behind the jamming front (as opposed to pulse-style flooding after a jam is breached). Ice jam floods can also occur on shallow, braided sections of the Klondike River and on nearby Rock Creek. The probability of an ice jam flood is between 3% and 5% in any given year, based on gauged data and paleoflood reconstructions (Livingstone et al., 2009; NCE, 2011). Major flooding in the community in 1979 (discussed in more detail later in this report) was the result of heavy snowfall and ice jams that formed on the Yukon, Indian and Klondike rivers. After this flood, a permanent dike was constructed to 321.0 m, which has since protected the community from major river-related flooding.

In order to evaluate discharge patterns, both average monthly and peak discharge are examined. The Water Survey of Canada (WSC) has maintained several gauging stations in the region over the past several decades, some of which provide real-time hydrometric data. (See Table 1 for a summary of station information.) The WSC reports daily average, monthly average, and peak yearly discharge for each station (Water Survey of Canada, 2015). Hydrographs of monthly average discharge for both the Klondike and Yukon rivers are shown in Figures 6 and 7, respectively. Discharge records for the Klondike River above Bonanza Creek are available for the period 1966-2013, whereas discharge records for the Yukon River at Dawson are available for the period 1945-

1980. For the sake of comparison to more recent data, Figure 7 also contains monthly average discharge for the Yukon River at Eagle, Alaska (downstream of Dawson; the period of record at this station spans 1983-2013).

Table 1. Summary of Water Survey of Canada's stations in the Dawson region (Water Survey of Canada, 2015). Stations are listed roughly in the order that they appear, from headwaters to mouth.

Station name	Station ID	Latitude	Longitude	Gross drainage area (km^2)	Period of record*
Yukon River above White River	09CD001	63.1	-139.5	149 000	1956-2012
Sixty Mile River	09EB004	63.7	-140.2	3060	1998-2013
Indian River at mouth	09EB003	63.8	-139.6	2210	1982-2013
North Klondike River near mouth	09EA004	64.0	-138.6	1090	1975-2013
Klondike River above Bonanza Creek	09EA003	64.0	-139.4	7810	1974-2013
Yukon River at Dawson	09EB001	64.1	-139.4	264 000	1968-1980
Yukon River at Eagle	09ED001	64.8	-141.2	288 000	1983-2013

* Periods of record do not always contain complete datasets.
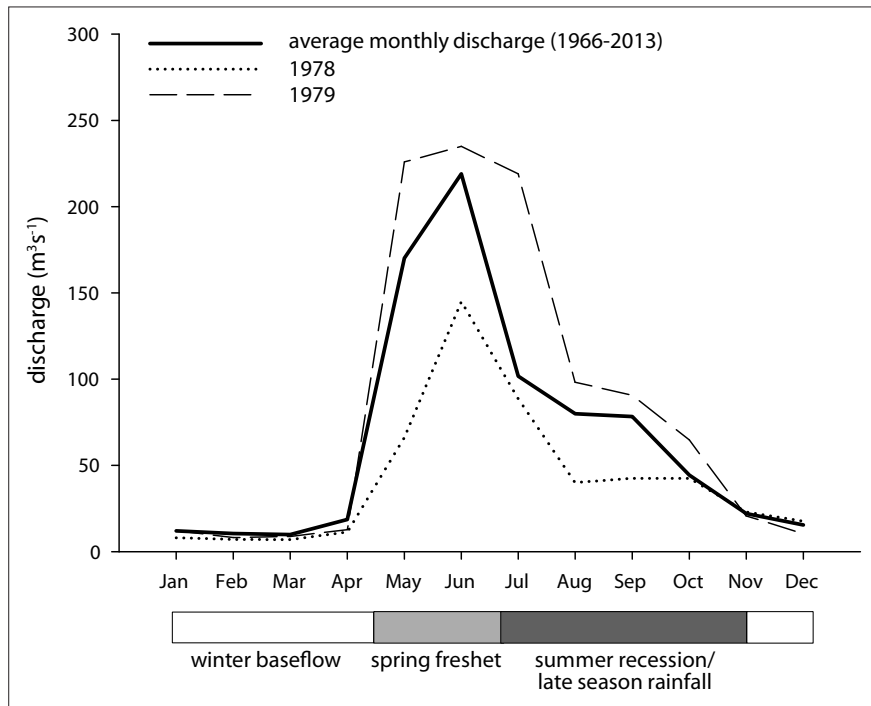
Figure 6. Average monthly discharge hydrograph for the Klondike River above Bonanza Creek (heavy solid line). Also shown are hydrographs for the years 1978 (dotted line) and 1979 (long-dashed line), demonstrating low and high measured peak discharge, respectively (Water Survey of Canada, 2015).
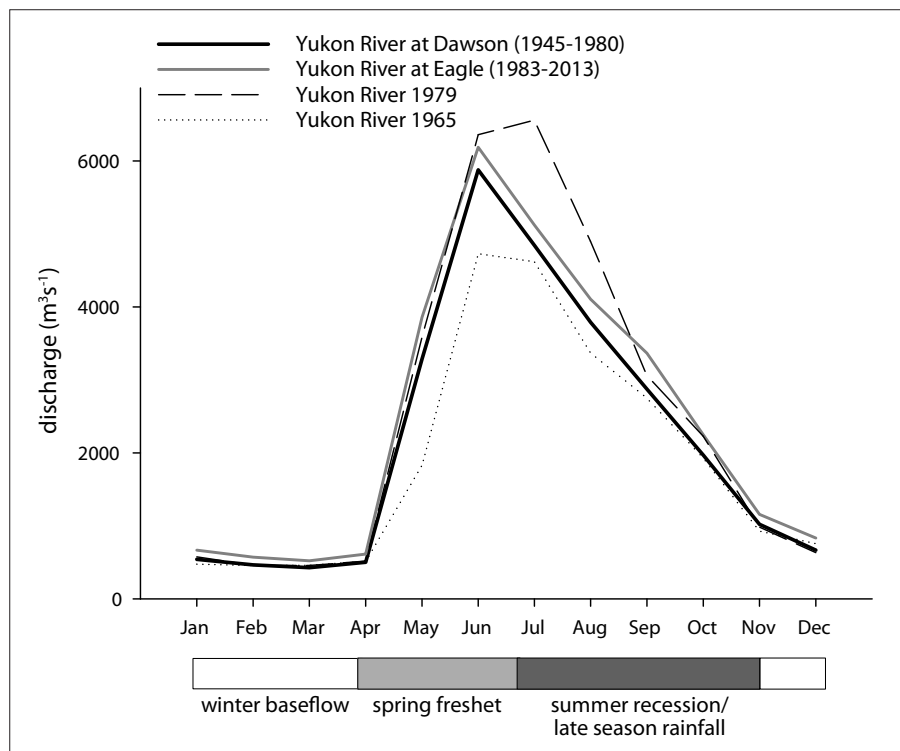
Figure 7. *Average monthly discharge hydrograph for the Yukon River at Dawson (heavy solid line) and Eagle (heavy grey line). Also shown are hydrographs for the years 1965 (dotted line) and 1979 (long-dashed line), demonstrating low and high measured peak discharge, respectively (Water Survey of Canada, 2015).*

Both hydrographs demonstrate the typical seasonal pattern of a river in Yukon's Interior Hydrologic Region, with rapid increases in discharge in April, May and June, followed by a recession through summer and autumn. Average monthly discharge is low throughout the winter months, when groundwater is the only input to the river; the lowest flows occur in March, prior to the spring freshet. Average monthly discharge for 1979, the year in which major flooding occurred in Dawson, is also superimposed on both hydrographs. Interestingly, high average monthly flows in the spring of 1979 are notable on the Klondike River hydrograph, whereas Yukon River discharge in 1979 shows a more sustained high-flow peak later in summer, with a less noticeable peak in May when the flooding took place. For reference, two years with low discharge (1965, Yukon River; 1978, Klondike River) are also included on Figure 6 and Figure 7, respectively.

There is also an extensive record of Yukon River spring breakup dates, which dates back to 1896 (Figure 8; http://www.yukonriverbreakup.com/statistics). Data records suggest a shift towards earlier breakup dates by about 7 days over the last century, although breakup dates in recent years do fall within the range of natural variability exhibited by the dataset. Historical data can also be examined using Water Survey of Canada discharge records. Figure 9 illustrates historical discharge peaks measured at Water Survey of Canada stations in the Dawson region. While records do not always cover the same period, enough data is available to demonstrate that peaks in river discharge at upstream stations (e.g., Yukon River above White River and Sixty Mile River) translate downstream (e.g., Yukon River at Dawson and Eagle). This applies to main stem Yukon River stations as well as smaller order streams like the Klondike, North Klondike and Indian rivers, suggesting that headwater snowpack plays an important role in downstream discharge characteristics. Interestingly, peak water levels measured in 1979, the year of major flooding in

Dawson, were comparable to average values for the periods of record at each station. This may be related to localized flooding and water level increases behind the ice jam near Dawson, which may not have resulted in elevated discharge peaks at the monitoring stations at the Yukon River above White River and the North Klondike River. Additionally, the period of record for the Yukon River at Dawson is too short to examine discharge peaks in relation with other periods; for example, discharge peaks measured between 1975 and 1980 may all be elevated compared to earlier or later years, but data is not available to make such a comparison. Nonetheless, data records do not show major trends in river discharge over the periods of record at any station.
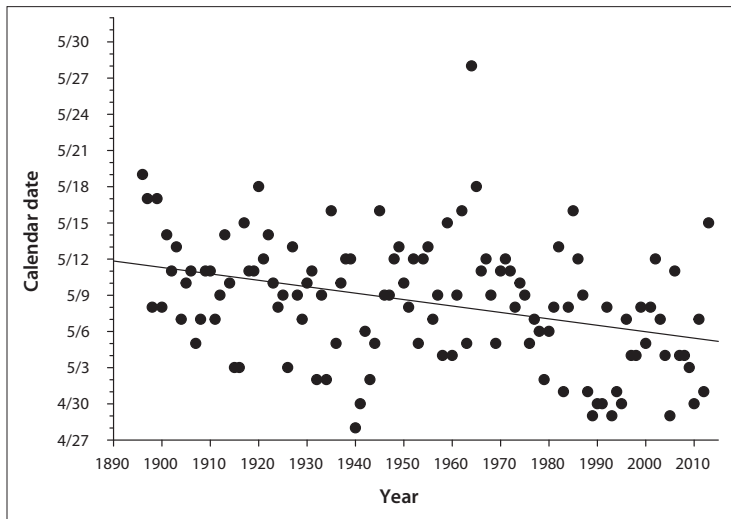
Figure 8. Spring breakup dates for the Yukon River between 1896 and 2013 (from http://www. yukonriverbreakup.com/statistics). The solid line represents a best-fit regression through the complete dataset.
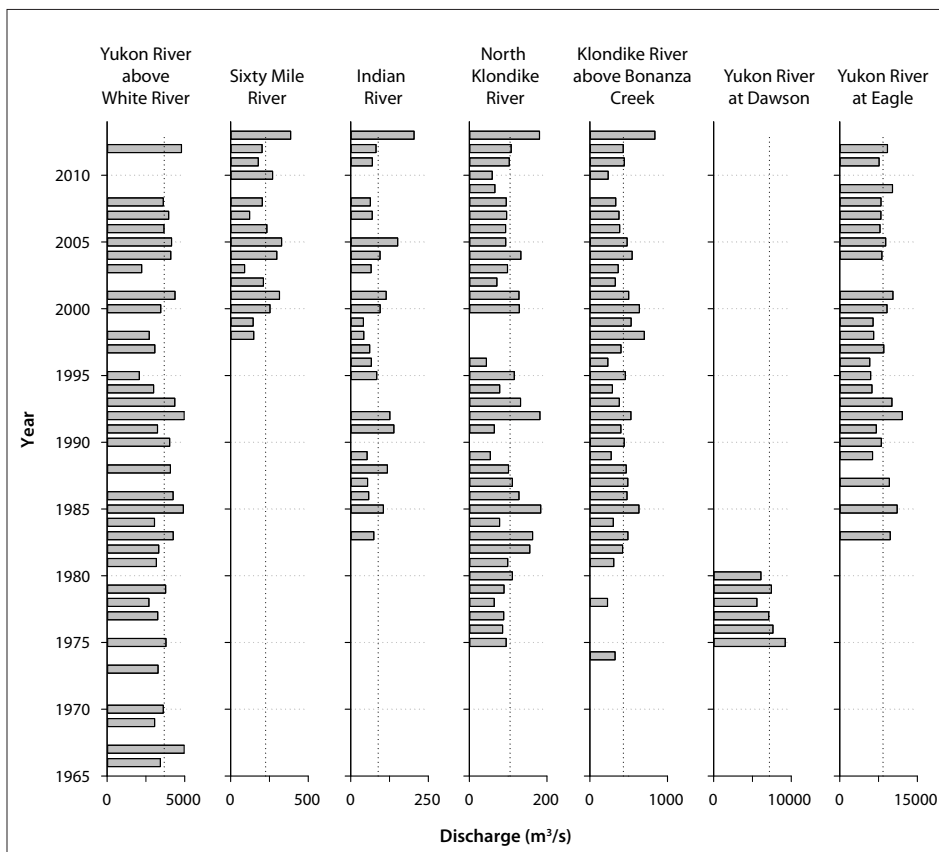
Figure 9. Peak discharge at WSC stations with multi-year records, arranged generally upstream (left) to downstream (right). Vertical, long-dashed lines indicate average peak discharge for each station for its period of record (Water Survey of Canada, 2015).

Modelled flood extents

As part of a complementary Aboriginal Affairs and Northern Development Canada-funded project in Yukon communities (http://northernadaptation.ca/sites/default/files/flood_risk_mapping. pdf), LIDAR (light imaging and ranging) imagery was captured along a swath of the Yukon River in the vicinity of Dawson City in the summer of 2014, and a high-resolution digital elevation model (DEM) of the image area was created by Yukon Government (horizontal accuracy = 50 cm, vertical accuracy = 10 cm). Based on this DEM, project researchers developed modelled flood risk maps for the image area that depict potential flood extents based on increases in Yukon River level, simulating floods of different elevations. The models are simplistic and do not integrate hydraulic gradient, the role of secondary input sources to the Yukon River (e.g., local creeks), or upstream or downstream propagation of flood events over time. However, given that the most notable floods in the Dawson region have historically been caused by ice jam events upstream of the townsite, the model is still informative.

It is important to note that any elevations within the LIDAR imagery area that fall within the elevation of each flood extent are depicted as being inundated. In other words, areas behind Dawson City's dike that are at an elevation of 318 m will appear to be flooded under the scenario that models river levels of 318 m, regardless of the fact that a 321 m-high dike is present along the riverfront. While flooding within the townsite would be unlikely under a water level increase of 318 m, this exercise demonstrates potential areas of flooding if there were to be a breach of the dike during a flood event, and is an important consideration in the context of assessing hazard risk.

Flood extent maps developed for the imagery area show flood extents under a series of scenarios depicting increases in the level of the Yukon River of between 318 m and 322 m (relative to the Canadian Geodetic Datum; Figure 10). The townsite of Dawson, the Klondike River valley near the confluence of the Klondike and Yukon rivers, and the western shore of the Yukon River upstream from Dawson are susceptible to flooding river level increases of 318 m to 322 m (and beyond, although elevations greater than 322 m have not been modelled as part of this exercise). As described above, it is unlikely that the townsite of Dawson would flood under water level increases below 321 m due to the presence of the dike; however, the Klondike River valley and the west shore of the Yukon River would likely be impacted by flooding if water levels rose to 318 m or greater. This is consistent with observed flood levels for the Dawson region, which are reported to be ~318 m (R. Janowicz, pers. comm.) and flood hazard zones of ~318.5 m in the vicinity of the Tr'ochëk heritage site near the confluence of the Klondike and Yukon rivers (Janowicz, 2002).

Model results also provide areal extent and building numbers within the LIDAR footprint that would be impacted by flooding under each modeled scenario, and these are presented in Table 2.

To examine flood extents at the Dawson City townsite more closely, Figure 11 presents an amalgamation of flood extents at the townsite and near the mouth of the Klondike River, and Figures 12a and b show the extent of individual modelled water levels. As described above, the model does not integrate the dike as a protective structure; rather, it shows as a sinuous line bordering the town that is flooded only at a flood elevation of 322 m. However, results show that should a breach of the dike occur, flooding would occur in isolated portions of the townsite at a water level elevation of 318 m, and would spread from the southwestern portion of Dawson City to the north as water levels increased. Under a flood level of 322 m, the dike would be overtopped, and the majority of the community would be flooded.
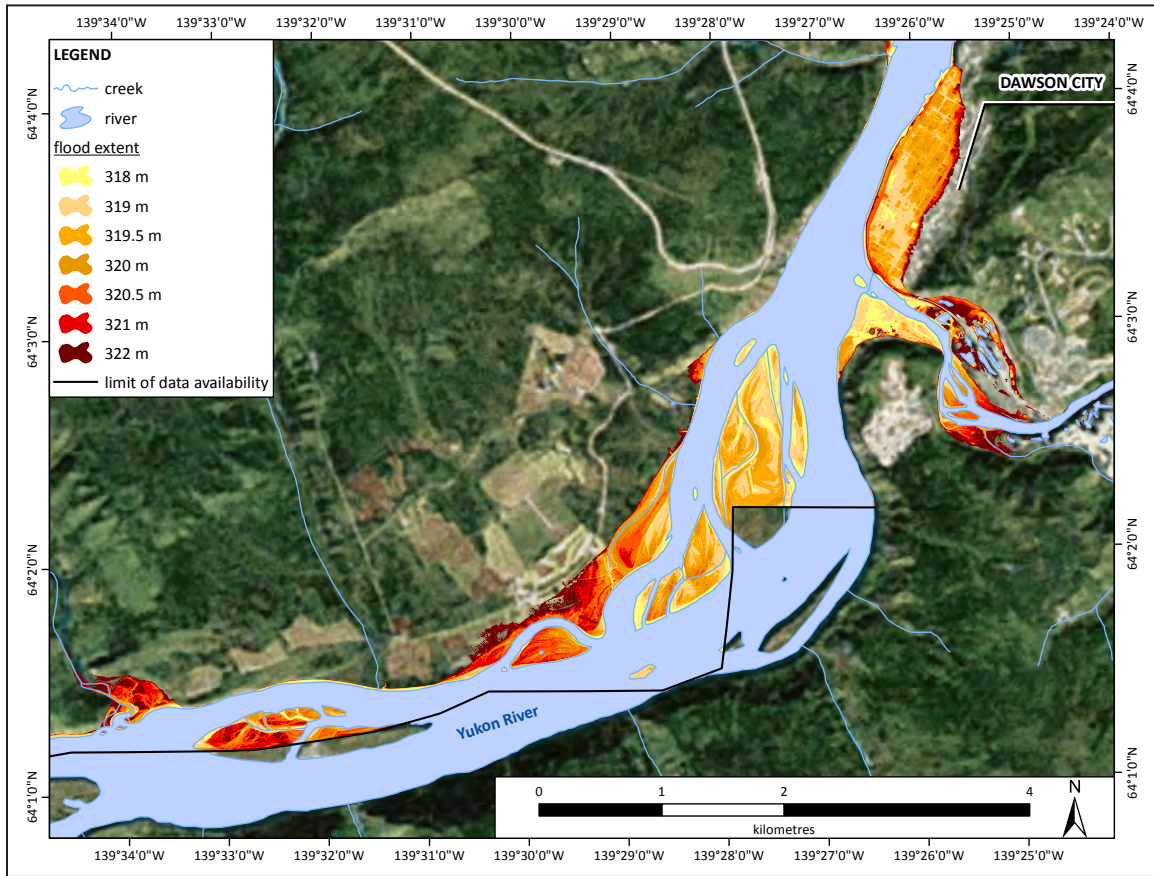
Figure 10. *Modelled flood extents for Dawson City and surrounding area illustrating Yukon River levels between 318 m and 322 m (relative to the Canadian Geodetic Datum). Note that the dike at Dawson City is not integrated as a barrier to flooding. Model results are based on LIDAR imagery provided by the Yukon Government. Background image source: ERSI, DigitalGlobe, GeoEye.*

Table 2. Summary of total flooded area and number of impacted buildings under Yukon River flood scenarios. Flood extents represent Yukon River water level relative to the Canadian Geodetic Datum. Note that the dike at Dawson City is not integrated as a barrier to flooding.

Flood extent (m)	Flood area (km²)	Buildings flooded (#)
318	0.46	4
319	1.26	71
319.5	1.93	181
320	2.51	322
320.5	2.95	373
321	3.31	409
322	3.74	439
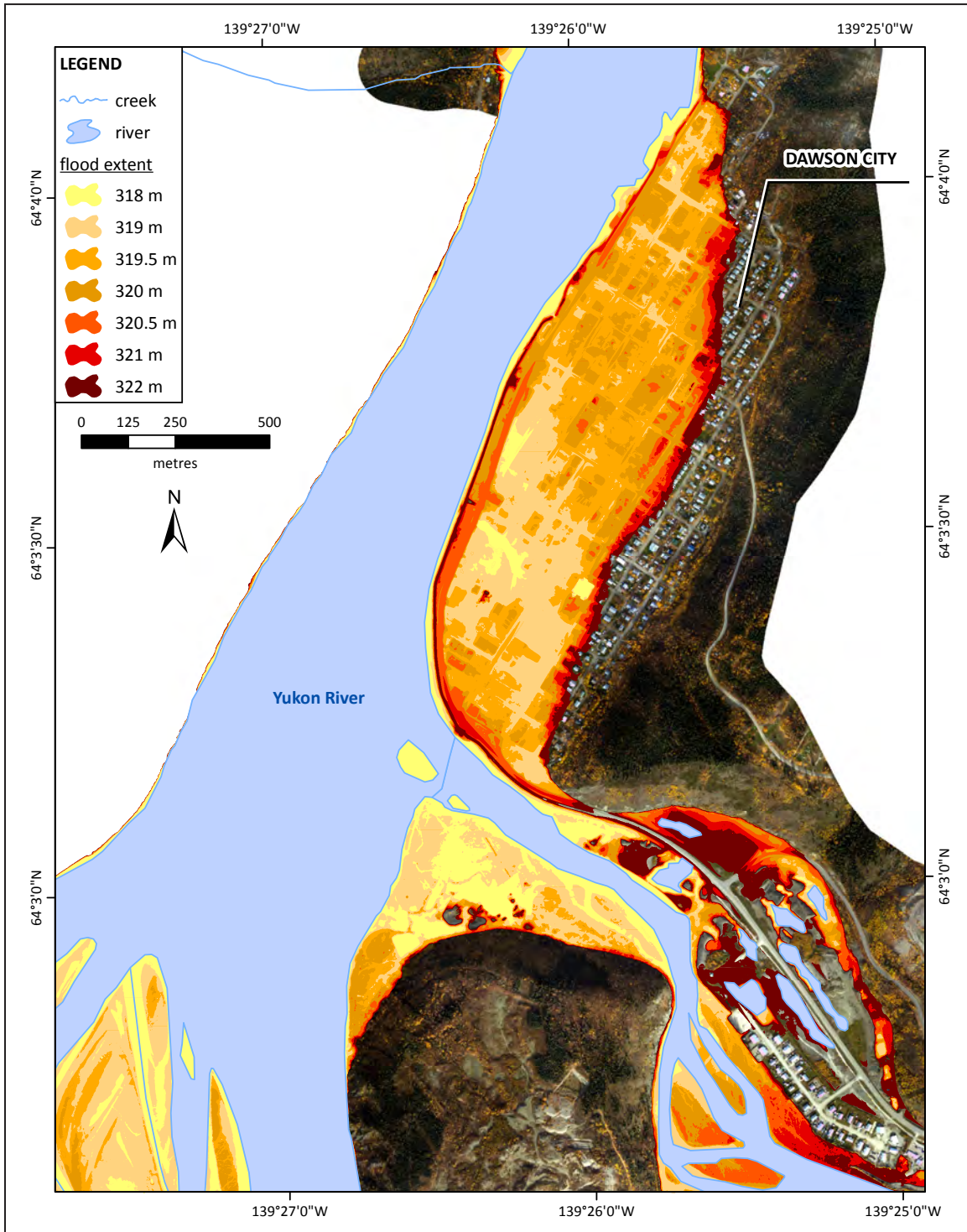
Figure 11. Close-up of amalgamated modelled flood extents for Dawson City illustrating Yukon River levels between 318 m and 322 m (relative to the Canadian Geodetic Datum). Note that the dike is not integrated as a barrier to flooding. Model results are based on LIDAR imagery provided by the Yukon Government. Background image source: ERSI, DigitalGlobe, GeoEye.
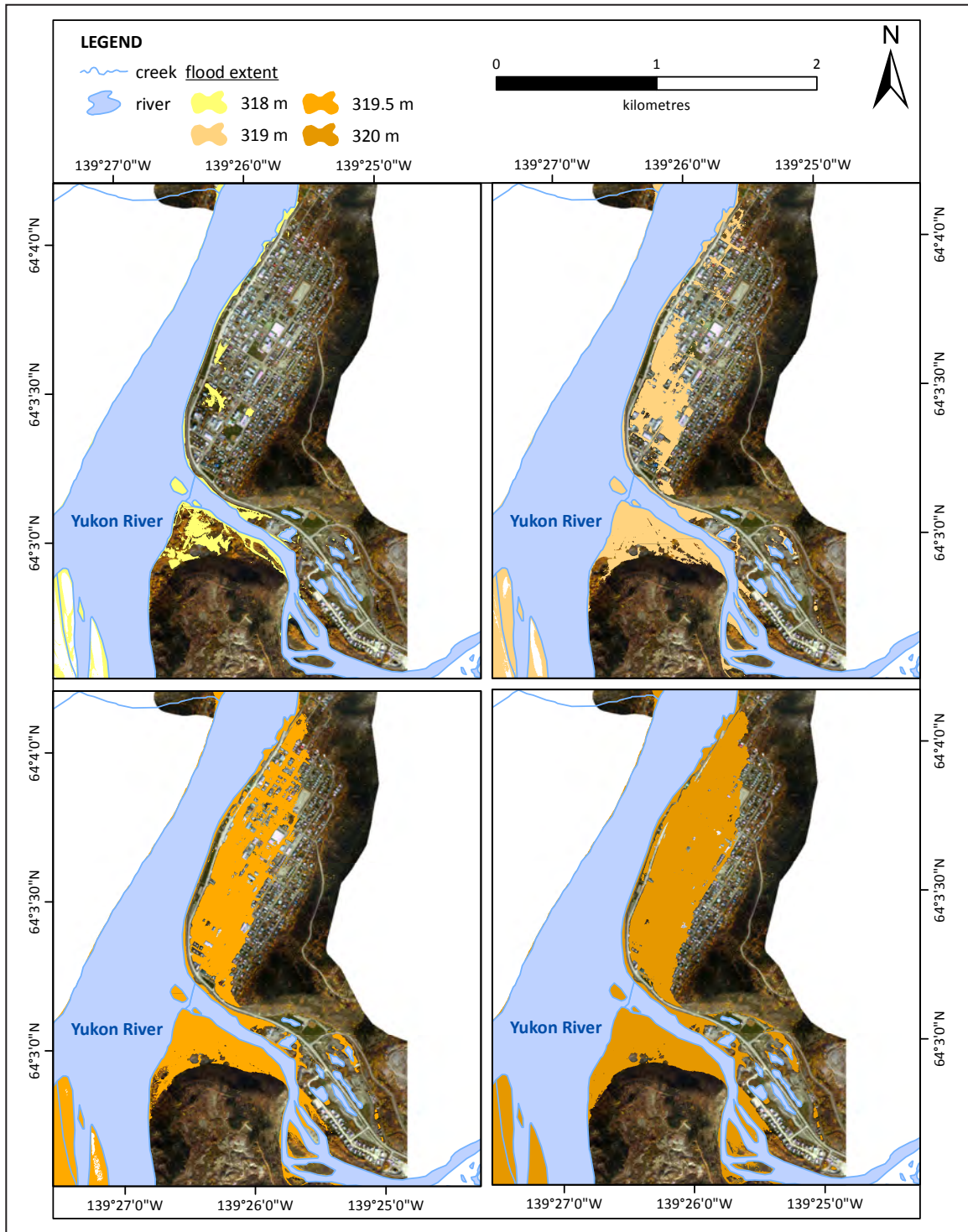
Figure 12a. Modelled flood extents for Dawson City depicting flood extent for individual Yukon River levels (relative to the Canadian Geodetic Datum) including river levels of 318, 319, 319.5 and 320 m. Note that the dike is not integrated as a barrier to flooding. Model results are based on LIDAR imagery provided by the Yukon Government. Background image source: ERSI, DigitalGlobe, GeoEye.
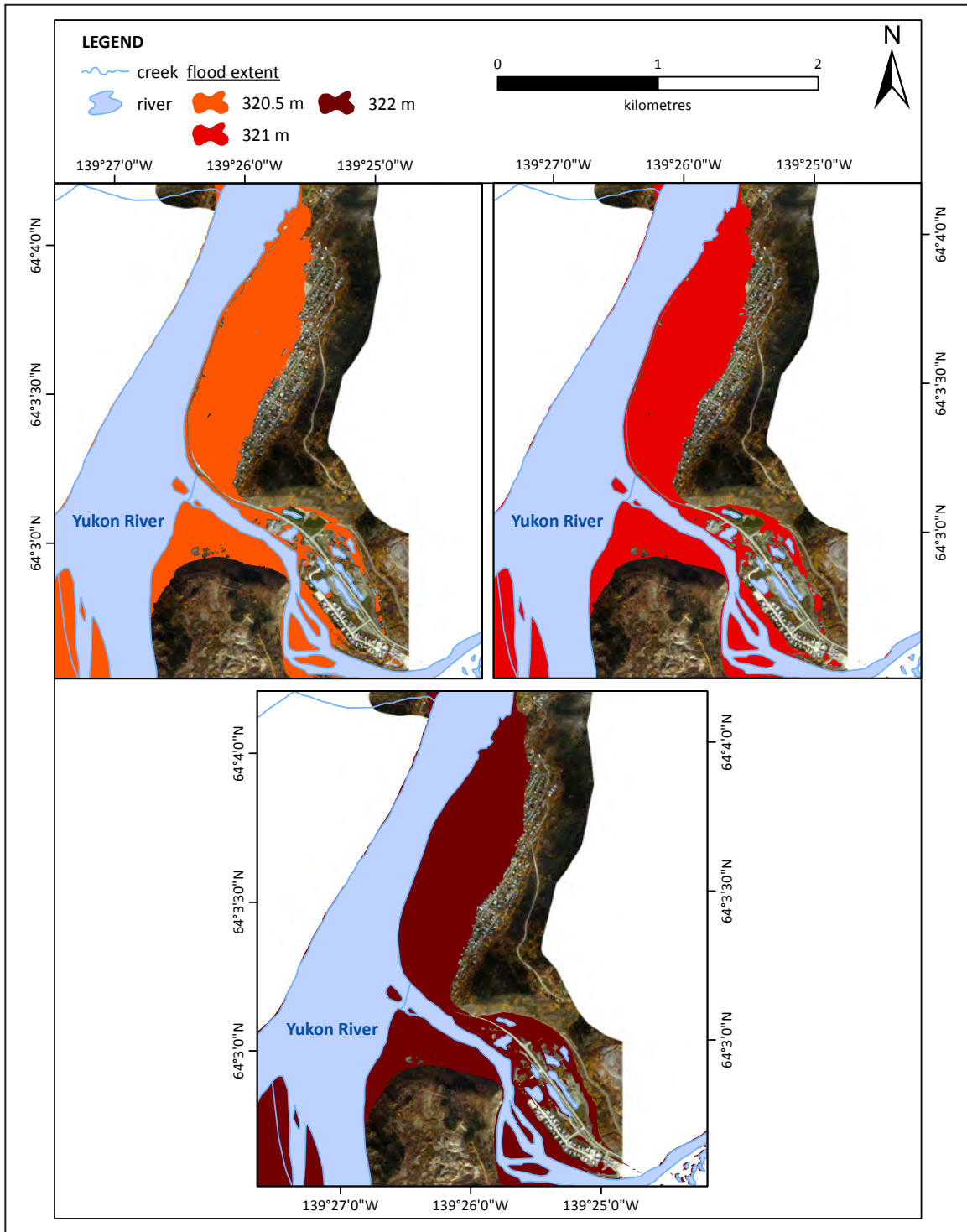
Figure 12b. Modelled flood extents for Dawson City depicting flood extent for individual Yukon River levels (relative to the Canadian Geodetic Datum) including river levels 320.5, 321 and 322 m. Note that the dike is not integrated as a barrier to flooding. Model results are based on LIDAR imagery provided by the Yukon Government. Background image source: ERSI, DigitalGlobe, GeoEye.

GROUNDWATER

Limited information regarding groundwater for Dawson City is available. No long-term monitoring records were identified as part of this project. However, as Dawson City is located on the floodplain of the Yukon River and is protected by a dike, it is likely that the water table under the community is quite shallow, and flow is generally towards the Yukon River. Most water wells in Dawson City are located with a shallow unconfined aquifer that recharges from surface runoff and infiltration from nearby streams and rivers (Gartner Lee Limited, 2003).

Interestingly, Dawson City may have been the first community in Yukon to use wells as a water source – reports indicate community wells were installed as early as 1903 (Intera, 1975). Presently, several municipal wells, operated by both the City of Dawson's Public Works Department and Yukon Government's Property Management Division are located in Dawson City. Wells operated by the City of Dawson are located west of Front Street, between Church and Turner streets. (Incidentally, the division between permafrost and non-permafrost areas of the community runs approximately along Church Street. The wells are located in an area where permafrost is not likely present.) Static water levels in these wells have been measured between 3 m and 7.3 m below ground surface (Gartner Lee Limited, 2003).

ENVIRONMENTAL DISTURBANCE HISTORY

Throughout history, many settlements have evolved in proximity to water in order to facilitate transportation, sanitation and support agricultural systems (Beasley, 2010). Dawson City was no exception, built at the confluence of the Yukon and Klondike rivers. Since the founding of the settlement, Dawson residents have dealt with a range of environmental stresses (NCE, 2011). The influx of thousands of miners to the Yukon during the Gold Rush (1896-1900) was the first major anthropogenic pressure on the land and water (Willis, 1997). Transforming the area from a small First Nations camp to, at the time, the largest city west of Winnipeg, the Klondike Gold Rush resulted in extensive deforestation (with subsequent implications for ecosystem health), water diversions (affecting fish habitat), loss of permafrost (influenced by mining and land clearing) and increased wildlife harvesting to feed the early mining population of Dawson (NCE, 2011). Effects caused by these changes to the land were devastating, and many consequences of this environmental disturbance remain today (Willis, 1997).

In Yukon, early settlers viewed floodplains to be hospitable locations for townsites given their level building surface and valley walls that provided protection from harsh climates (Beasley, 2010). Over time, the dynamic hydrology in the region and an understanding of the changing climate became known, revealing the challenging aspects of living on a floodplain. For example, Dawson City was quite exposed to the risk of floods (Beasley, 2010). Due to Dawson being the territory's most flood-affected settlement, a small dike was constructed in 1959 to provide protection to the town and its residents. Dawson City experienced some degree of flooding at least twelve times since its establishment in 1897, and the dike had to be raised on two occasions to accommodate the frequency of the floods. The worst flood occurred in 1979, and was the result of heavy snowfall and ice jams that formed on the Yukon, Indian and Klondike rivers. Despite efforts to build a sandbag dike between the river and the community, floodwaters quickly inundated much of the townsite, in some cases causing floodwaters of up to two metres deep (Whitehorse Daily Star, 1979). Gauged records indicate that water levels on the Yukon River reached 320.6 m in elevation (Janowicz, 2002). After this flood, a permanent dike was constructed to 321.0 m, which has since protected the community from major river-related flooding.

Human impacts on permafrost have also resulted in environmental disturbance in the region. Dawson City is located at the northern limit of the discontinuous permafrost zone. Permafrost

is up to 60 m thick under the town site and close to surface (NCE, 2011). Over the past century, the distribution of permafrost in the Dawson region has been heavily influenced by Gold Rush-era deforestation and hydraulic placer mining, and evidence of permafrost thaw associated with early twentieth century gold rush activity persists in the region (Calmels et al., 2012). In some valley bottoms surrounding Dawson, permafrost is thawed and destroyed by placer mining, which involves removing surface vegetation to reach the gold found in buried creek gravel deposits (Willis, 1997). In addition, large gold dredges altered river and creek routes, leaving behind tailing piles that are free of permafrost.

Over the years, agricultural development has also taken place in Dawson. The challenge with developing permafrost terrain for agricultural use is the thawing of the underlying permafrost; this is often done to facilitate drainage and land workability. When attempted, it is a time consuming process that involves careful timing of activities and drainage of the area to prevent the loss of substantial topsoil material (McKenna, 2013). In the Dawson region, where long days and warm temperatures make agricultural activities possible, farming has been carried out for some time. Soils in the region are also conducive to growing, as they are composed mainly of silt loam to fine sandy loam. Records indicate that farming activities in Dawson began before 1949, and that in the Sunnydale region (west of the Yukon River, and south of West Dawson), clearing for agriculture continued into the 1960s (McKenna, 2013). In this region, low-lying areas that are not suitable for building major infrastructure due to flood risk are still used to grow hay and other crops.

An additional pressure on permafrost preservation is the consistent annual forest fire activity that affects the region. Over the last fifty years, relatively few areas in the greater Dawson region have gone untouched by fire (NCE, 2011). It appears that the incidence of fire has increased over time, most specifically between the years of 1980 and 2000 (NCE, 2011). In the study area region, most forest fire activity occurred in the 1950s and in more recent decades (Figure 13). Environmental disturbance as a result of the forest fires includes changes in vegetation and re-establishment of early successional species. However, subsequent impacts on permafrost are also possible. Because the organic mat on the forest floor acts as an insulator for permafrost, its disturbance can result in deepening of the active layer, alterations to surface albedo, and accelerated permafrost thaw or the development of taliks (an unfrozen layer between the seasonally thawed active layer and the permafrost) (Yoshikawa et al., 2003).
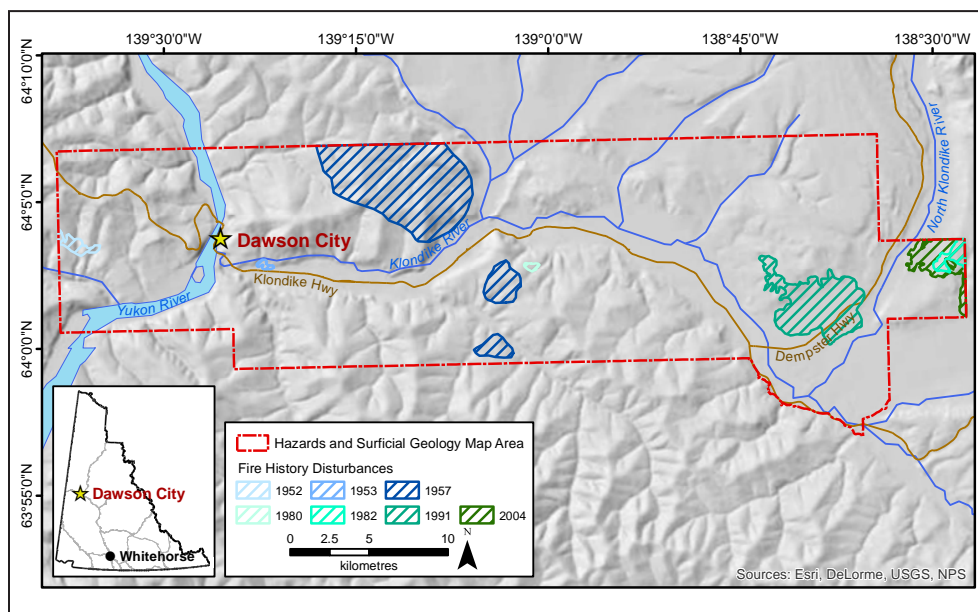
Figure 13. Fire history for the Dawson region, denoting the extents of notable fires in the study area. Fire history records provided by Government of Yukon.

21

LANDSCAPE EVOLUTION

The concept of 'landscape' comprises both the physical elements of landforms (mountains, valleys and plateaus), water bodies (rivers, lakes and ponds), elements of the cryosphere (glaciers and permafrost), and the living parts of the landscape such as the presence and modifying pressures of plants, animals and humans. The physical and geological landscape of the study area has been modified by millions of years of tectonic activity, fluvial (water) erosion and deposition, the advance and retreat of glaciers, and more recently, the modifying effects of eolian (wind), colluvial (gravity), permafrost (perennially frozen ground), and human processes.

The study area for this project is situated in a unique region of Yukon. The map area straddles the boundary between a landscape affected by extensive, repeated phases of advance and retreat of continental-scale ice sheets, and a landscape of deeply weathered, unglaciated terrain that was part of a much larger unglaciated landmass known as Beringia (Figure 14). Because the unglaciated landscape has never been 'stripped' by the scouring action of glaciers, the unconsolidated sediments that comprise the surficial geology of the region extend much further into geologic history than those of glaciated regions. As a result, surficial sediments in the map area range in age from most recent Holocene to greater than 2.6 million years. Underlying bedrock geology comprises various rock types that are as old as Devonian or greater than 350 million years.

In discussing the evolution of the landscape in the Dawson region, we can broadly divide the surface and bedrock geology into components that were formed prior to the epoch of frequent glacial episodes (the Tertiary Period and earlier; Figure 15), those that were formed during the epoch of glacial episodes (the Pleistocene Epoch of the Quaternary Period), and those formed in the modern, post-glacial time (the Holocene Epoch of the Quaternary Period).
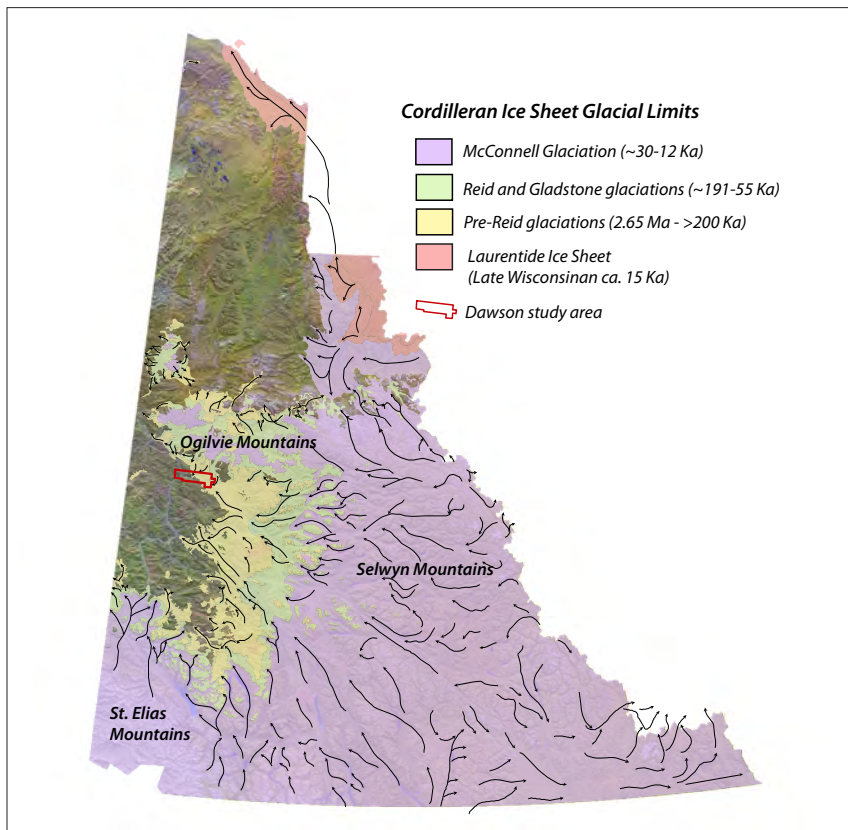
Figure 14. *The study area for the Dawson Landscape Hazards Mapping Project is at the furthest extent of Pleistocene ice sheets in western Yukon. Advances of the Cordilleran Ice Sheet in Yukon became less extensive throughout the Pleistocene and the study area is thought to have only been glaciated by the earliest, Pre-Reid advances. Unglaciated areas of Yukon were part of the landmass known as Beringia, which remained unglaciated throughout the Pleistocene. Arrows indicate ice-flow directions. Figure modified from Duk-Rodkin (1996).*

Mya	PERIOD	EPOCH	
		HOLOCENE	post-glacial era; warming to modern climate
0.01	QUATERNARY	PLEISTOCENE	era of frequent glaciation in the northern hemisphere; depostion of Klondike gravel and glacial deposits in the study area
2.58			
	TERTIARY	PLIOCENE	era of gradual cooling, warmer than modern climates; deposition of White Channel gravel in the study area
5.3			
	beginning 65 Mya	MIOCENE beginning 23 Mya	warmer than modern climates

Figure 15. A simplified geologic timescale including those periods of rapid landscape evolution that occurred in the study area. Mya = millions years ago.

THE TERTIARY PERIOD AND EARLIER

Landscape building in the study area is thought to have begun with two periods of volcanic arc activity at the western margin of the ancestral North American continent (Gordey and Ryan, 2005). Arc activity took place in the Devonian-Mississippian Period (~350 million years ago (Ma)) and again in the Permian (~260 Ma). Arc volcanic and plutonic rocks were deposited on top of, and intruded into, older siliciclastic rocks of the ancestral continental margin; these rocks are collectively represented today by the Yukon-Tanana terrane (Figure 16; Figure 17). The volcanic arc was separated from the ancestral North American margin by a small ocean (comparable to the modern Sea of Japan) between Mississippian and Permian time (~350-250 Ma). Rocks deposited in this ocean basin correspond to the Slide Mountain terrane (see Figures 16 and 17).

By the Triassic, this small ocean closed, the Yukon-Tanana and Slide Mountain terranes were accreted to the continental margin and were deformed and metamorphosed. Rapid uplift of these rocks first occurred in the Early Jurassic (~190 Ma) with subsequent and contemporaneous episodes of arc activity in the Jurassic and Cretaceous (~200-100 Ma; Gordey and Ryan, 2005). Local occurrences of Cretaceous conglomerate (~100 Ma) marked the cessation of this period of mountain building, and it is likely that much of the modern topography of the Klondike Plateau had been in place by that time (Gordey and Ryan, 2005). Extensive outpouring of basalt and dacite in the Late Cretaceous (~70 Ma) covered the landscape and was accompanied by minor faulting. The last major geological event in the region is the substantial regional offset along the Tintina fault in the Eocene (~55-35 Ma).

Most recent landscape evolution and the deposition of unconsolidated sediments in the Dawson area began ~5 Ma ago, in the late Tertiary (~65-2.58 Ma), when the landscape was drained by river systems that were substantially different than the Klondike and Yukon rivers we see in the study area today. It is likely the paleo-Klondike River flowed southward, draining the eastern part of the map area from its headwaters at a paleo-divide near the modern Rock Creek. In the western part of the map area (Figure 18a; see page 26), the drainage of Hunker and Bonanza creeks likely

flowed westward before joining a south-flowing, paleo-Yukon River (Tempelman-Kluit, 1980; Duk-Rodkin et al., 2001).
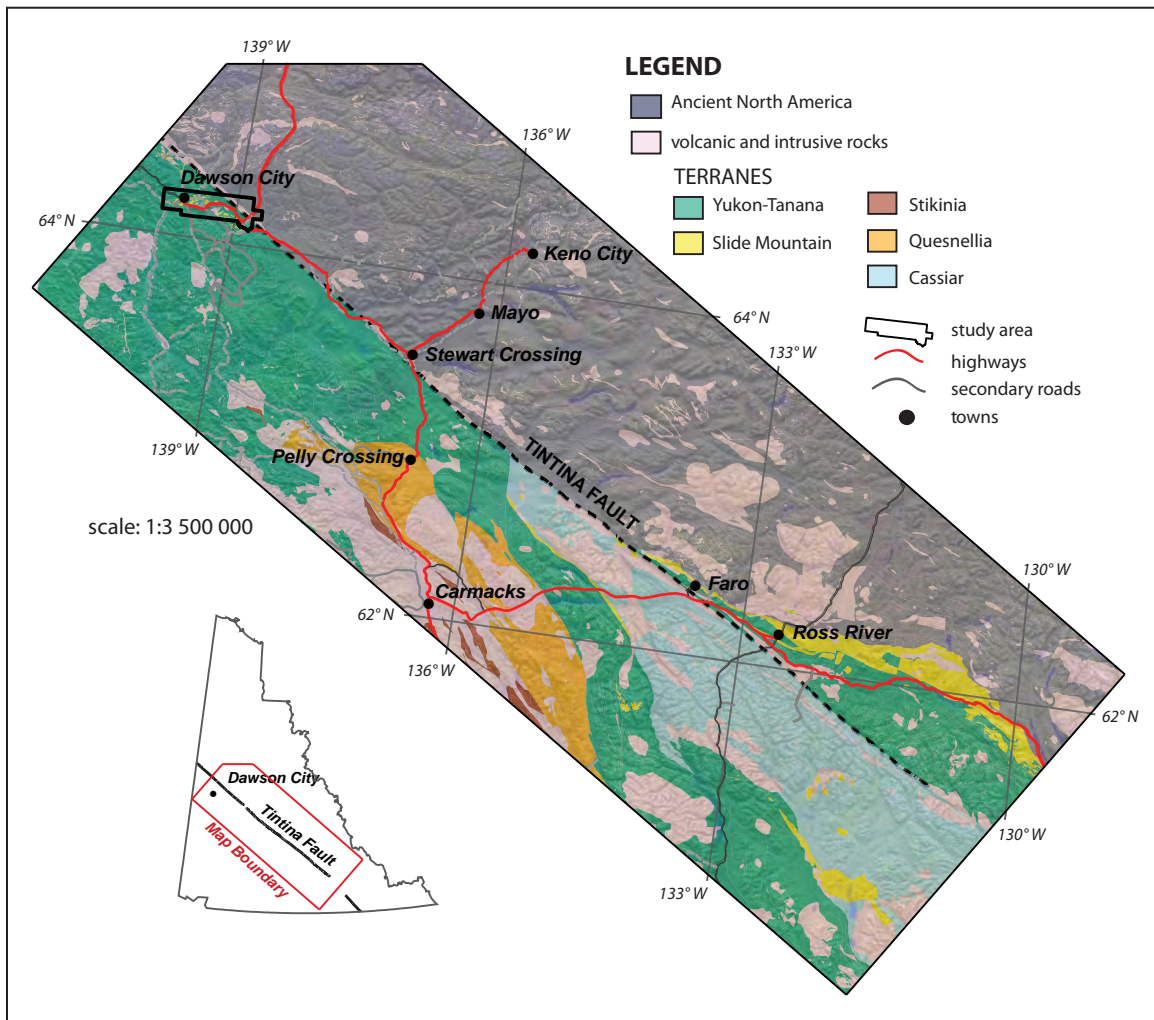
Figure 16. *Simplified terrane map of the study area and surrounding regions. The majority of the bedrock in the study area comprise rocks of Yukon-Tanana and Slide Mountain terranes. From Colpron (2014).*

Gradual incision of the Klondike Plateau by Tertiary streams resulted in a landscape characterized by broad hills, shallow valleys, and deeply weathered bedrock. An extended period of fluvial aggradation initiated by a gradual cooling of global climate (Jackson et al., 2009), or possibly differential regional uplift (Hughes et al., 1972; Milner, 1977), is recorded in distinctive light grey to white quartz-rich gravel deposits known as the 'White Channel' gravel that occur at elevations 50 to 100 m above modern stream levels (Figure 18b and Figure 19).

When first encountered by geologist R.G. McConnell in 1898, the "quartz-drift" was unlike any deposit the geologist had previously encountered (McConnell, 1900). Systematically ruling out glacial, lacustrine and marine environments for deposition, McConnell ultimately concluded the deposit was composed of "stream gravel deposited under… exceedingly slow accumulation in streams of easy grades and comparatively slack currents" (McConnell, 1905). Citing the uniform and highly weathered clasts in the gravel (less resistant lithologies had been weathered away), its unusually high compaction (requiring a long period of time), and evidence of iron leaching

(indicating warmer climates and unfrozen sediments), McConnell (1905) further suggested the White Channel gravel was a residual Pliocene stream deposit, having been emplaced over a long period of stream action under warmer climates than that of today.
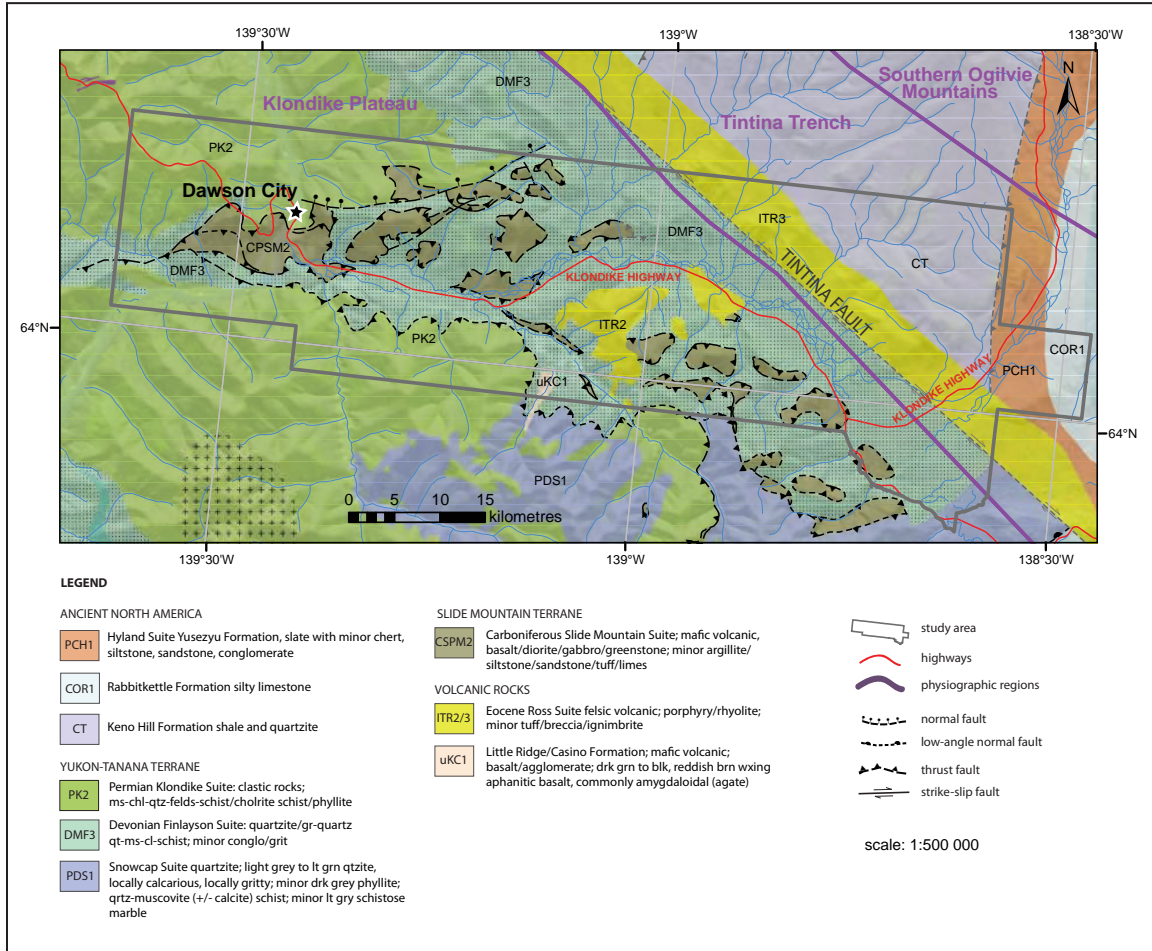
Figure 17. *Simplified geology map of the study area including physiographic regions, faults, and simplified descriptions of the rocks of Slide Mountain and Yukon-Tanana terranes; ancient North America; and intrusive volcanics. From Colpron (2014).*

Very little of McConnell's interpretation of the genesis of the White Channel gravel has changed in the more than 100 years since he first published his observations. Detailed sedimentological studies have interpreted the gravel as originating in a braided stream environment that evolved over an extended period of weathering and erosion in the drainage basin (Morison, 1985; Morison and Hein, 1987). As originally suggested by McConnell (1905), the gravel is derived entirely from local bedrock lithologies that underwent extensive weathering prior to deposition, as well as strong in-situ leaching by hydrothermal fluids (Tempelman-Kluit, 1982; Dufresne et al., 1986). Early authors divided the White Channel gravel into upper and lower units largely based on colour and staining (McConnell, 1905), however, there is no distinct break in sedimentation between the units at most locations (Morison, 1985) and more recent descriptions have characterized the upper unit by evidence of periglacial conditions (Froese and Westgate, 2001).
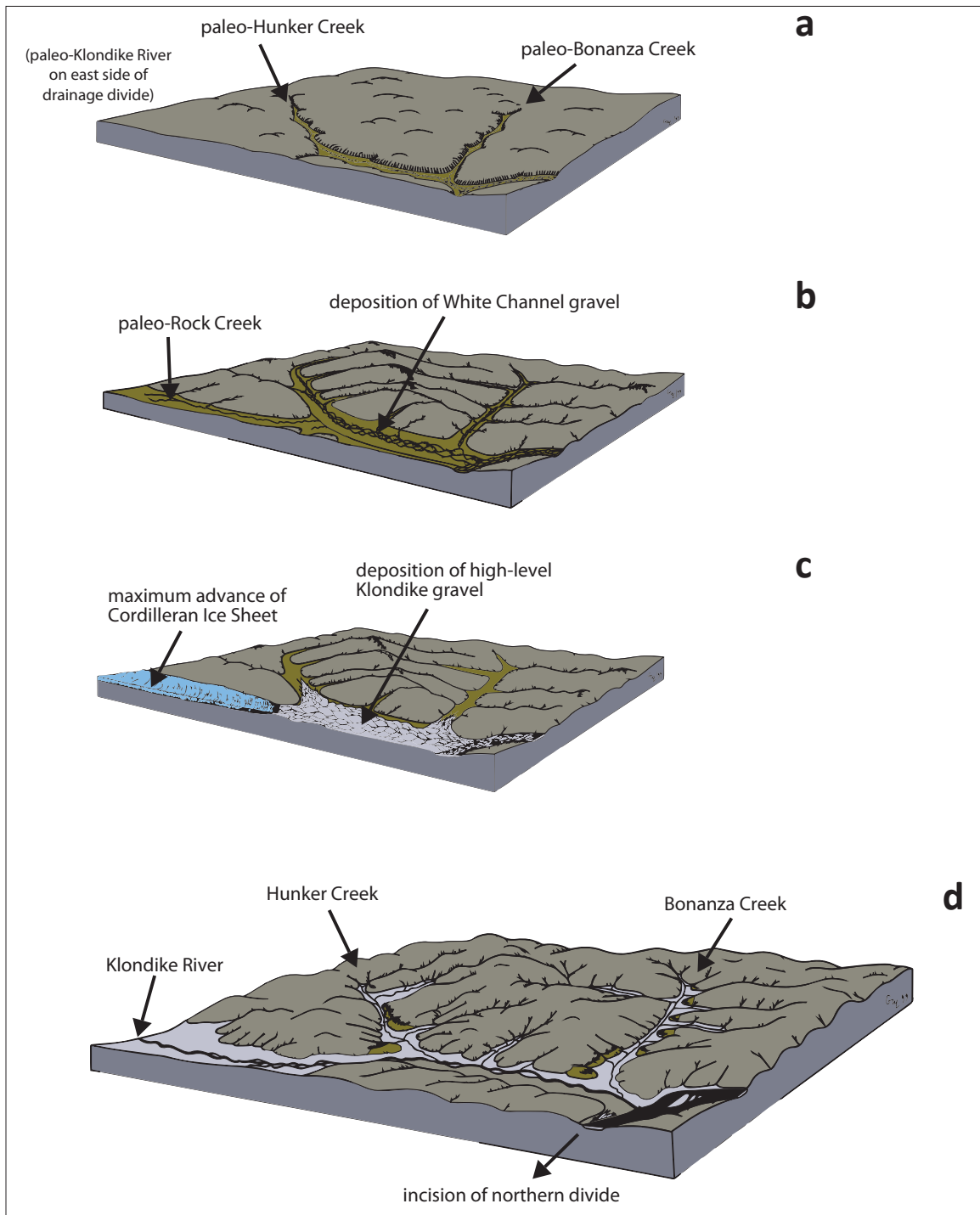
Figure 18. *Evolution of the late Tertiary landscape:* **(a)** *Accumulation of the White Channel gravel begins in the early Miocene; broad, low-angle drainages of the paleo-Hunker and paleo-Bonanza creeks formed the headwaters of a south-flowing, paleo-Yukon River.* **(b)** *Continued aggradation of the White Channel gravel under a cooling climate in the late Tertiary; Rock Creek is a small tributary to the Hunker Creek drainage.* **(c)** *During the maximum advance of the Cordilleran Ice Sheet into the study area, ice overtopped the Rock Creek drainage divide, eroded the Klondike Valley, and deposited the high-level, Klondike gravel.* **(d)** *Eventual establishment of the northward flow of the Yukon River led to a lowering of base-level and incision of high and intermediate-level terraces; modern drainages are deeply incised and underfit for their broad valley profiles. Figure modified from Lowey (2004; Figure 24).*
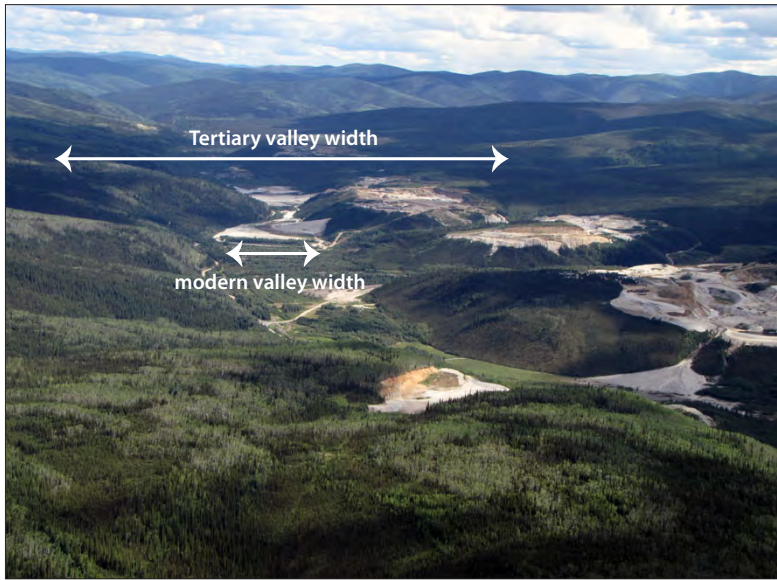
Figure 19. *Photo looking south toward the headwaters of Hunker Creek showing the broad valley floor of the Tertiary fluvial system (benches currently being mined) and the narrow, inset valley of the modern Hunker Creek drainage. White Channel gravel is a distinctive deposit that makes up benches up to 100 m above modern stream levels.*

Deposition of the lower White Channel gravel likely began >5 Mya (in the earliest Pliocene) while periglacial conditions of the upper White Channel gravel began in the mid-Pliocene (Froese and Westgate, 2001; Westgate et al., 2003). By the latest Pliocene (~2.64 Ma), the first glacial sediments were deposited in the study area and a renewed period of valley incision began (Hughes et al., 1972; Froese et al., 2000; Westgate et al., 2003; Hidy et al., 2013).

THE PLEISTOCENE EPOCH

Multiple Cordilleran and Ogilvie Mountain glaciations during the early and middle Pleistocene are recorded in glaciogenic sediments preserved in Tintina Trench to the north and west of the study area (Duk-Rodkin et al., 2010; Barendregt et al., 2010). Only the maximum Cordilleran Ice Sheet advance is thought to have reached the study area in the earliest Pleistocene, and subsequent, less-extensive advances during the Pre-Reid (up to 7 undifferentiated advances lasting from ~2.65 to 0.2 million years ago), Reid (~191-125 thousand years ago) and McConnell (~30-12 thousand years ago) glaciations likely reached their maximum just south of the study area (see Figure 14). Pleistocene glaciations were initiated by expansion of alpine glaciers in the high mountains that eventually coalesced into major ice sheets. At its maximum Pre-Reid extent in the study area, ice from the Selwyn Lobe (originating in the Selwyn Mountains of eastern Yukon) advanced north along Tintina Trench and coalesced with ice formed in the Ogilvie Mountains to the northeast of the study area (see Figure 14). The extent of the Cordilleran Ice Sheet became increasingly limited with successive glaciations during the Pleistocene, and it is likely the Ogilvie Mountain lobe was only able to coalesce with the Selwyn Lobe during Pre-Reid glaciations.

High-level gravel

Overlying (and in some localities interbedded with) the upper White Channel gravel, the Klondike gravel (also known as the Klondike 'wash' or 'outwash') marks the first episode of Pleistocene glaciation to be recorded in the study area. The gravel is a glaciofluvial outwash that was deposited 2.64 ± 0.2 Mya (Hidy et al., 2013), at the transition between the Pliocene and Pleistocene epochs, a globally recognized time of ice sheet growth after gradual cooling during the Pliocene (e.g., Haug et al., 2005; Balco and Rovey, 2010).

Found at high elevations (up to 200 m above the Klondike River) from the Flat Creek beds south of the North Klondike River, and westward to at least the Alaska border (Duk-Rodkin, 1996),

the Klondike gravel was originally described by McConnell (1905) as high-level "stream gravel" because of the unit's similar appearance to modern gravel in the valley bottoms. The Klondike gravel is distinctly grey in colour and contains pebbles of chert, quartzite, and slate lithologies that are foreign to the paleo-Hunker Creek drainage basin. These 'extra-basinal' clasts are interpreted to have been transported into the Klondike River valley by glacial meltwater generated by the maximum, and earliest, advance of the Cordilleran Ice Sheet in the region (Hughes et al., 1972; Froese et al., 2000; Hidy et al., 2013). Paleoflow measurements of the Klondike gravel at Flat Creek are further evidence that the maximum early Pleistocene glaciation in the region was from a westerly advancing Cordilleran Ice Sheet rather than local glaciation in the Ogilvie Mountains (Bond, 1997).

Yukon River reversal

The maximum extent of the Cordilleran Ice Sheet in the map area (see Figure 18c) was achieved after a westward advance up the paleo-Klondike valley. The glacial advance spilled meltwater over the Tertiary surfaces of the paleo-Hunker drainage (depositing the Klondike gravel) and eventually incised a channel through the divide at Rock Creek to form the modern Klondike River (see Figure 18d). Incision of the lower Klondike Valley likely took advantage of a pre-existing fault (Duk-Rodkin et al., 2001) and was driven by a change in base level on the Hunker Creek side of the divide initiated by the establishment of the northward flow of the Yukon River. It is thought the maximum advance of the Cordilleran Ice Sheet in the early Pleistocene impounded a south-flowing paleo-Yukon River, forming a large pro-glacial lake that overtopped the Yukon River paleo-divide near the modern Fortymile River and established the modern northward course of the Yukon River (Duk-Rodkin et al., 2001). The restructuring of the Yukon River drainage precipitated significant base level change, effectively driving the abandonment of the high-level Tertiary surface through incision of the broad paleo-valley floor and establishment of the modern, narrow inset valleys of the Klondike and Yukon rivers and their tributaries (see Figures 18d and 19).

Intermediate-level gravel

Between the high-level Klondike gravel and the modern valley floor, intermediate-level terraces incised into Pliocene sediments (White Channel gravel) and bedrock record a gradual cutting of the modern valley over 2.6 million years. The intermediate terraces are generally poorly preserved and occur preferentially on the north side of the Klondike Valley (Figure 20). Terraces range in elevation from 40 to 150 m above the modern river and likely represent intermittent periods of channel aggradation and terrace formation driven by glacial advances to the north, east and south (Jackson et al., 2009).
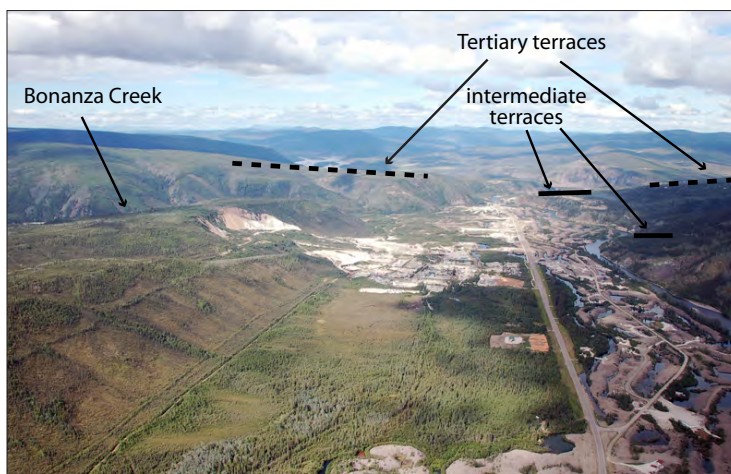
Figure 20. Photo of the lower Klondike River valley (view west toward the Yukon River) with broad Tertiary fluvial surface high on the hillside, intermediate terraces on the north side of the valley, and the narrow Quaternary valley occupied by the modern drainage.

Two of the intermediate-level terraces, Archibald's Terrace and the Midnight Dome terrace, have been studied in detail. Incised 60 m into Tertiary White Channel deposits, the gravel at Archibald's terrace is overlain with silt containing the 1.37 million year old Mosquito Gulch tephra (Naeser et al., 1982; Preece et al., 2011). Similarly, at Midnight Dome, ~2 m of non-glacial fluvial gravel and ~2-5 m of glacial outwash (Froese and Hein, 1996) are overlain by up to 15 m of silty loess with a paleomagnetic signature that records up to 1.5 million years of deposition and four cycles of glacial-interglacial sedimentation (Froese et al., 2000; Froese and Schweger, 1999; Schweger et al., 1999). The Midnight Dome terrace is incised ~100 m into the Tertiary surface, and with an inferred age ~1 million years younger than the Klondike gravel, provides a rough constraint on the rate of incision of the Klondike Valley.

Valley-bottom gravel

During the penultimate Reid Glaciation, glaciers from the Ogilvie Mountains advanced into the study area and achieved their maximum ~10 km upstream of the confluence of the North Klondike River with the South Klondike River. Landforms from this event include moraines and glaciofluvial terraces in the lower North Klondike River valley (McKenna and Lipovsky, 2014; see map included in back pocket of this report), and glaciofluvial terraces in the Klondike River Valley ~40 m above modern river level (Tarnocai et al., 1985; Duk-Rodkin, 1996).

During the most recent McConnell Glaciation (~20,000 years ago), Ogilvie Mountain ice reached its maximum some 100 km from the study area, near Tombstone Territorial Park. Glaciofluvial terraces produced from this advance, as well as from the McConnell maximum in the Stewart and Yukon river valleys (~200 km southwest of the study area), grade into Holocene and modern fluvial terraces in the Klondike River valley (Duk-Rodkin, 1996).

The restructuring of the Yukon River drainage (from south-flowing to north-flowing) contributed to the formation of the region's richest placer gold deposits in the Klondike River and its north-flowing tributaries (mainly Bonanza and Hunker creeks). Gold-bearing Tertiary and Pleistocene gravel was reworked as the drainages incised new, deeper channels, effectively 'sluicing' the older deposits and leaving behind a much richer placer than was contained in the original high and intermediate-level gravel. The valley-bottom creek gravel also contains abundant fossil remains of Pleistocene mammals (McConnell, 1905; Froese et al., 2009).

Loess, colluvium and muck

As advances of the Cordilleran Ice Sheet became less extensive during the Pleistocene, sediment deposition in the study area was dominated by colluvial and eolian processes. Changes to the landscape during the late Pleistocene include the deposition of a mantle of wind-blown silt and sand (loess), and blankets, aprons, and fans of colluvium.

Loess deposits are found on both upland and lowland surfaces in the Klondike, but commonly occur in greater thicknesses in steep gullies, and overlying creek bottom and intermediate terrace gravels (McConnell, 1905; Fraser, 1995; Bond and Sanborn, 2006). The silt, comprising the bulk of loess deposits, was likely generated from local stream beds and unglaciated soils (Tarnocai et al., 1985; Fraser and Burn, 1997) under regional winds and strong katabatic flow from the ice sheets to the south (Muhs et al., 2003; Muhs and Budahn, 2006). While much of the loess in the study area was deposited during the late Pleistocene and Holocene (Fraser and Burn, 1997; Kotler and Burn, 2000), loess deposition and colluviation processes have probably been ongoing throughout the Pleistocene (Westgate et al., 1990; Froese et al., 2000; Preece et al., 2000).

Numerous volcanic ash (tephra) beds preserved within loess sequences on intermediate-level benches and narrow gullies of the Klondike have demonstrated the antiquity of loess deposits in the study area (Preece et al., 2011). Dated tephra deposits span more than two million years and

provide evidence of the long-term maintenance of loess depositional processes through many glacial and interglacial cycles.

Primary loess deposits are commonly retransported by cryoturbation and downslope colluvial processes. Where loess becomes incorporated with organic and mineral surface materials, the resulting organic-rich, colluvial silt and sand is commonly known as 'muck' (Fraser and Burn, 1997; Figure 21). A silt-rich lower member of the 'muck' deposits in the Klondike was deposited during full-glacial conditions in the Pleistocene and preserves flora and fauna representative of dry grasslands (Fraser and Burn, 1997; Zazula et al., 2006). Relict ice wedges are common in the upper part of the silt 'muck' unit and are typically overlain by a thaw unconformity (Fraser and Burn, 1997; Froese et al., 2008). Ice wedges record thermal cracking of the ground surface primarily during the late Pleistocene (Kotler and Burn, 2000); however, tephra records show that some ice wedges have been preserved since the early to middle-Pleistocene (Froese et al., 2008).

Figure 21. Ice-rich 'muck' deposits on a north-facing slope in the Hunker Creek valley.

Downslope colluviation of all surface materials in the study area is largely driven by gravity and permafrost processes. In particular, slow periglacial wasting mechanisms (e.g., solifluction, slopewash) have likely dominated colluvial processes throughout the Pleistocene and Holocene. In general, colluvial deposits of weathered bedrock thicken downslope and become increasingly mixed with other surficial deposits such as loess, glacial deposits, and high-level fluvial gravels. In the region, downslope processes are strongly controlled by aspect, whereby permafrost processes are present on north and east-facing slopes and largely absent on south-facing slopes (Bond and Sanborn, 2006; Smith et al., 2009).

The Holocene Epoch

Holocene landscape evolution in the study area was modified by the amelioration of periglacial conditions and a gradual infilling of the valley bottoms that had been carved by glacial outwash. Warmer and wetter conditions in the Holocene initiated the development of peat and bog landscapes (Fraser and Burn, 1997; Kotler and Burn, 2000). These ice-rich, perennially-frozen organic accumulations are frequently referred to as 'muck', however they lack the typical mineral silt component that defines these types of deposits, and are interpreted to be primary and colluvial organic deposits that accumulated slowly through the Holocene (Fraser and Burn, 1997). Valley-

side colluvial deposits, thick eolian blankets, and a climatically driven abandonment of much of the floodplain of the Klondike River resulted in the modern narrow fluvial channels within a broad, poorly drained valley floor (see Figure 20).

Landscape evolution of the Dawson map area continued in most recent historic times as the result of extensive mining and community development on the creek bottoms and stream terraces of the Yukon and Klondike rivers and their tributaries. The largest and most well-known modification to the landscape resulted from the wholesale redeposition of many creek bottom gravels through dredging. The 'made land' comprising the dredge tailings represents a significant portion of land available for development in the map area and has its own unique set of material characteristics discussed in the following section.

Changes in climate through the Holocene must have impacted the development and degradation of permafrost. In general, permafrost may take decades to centuries to form, and equally long periods to degrade, although degradation can accelerate if surface ponding occurs or if ice within the ground is exposed. The surface organic mat can help preserve the permafrost for some decades during a warming phase, leading to what is termed ecosystem-protected permafrost (Shur and Jorgenson, 2007). Forest fire, which destroys the organic mat, may lead to the permanent loss of permafrost at warmer sites, whereas taliks (an area of year-round unfrozen ground surrounded by permafrost) may form at locations with colder microclimates, with permafrost eventually aggrading as vegetation succession takes place. The current state of permafrost in the Dawson region reflects the combined impacts of the most recent climate changes (the cooler period of the Little Ice Age which lasted for several centuries up to the end of the 19th century; and the 20th century climatic warming which has continued through to present), and disturbance associated with mining activities (Calmels et al., 2012), settlement, agriculture and forest fire. Given lags in the reaction of permafrost, permafrost in the area is undoubtedly in a phase of slow warming and thaw may be occurring at some locations. The impacts of thaw depend on many factors, but especially on the ice-content of the permafrost, which varies considerably from site to site.

SURFICIAL MATERIALS

The mapping of surficial landforms and their contained sediments is achieved primarily through air photo interpretation followed by ground truthing. While ground truthing, geologists examine riverbank exposures, road cuts, and dig small pits in order to characterize the various surficial deposits. Textural and stratigraphic information of surficial landforms is also gained through geophysical profiles of the subsurface (using Ground Penetrating Radar and Direct Current Electrical Resistivity), as well as shallow boreholes. Surficial materials are characterized based on their texture or grain size (e.g., very fine to very coarse sand); sorting (e.g., poorly sorted = inconsistent grain size); structure (e.g., layering or bedding); and the general distribution of the material.

Surficial deposits in the study area are derived from the following processes: glacial (ice, glacial streams and lakes); fluvial (rivers and streams); colluvial (downslope movement or creep); eolian (windblown); and organic processes (soil development). Detailed descriptions of the surficial materials found in the study area are also located in the map legend (see accompanying map "Surficial geology, Dawson region, Yukon; parts of NTS 115O/14 & 15 and 116B/1, 2, 3 & 4"; McKenna and Lipovsky, 2014).

Bedrock and weathered bedrock

Bedrock in the map area consists of a widespread suite of schists (commonly referred to as the 'Klondike Schist'; Figure 22); lesser amounts of carbonaceous quartzite (the 'Nasina Formation');

and uncommon greenstone, serpentinite and harzburgite from the Carboniferous Dawson-Clinton Creek Assemblage (Figure 23). Bedrock (R) is mapped on steep cliffs and slopes along the Klondike and the Yukon river valleys and are exposed by large landslides or glacial or glaciofluvial erosion.

Figure 22. Example of Klondike Schist found in the map area.

Figure 23. Example of serpentinite associated with Slide Mountain terrane rocks in the map area. This example is from the materials comprising the Dawson City landslide (Moosehide Slide).

Bedrock in the uplands and along ridge tops of the unglaciated portion of the map area is uniformly mapped as 'weathered bedrock' (D). Weathered bedrock deposits are frequently composed of blocks and boulders in a silty matrix created through frost shattering, colluviation, and chemical weathering processes. Weathered bedrock units typically contain a component of loess-derived silt and are subject to sorting and mixing from cryoturbation and other periglacial processes.

Permafrost is present in both bedrock and weathered bedrock in the map area.

MORAINE DEPOSITS

Moraine deposits include materials that have been deposited directly by a glacier or ice sheet without modification by any other agent of transportation (Howes and Kenk, 1997). Moraine deposits are typically compact, lack any structure (e.g., bedding or grading), and are poorly sorted containing a wide range of particle sizes (i.e., from clay-sized particles to boulders). Moraine deposits in the study area are assigned to either Pre-Reid glaciations (up to 7 undifferentiated advances lasting from ~2.65 to 0.2 million years ago) of the Cordilleran Ice Sheet or the Reid Glaciation (~191-125 thousand years ago) of the Ogilvie Mountains.

Pre-Reid ($M^{>R}$) moraine deposits in the study area are mapped predominantly on uplands and valley sides north of the Klondike River and between Rock Creek and the North Klondike River (see McKenna and Lipovsky, 2014, map included in back pocket of this report and Figure 24). These thick glacial deposits (till) consist of abundant pebbles, cobbles and boulders in a silty-sand matrix. Deposits are usually oxidized and contain a high percentage of weathered clasts. Extensive

loess from Pre-Reid and more recent glacial events was likely deposited on top of the till. Pre-Reid moraine in the study area has been heavily modified by colluviation, weathering, and periglacial processes. Occurring as thin (<1 m) veneers to thick (>1 m) blankets on shallow to steep slopes and plateau surfaces, Pre-Reid moraine deposits are usually secondary deposits having undergone extensive downslope colluviation and periglacial mixing. Both processes serve to incorporate younger sediments (i.e., loess) into the morainal deposits and result in a less compact deposit than younger morainal materials. Additionally, Pre-Reid moraine deposits have been subjected to a lengthy period of post-depositional weathering, likely resulting in higher clay contents than the primary deposit.
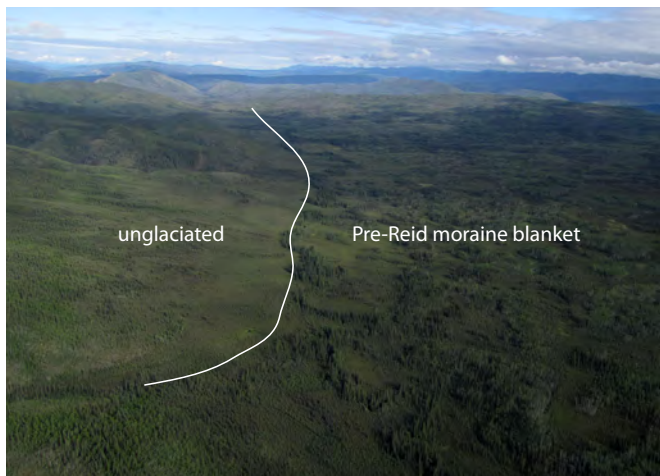
Figure 24. *Moraine blanket deposited by the Pre-Reid advance of the Cordilleran Ice Sheet in Tintina Trench. View is to the north.*

Reid (M^R) moraine deposits in the study area are limited to a few small units in the lower North Klondike River valley that are associated with moraines marking the maximum extent of the Reid-age advance of ice from the Ogilvie Mountains (see McKenna and Lipovsky, 2014; map included in back pocket). Like the Pre-Reid moraine in the study area, these deposits are comprised of poorly sorted silt, sand and clay, and abundant pebbles, cobbles and boulders which are commonly oxidized and have little structure such as bedding or grading. However, Reid-age moraine deposits have undergone significantly less weathering and retransport from colluvial and periglacial processes than Pre-Reid deposits, and are thus more compact, less mixed, and more closely resemble a primary deposit compared to the Pre-Reid moraine in the study area.

Both Reid and Pre-Reid moraine deposits are affected by permafrost, and these compact, poorly drained materials may be ice-rich.

GLACIOFLUVIAL DEPOSITS

Glaciofluvial deposits consist of sediment deposited by glacial streams on, within, adjacent to, and in front of a melting glacier (Howes and Kenk, 1997). Glaciofluvial deposits that formed at the toe (front) of the glacier are typically poorly sorted and lack structure due to their rapid aggradation (deposition and building up of sediment); however, deposits that are more distal to the ice front are more commonly moderately to well-sorted and stratified. These deposits generally contain less silt and clay-sized particles, are less compact, and better drained compared with morainal deposits and therefore ice-rich permafrost may or may not be present.

Glaciofluvial sediments in the map area consist of moderately to well-sorted, rounded, stratified sand and gravel, although the nature and texture may vary locally depending on transport distance. In general, glaciofluvial sediments associated with Pre-Reid glaciations were close to the ice front,

and contain more silt and clay-sized particles, and are more poorly stratified and sorted compared to deposits of Reid-age glaciofluvial sediments. Glaciofluvial deposits related to the McConnell glaciation (~30-12 thousand years ago) are limited in the study area and are indistinguishable from Holocene fluvial deposits, apart from small differences in the elevation of terrace deposits.

Glaciofluvial deposits are mapped on valley-side and valley-bottom terraces in the North Klondike, Klondike, and Yukon rivers, as well as in numerous smaller tributary valleys (McKenna and Lipovsky, 2014; map included in back pocket). High-level (up to 200 m above the modern river) and intermediate-level (40-150 m above the modern river) terraces are assigned to Pre-Reid ages, although the actual timing of deposition of these materials likely spans more than a million years.

The high-level Klondike gravel is the most extensive Pre-Reid (FG$^{>R}$) glaciofluvial deposit in the map area and overlies Tertiary-age fluvial gravel on the south side of the Klondike valley near the mouths of Hunker and Bonanza creeks (Figure 25). The Klondike gravel is interpreted as braided stream deposits (Froese et al., 2000) which grade from massive imbricate beds at Flat Creek (the extreme southeast corner of the map sheet) to less-energetic, planar-tabular, cross-bedded deposits in the western Klondike Valley (Froese et al., 2000). The Klondike gravel has a gradational lower contact with underlying Tertiary fluvial gravel that is defined by the addition of chert, quartzite and slate clasts derived from rocks found north of the Tintina Trench.

Figure 25. *Klondike gravel overlies Tertiary, White Channel gravel at Jackson Hill near the mouth of Bonanza Creek.*

Less extensive Pre-Reid glaciofluvial gravels are preserved on intermediate level terraces (e.g., Midnight Dome Gravel) in the Klondike Valley. Glaciofluvial gravel is described by Froese and Hein (1996) at the Midnight Dome terrace as a massive to crudely imbricate cobble-gravel overlying interglacial, fluvial pebble-gravel similar to deposits of the modern Klondike River. Glaciofluvial gravel was also exposed at the base of the Klondike River valley in placer mining cuts (Yukon Placer Mining Industry 2010 to 2014; Figure 26). Striated boulders in the gravel were noted near the contact with the underlying bedrock, which suggests a pre-Reid glaciation was likely responsible for its deposition.

Two distinct levels of intermediate terraces have been mapped along the Yukon and Klondike rivers. Pre-Reid glaciofluvial terraces are best expressed near the confluence of the North and

South forks of the Klondike River. Reid (FG^R) glaciofluvial terraces are mapped east and north of Rock Creek and are often covered by organic veneers, and in some places blankets of organic material.
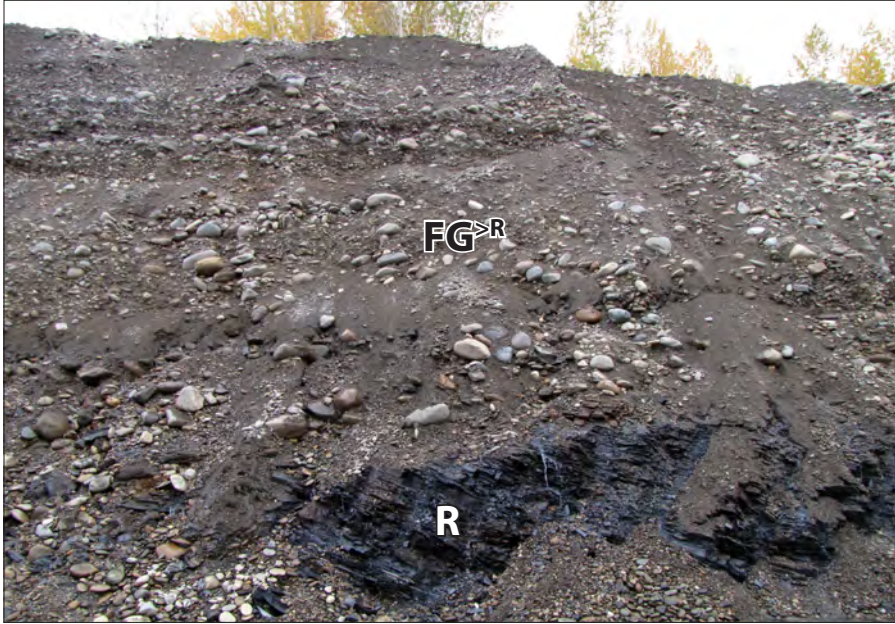
Figure 26. Pre-Reid glaciofluvial gravel (FG$^{>R}$) deposited on bedrock (R) in the Klondike Valley and overlain by modern fluvial deposits.

The lowest terraces above recent fluvial deposits date from the late Pleistocene McConnell glaciation. They are found along the Klondike and Yukon rivers. Many of these terraces are covered by a veneer of organic deposits (McKenna and Lipovsky, 2014; map included in back pocket).

Near-surface ground ice may be absent in glaciofluvial deposits especially at the edges of terraces where they are not overlain by more than 20 cm of silty loess and organic material.

FLUVIAL DEPOSITS

Fluvial deposits are derived from modern and ancient rivers and streams and are composed of stratified beds of gravel and/or sand with sand and/or silt and/or organic materials (and rarely clay) (Howes and Kenk, 1997). Fluvial sediments mapped in the study area are predominantly those associated with floodplains, fluvial terraces and channels of the Yukon, Klondike and North Klondike rivers, as well as Rock Creek and smaller tributary streams. Mapped fluvial materials include Tertiary-age gravel in high-level terraces, Pleistocene interglacial gravel largely found on intermediate-level terraces, and a large range of late-Pleistocene to Holocene-age fluvial deposits that comprise the modern valley-bottom floodplains, channels and terraces. Fine-grained fluvial deposits tend to be poorly drained and may be ice-rich, whereas coarse-grained fluvial deposits are typically well drained and ice poor.

Tertiary fluvial deposits (F^T) are characterized by the White Channel gravel which occurs as a light grey to white, quartz-rich pebble-cobble gravel with minor, discontinuous sand and mud interbeds (Figure 27; see also Figure 25). The unit is deposited in thicknesses up to 35 m on irregularly distributed benches bordering the modern valleys, 50 to 100 m above the modern floodplain (Morison and Hein, 1987). The unit has an unconformable lower contact with gently inclined bedrock benches, and both gradational and unconformable upper contacts with overlying glaciofluvial gravel (Froese et al., 2000). The White Channel gravel comprises a lower unit displaying more intense hydrothermal leaching and alteration (Tempelman-Kluit, 1982; Dufresne

et al., 1986) and an upper unit differentiated based on the presence of periglacial features (Froese et al., 2000). Both upper and lower units are thought to be conformable and are interpreted as a braided stream deposit whose upper unit aggraded under significantly colder conditions than the lower unit (Morison and Hein, 1987). Ice wedge casts and involutions related to cryoturbation in the upper White Channel gravel record the earliest evidence of permafrost in the region more than 2.65 million years ago (Hidy et al., 2013).

Figure 27. Quartz-rich, pebble-cobble gravel of the Tertiary 'White Channel gravel' exposed at Australia Hill.
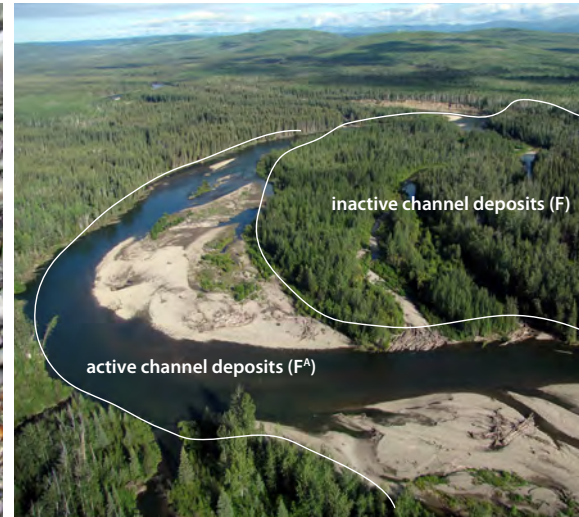
Figure 28. Late-Pleistocene to Holocene fluvial deposits on the Klondike River. Active fluvial deposits (F^A) include stream materials that are subject to regular flooding. Inactive fluvial deposits (F) include terraces above the floodplain and valley bottom deposits no longer part of the active floodplain.

Early to mid-Pleistocene interglacial fluvial deposits (F$^{>R}$) are found overlying bedrock on intermediate-level terraces in the Klondike Valley and commonly occur adjacent to, or interbedded with, glaciofluvial gravel. Fluvial deposits at Midnight Dome are characterized by planar tabular cross-bedded, imbricate gravel similar to the modern Klondike River fluvial deposits (Froese and Hein, 1996). The interglacial gravel hosts economic placer gold deposits and is overlain by glaciofluvial gravel (Froese and Hein, 1996).

Late Pleistocene to Holocene fluvial deposits encompass the bulk of mapped fluvial materials in the study area (McKenna and Lipovsky, 2014; map included in back pocket). Of these, fluvial deposits can be active (F^A) or inactive (F). Inactive Holocene fluvial deposits (F) include terraces above the modern floodplain, abandoned back-channel deposits, and valley bottom deposits no longer part of the active floodplain (Figure 28 above). These deposits range from silty, sand-rich gravel channel deposits to fine-grained sand and silt overbank and back-channel materials. Inactive fluvial deposits are commonly overlain by organic and eolian materials, and where these deposits occur, permafrost is also common.

Active Holocene fluvial deposits (F^A) comprise sand and gravel stream materials that are subject to regular flooding. These deposits include both coarse, channel gravel and fine overbank flood deposits (Figure 29). Main channel gravel deposits are moderately to well sorted, and contain rounded clasts in a sandy matrix (Figure 30). Overbank deposits are represented by fine-grained

sediments of silt, sand and organics that are massive (lacking structure) to thinly laminated, and may contain interbeds of gravel.

Figure 29. *Holocene channel and overbank deposits on the Klondike River.*

Figure 30. *Rounded clasts in a sandy matrix is a common texture for coarse, main channel deposits of the modern, active floodplain of the Klondike River.*

In the study area, fans, or complexes of coalesced fan-shaped landforms can be either active or inactive. Fans typically consist of large amounts of resedimented silt and sand derived largely from upstream loess, and minor deposits of gravel derived from colluvial or glaciofluvial material. Fans were likely formed fairly quickly at the end of the late-Pleistocene McConnell Glaciation and may be ice-rich, especially where they are located on the north-facing side of the valley.

Eolian deposits

Eolian deposits are materials transported and deposited by wind. These deposits generally consist of medium to fine sand and coarse silt that is well sorted, non compacted, and may contain internal structures such as cross-bedding or ripple laminae, or may be massive (i.e., no structure) (Howes and Kenk, 1997). Eolian deposits mapped in the study area are predominantly loess, a loose deposit composed primarily of silt-sized quartz particles with a smaller fraction of fine sand. Loess deposits are typically weakly stratified with variations in mean grain size, and contain repetitive sequences of buried paleosols (Pecsi, 1990; Wright, 2001).

Loess deposits are found on both upland and lowland surfaces in the Klondike, but commonly occur in greater thicknesses in steep gullies and overlying creek bottom and intermediate terrace gravel deposits (McConnell, 1905; Fraser, 1995; Bond and Sanborn, 2006). Resedimented loess is a major component of colluvial aprons and fluvial fans in the area. Where the loess has been reworked extensively and shows flow lines, it has been mapped as a silty fluvial veneer (zFv\sgFGt). Reworked loess on the broad glacial outwash terraces north of the junction of the north and south forks of the Klondike River (McKenna and Lipovsky, 2014; map included in back pocket) is finer in texture and contains some clay which could be derived from till deposits.

Aspect is a strong controlling factor on loess distribution. South-facing aspects have a distinct loess layer that forms part of the B-horizon in soils, whereas on permafrost-affected, north-facing slopes, enhanced colluviation and cryoturbation mixes loess into the underlying weathered-bedrock soil parent material (Figure 31). When reworked through periglacial processes, the only evidence for the loess is an increase in silt content toward the top of surficial deposit, which is also reflected in the soil geochemistry (Bond and Sanborn, 2006). Active landforms such as fluvial channels or colluvial fans are unlikely to have noticeable accumulations of eolian deposits.

Silt-rich eolian deposits are generally affected by permafrost and are commonly ice-rich.
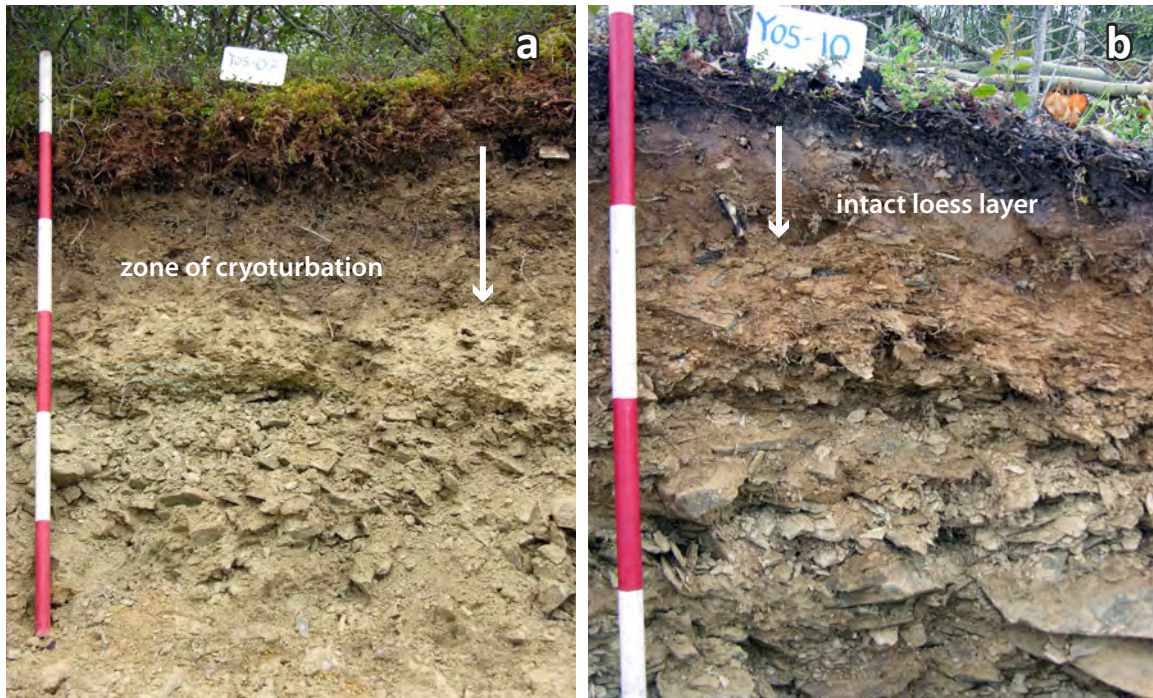
Figure 31. (a) A north-facing hillslope with a well-mixed soil profile; and *(b)* a south-facing hillslope with the loess layer intact. Coloured bands on rod are 25 cm.

Colluvial deposits

Colluvial deposits are materials that have moved downslope, primarily due to gravitational forces (Howes and Kenk, 1997). Deposits range from massive to moderately well stratified, non sorted to poorly sorted, and particle sizes may range from clay to boulder-size. Transportation of colluvial sediment is usually not very far from the source material, therefore particles tend to be angular to sub-angular in shape; however, colluvial deposits originating from morainal, glaciofluvial and fluvial material may contain rounded to well-rounded clasts.

Colluvium is the dominant surficial material in the unglaciated uplands near the Klondike River and west of the Yukon River (McKenna and Lipovsky, 2014; map included in back pocket). It commonly has a stratified structure with a highly variable texture and composition that is controlled by the parent material, transport mechanism, and travel distance. On steeper slopes, colluvium is generally coarse grained, as it has been deposited by rapid mass wasting or landslide processes such as rock fall, debris flows and avalanches. Slow mass wasting is generally achieved through periglacial processes such as solifluction and frost creep, and occurs more commonly on gentle slopes resulting in thick accumulations of loess. Colluvium produced through slow mass wasting

processes is characterized by fine-grained silt and sand, and commonly contains near-surface permafrost.

Colluvium on uplands and slopes is generally derived from weathered bedrock and loess, resulting in a silt-rich diamicton containing angular, local bedrock clasts (Figure 32; Bond and Sanborn, 2006). Where permafrost is largely absent on south-facing slopes, colluvium is typically composed of weathered bedrock and overlain by loess that has not been mixed by cryoturbation (Bond and Sanborn, 2006). North-facing aspects in the map area commonly contain permafrost, and colluvium deposited on these slopes is typically modified by cryoturbation to depths of up to 50 cm, resulting in a mixed profile with loess (silt) incorporated into the weathered bedrock colluvium (Bond and Sanborn, 2006). In general, where permafrost is present, colluvial processes in upland sites are limited to the depth of the active layer (Bond and Sanborn, 2006). North of the Klondike River, Pre-Reid moraine deposits have been extensively modified by colluviation and solifluction. These slopes are mapped as complexes of colluvial and morainal materials (McKenna and Lipovsky, 2014; map included in back pocket).
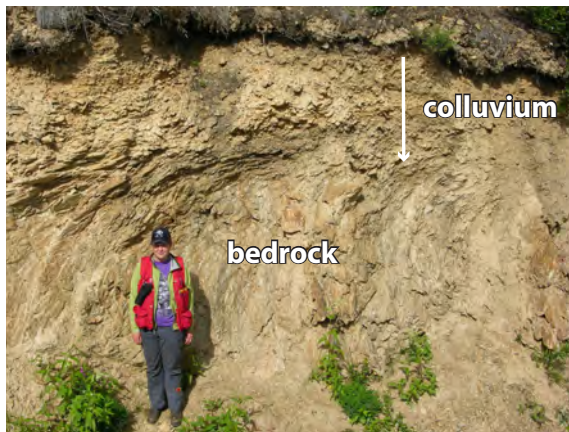
Figure 32. Hillslope colluvium generated from weathered bedrock.

Figure 33. Colluvial aprons (outlined) are commonly comprised of resedimented colluvium and loess near the Klondike River.

Colluvial aprons mapped in the valley bottom, on lower hillslopes (Figure 33 above), and on the uphill-side of terraces are typically composed of resedimented loess and peat and are commonly ice-rich. When occurring as dark brown to black ice-rich silt, these sediments are commonly referred to as 'muck' (see Figure 21, p. 30) and are derived from resedimented and primary loess deposits which cover valley-bottom gravel deposits in much of the Klondike district. Colluvial 'muck' deposits are limited in elevation to ~80 m above valley bottoms and are preserved preferentially at the base of north-facing slopes (Fraser, 1995).

Organic deposits

Organic deposits are defined as containing at least 30% organic matter by weight and are formed by the accumulation of vegetative matter (Howes and Kenk, 1997). Organic deposits typically form in low-lying areas and valley floodplains where the ground is saturated. They may also form over inorganic materials that contain high concentrations of silt and clay and where drainage is poor. Due to the poorly drained nature of these materials, ice-rich permafrost is common in these deposits (Smith et al., 2009).

The ultimate distribution of organic materials in the study area is dependent on landscape position, slope aspect, slope angle and the presence of near-surface permafrost (Smith et al., 2009). In particular, organic materials accumulate preferentially on cold aspects (e.g., east and north-facing slopes) with gentle slopes and poor drainage (Figure 34). In the study area, organic materials accumulate on top of most surficial units including colluvial and morainal slopes, eolian deposits, old fluvial and glaciofluvial terraces, as well as post-glacial fluvial floodplains.

Accumulations of vegetative matter thicker than one metre are mapped as organic blankets and are found on floodplains in old meander scars, pockets on cool north-facing slopes (Figure 35), and on some cool, poorly drained, glaciofluvial terraces. Veneers of organic material (20 cm to 100 cm thick) are widespread in the map area and present on most gently sloped morainal, colluvial, eolian, and fluvial deposits. Organic veneers are not mapped on all surficial units, but are almost always present on poorly drained sites, and cold, north and east-facing slope aspects.

Organic materials commonly contain near-surface, ice-rich permafrost.

Figure 34. Preferential accumulation of organic material on a north-facing slope near the study area.

Figure 35. Organic blanket (>1 m thick) on a north-facing slope near the map area.

ANTHROPOGENIC DEPOSITS

Anthropogenic deposits are surface materials modified by human activities such that their original physical properties have been significantly altered (Howes and Kenk, 1997). Anthropogenic deposits in the map area include mine and dredge tailings in the Klondike Valley, lower Hunker and Bonanza creeks, and a number of smaller mined creek bottoms (Figure 36). Quarry pits, some large building pads, and the Dawson Airport have also been mapped as anthropogenic deposits (McKenna and Lipovsky, 2014; map included in back pocket).

Most fine sand, silt and clay found in mined fluvial gravel in the Klondike Valley was removed by dredging and the remaining tailings of coarse cobble gravel is unusually porous (Figure 37). Ponded water surrounds the tailings piles, and gravel deposits in the area appear saturated. Much of this water likely represents groundwater flow (Gartner Lee, 2003). In lower reaches of the Klondike River floodplain, dredging has led to a decline in isostatic pressure in response to increased ground permeability (Beasley, 2010), and flooding can occur from below – that is, high river levels produce a corresponding increase in the groundwater table (Inukshuk Planning and Development, 2000).
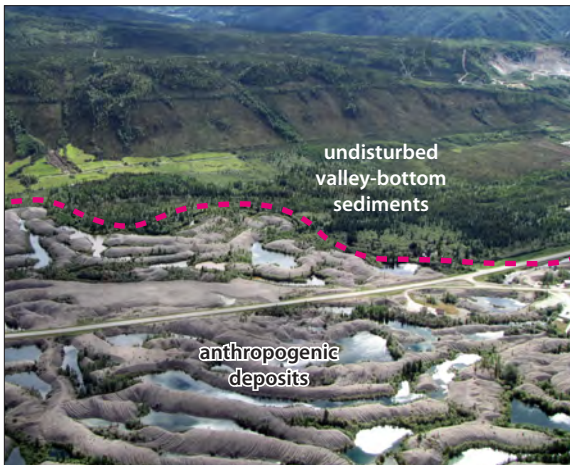
Figure 36. Arial view of anthropogenic deposits (e.g., dredge tailings) and vegetated, undisturbed sediments in the Klondike River valley.

Figure 37. Coarse-grained gravel containing cobbles and pebbles compose dredge tailings, making them unusually porous and subject to high rates of groundwater movement.

STRATIGRAPHY

An idealized cross-valley profile for the lower Klondike River valley is presented in Figure 38. High bedrock terraces formed in the Tertiary are present on both sides of the valley, and are almost always overlain by fluvial gravel deposits representing a former river much higher than the modern river level. Stepped, intermediate-level terraces are better preserved on the north side of the valley, but terrace expression everywhere is subdued by a blanket of loess and colluvium that drapes the landscape. The modern Klondike River occupies only a small part of the valley-bottom floodplain, much of which has been heavily modified by dredging.
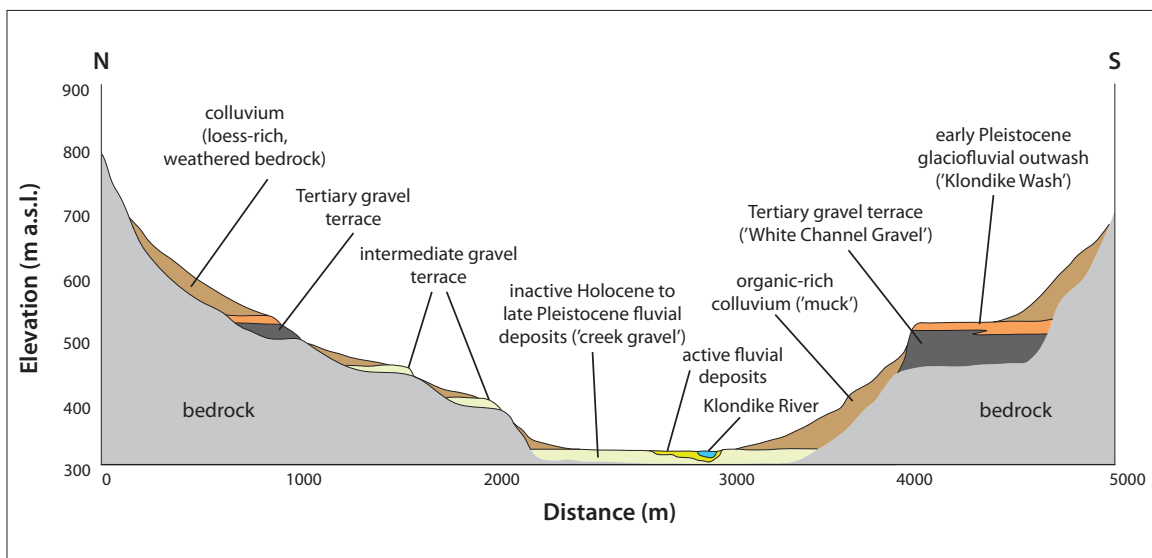
Figure 38. An idealized cross-valley profile for the lower Klondike River valley. View is looking up the Klondike River near its confluence with the Yukon River.

PERMAFROST

In the study region, the permafrost profile is made up of several different components which must be considered collectively to accurately characterize local permafrost conditions. These components, and comments about their relevance to the Dawson region, are described in the following section.

FOREST COVER

The forest cover keeps the ground cool by providing shade, increasing the soil moisture (increase in heat capacity), and increasing energy diffusion before it hits the ground surface. In the winter, trees retain snow, which locally reduces snow cover on the ground that is acting as an insulating layer between the atmosphere and the ground (Brown, 1963; Brown and Péwé, 1973). Clearing of the forest cover by machinery or forest fire usually leads to a deepening of the active layer and degradation of upper portions of permafrost, which is commonly ice-rich. When the low-lying vegetation (e.g., bryophytes, grasses) is also removed, the effects are much more pronounced.

SOIL TEXTURE

Eight different surface material types were identified in the Dawson area based on the geotechnical characteristics of samples gathered during the permafrost-drilling program. They were classified using the Unified Soil Classification System (USCS) and are as follows: gravel, sand, silty sand, silty sand with gravel, sandy silt, sandy organic silt, organic silt and peat; each is described in more detail below.

Gravel

The gravel surveyed in the Dawson region was of fluvial or glaciofluvial origin (and observed at the downtown Dawson and West Dawson case study sites, respectively). Fluvial and glaciofluvial sediments are generally coarse-grained and therefore not frost-susceptible. Where permafrost is present, these sediments do not contain excess ice and are mechanically stable upon thawing. However, fluvial gravel sometimes contains a significant amount of fine-grained material such as silt in the matrix of the deposit, or as thin beds and interlayers. In these cases, the sediment has high ice-segregation potential. When contained in permafrost, these deposits display layers with ice-rich cryostructures and are characterized by differential thaw settlement.

Sand

Sand layers are generally well drained and do not contain excess ice. However, fine and very fine sand are frost susceptible, and may contain excess ice in the form of alternating ice lenses. Upon thawing, soils with excess ice will undergo thaw settlement and will drain slower than coarser sand deposits (i.e., medium to very coarse sand).

Silty sand and sandy silt

Where surficial hydrologic and thermal regimes allow, coarse silt and fine sand may contain a considerable amount of excess ice in various forms, because these material types have high ice segregation potential (Darrow et al., 2008). However, if present in under-saturated conditions, these sediments do not contain excess ice and will be mechanically more stable upon thawing, although they may be deformed by creep.

Sandy organic silt and organic sand

Any organic matter present in sandy or silty deposits will increases water retention and the water capacity of a soil; this may lead to the development of excess ice cryostructures in permafrost, and increase settlement potential under a load.

Peat

Peat layers have a high porosity, can retain water, and are highly compressible when thawed. In permafrost, peat is usually ice-rich. When it thaws, the water is drained and the ground is susceptible to considerable settlement, especially under a load.

CONTEMPORARY PERMAFROST DISTRIBUTION

The Dawson region is included in the extensive discontinuous permafrost zone (50-90% of the land is underlain by permafrost) in the Permafrost Map of Canada (Heginbottom et al., 1995). A more detailed assessment of the spatial pattern of current permafrost conditions in the Dawson region can be extracted from a model of permafrost probability developed for the southern half of Yukon (Bonnaventure et al., 2012). This model is essentially climatically based, taking into account the impacts of air temperature trends with elevation (Lewkowicz and Bonnaventure, 2011) and solar radiation, but not accounting for site-specific factors such as snow depth or surficial materials. The calculated probabilities are for typical snow cover conditions and there can be considerable sub-grid cell variability where sites are locally blown clear of snow, resulting in a higher probability of permafrost, or at sites that accumulate early and deep snow covers, resulting in a lower probability of permafrost (Lewkowicz and Ednie, 2004). Results portray the broad spatial trends in permafrost conditions across the landscape but cannot be used for site-specific predictions. For example, if an area is shown as having a probability of 0.5 to 0.6, this means that 50-60% of the grid cells are predicted to be underlain by permafrost, but it does not indicate which of the cells may have permafrost and which may not.

Predictions from the regional model described above have been compared to the following: 1) field observations in the Sa Dena Hes region, which were not used in the derivation of the model (Lewkowicz and Bonnaventure, 2011); 2) permafrost zone boundaries from the national permafrost map of Canada (Heginbottom et al., 1995); 3) a database of Yukon rock glaciers (Page, 2009); and 4) temperature measurements in instrumented boreholes (Global Terrestrial Network for Permafrost, 2013). The results suggest that the model may slightly over-predict permafrost probabilities where they are >0.5 and slightly under-predict at probabilities <0.5. However, the overall trends reflect observed probability patterns (Bonnaventure et al., 2012).

Model results for the Dawson region were extracted from the regional model (Figure 39) indicate that the highest probability of permafrost presence in the area is in the valley bottoms, where probabilities are in the 90-100% range. As elevation increases up to treeline, mean annual air temperatures rise, and permafrost probabilities decrease, so that permafrost probabilities at the highest elevations in the study area are 40-50%. This is due to inverted surface lapse rates in the region, which promote cold air drainage to valley bottoms during the winter months. Additionally, results indicate that permafrost probability is higher on north-facing slopes than south-facing ones, suggesting aspect also plays a role in determining the spatial distribution of permafrost in the Dawson region. The influences of increases in mean annual air temperature on permafrost distribution shown in this model are discussed later in this report.
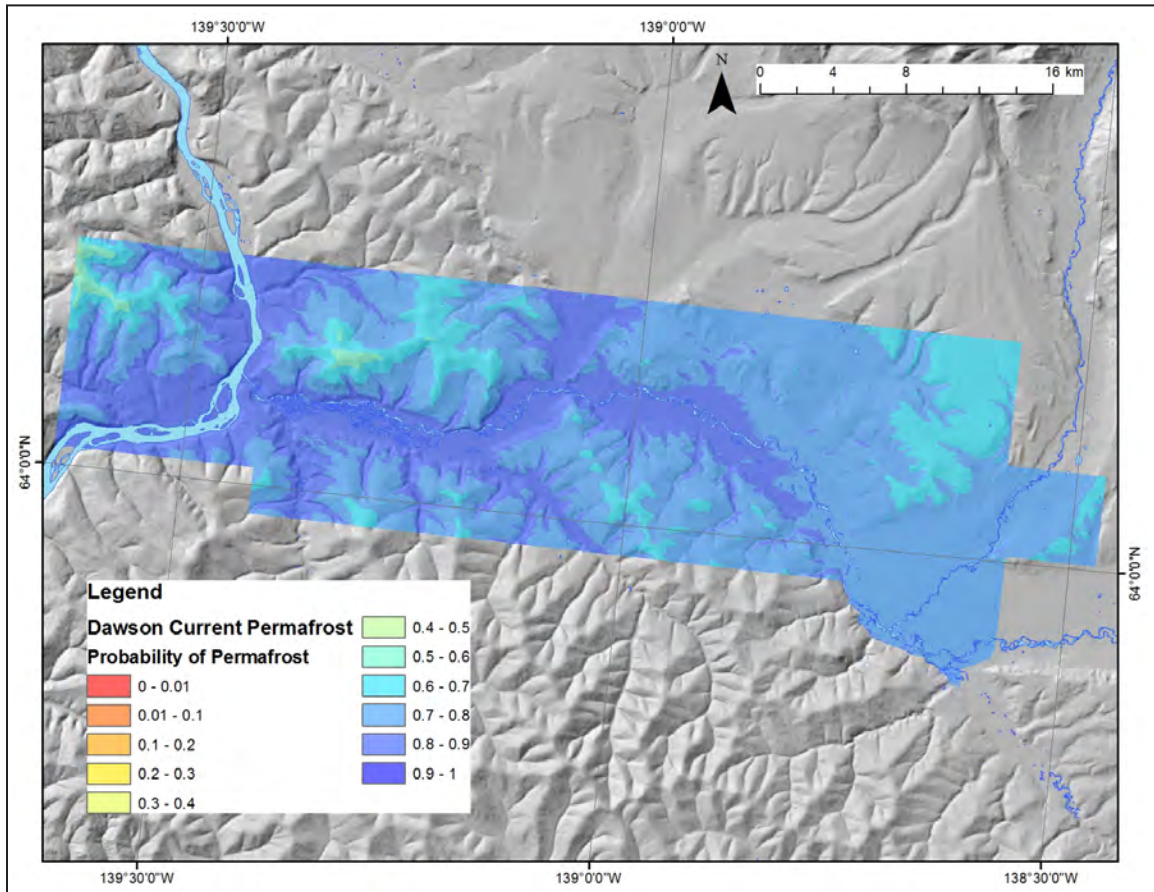
Figure 39. *Permafrost probability for the Dawson region under current climate conditions.*

POTENTIAL HAZARD RISKS FOR THE DAWSON REGION

Potential landscape hazards encountered in the Dawson study area include seismic activity associated with geological faults, mass wasting of hillslope and bedrock materials, flooding, and permafrost-related hazards. Each of these is described in more detail below.

SEISMICITY

Seismic hazards in the Dawson area are considered moderate (Figure 40) and minor earthquakes do occasionally occur. Thirty-four earthquakes have been recorded within 50 km of Dawson since 1980 (Natural Resources Canada, 2013), and of these, the largest was magnitude 4, and the remainder were all below magnitude 4. While the town is situated close to the Tintina fault, which is a major structural feature, the fault has not been active since the early Tertiary (Tempelman-Kluit, 1980), over 50 million years ago. Numerous other inactive faults are associated with the Tintina fault and present a similarly small risk of earthquakes, surface ruptures, and landslides in the study area.

If a large earthquake were to occur in the Klondike region, materials most likely to generate subsequent landslides include highly fractured ultramafic rocks, poorly consolidated surficial materials, and any recently thawed portions of ice-rich glacial, colluvial, eolian and organic materials.
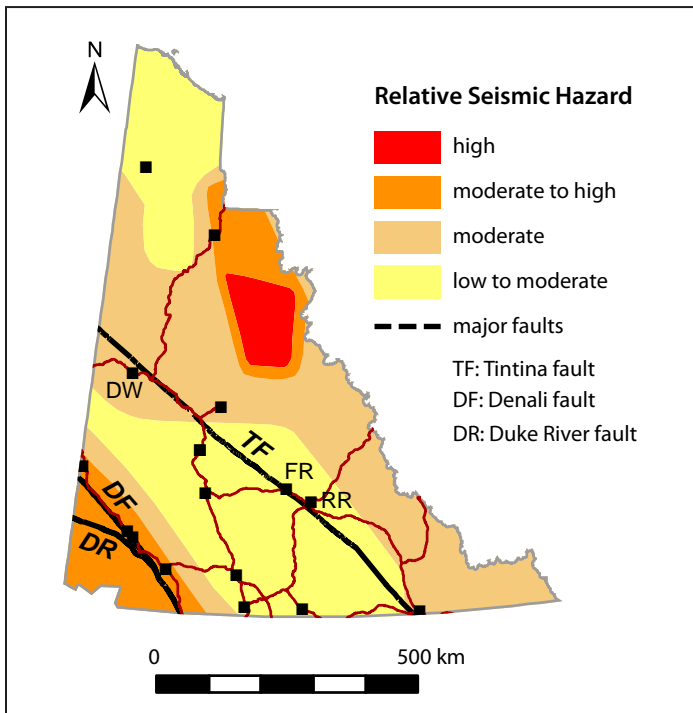
Figure 40. *Simplified version of the National Building Code of Canada's 2010 seismic hazard map (for spectral acceleration at a 0.2 second period (5 cycles per second)), illustrating the relative likelihood of experiencing earthquakes strong enough to potentially damage some, but not all, single family (one and two-story) dwellings (Natural Resources Canada, 2013). Dawson (DW) is located in the moderate hazard zone, where there is a 5-15% chance that significant damage will occur every 50 years. FR = Faro; RR = Ross River*

MASS WASTING

Mass wasting (the downslope movement of surficial materials and/or bedrock fragments, often mixed with vegetative debris) may be restricted to very shallow surface layers, or be deep-seated and extend into thick packages of sediment or bedrock. Mass wasting events may be rapid, occurring in seconds to minutes, or gradually creep or rotate over years to centuries. Depending on slope geometry and sediment water content, debris may free fall, slide, rotate, and/or flow. Mass wasting processes in the study area can be grouped into three primary types: large landslides, small landslides, and mechanisms of slow periglacial wasting.

LARGE LANDSLIDES

Landslides generally occur on moderate to steep slopes due to a variety of contributing and triggering factors that include: intense rainfall or snowmelt events, permafrost degradation, forest fires, river erosion, groundwater flow, and/or earthquakes. In many cases, several of these contributing and triggering factors act in combination. Large landslides have been mapped along the lower Klondike River valley, lower Rock Creek valley, and in the townsite of Dawson. Of these, only the landslide in the townsite of Dawson has been studied in detail. The 'Moosehide Slide' (also known as the Dawson City landslide) occurs on the western slope of Midnight Dome, with a headscarp immediately above the town, and downslope landslide debris that underlies temporary infrastructure and recreational trails (Figure 41).

The initial prehistoric pseudo-circular slope failure is interpreted as having occurred at, or near, a geological contact between serpentinite and underlying metasedimentary rocks, and may have been triggered by high pore-water pressures and seismic acceleration (Brideau et al., 2012). The contact regionally represents the overthrust of a sliver of oceanic crust (Slide Mountain terrane) onto a volcanic-arc assemblage (Yukon-Tanana terrane) but has not been located in outcrop in the slide area (Brideau et al., 2012). While the landslide is thought to have occurred in prehistoric times (Brideau et al., 2007) continued slope instability has been recorded on both the headscarp and the lower landslide deposit (Figure 42).

Figure 41 (above). The 'Moosehide Slide', or Dawson City Landslide, as seen from the Klondike River, showing the headscarp, central landslide debris, and lower landslide debris which has been modified by development.
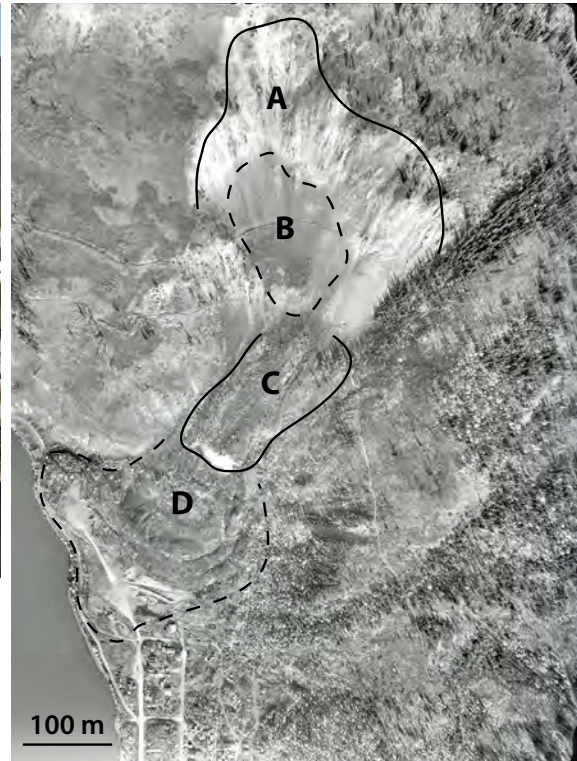
Figure 42 (above right). The 'Moosehide Slide', or Dawson City Landslide, as seen from above in an aerial photo. Black lines indicate the headscarp or initiation zone (A), the upper talus cone of sloughing debris from the headscarp (B), the middle section of landslide debris that is moving (C), and the lower section of landslide debris that has been altered by quarrying and recontouring (D).

Headscarp movement is characterized by tension cracks, split trees (Figure 43), and a large unstable block of rock (Brideau et al., 2007; Brideau et al., 2012). The headscarp regularly generates minor rockfalls that have formed a small talus cone of rock debris at the base of the slope. The landslide debris deposit itself comprises a central section in the form of an elongate lobe that displays downslope movement, and a lower section that has undergone significant anthropogenic modification and continues to the bank of the Yukon River before dropping off steeply (Brideau et al., 2007). The central mass of landslide material contains shear zones, tension cracks, split trees, stretched roots, and has a steep snout at its terminus; it is likely moving through earth flow (movement of interstitial clay and silt under wet conditions) or rock glacier (movement of interstitial ice) mechanisms (Brideau et al., 2007). Monitoring over a five-year period from 2006-2011 showed that the unstable section of the headscarp is moving downslope at a rate of 4 to 12 cm/year, whereas the lower landslide deposit is moving at a rate of 9 to 20 cm/year (Brideau et al., 2012).

Figure 43. A sequence of photos showing the progressive splitting of a tree growing over a tension crack on the Dawson City landslide. Photos courtesy of M.-A. Brideau.

A 200 m-long ERT profile (5 m electrode spacing) was run on September 7, 2014 down the lobate mass that is at the foot of the steep, unstable headwall (Figure 44). The surface along most of the profile was covered by coarse material (including boulders up to one metre in diameter), and very sparse vegetation. The steep front of the lobe was unvegetated and unstable having exposed fines as well as some large boulders and cobbles. Downslope of this front, the surface was covered with shrubs and grasses in some places with scattered boulders.
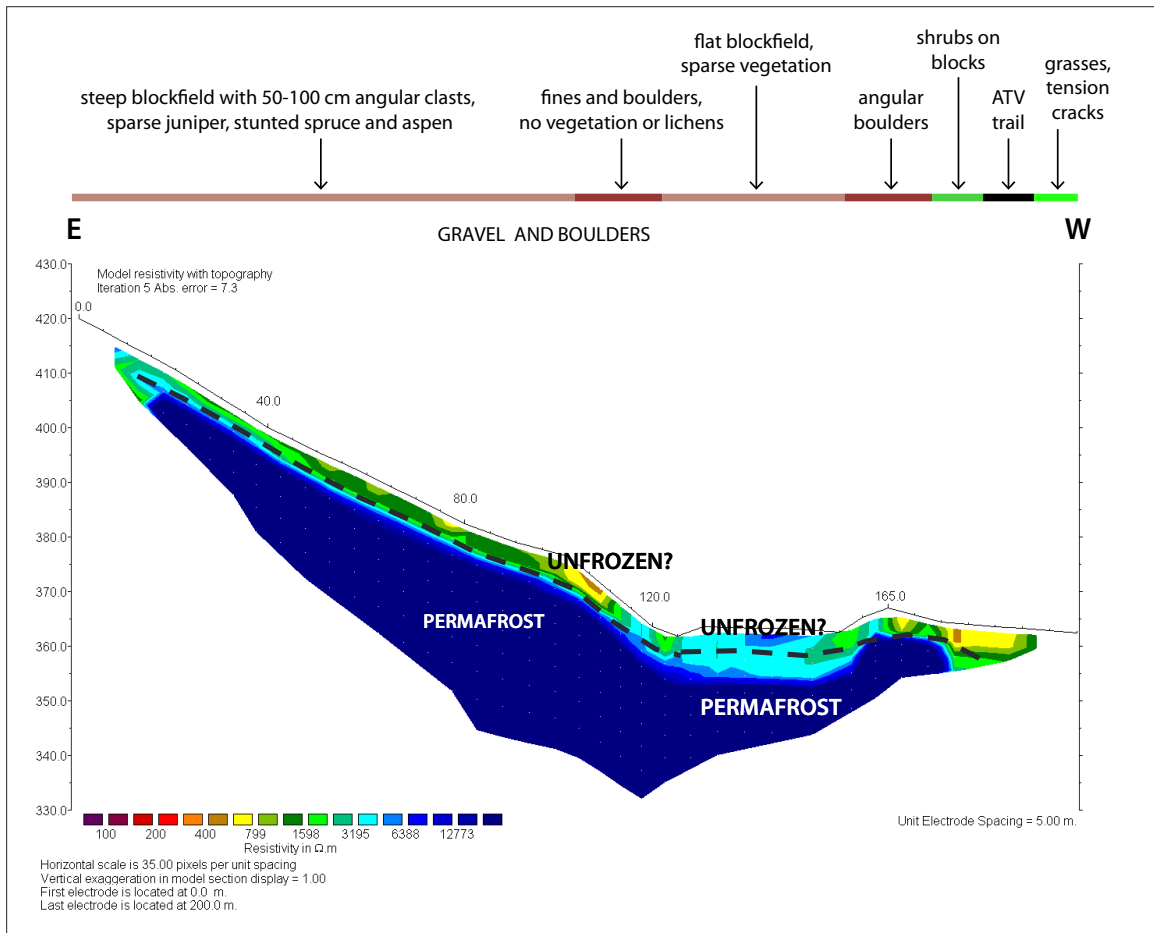
Figure 44. *ERT profile for the Moosehide Slide (200 m long) was run down the lobate mass at the foot of the steep, unstable headwall of the slide. The profile has a maximum penetration depth of about 30 m. Likely areas of permafrost are outlined by black dashed lines.*

The ERT profile depicts a relatively low resistivity layer 3-5 m thick overlying a very high resistivity layer that extends to the base of the profile at about 30 m depth. All the apparent resistivity values, including those in the near surface are greater than 400 ohm m, which elsewhere in the region would indicate frozen surface materials or soils. However, a more appropriate boundary value between frozen and unfrozen materials or soils for this site, because of its dry, coarse sediments, is 1000 ohm m. The interpretation of the profile is, therefore, a deep active layer overlying permafrost. The resistivities at depth, which exceed 100 kilo-ohm m, represent the highest values recorded in the Dawson area, and suggest low unfrozen moisture contents that are associated with coarse materials, as well as relatively cold permafrost temperatures. ERT profiles of rock glaciers in the European Alps typically also exhibit very high apparent resistivities, in the 100 kilo-ohm m range or higher. The interpretation suggests that the Moosehide Slide may be deforming

as a result of a core of permafrost and that ongoing movements reported by Brideau et al. (2007; M.-A. Brideau pers. comm., 2014) may be due to the creep of ice-rich permafrost on a steep slope, assuming such material is present at the site.

Other large, deep-seated rock failures in the map area include complex scarps on the south-facing slope of the Klondike Valley across from Lovett Hill and the municipal airport; a large north-facing failure on upper Bradley Creek in the northernmost part of the map area; east-facing failures on lower Rock Creek; and both east and west-facing landslides above Germaine Creek in the Klondike River valley (see Figure 41 and McKenna and Lipovsky, 2014; map included in back pocket).

Figure 45 is a map of the study area and includes documented landslides and units of the Slide Mountain terrane (yellow) and volcanic rocks (pink). Red stars represent large, deep-seated landslides that are potentially caused by bedrock failures. White stars represent smaller landslides that may be hosted in surficial sediments. Four large landslides are mapped in rocks of Slide Mountain terrane and all occur on slopes that were likely over-steepened by glaciers or fluvial incision.
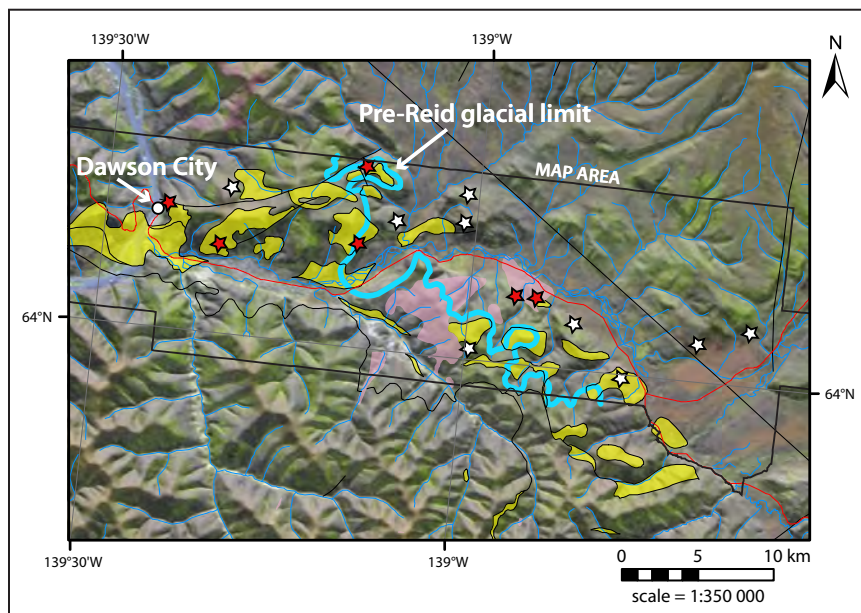
Figure 45. *Map area illustrating ultramafic Slide Mountain terrane rocks (yellow), volcanic rocks (pink) and landslides (stars). Red stars indicate deep-seated bedrock slides; and white stars are small landslides, and landslides in glacial moraine material.*

Some of these features are likely very old, as in the case of the slide across the Klondike Valley from the Callison Subdivision. This slide was mapped only by the presence of a head scarp high on the hillside, indicating that this feature may have been caused by valley incision early in the Pleistocene and is largely a relict feature. The area north of the Klondike River in the Tintina Trench within the Pre-Reid glacial limits has experienced extensive slope failures (Duk-Rodkin, 1996) which most certainly occurred in the late Pleistocene or Holocene. These slides may be related to glacial over-steepening of hillslopes, or involve unstable glacial moraine materials.

SMALL LANDSLIDES

Small landslides are mapped in morainal materials in the study area on south-facing slopes above the confluence of the north and south forks of the Klondike River, and on north-facing slopes on upper Coal Creek (a tributary to Rock Creek).

Landslides too small to be mapped but pervasive enough to have modified surface materials include active-layer detachments or thaw flow slides (Figure 46), a type of fast periglacial mass

wasting usually designated with the modifier -Xf in the polygon unit labels (see accompanying map in back pocket). These landslides occur where the thawed or thawing portion of the active layer detaches from the underlying frozen material and moves downslope through sliding and sometimes flowing of the thawed debris (Lipovsky et al., 2006). Events that cause rapid thickening of the active layer, such as forest fires and hot and/or wet weather, commonly trigger active-layer detachments (Lewkowicz, 1992; Lewkowicz and Harris, 2005).

Hot, dry weather in the summer of 2004 contributed to a severe forest fire season for the Dawson region, and created conditions for the later initiation of widespread active-layer detachment slides (Lipovsky et al., 2006; Coates, 2008; Lewkowicz et al., 2011). A 2005 study of nearly one hundred and fifty detachments slides in the Dawson region concluded the failures generally initiated in silty colluvium at shallow depths (<65 cm) within the active layer (the frost table was generally at 1 m depth) and were on the order of 5-20 m wide and 10-100 m long (Lipovsky et al., 2006). The landslides were documented on all slope aspects, provided permafrost was present, and on both steep and gentle (as low as 10°) slopes (Lipovsky et al., 2006).

Active-layer detachments generated after the 2004 fire season were largely in remote locations where there exists little infrastructure or human habitation. Nonetheless, the slides blocked roads, trails, and access routes (Figure 47); impounded waterways; and contributed significant amounts of suspended sediment to nearby streams (impacting both fisheries and placer mining industries). Were landslides of similar size and magnitude to occur within the developed regions of the map area, they could pose a significant risk to both infrastructure and human life.

Figure 46. Two active layer detachment slides near the map area that were generated after intense forest fire activity in 2004.

Figure 47. A series of active layer detachment slides generated after intense forest fire activity in 2004 blocked roads and access routes.

Slow periglacial wasting

Periglacial wasting is a general term that describes cold-climate colluvial processes that are initiated by freeze-thaw and permafrost conditions (French, 1983). Periglacial wasting includes both slow processes such as solifluction, slopewash, solution and nivation; and rapid processes such as active layer detachments (described in previous section). Slopewash (modifier -Xs on accompanying map), and to a lesser degree solifluction, operate on upland slopes in the study area and contribute to downslope colluvial processes.

Solifluction, the slow downslope movement of saturated sediments, can be identified by distinctive slope morphology of lobes and terraces on moderate slopes, but can also occur in broad sheets

on low-angle slopes (French, 1983). Slopewash (also known as sheetwash), is difficult to qualify, but is likely a significant modifier of the landscape in the map area. Slopewash is characterized by unconcentrated surface wash where particles are carried downslope in an overland flow and deposited as fine unconsolidated sediment, typically at the foot of slopes as the result of the continual percolation of water downslope (French, 1983). While unlikely to cause catastrophic events, slow periglacial wasting can be a significant hazard to infrastructure that is built upon, or at the base of, landforms that are experiencing gradual downslope movement.

PERMAFROST PROCESSES

Hazards related to permafrost have the potential to impact several elements such as ground stability, hydrology, and infrastructure integrity. The following section provides a general description of permafrost structure and characteristics, in order to present a more comprehensive picture of the risks associated with permafrost thaw.

Permafrost development

In permafrost regions, the distribution of ice in surface materials or soil (i.e., cryostratigraphy) is related to the manner in which permafrost has aggraded and degraded through time. The understanding of permafrost genesis at a given site is important because permafrost structure and composition is directly related to the type of permafrost development. Permafrost genesis can be divided into four main types: epigenetic, syngenetic, quasi-syngenetic, para-syngenetic and polygenetic (French and Shur, 2010; O'Donnell et al., 2012). Epigenetic permafrost forms in bedrock and sediments following deposition. The ice content of epigenetic permafrost usually increases with depth, and the sediment layers in between ice features are usually ice-poor and over-consolidated or stiff (Stephani et al., 2010). The syngenetic growth of permafrost occurs when material is deposited at the surface while freezing is in progress. Thus, the permafrost is approximately the same age as the sediment in which it is found. The ice content of syngenetic permafrost is more likely to be uniform and ice-rich throughout the soil column (Fortier and Allard, 2004; Kanevskiy et al., 2011). Quasi-syngenetic permafrost forms when the permafrost table shifts upward in response to vegetation growth at the surface, leading to the formation of an intermediate, ice-rich layer at depth. Para-syngenetic permafrost is defined by multidirectional refreezing of a talik zone (e.g., those areas of unfrozen ground under drained lakes). The ice content of para-syngenetic permafrost relates to the degree of saturation of the material prior to refreezing. If the permafrost has more than one origin it can be defined as polygenetic (Lunardini, 1994; French and Shur, 2010).

Geotechnical properties

The cryostratigraphy and geotechnical properties of the ground are important characteristics as they influence permafrost dynamics and the thermal and mechanical sensitivity of frozen ground. Cryostratigraphy is defined as the study of frozen layers in the Earth's crust and is used to reconstruct the deposition history of a given site, define the type of permafrost present, determine how ice developed, and how the ice is distributed within the permafrost. It is useful to predict the rheology (rate and type of deformation) of surface and sub-surface materials in the context of permafrost thaw (French and Shur, 2010). Cryostratigraphy is defined by cryofacies (e.g., ice-rich or ice-poor sediments), which are characterized by typical cryostructures.

Cryostructures are determined by the amount and distribution of ice within the pore structure, and by ice in excess of the porosity (e.g., lenses, layers of segregated ice; French and Shur, 2010). Table 3 presents typical cryostructures that may be observed in permafrost. Layered, lenticular, and microlenticular cryostructures are present in ice-rich permafrost. They are the result of

ice segregation in the sediment and are typical of fine-grained syngenetic permafrost. When permafrost thaws, the water from the melting of excess ice is drained, leading to settlement of the ground. Porous visible and porous invisible cryostructures are ice-poor and result from in-situ freezing of water trapped in the soil pores with little to no migration of water to the freezing front (cryosuction) within the freezing soil. These types of cryostructures are common in coarse-grained sediments, but can also develop in fine-grained sediments that were originally ice-rich, thawed, drained, and subsequently refrozen (Stephani et al., 2010). Because there is no excess ice present, no significant subsidence of the ground is expected upon thawing (Stephani et al., 2014).

Table 3. Cryostructure classification, from Stephani et al. (2014) and based on Murton and French (1994).

Name	Equivalent	Description	Sediment type	Illustration*
Lenticular	Lenticular[1]	• lens-shaped ice in sediment • generally continuously shaped • generally horizontal (parallel to freezing front) • may be straight, wavy, inclined, interlaced • may contain air bubbles • thickness: ≥1 mm: Syngenetic permafrost: mm to cm thick Epigenetic permafrost: cm to dm thick • usually ice-rich sediment	silt to fine sand; silty clay	see Fig. 3.1A
Microlenticular	Lenticular[1,2]	• lens-shaped ice in sediment • generally discontinuously shaped • generally horizontal (parallel to freezing front) • may be straight, wavy, inclined, interlaced • very few air bubbles • thickness: <1 mm • usually ice-rich sediment: Syngenetic permafrost: >50% volume Epigenetic permafrost: 30-50% volume	silt to fine sand; peat	see Fig. 3.1A
Layered/belt-like structure	Layered[1]	• assemblage of lenticular cryostructures • thickness: centimetre to decimetre • usually ice-rich sediment	silt to fine sand; peat	see Fig. 3.1C
Ice veins		• ice-filled crack or fissure in sediment • thickness variable (millimetre to centimetre) Frost crack: 1-5 mm thick Dilation/extension cracks: cm to dm thick	all types	
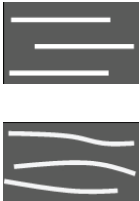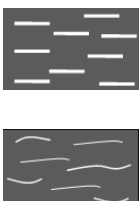
Table 3, *continued*. Cryostructure classification, from Stephani et al. (2014) and based on Murton and French (1994).

Name	Equivalent	Description	Sediment type	Illustration*
Reticulate	Reticulate[1,2]	• net-like cryostructure of interconnected sub-horizontal ice lenses and sub-vertical ice veins • usually ice-rich to very ice-rich sediment (~35-95% volume)	silt to fine sand	see Fig. 3.1F
Suspended	Suspended[1]; Ataxitic[2]	• suspended aggregates in ice • usually very ice-rich sediment (up to 90-95% volume) • common in upper part of permafrost	silt to fine sand; occasionally peat; silty clay	see Fig. 3.1E
Crustal	Crustal[1,2]	• ice-coating around rock fragments, aggregates or wood fragments • usually partial coating, occasionally total • common just beneath permafrost table • thickness: few millimetres to centimetre-thick coating	gravel/rock fragments; diamicton	see Fig. 3.1D
Porous visible	Ice cement[1]; Massive[2]	• pore ice that is visible to the unaided eye • usually ice-poor sediment (<30% volume)	gravel/rock fragments; diamicton	see Fig. 3.1F
Porous invisible	Ice cement[1]; Massive[2]	• pore ice not visible to the unaided eye • usually very ice-poor sediment (<10-30% volume)	all types	see Fig. 3.1F
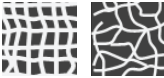
***Illustrations modified from Murton and French, 1994

[1] Murton and French (1994); [2] Kudryavtsev (1979)

Legend: grey = sediment; dark grey = aggregate or wood fragments; white = ice.

Generally, dry or unsaturated frozen materials or soils do not present a high risk upon thawing, as the water will remain in the soil porosity or will drain away. In contrast, when a saturated soil thaws, it presents a much higher risk of settlement, mass movement, or ponding in response to poor drainage. Hazards related to the thawing of ice-rich materials or soils is affected by factors such as stratigraphy and the grain size distribution of the stratigraphic layers, as well as external factors such as slope, surface roughness, and vegetation (Stephani et al., 2014).

For thaw-settlement hazard assessments, cryostratigraphy is used to locate ice-rich and ice-poor layers, and determine the geometry and distribution of massive ice (e.g., patterns of ice wedges). Generally speaking, the presence of ice-rich deposits raises concern in terms of hazard potential. Where ice-rich deposits overlie ice-poor layers, the thaw-settlement hazard is high in the short term, and the rate of change is fast. Conversely, when ice-poor deposits overlie ice-rich sediment, the thawing of the upper layer is rapid but with minimal thaw settlement and will be followed by the slow, but constant thawing of the underlying ice-rich layer resulting in differential thaw settlement.

The grain size distribution of sediments determines the porosity and hydraulic conductivity of the ground. Coarse material (medium sand and coarser) has a high hydraulic conductivity and readily drains water as ice melts, whereas fine-grained material drains poorly once it thaws due to its low hydraulic conductivity. Furthermore, fine-grained sediments often contain excess ice (i.e., the volume of ice in excess of the total pore volume of the ground when unfrozen) and may form ice lenses or layers by ice segregation. On flat terrain, ground with excess ice will undergo severe thaw settlement; likewise, on slopes, silt and clay deposits may experience mass movement when the pore water pressure created by melting ice is high. For slope deposits, the plastic and liquid limits of the material are used to evaluate the potential of ground failure.

Permafrost as a hazard risk

The ground thermal regime of permafrost is influenced by climate, surface conditions, and the complex interactions of geophysical factors such as hydrography, topography, vegetation, soil texture and ground-ice content (Jorgensen and Osterkamp, 2005). As a result, variations in climate or terrain conditions (e.g., environmental changes or human interventions) can both have a great impact on permafrost stability. Higher surface temperatures, variation in snow cover depth, active-layer hydrology variations, infrastructure, and fire disturbances are good examples of changes that can play, at various scales, a major role in permafrost degradation (Stephani et al., 2014). Additionally, since it is closely linked to local factors, permafrost response to environmental change can be spatially and temporally heterogeneous and can respond differently to geomorphological processes due to different terrain conditions. Therefore, permafrost landscapes will have a dynamic response to environmental change and must be considered holistically, at diverse spatio-temporal scales.

Because permafrost stability is essentially maintained by the bonding between ice and the ground particles, when ice melts, cohesion is lost and soil stability is diminished (French, 2007). Following an increase in air temperature, the active layer is expected to deepen as the ice contained in the upper part of the permafrost (right below the bottom of the active layer) melts. If the volumetric water content of the ground is lower than the volume of soil pores, the ground is not saturated. Thawing of this type of ice-poor soil results in moderate surface settlement and is essentially due to the loss of volume upon ground ice melting and subsequent soil consolidation. If the volumetric water content of the ground is equal to, or slightly above the volume of soil pores when unfrozen, the soil is saturated. Thawing of this type of ice-rich soil results in poorly drained surface conditions, and the soil will be unable to consolidate due to the high pore-water pressure. If the volumetric water content of the ground is higher than the volume of soil pores, the ground is super-saturated and contains excess ice in its frozen state. Thawing of this type of ground results in severe surface settlement, and is essentially due to the loss of volume upon ground ice melting and soil drainage (Nelson et al., 2002). In gently sloping areas, water ponding is frequent; on steep slopes, the release of water builds excess pore water pressure in the soil pores, which is conducive to rapid mass movements (e.g., slides, slumps and debris flows). When the material is coarse-grained, soil water is drained according to the hydraulic conductivity of the material and there is minimal settling or movement of the sediment. When the material is fine-grained, the drainage is slow and pore water pressure may trigger slow mass movement (e.g., solifluction). Depending on the nature of the soil material and the amount of ground ice present, significant hazards may develop. Permafrost-related hazards represent some of the principal challenges for planning and development in northern environments.

To assess permafrost stability for land-planning purposes, an estimation of the maximum thaw depth that could be reached under changing climatic conditions is essential, mainly to evaluate the potential deformation that the soil may undergo in the future (Instanes, 2003). The rate and type of deformation is closely linked to the type of surficial deposits, the ground ice content and its distribution, the ground temperature, and the soil hydrological regime.

Permafrost is present in much of the map area, and may be found within any of the materials described on the accompanying map. Ice-rich permafrost is common on cold (north and east-facing) aspects with poor drainage, but may be present on all aspects, as well as in moderately to well-drained materials. Near-surface permafrost (i.e., within one metre of the surface) is encountered on most north-facing slopes as well as on more level valley-bottom sites where there is an insulating cover of organic material and/or finer textured soils. High ice contents are common especially where there is, or has been, subsurface water flow associated with large rivers systems, as well as surface water related to smaller drainages and alluvial fans.

Permafrost influences slope stability by strongly affecting drainage (which is restricted by the permafrost table), soil moisture (which may increase in response to rapid thaw of ground ice), and strength (through bonding of frozen soil particles).

Disturbance or clearing of the organic cover, and/or changes in surface or subsurface drainage, can cause changes to the soil thermal regime and result in thermokarst development, subsidence, and terrain destabilization. Thermokarst collapse features, generally occupied by small ponds or lakes, occur in scattered locations around the map area, particularly near, or on, the floodplain of the Klondike River (Figure 48). Thermokarst depressions result from the thaw of ground ice and subsequent settlement of the ground surface. Fine-grained, ice-rich sediments are most susceptible to thermokarst collapse following some kind of surface disturbance which exposes ground ice. Thermokarst depressions may grow in size for decades until the supply of ground ice is exhausted.
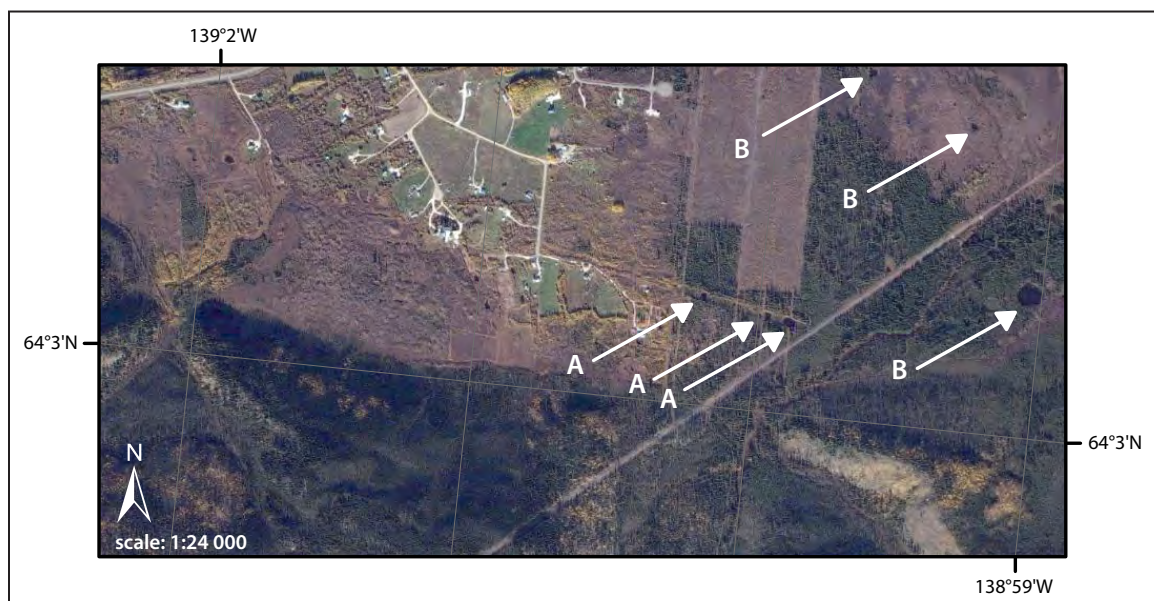
Figure 48. A satellite image of Henderson's Corner shows human-induced thermokarst where vegetation was cleared along a linear path (A), and natural thermokarst ponds in the floodplain of a fluvial fan (B).

ASSESSING CURRENT HAZARD RISKS FOR THE DAWSON REGION

CASE STUDY SITES

To assess the risk of the hazards described above for the Dawson region, the research team focused on several case study sites (Figure 49). Findings from case study sites were then used to assess risk on a regional scale.
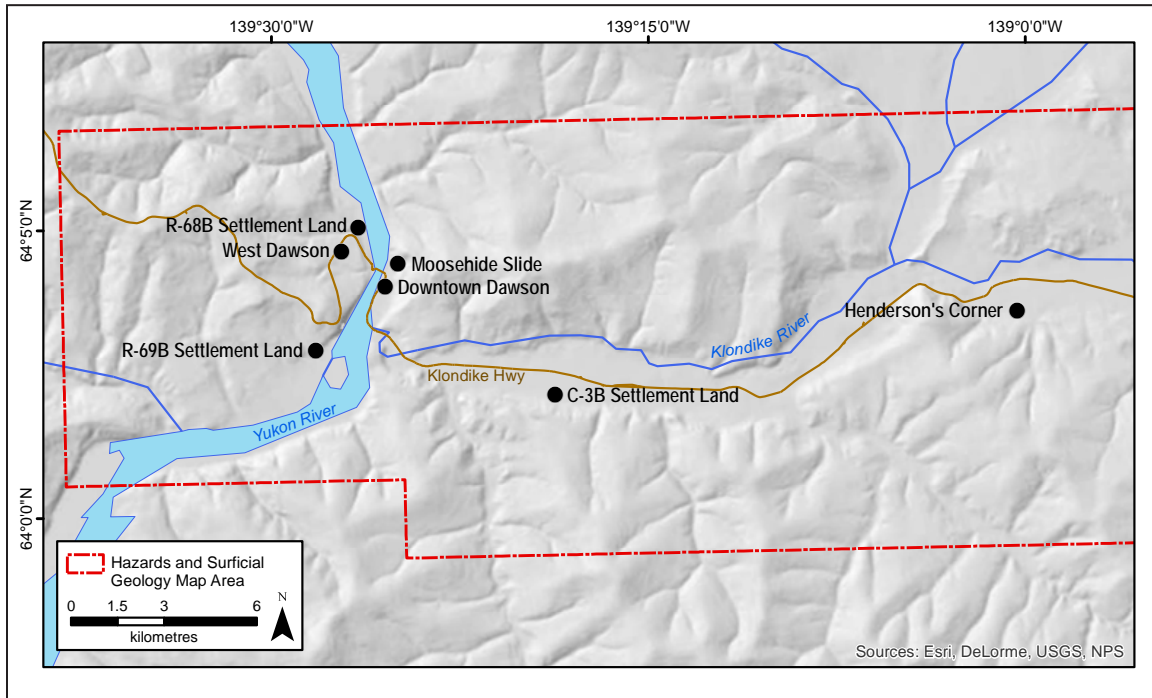
Figure 49. Overview map of all case study site locations for the Dawson area.

The case study sites for Dawson City were determined in consultation with the community – they reflect areas where there are hazards-related concerns, or where future development may take place. Case study sites were also chosen to cover a variety of landscape types. Case study sites are: 1) West Dawson; 2) C-3B Settlement Land; 3) R-68B Settlement Land; 4) R-69B Settlement Land; 5) downtown Dawson; and 6) Henderson's Corner. The locations of the case study sites are shown in Figure 49. At each site, researchers used a combination of geophysical approaches (ERT and GPR), permafrost borehole and soil pit observations, and examined exposed surficial material where possible. (Note: not all techniques were used at every site.) Results from each case study site are described below.

WEST DAWSON

The West Dawson case study site (Figure 50) is situated on a glaciofluvial terrace ~100 m above the Yukon River between Benson and Dawson creeks in West Dawson. The terrace sediments were likely deposited in the middle or early Pleistocene (up to 2.6 million years ago) and are colluviated on adjacent landforms. Terrace deposits are composed of sand and gravel with minor silt and are often overlain by thin veneers of organic material or eolian silt. Geophysical surveys and borehole drilling were conducted at a site where thin organics cover glaciofluvial deposits of sand, and sand and gravel.

Figure 50. Map illustrating locations of detailed site investigations for the West Dawson case study site. Refer to Figure 49 for case study location.

Borehole *DC_BH01* was drilled on the western side of the Yukon River in a small subdivision. The site is located approximately 90 m above the riverbed, in a black spruce forest (about 15 m high). The borehole was drilled off a trail, along ERT profile *DC_ERT01b* and GPR profile *DC_GPR01* (Figure 50). The ground was covered with a 0.17 m-thick moss and lichen layer as well as 0.3 m-tall grasses (*Carex sp.*). The permafrost table was encountered at a depth of 83 cm. The permafrost (epigenetic) contained a layer of sandy silt (0.83 to 0.9 m deep) overlying silty sand with gravel (0.9 to 1.15 m deep). The borehole was drilled to a depth of 1.15 m, at which point the presence of cobbles prevented further coring. At 0.83 m, the permafrost had a porous-invisible cryostructure with an excess ice volume content of 30%. The complete borehole log is shown in Appendix B, and grain size analysis and ice content results are shown in Appendix C.

Ground truthing was completed at an existing exposure cut (*DC_CUT01*) approximately 500 m north of *DC_BH01* in a gravel pit. The elevation at the top of the pit corresponded to the elevation at the top of borehole *DC_BH01*. The same stratigraphy was encountered in the pit as in borehole *DC_BH01*, but the lowermost gravel layer was noted to a depth of at least 3 m. Additional ground truthing (*DC_CUT02*) was performed in a sand pit approximately 780 m southwest of *DC_BH01*. The elevation of the bottom of the cut corresponded to the elevation at the top of the borehole. The section was composed of fine to medium sand layers overlying a slightly humid to dry, disturbed, top sand layer. No water or permafrost table was reached. Gravel (2 to 10 cm in diameter) was encountered at the bottom of the cut (240 cm).

Two ERT profiles were run from north to south across the borehole site in West Dawson. The first (*DC_ERT01b*) was 160 m long and penetrated to a depth of 25 m (Figure 51) while the second

(*DC_ERT01a*) was 400 m long and penetrated to 60 m (Figure 52). The two surveys were centred on approximately the same point (80 m in the first and 200 m in the second; see Figure 50) and concur in the general resistivity pattern and values for their common areas, except just below the surface where there is higher resolution in the shorter survey (*DC_ERT01b*). The vegetation along the profiles consisted of spruce forest with an understorey of Labrador tea (*L. groenlandicum*) and a well-developed organic mat. The northern half of each survey was run in forest but parallel to a gravel road, whereas the southern half was well away from any recent disturbance. Frost tables averaging a depth of 0.52 m (n=62) were encountered across the length of both profiles except where probing was impossible beneath the gravel road. As described above, the borehole drilled in a clearing at the centre point of each profile (*DC_BH01*) encountered permafrost.
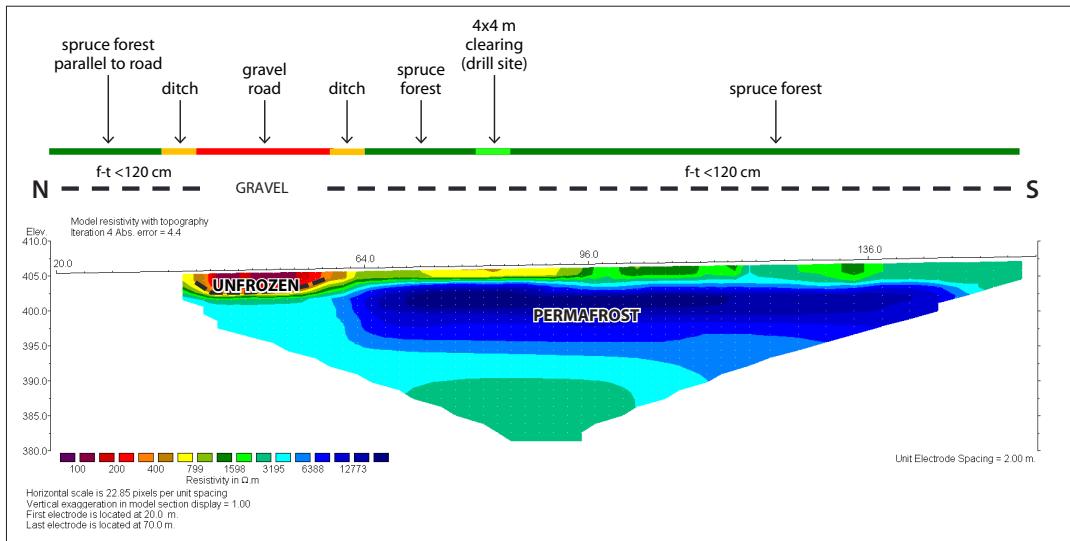
Figure 51. *ERT profile DC_ERT01b is 160 m long and runs north to south, and parallel to DC_ERT1a (see Figure 50 for location). The profile has a maximum penetration depth of ~25 m. Likely areas of permafrost are outlined by black dashed lines; f-t = frost table.*
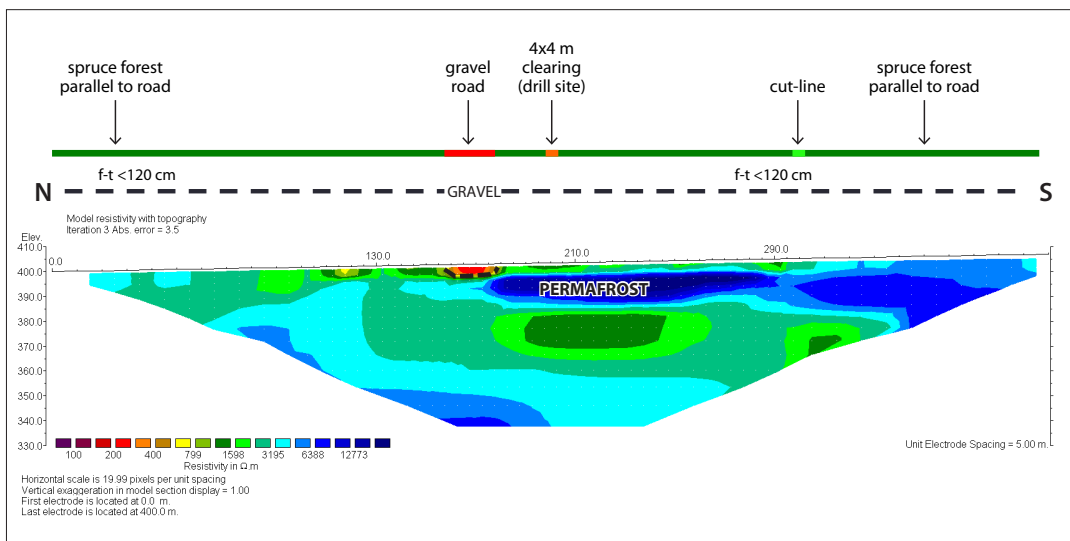
Figure 52. *ERT profile DC_ERT01a, is 400 m long and runs parallel to DC_ERT01b (see Figure 50 for location). The profile has a maximum penetration depth of ~60 m. Likely areas of permafrost are outlined by black dashed lines; f-t =frost table.*

The profiles reveal a relatively low resistivity layer near surface over a higher resistivity layer that exhibits a gradual drop in values towards the base of the profile; however, resistivities remain above 1000 ohm m. Where the profiles cross the road, lower resistivities are evident on both profiles with values below 400 ohm m extending to a maximum depth of 2.5 m. Both ERT profiles clearly indicate the presence of frozen ground to their respective bases, therefore demonstrating permafrost depths of >60 m. The active layer is too shallow to be represented by resistivity values that directly indicate thawed ground because the electrical contrast between the underlying permafrost and the thawed active layer is so great. Deeper seasonal thaw is evident beneath the road, but there is no indication of a talik (perennially unfrozen zone). The gradient in resistivities between 10 and 15 m depth is likely due to a stratigraphic change which may also coincide with a change in ice content.

A 95 m-long GPR transect (*DC_GPR01*; Figure 53) was completed in the same location as ERT transect *DC_ERT01b*, starting at borehole *DC_BH01*. A strong, undulating layer was observed near the surface to a depth of one metre, which may correspond to the permafrost table, based on the units described in borehole *DC_BH01* (see Appendix B for the complete borehole log). A second strong but discontinuous layer was observed at a depth of ~1.5-2.5 m, corresponding to the gravel layer identified in borehole *DC_BH01*. A third contact with opposite polarization was observed at a depth of ~5.5 m, and a fourth is present at a depth of about ~7 m. These two layers are partially masked by numerous hyperbolic reflectors, which suggest the presence of very coarse materials at depth (e.g., cobbles and boulders).
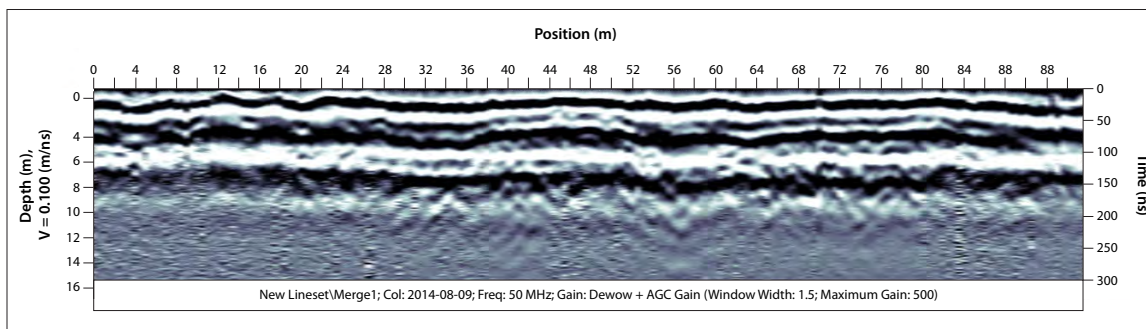
Figure 53. *GPR profile DC_GPR01 from the West Dawson case study site, showing a strong, undulating layer from 0-1 m depth, which may correspond to the top of the permafrost table.*

C-3B SETTLEMENT LAND

The C-3B case study site (Figure 54) is located on the southern edge of the Klondike River floodplain, on the north-facing side of the valley (just east of the Callison Industrial subdivision). Late Pleistocene glaciofluvial sand and gravel (indistinguishable from modern floodplain sediments) is overlain by silt, sand and gravel of a fluvial fan and/or apron that has been built onto the floodplain from drainage off the adjacent slope. The site is overlain by a discontinuous organic layer, and is affected by permafrost processes.

Two sites were investigated in this study area (Figure 54). Borehole *DC_BH02* was drilled in an open black spruce forest (up to 15 m high) along ERT profile *DC_ERT02* and GPR profile *DC_GPR02*. The undergrowth was composed of shrubs ranging from 0.3 m to 2 m high (i.e., *Salix sp.*, *Rhododendron groenlandicum*) and a thick moss and lichen cover (0.21 m thick). The permafrost table was encountered at a depth of 0.52 m, under a 0.31 m-thick layer of tephra. The permafrost stratigraphy was composed of an ice-rich lenticular sandy organic silt layer (0.52 to 0.88 m deep) overlying layers of microlenticular sandy organic silt (0.88 to 1.23 m deep), and porous invisible

silty sand with gravel (1.23 to 3.08 m). These silty sand with gravel deposits were very dry and ice poor and had an average of 19% excess ice content by volume, compared to 26% for the silty sand deposits near the top of the permafrost. At the boundary between the active layer and the permafrost, ice lenses up to 3 cm thick were observed. Thaw settlement and consolidation test results revealed 48% total settlement under a stress load of 25 kPa, and 50% under a stress load of 150 kPa. In silty sand deposits at greater depths, the thaw settlement and consolidation tests resulted in 24% total settlement under a stress load of 25 kPa, and 28% total settlement under a stress load of 150 kPa. The complete borehole log is shown in Appendix B, and grain size analysis and ice content results are shown in Appendix C.

Figure 54. Map illustrating locations of detailed site investigations for the C-3B case study site. Refer to Figure 49 for case study location.

A second site (*DC_PIT01*) was investigated south of *DC_BH02* (just outside the C-3B settlement land boundary), where surface vegetation and soil were cleared within the last decade for placer mining. At the time of investigation, only tall grass (0.5 m, *Carex sp.*) and shrubs (*Salix sp.*) were present. A stratigraphic test pit of 1.55 m was dug about one third of the way along ERT profile *DC_ERT02*, near the end of GPR profile *DC_GPR03*. No permafrost was encountered, but the water table was reached at 111 cm. The soil stratigraphy was composed of a thin moss cover (0.1 m thick) overlying sandy silt layers (0.1 to 0.92 m) and interlaced layers of iron oxide-stained, silty sand and dark organic deposits (0.92 to 1.55 m). The complete borehole log is shown in Appendix B.

A 200 m-long ERT profile at this site (*DC_ERT02*) illustrates clearly the effect of surface disturbance (i.e., land clearing) on permafrost in the Dawson area. The survey was run from south to north across a cleared area, through spruce forest, and finally through terrain covered by a deciduous

forest. In the cleared area, there is a continuous low resistivity layer near-surface that overlies a much higher resistivity layer that extends to the base of the profile at 25 m (Figure 55). The same pattern persists beneath the spruce forest but the near-surface low resistivity layer is thin and discontinuous, and the resistivities are not as low as those beneath the cleared area. The northern end of the profile beneath the deciduous forest exhibits moderate resistivities in the 300-800 ohm m range without an obvious layered pattern.
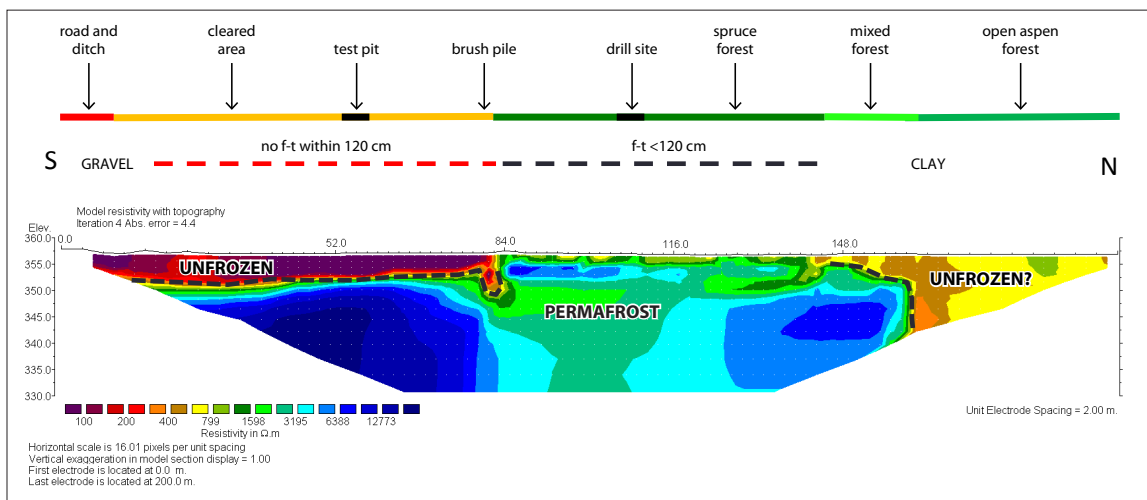
Figure 55. *ERT profile DC_ERT02, which is 200 m long and runs south to north across a cleared area and into forest at the C-3B case study site (see Figure 54 for location). The profile has a maximum penetration depth of ~25 m. Likely areas of permafrost are outlined by black dashed lines; f-t = frost table.*

The ERT profile is interpreted as having a supra-permafrost talik extending across the field over permafrost that is at least 25 m thick. The top of the permafrost is at a depth of approximately 3-5 m, which accounts for its absence in the test pit. There is a slightly deeper thaw depth at the very edge of the field beneath the brush pile, likely due to snow accumulation in the winter, causing ground warming. The permafrost beneath the forest has some layers that exhibit excess ice contents. Borehole data reveal an active layer averaging 0.55 m (n=16). The interpretation of the latter part of the profile is ambiguous. The resistivity values suggest frozen ground, and field measurements while probing document resistance at an average depth of 0.40 m (n=13). However, the probing also indicates that the substrate is cohesive, making the values suspect. The absence of layering in the resistivity profile, the dry surface, the absence of a thick organic mat, and the presence of large deciduous trees, all suggest that permafrost is absent. However, an alternative explanation is that frozen ground is very close to 0°C because of the differences in forest and ground cover, causing high unfrozen moisture contents and lower resistivities than in the central part of the profile. Determining whether or not there is frozen ground would require further investigation (e.g., by completing a borehole or deep pit).

Two GPR surveys were completed at this site. The first (*DC_GPR02*; Figure 56) was 40 m long and was conducted in the spruce forest. The penetration depth of the signal was ~6 m and the penetration speed was 0.1 m/ns. An upper reflection, which was present along the entire profile, was located near surface, at a depth between 0.3 m and 1 m, and likely corresponds to the permafrost table (also identified in *DC_BH02*; see Appendix B for the complete borehole log). A second layer, which is relatively constant and has a strong reflection, is present at a depth of ~2 m, and likely corresponds to a gravelly layer noted in borehole *DC_BH02*. A third layer can

be observed in the second half of the profile at a depth of ~3 m but the nature of the material creating this reflection is unknown. An anomaly was detected at a depth of ~4-6 m, but because this is below the base of borehole *DC_BH02*, the nature of the anomaly is unknown. The second survey (*DC_GPR03*; Figure 57) was 59 m long and was carried out in the cleared area. It paralleled ERT survey *DC_ERT02* from the trail to the boundary between the clearing and the spruce forest (see Figure 54). The penetration depth was ~7 m and the penetration speed was 0.1 m/ns. A weak but relatively constant, undulating contact was visible at a depth of ~2 m, possibly corresponding to the gravelly layer reported in *DC_BH02*. A second strong and constant reflection was noted at a depth of ~4 m, and the nature of this contact is unknown. A third undulating layer, also of unknown composition, is visible as a more subdued reflection at a depth of ~5 m at the beginning of the profile, and at a depth of ~7 m in the centre of the profile.
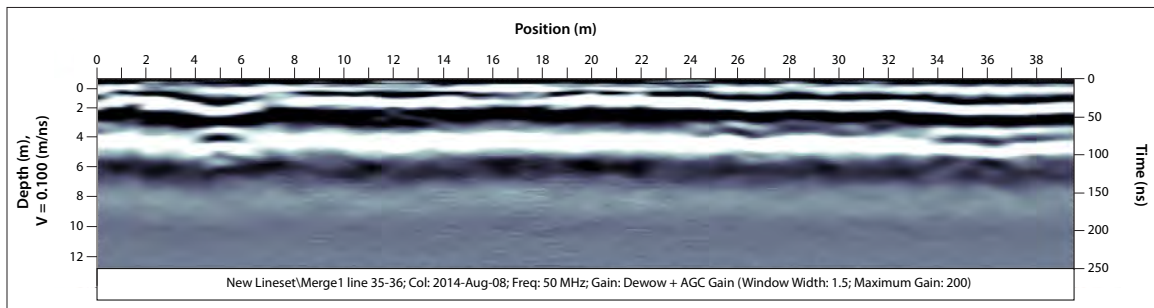
Figure 56. GPR profile DC_GPR02 from the C-3B case study site, showing a reflection at a depth of 0.3-1 m, which may correspond to the top of the permafrost table.
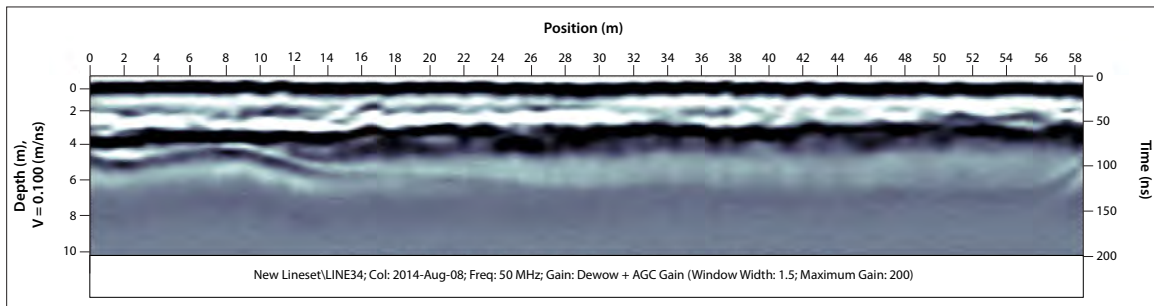
Figure 57. GPR profile DC_GPR03 from the C-3B case study site, showing a weak, undulating reflection at a depth of ~2 m, possibly corresponding to a gravelly layer.

R-68B SETTLEMENT LAND

The R-68B case study site (Figure 58) is underlain by a number of surficial geological units formed by modern streams, glacial streams, and downslope colluviation of sediments. The unconsolidated surface materials (largely sand and gravel overlain by organic material) are deposited on bedrock which can be seen upstream on both sides of the Yukon River.

Geophysical surveys and borehole drilling were conducted on a fluvial terrace ~25 m above the Yukon River floodplain. The terrace is composed of silt, sand and gravel, and is overlain by organic material ranging in thickness from a few centimetres to more than 1 m. At the borehole location, a silty to sandy fluvial fan is incorporated into the terrace materials, and also overlain by organic material. The entire site is affected by permafrost processes and can be inundated by water seasonally.
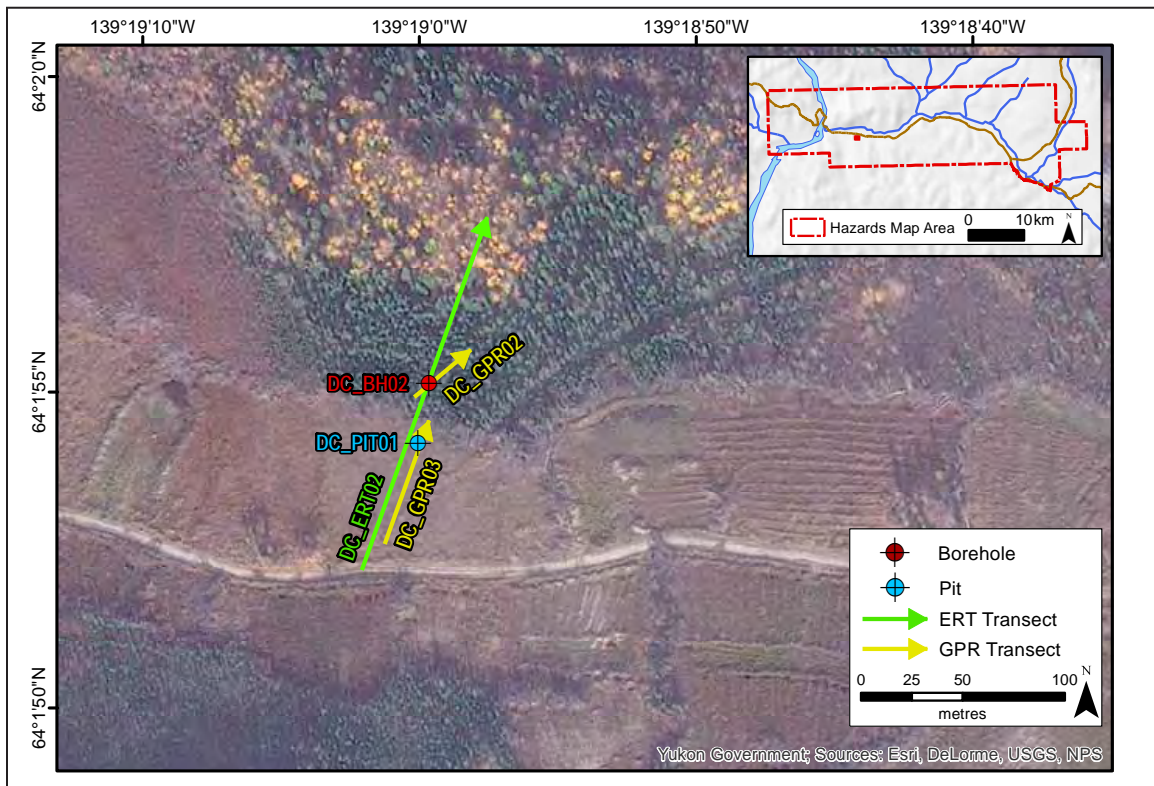
Figure 58. Map illustrating locations of detailed site investigations for the R-68B case study site. Refer to Figure 49 for case study location.

Borehole *DC_BH03* was drilled in a muskeg approximately 110 m from the Yukon River bank and 105 m along ERT profile *DC_ERT04*. The vegetation was composed of black spruce (1 to 3 m high), shrubs (i.e., *Salix sp., Rhododendron groenlandicum*), and a thick organic moss cover (0.30 m). The borehole was drilled to a depth of 4.10 m. The permafrost table was encountered at a depth of 0.30 m, 0.15 m below the water table. The permafrost stratigraphy was composed of interlaced layers of ice-rich microlenticular and porous visible sandy organic silt, overlying layers of porous visible and invisible sandy organic silt. In the lower half of the stratigraphy, some layers of ice-rich microlenticular cryostructures were also observed in silty sand deposits. Excess ice content was at its highest at the top of the permafrost having values ranging from 26 to 30% by volume. Below, in silty sand deposits, the volumetric excess ice content values dropped considerably to 4%. However, where the ratio of silt to sand increased, the excess ice content also increased to 19%. At a depth of 1.14 m, in ice-rich permafrost, thaw settlement and consolidation test results exhibited 44% total settlement under a stress load of 25 kPa, and 58% total settlement under a stress load of 150 kPa. Deeper, in drier and ice-poor permafrost, thaw settlement and consolidation test results revealed 13% total settlement under a stress load of 25 kPa, and 17% total settlement under a stress load of 150 kPa. The complete borehole log is shown in Appendix B, and grain size analysis and ice content results are shown in Appendix C.

A 400-m ERT profile (*DC_ERT04*) was run from east to west from a beach along the Yukon River, through dense deciduous regrowth surrounding an old paddle wheeler wreckage, to an open dwarf-spruce forest (Figure 59). Frost tables less than 1.20 m depth were encountered throughout the profile except beneath the beach. The average depth of thaw was only 0.42 m (n=39), and given the time of year the survey was taken, this represents the actual active layer thickness.

The borehole described above showed moderately ice-rich materials to a depth of 4.1 m. Air temperatures have been recorded since 2007 at a station located at 100 m along the profile and the mean annual average is approximately -4.3°C. This is slightly colder than the mean annual air temperature recorded at treeline in the area due to the consistent air temperature inversions that occur for five months over the winter (Lewkowicz and Bonnaventure, 2011). Ground temperatures in a borehole at the same location averaged about -2°C (A. Lewkowicz, unpublished field data). Typically, the geothermal gradient within permafrost is 1°C per 30-50 m; based on these measurements, the permafrost thickness is interpreted to be 60-100 m at this site.
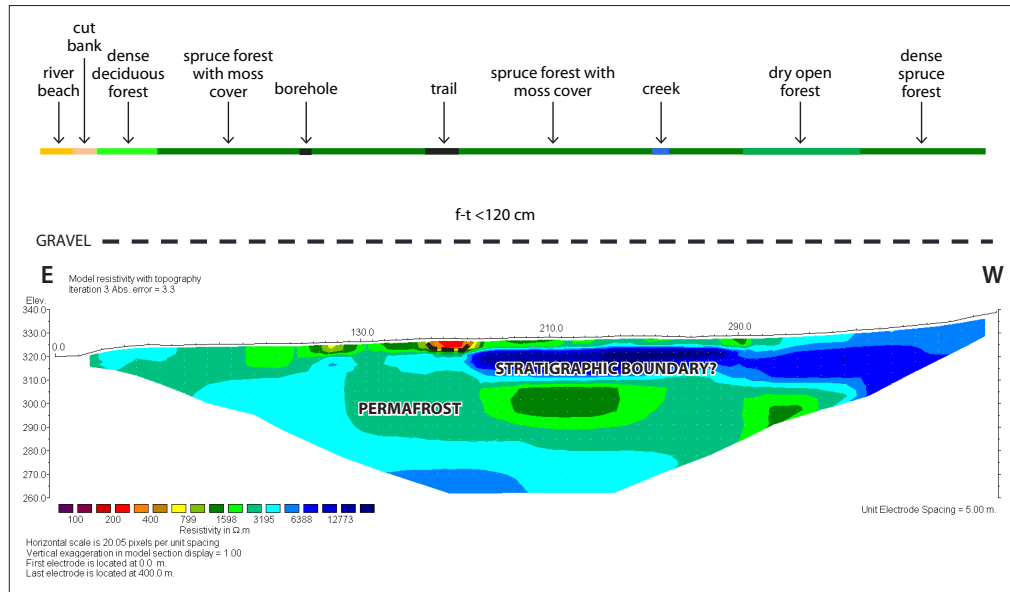
Figure 59. *ERT profile DC_ERT04, which is 400 m long and runs east to west from a beach along the Yukon River, into an open dwarf spruce forest (see Figure 58 for location). The profile has a maximum penetration depth of ~60 m. Likely areas of permafrost are outlined by black dashed lines; f-t = frost table.*

The ERT profile shows a low, near-surface resistivity layer that is almost continuous in the more-detailed, central 200 m of the profile. This layer overlies higher resistivity layers extending to a depth of 15 m, and the resistivities beneath these generally decrease gradually towards the base of the profile at ~60 m. With the exception of a small patch beneath a trail at 170 m along the profile, all the resistivity values indicate frozen materials. The profile is interpreted as having permafrost that extends to the base of the profile; this interpretation concurs with temperature estimates recorded in borehole *DC_BH03*. The near-surface, low resistivity layer is believed to be the result of the combined effect of a thin active layer and relatively warm upper permafrost. Below the trail, there is a slightly deeper active layer due to surface disturbance, however not enough to cause a talik to develop.

The forest at this site was cut down at the end of the 19th century, and the current vegetation represents regrowth since that time. Given the site's current condition, which is relatively undisturbed, it shows what permafrost and the active layer might be like beneath the Dawson townsite if there were no buildings or roads. Since ground temperatures in the northern part of Dawson are about -0.5°C, this suggests that the impact of the development of the town has warmed permafrost by about 1.5°C; however, in developed areas that are underlain by coarse sediment, the effect would be less significant.

R-69B SETTLEMENT LAND

The R-69B case study site (Figure 60) is located on fluvial and glaciofluvial materials on the west bank of the Yukon River, upstream of Dawson City. Geophysical surveys and borehole drilling were conducted on a fluvial fan comprised of silt and sand. Thermokarst ponds and other permafrost-related processes are expressed in the surface materials. Seasonal inundation by water may also occur at this site.
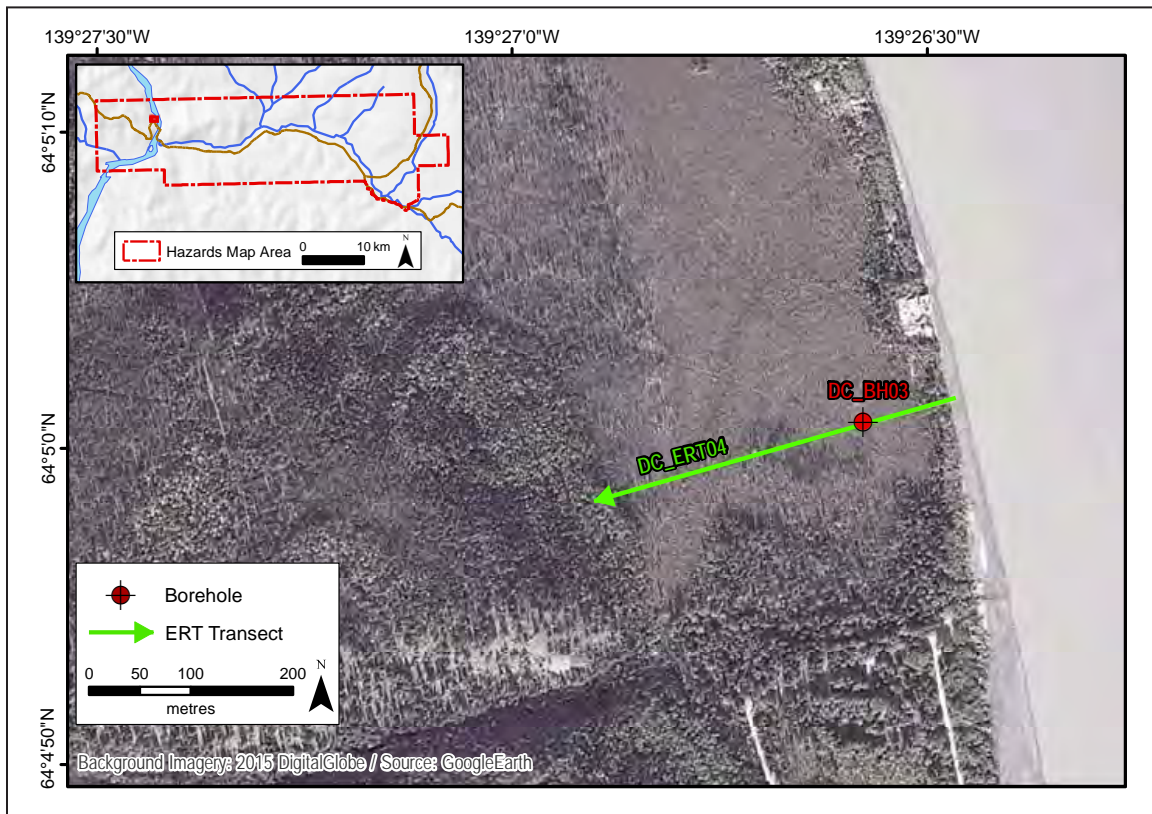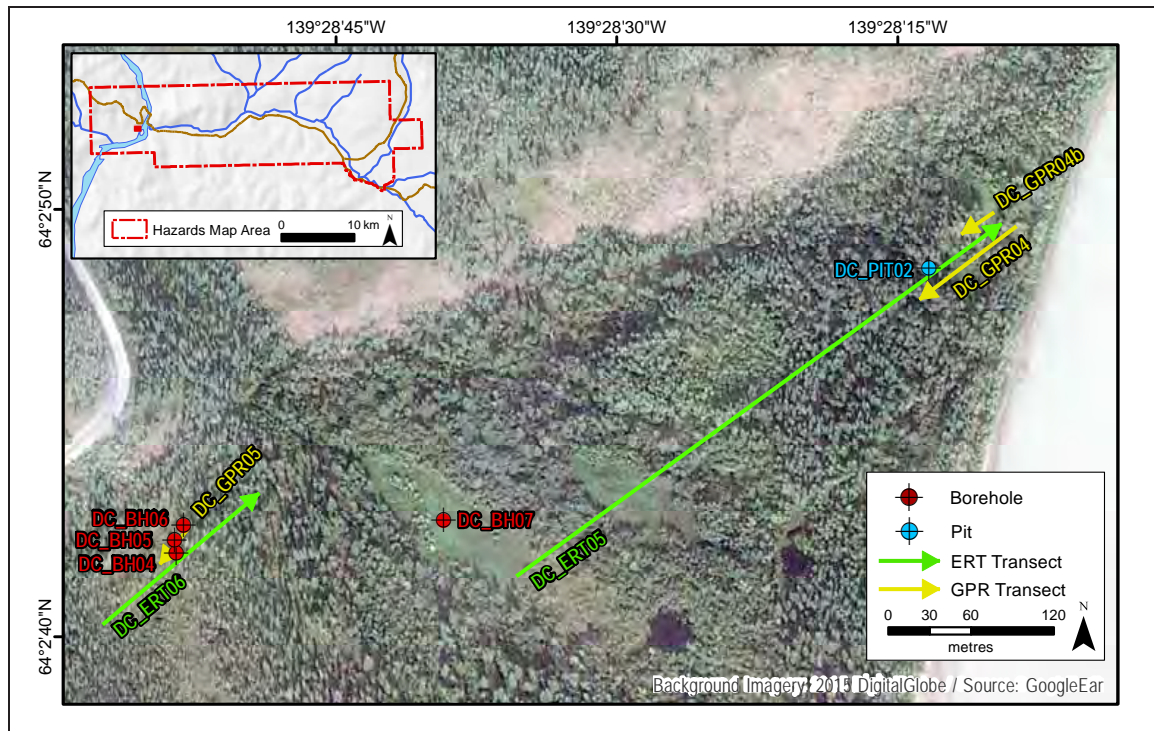

Figure 60. *Map illustrating locations of detailed site investigations for the R-69B case study site. Refer to Figure 49 for case study location.*

DC_PIT02 was dug on the western side of the Yukon River, 2 km upstream from Dawson City and 80 m from the river bank. It is located adjacent to GPR transect *DC_GPR04* and along ERT profile *DC_ERT05*. The site is situated in an open poplar forest (up to 30 m high) with scattered black spruce; the undergrowth was composed of shrubs ranging from 0.30 m to 2.0 m high (i.e., *Carex sp., Rosa sp.*) and a 0.17 m-thick organic humus cover. The pit was first excavated, followed by borehole drilling to a depth of 3.66 m. A temperature of -0.04°C was recorded in situ at a depth of 2.26 m. The water table was not reached. The stratigraphy consisted of interlaced layers of very dry, silty sand and sandy silt to the bottom of the borehole. An iron oxide-stained organic layer was observed near the middle of the borehole from 0.79 to 1.10 m. The complete borehole log is shown in Appendix B.

Borehole *DC_BH04* was drilled at a slightly higher elevation than *DC_PIT02*, along ERT profile *DC_ERT06* and GPR profile *DC_GPR05*, on the top of a mound. This site was significantly damper, and the topography was a succession of dry mounds (about 2 m high) and wet depressions. The vegetation was composed of black spruce (30 m high), shrubs (i.e., *Salix sp., Rhododendron groenlandicum*), and a 0.2 m-thick organic moss and lichen cover. The borehole was drilled to a depth of 4.28 m. The permafrost table was encountered at a depth of 0.50 m. The permafrost stratigraphy was composed of interlaced layers of microlenticular and lenticular, silty sand

overlying layers of porous visible and invisible sandy organic silt. A layer of ice-rich, microlenticular cryostructure was observed between 1.78 and 1.85 m. At the bottom of the borehole (4.28 m), layers of sand and fine gravel were noted. Excess ice content was at its highest in the fine-grained deposits, (i.e., silty sand) with values ranging from 18-36% by volume. Below, in sandy and gravelly deposits, the excess ice content values dropped considerably to 6%. At a depth of 1.1 m, where volumetric ice content results were the highest, thaw settlement and consolidation test results revealed 20% total settlement under a stress load of 25 kPa, and 24% under a stress load of 150 kPa. Deeper, in layers containing higher concentrations of organic matter (57%), thaw settlement and consolidation tests resulted in 10% total settlement under a stress load of 25 kPa, and 19% under a stress load of 150 kPa. The complete borehole log is shown in Appendix B, and grain size analysis and ice content results are shown in Appendix C.

Borehole *DC_BH05* was drilled on top of a mound, 12 m from *DC_BH04*, in a forest of black spruce 30 m high. The undergrowth was composed of shrubs ranging from 0.3 to 2 m high (i.e., *Salix sp., Rhododendron groenlandicum*), and by a 0.43 m-thick moss and undecomposed fibric peat cover. The borehole was drilled to a depth of 4.46 m. The permafrost table was encountered at a depth of 0.43 m. The permafrost stratigraphy was composed of interlaced layers of porous visible sandy organic silt overlying layers of microlenticular and lenticular, silt deposits. Layers of coarse sand and small pebbles were encountered at the bottom of the borehole. Excess ice volume content was at its highest in the first half of the borehole (i.e., in silty sand) with values ranging from 20-47% by volume. Below, in slightly coarser sediments, the volumetric ice content values dropped to an average of 18%. The complete borehole log is shown in Appendix B, and grain size analysis and ice content results are shown in Appendix C.

Borehole *DC_BH06* was drilled in a depression between the mounds described above. The ground was saturated with water, and composed of fibric organic matter (0 to 0.25 m) overlying unfrozen silt to the bottom of the borehole (1.10 m).

Borehole *DC_BH07*, located 192 m east of *DC_BH05*, was drilled to a depth of 2.85 m in an open field using a hand auger. The field was covered with 0.50 m-high grasses (*Carex sp.*). A temperature of 0.54°C was recorded in situ at a depth of 2.85 m. The stratigraphy consisted of a sandy organic silt layer (0.89 m thick), overlying dry, silty sand mixed with pebbles from 1.0 m to the base of the borehole at a depth of 2.85 m. The complete borehole log is shown in Appendix B. No permafrost was encountered, and the water table was not reached.

Two ERT surveys were undertaken at this site. The first was a 500 m-long profile (*DC_ERT05*) that was run from southwest to northeast, with a depth of penetration of approximately 60 m (Figure 61). The survey crossed cleared fields and forested sections which is clearly reflected in the ERT profile by the differing resistivities and patterns produced by frozen versus thawed ground. The frost table was reached within 120 cm only at a very small number of points along the profile.

The *DC_ERT05* profile exhibits a low resistivity layer of variable thickness (up to 20 m) with values as low as 100 ohm m, overlying higher resistivities (up to several thousand ohm m) which extend to the base of the profile. The main features of the ERT survey are the six bodies of low resistivity in the near surface that are interpreted as a combination of deep active layers and supra-permafrost taliks. The borehole (*DC_PIT02*) at 315 m along the transect reached cryotic (frozen) ground at ~220 cm suggesting that at this location there may be a deep active layer. The link between the surface disturbance (cleared fields) and unfrozen ground in the southwest part of the profile is obvious; however, taliks are also present beneath the deciduous forest in the central part of the profile. The latter may be due to regrowth on formerly cleared fields or following fire, but it appears that permafrost has degraded to a considerable depth in this area, likely over several decades. Nevertheless, it persists beneath the taliks.
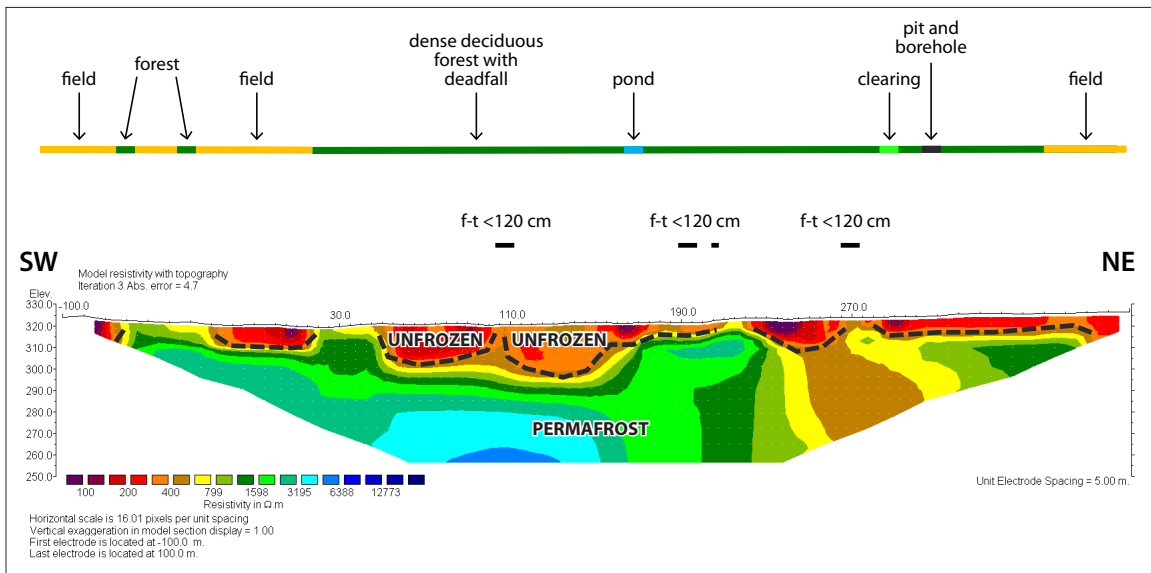
Figure 61. *ERT profile DC_ERT05, which is 500 m long and runs southwest to northeast through forest towards the Yukon River (see Figure 60 for location). The profile has a maximum penetration depth of ~60 m. Likely areas of permafrost are outlined by black dashed lines; f-t = frost table.*

A second ERT survey (*DC_ERT06*) was run near boreholes *DC_BH04*, *BH05* and *BH06*. This survey was located ~100 m west of *DC_ERT05* and ~15 m higher in elevation, but traversed similar terrain (see Figure 60 for location). The vegetation cover consisted of generally open spruce and mixed forest, and a ground surface covered with an organic mat. Frost tables were encountered by frost probe along most of the profile, with the exception of very wet locations. Where measured, the average depth to the frost table was 0.58 m (n=26).

The *DC_ERT06* survey was 160 m long with a maximum penetration depth of 25 m. The profile shows a continuous low resistivity layer overlying a layer with variable resistivities ranging from moderate (less than 1000 ohm m) to high (greater than 6000 ohm m) (Figure 62). The low-resistivity layer in the profile is interpreted as the active layer which overlies permafrost (moderate to high resistivity) that extends to the base of the profile at a depth of 25 m. Although the low resistivity layer appears to extend to a depth of about 2 m along much of the profile, probing revealed that the unfrozen ground is actually much shallower. The discrepancy is believed to be as a result of very low values from a wet active layer which is in contact with much higher values from the underlying permafrost. Only two short sections showed no measurable frost table and these corresponded to slightly deeper apparent thaw depths. Two of the small mounds described above had slightly higher apparent resistivities and shallower frost table depths than the adjacent terrain. These are thought to represent remnants of a higher elevation surface which has subsided following permafrost degradation along preferential groundwater flow paths. Within the permafrost body, there is a considerable difference between resistivity values at a depth of 3-8 m from 96-118 m along the profile and the remainder of the profile beyond 118 m. This may represent a stratigraphic boundary but could also be due to colder permafrost with a lower unfrozen moisture content in soil pores.
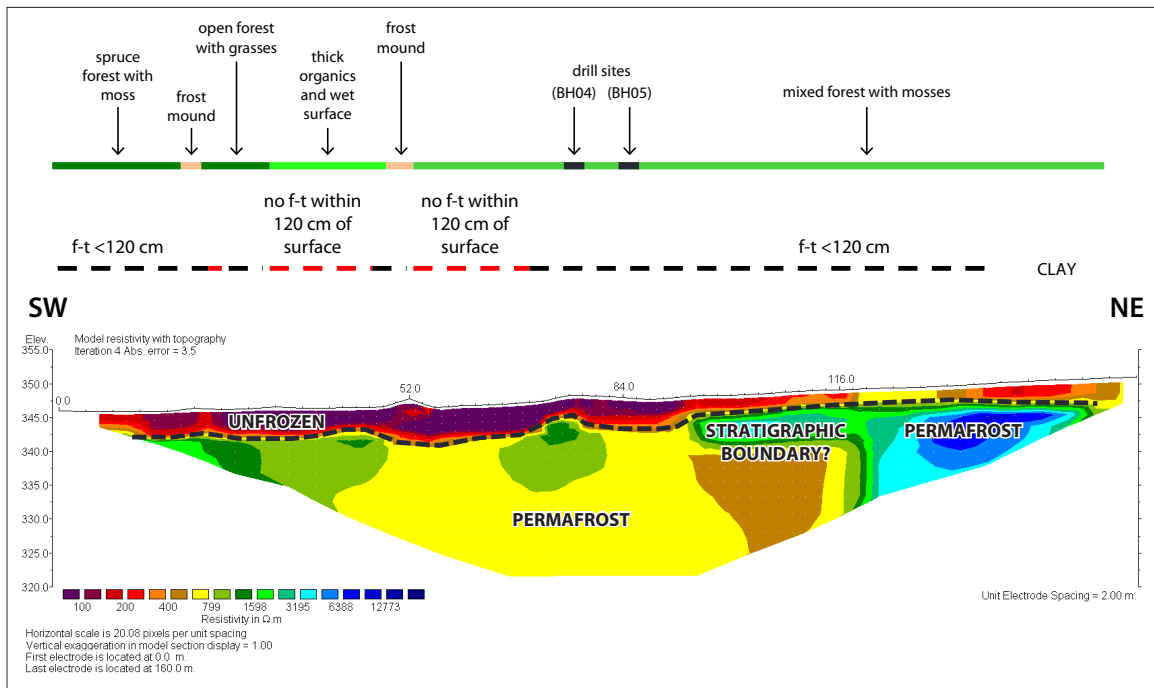
Figure 62. *ERT profile DC_ERT06, which is 160 m long and runs southwest to northeast approximately 100 m west and 15 m upslope of DC_ERT05 (see Figure 60 for location). The profile has a maximum penetration depth of ~25 m. Likely areas of permafrost are outlined by black dashed lines; f-t = frost table.*

Three GPR surveys were completed at this site (see Figure 60 for locations). GPR survey *DC_GPR04* (Figure 63) was 64 m long and was run from the end of ERT profile *DC_ERT05* to pit *DC_PIT02*. Signal penetration depth was ~4 m with a penetration speed of 0.1 m/ns. The profile shows a strong contact at a depth of about 1-2.5 m. A weaker and irregular reflection was present ~1 m below the upper contact. Based on other nearby field data, the first contact may represent the top of the permafrost table (see the log for *DC_PIT02* in Appendix B). The nature of the second reflection is unknown, although it is likely a stratigraphic contact. The deformed nature and disruption in the reflection below 2 m may be related to local permafrost degradation, or to thawed and partially refrozen permafrost. The second GPR survey (*DC_GPR04b*; Figure 64) was run across an open meadow beside an abandoned cabin, to the forest-meadow boundary. There is a strong reflective layer at a depth of ~2 m which may correspond to the top of the permafrost table. A third GPR survey (*DC_GPR05*; Figure 65) was run at a forested site, roughly parallel to ERT survey *DC_ERT06* (see Figure 60). The survey followed a succession of nearby mounds and depressions. The survey was 41 m long and the signal penetration depth was ~4 m with a penetration speed of 0.1 m/ns. The survey was carried out over boreholes *DC_BH04*, *BH05* and *BH06*. A strong contact was detected near surface (between 0.2 and 0.5 m), corresponding to the top of the permafrost table, which was also described in the borehole logs (see Appendix B). A second contact is visible at a depth of ~2 m. Signals were stronger under the mounds than those under the depressions. Under the mounds, the signal is interpreted as a reflection of ice-rich, silty-sandy permafrost. Under the depressions, the signal is likely weakened due to a high water content.
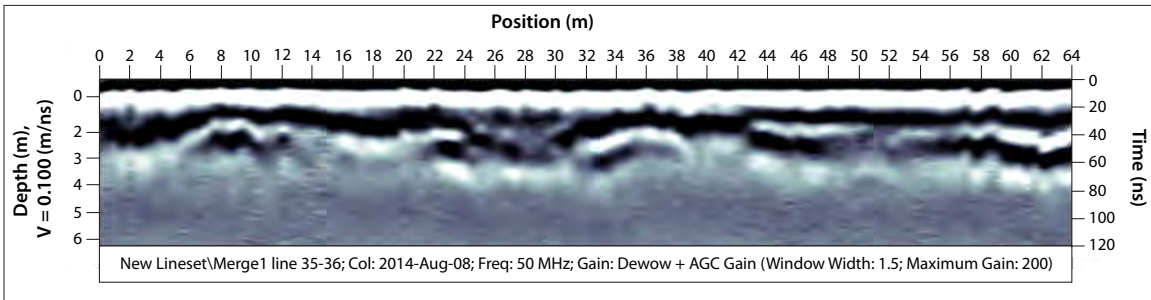
Figure 63. GPR profile DC_GPR04 from the R-69B case study site, showing a strong reflection at a depth of between 1 and 2.5 m, which may correspond to the top of the permafrost table.
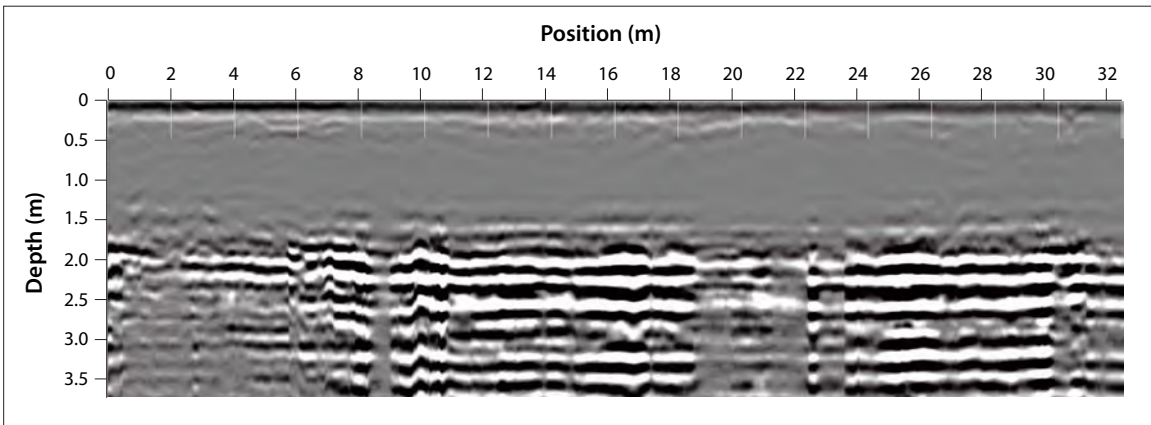
Figure 64. GPR profile DC_GPR04b for the R-69B case study site, showing a strong reflection at a depth of ~2 m.
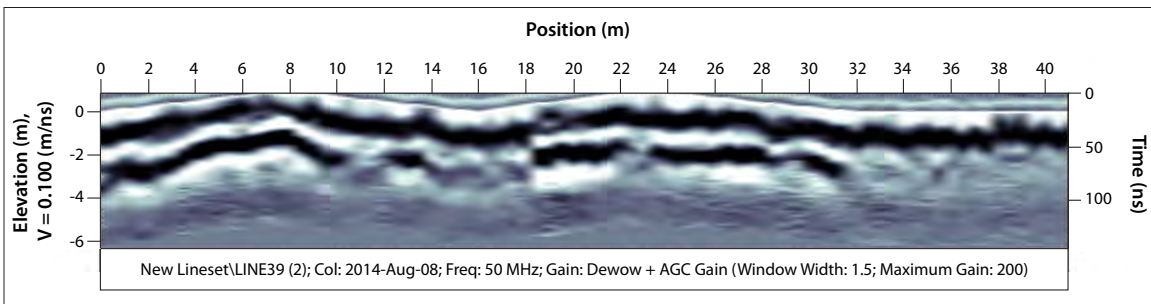
Figure 65. GPR profile DC_GPR05 from the R-69B case study site, showing a strong reflection near surface (between 0.2 and 0.5 m), likely corresponding to the top of the permafrost table.

DOWNTOWN DAWSON

Downtown Dawson (Figure 66) is situated on a fluvial plain comprised of sand, silt and gravel that was part of the active Yukon River floodplain before flood control measures were implemented (i.e., construction of the dike).
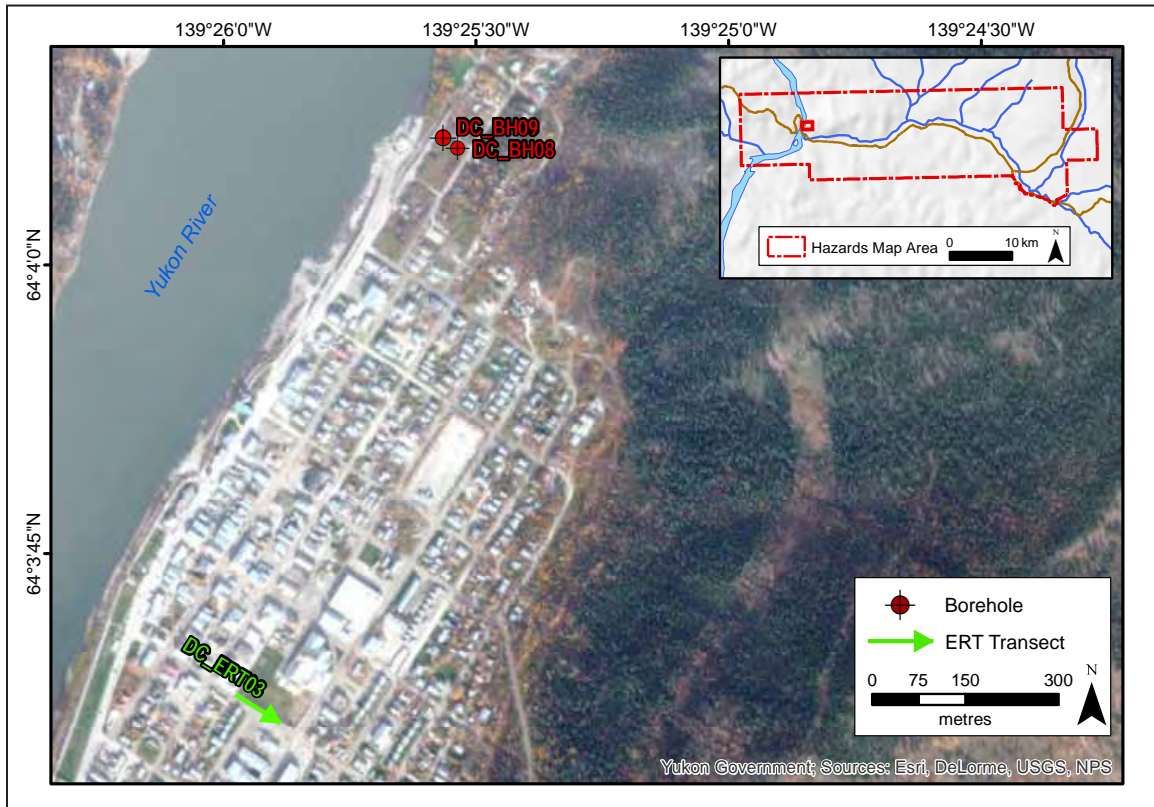
Figure 66. Map illustrating locations of detailed site investigations in downtown Dawson. Refer to Figure 49 for case study location.

Borehole *DC_BH08* was drilled by Northern Climate ExChange researchers in August 2011 as part of a different project. It was located in a poplar forest (average tree height 20 m), 85 m from the Yukon River bank, and 5 m from George Street in the north part of the town. There were signs of past surface disturbance at the site. The ground surface was covered with a thick litter composed of branches and dead leaves. The active layer was comprised of a 0.2 m-thick peat layer overlying organic-rich, disturbed silt and gravel (0.3 m thick) and fine silt deposits (0.5 m thick). The permafrost table was encountered at a depth of 1.0 m. The borehole was drilled to 5.12 m. The stratigraphy within permafrost was composed of layers of microlenticular silty sand overlying layers of porous invisible sandy organic silt. In the uppermost part of the stratigraphy, some layers of frozen, fibric peat were observed. Excess ice content was higher towards the top of the permafrost with values ranging from 14 to 42% by volume. Below, in dryer deposits, the volumetric excess ice content dropped considerably to 2%. The complete borehole log is shown in Appendix B, and grain size analysis and ice content results are shown in Appendix C.

Additional ground truthing (*DC_BH09*) was completed during the current study using a manual hand auger, 30 m west of *DC_BH08*, in the same forested site. The stratigraphy consisted of a very thin organic layer (0.03 m thick), overlying iron oxide-stained, silty sand with traces of pebbles (0.03 to 0.3 m deep); silt with rootlets (0.3 to 0.74 m); fibric undecomposed peat

(0.74 to 1.02 m deep); interlaced layers of sandy organic silt (1.02 m to 1.4 m deep); and grey silt with wood fragments down to the base of the borehole (at 2.2 m). The water table was encountered at a depth of 1.65 m and the water level quickly rose to the top of the borehole. Frozen ground was reached at a depth of 2.2 m. The complete borehole log is shown in Appendix B.

A short ERT profile (*DC_ERT03*) was undertaken adjacent to the Robert Service School with the help of a participating class. The survey was run a total distance of 80 m from northwest to southeast along the southwestern side of the playground. The ground surface was covered in grass and the substrate was gravelly in composition and no frost tables were noted. The ERT profile shows a thick, low resistivity layer extending to depths of 5 to 9 m. Below this is a high resistivity layer that extends to the base of the profile at approximately 13 m (Figure 67). Results from the profile are interpreted as representing a talik overlying permafrost. Resistivity values for the frozen ground suggest low unfrozen moisture content and possibly high ice content.
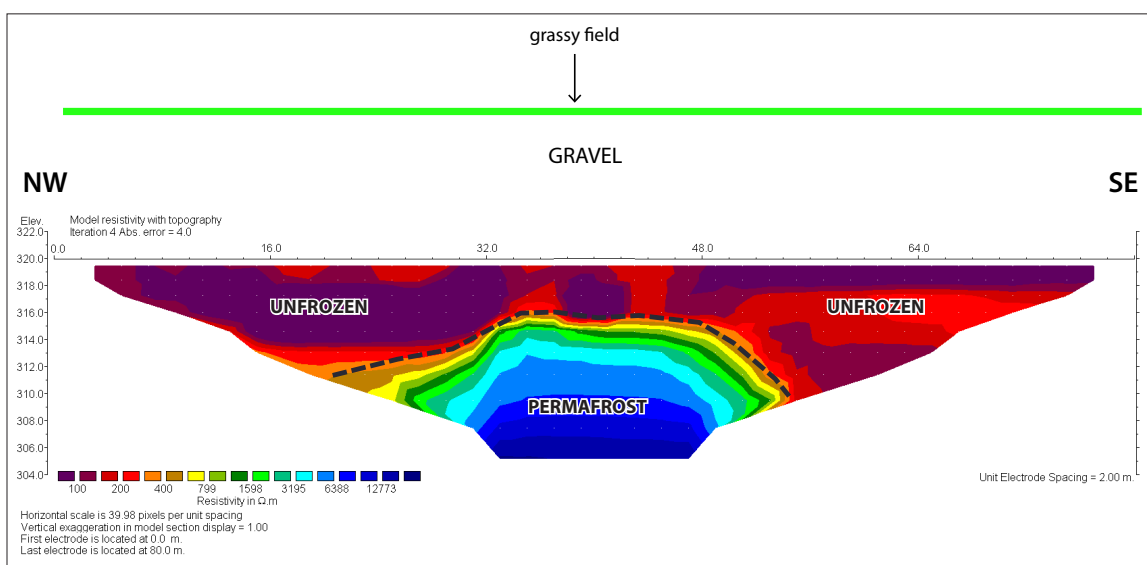
Figure 67. *ERT profile DC_ERT03, which is 80 m long and runs along the southern side of the schoolyard (see Figure 66 for location). The profile has a maximum penetration depth of ~13 m. A likely area of permafrost is outlined by a black dashed line.*

HENDERSON'S CORNER

Henderson's Corner case study site (Figure 68) is located within a small subdivision (of the same name), 22 km southeast of Dawson City. It is situated on a fluvial fan, which likely formed shortly after the McConnell glaciation (McKenna et al., 2014). The fan sediments are composed of silt and sand that has formed on the Klondike River floodplain at the base of Alki Creek (a north-flowing tributary to the Klondike River). The deposits are affected by permafrost processes, and thermokarst ponds and ice-wedge polygons are common, especially along the base of a nearby hill. Once a forested area, the residential lot investigated as part of this study was cleared for agricultural purposes in the 1990s, although other nearby areas were cleared as early as the mid-1970s. The ground is now covered with 30 cm-tall grasses (*Carex sp.*), and some water ponds have formed throughout the property. *DC_BH10* was drilled in a trough of an ice-wedge polygon. The soil stratigraphy revealed a 2.15 m-thick deposit of silt. Soil probing (to a depth of 1.2 m) in the centre of the same polygon revealed comparable deposits of silt to the base. Both samples were saturated and no permafrost was observed. This is consistent with other investigations in the local area, which also found no near-surface permafrost (R. Trimble, TetraTech EBA, pers. comm.).
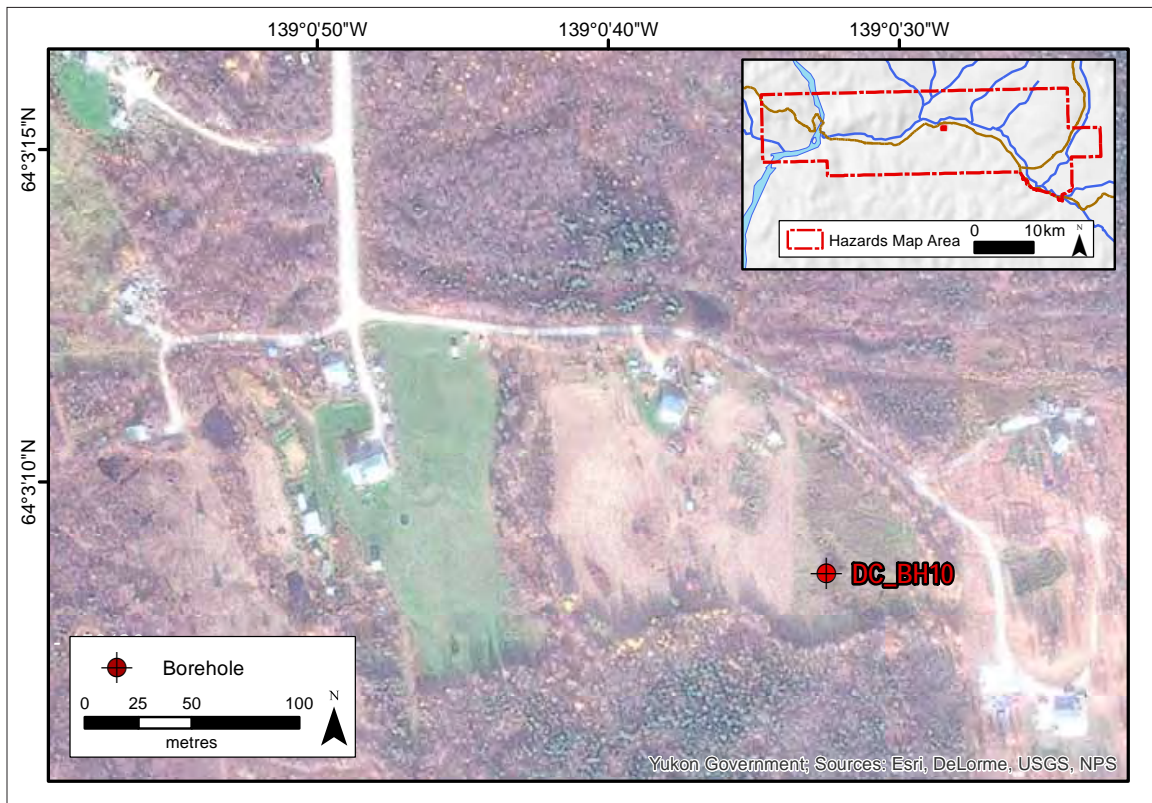
Figure 68. *Map illustrating location of detailed site investigation at Henderson's Corner. Refer to Figure 49 for case study location.*

HAZARD RISKS IN A CHANGING CLIMATE

PROJECTED CLIMATE CHANGE FOR THE DAWSON REGION

Climate projections for the Dawson City area were integrated into this project in order to evaluate how current environmental conditions may pose risk in the future as a result of changes in climate. Predicting future climate change around the globe has become a critical component in climate change science and adaptation. Scientists use a variety of Global Climate Models in combination with discrete scenarios in order to make a range of projections for numerous climate variables (e.g., temperature and precipitation).

GLOBAL CLIMATE MODELS

Global Climate Models (GCMs) – also referred to as Atmosphere-Ocean General Circulation Models – are mathematical representations of atmospheric and oceanic circulation in the world. There are several types of GCMs; however, three-dimensional global atmosphere and ocean models are most commonly used to generate future climate projections. GCMs are complex mathematical models that incorporate a wide range of climate variables including radiation, energy transfer by winds, cloud formation, evaporation and precipitation of water, and transport of heat by ocean currents (CCRUN, 2011). The model calculations are based on a complex grid system that covers the globe in both a horizontal and vertical dimension on the order of 200-500 km. Data for each grid box is input into the model equations to solve for atmosphere, land surface and oceans (CCRUN, 2011).

CLIMATE CHANGE SCENARIOS

In order to generate future climate projections, the Intergovernmental Panel on Climate Change – the leading international body for the assessment of climate change – developed several scenarios that outline a range of possible emission futures. There are a total of six scenario groups, each making different assumptions about the release of greenhouse gases (e.g., carbon dioxide (CO_2), methane (CH_4), nitrous oxide (N_2O) etc.; see Nebojša et al., 2000 for details). Projections used for Dawson were derived from regionally downscaled climate data provided by the Scenarios Network for Alaska Planning (SNAP) at the University of Alaska Fairbanks (SNAP, 2014). For the purpose of this project, SNAP applied three scenarios that best represented the possible shifts in climate for the Yukon communities. The three scenarios used are defined as follows (SNAP, 2014):

The B1 scenario – low to moderate degrees of climate change

- rapid economic growth (as in A1B), but with rapid changes towards a service and information economy

- population rising to 9 billion in 2050 and then declining as in A1 (see Nebojša et al., 2000)

- reductions in material intensity and the introduction of clean and resource-efficient technologies

- an emphasis on global solutions to economic, social and environmental stability

The A1B scenario – medium to high degrees of climate change

- rapid economic growth

- a global population that reaches 9 billion in 2050 and then gradually declines

- the quick spread of new and efficient technologies

- a convergent world, i.e., income and way of life converge between regions

- extensive social and cultural interactions worldwide

- a balanced emphasis on all energy sources

The A2 scenario – high degree of climate change

- a world of independently operating, self-reliant nations

- continuously increasing population

- regionally oriented economic development

- slower and more fragmented technological changes and improvements to per-capita income

The climate projections developed by SNAP were then enhanced to reflect local landscape heterogeneity (like mountainous terrain, which can create local temperature inversions that are not typically captured in models; see Appendix D for more details). Climate projections for three time periods (the 2020s, 2050s and 2080s) were produced, and maps of all projections are included in Appendix D.

Based on climate normal data measured at the Dawson Airport meteorological monitoring station for the period 1980-2010 (Environment Canada, 2014a), mean annual air temperature for the region is -3.6°C (Table 4). Interestingly, back-cast temperatures hindcasted for the period 1950-1979 using the modelling approaches described above, indicate mean annual air temperature for

the period was -5.0°C. This suggests a warming of 1.4°C might have already taken place over the region in the past ~50 years.

Table 4. Statistics generated for the B1, A1B and A2 climate scenarios, displaying mean, minimum and maximum air temperature in the 2020s, 2050s and 2080s.

Projection	Air Temperature (°C)		
	Mean	Minimum	Maximum
Current MAAT	-3.6	-4.0	-3.2
1950 - 1979	-5.0	-5.5	-4.7
B1 2020s	-3.6	-4.0	-3.2
B1 2050s	-3.0	-3.4	-2.6
B1 2080s	-1.9	-2.3	-1.5
A1B 2020s	-3.6	-4.0	-3.2
A1B 2050s	-2.3	-2.7	-1.9
A1B 2080s	-0.8	-1.3	-0.4
A2 2020s	-3.6	-4.0	-3.2
A2 2050s	-2.7	-3.1	-2.3
A2 2080s	-0.6	-1.0	-0.2

Projections of mean annual air temperatures in the Dawson region show continued warming over the next several decades. All three scenarios predict temperatures in the 2020s that are comparable to 1980-2010 climate normal conditions. By the 2050s, the B1 scenario predicts the lowest mean annual air temperature (-3.0°C), while A1B predicts the highest (-2.3°C). By the decade of the 2080s, both A1B and A2 predict mean annual air temperatures approaching 0°C (-0.8°C and -0.6°C, respectively). Even B1, the most conservative scenario applied, predicts a mean annual air temperature of -1.9°C by the 2080s, which is 1.6°C warmer than present. Importantly, all scenarios suggest mean annual air temperatures below 0°C by the 2080s, implying that undisturbed permafrost in the region may persist towards the end of this century. However, permafrost presence will also be affect by changes in snowcover, vegetation patterns, and hydrology, which may all vary in response to warmer mean annual air temperatures.

As discussed in earlier sections of this report, it is important to note that warming in the region will not be uniform – lapse rates (i.e., changes in temperature with elevation gain) are variable and differ significantly from the global average (Lewkowicz and Bonnaventure, 2011). Regardless of scenario, continued increase in mean annual air temperature has the potential to exacerbate hazards in the Dawson region in ways that will be described below.

PROJECTED CHANGES IN PERMAFROST DISTRIBUTION

Increases in mean annual air temperature will affect permafrost distribution in the Dawson area. Projections of permafrost distribution under different degrees of warming can be mapped based on the model of current permafrost distribution developed for Dawson (see Figure 39, p. 44).

To map future permafrost distribution, the contemporary permafrost probability model is perturbed by altering the input variable of equivalent elevation which represents mean annual air temperature. This effectively simulates a uniform regional temperature change, which is used to predict the probability of permafrost occurrence in the study area under differing degrees of warming. A range of mean annual air temperature increases from +1°C to +5°C were imposed,

based on widely accepted projections of change for the next several decades (e.g., see IPCC, 2015). A scenario approach was favoured over applying global or regional climate model predictions, because these tend to suffer from inadequate representation of the topography in the Yukon (see Burn, 1994).

The goal of imposing climate change scenarios on the regional permafrost probability model is to examine the sensitivity of permafrost to changes in mean annual air temperature over time. It is important to note that modelling is done for equilibrium conditions and therefore does not take into account the rate at which the change in climate might occur, nor the lag times associated with permafrost thaw. Still, it is a useful indication of potential changes in the spatial distribution of permafrost regionally, under a changing climate.

Increases in mean annual air temperature were simulated in the spatial model by uniformly decreasing the values of equivalent elevation in the transformed digital elevation model (Janke, 2005; Lewkowicz and Bonnaventure, 2011; Bonnaventure et al., 2012), and then running the model to produce an altered basal temperature of snow surface. This affects the predicted permafrost probabilities that are calibrated with the non-linear logistic regression coefficients determined for 1971-2000 climate normal conditions. An increase of 1°C is represented by a decrease in the equivalent elevation surface of 154 m. Even though the change is uniformly applied across the region, it results in differential responses that depend on the surface lapse rates below treeline. This methodology has the advantage of preserving all elements of the spatial model for a given area (i.e., Dawson) such as aspect, shading and slope, as well as the specific relationships that exist between changes in elevation and basal temperature of snow values. Although other environmental factors, such as snow, vegetation, hydrology, groundwater flow, soil moisture, surface subsidence and mass movements significantly influence permafrost distribution in the discontinuous zones (e.g., Smith and Riseborough, 2002) and are expected to change in the future (e.g., IPCC, 2015), the model cannot take such changes into account, as they are not part of the input variables.

As with contemporary permafrost probability modelling presented earlier in this report, results show probabilities on a scale of 0 to 1. If an area has a probability value of 0.6, this means that 60% of the grid cells in the area are likely to be underlain by permafrost. However, the model is not capable of distinguishing which grid cells in the area have permafrost; rather, it identifies local probabilities given local conditions.

The results of the perturbed permafrost probability modelling (see Figures 69-73) show that a relatively small increase in air temperature (1-2°C) is likely to have an impact on permafrost probability in the Dawson region. Under current conditions, the present probability of permafrost being present at any point in the region (defined by the boundaries of the hazards map; see Figure 1 for map area) is 77% which is consistent with the area being in the extensive discontinuous permafrost zone (50-90% permafrost by area). With a mean annual air temperature increase of 1°C, the probability of permafrost declines to 29%. This change is dramatic, and is compounded in the region by wintertime inversions in surface lapse rates, which subsequently result in a slightly inverted surface lapse rate through the forest annually. This means that in the Dawson area, the highest probability of permafrost is currently in the valley bottoms (90% probability; see Figure 39). With increased elevation toward treeline, permafrost probability decreases to 50%. Under air temperature increases, the Dawson region has a greater loss of permafrost for a given amount of warming than other communities in Yukon (e.g., see Bonnaventure and Lewkowicz, 2013). For example, under a 2°C increase in mean annual air temperature, the probability of permafrost presence in the map region becomes less than 10% (Table 5). This loss pattern is referred to as

bidirectional spatial loss, and typically results in the lowest probabilities of permafrost shifting to areas down valley from those areas close to treeline (Bonnaventure and Lewkowicz, 2013).

Table 5. Statistics displaying the probability of permafrost presence in the hazards map area under current and future scenarios of temperature increase.

Mean annual air temperature	Probability of permafrost presence		
	Mean	Minimum	Maximum
Current	0.77	0.49	0.90
+1°C	0.29	0.09	0.49
+2°C	0.08	0.02	0.23
+3°C	0.04	0.01	0.17
+4°C	0.02	0.01	0.14
+5°C	0.01	0.10	0.01
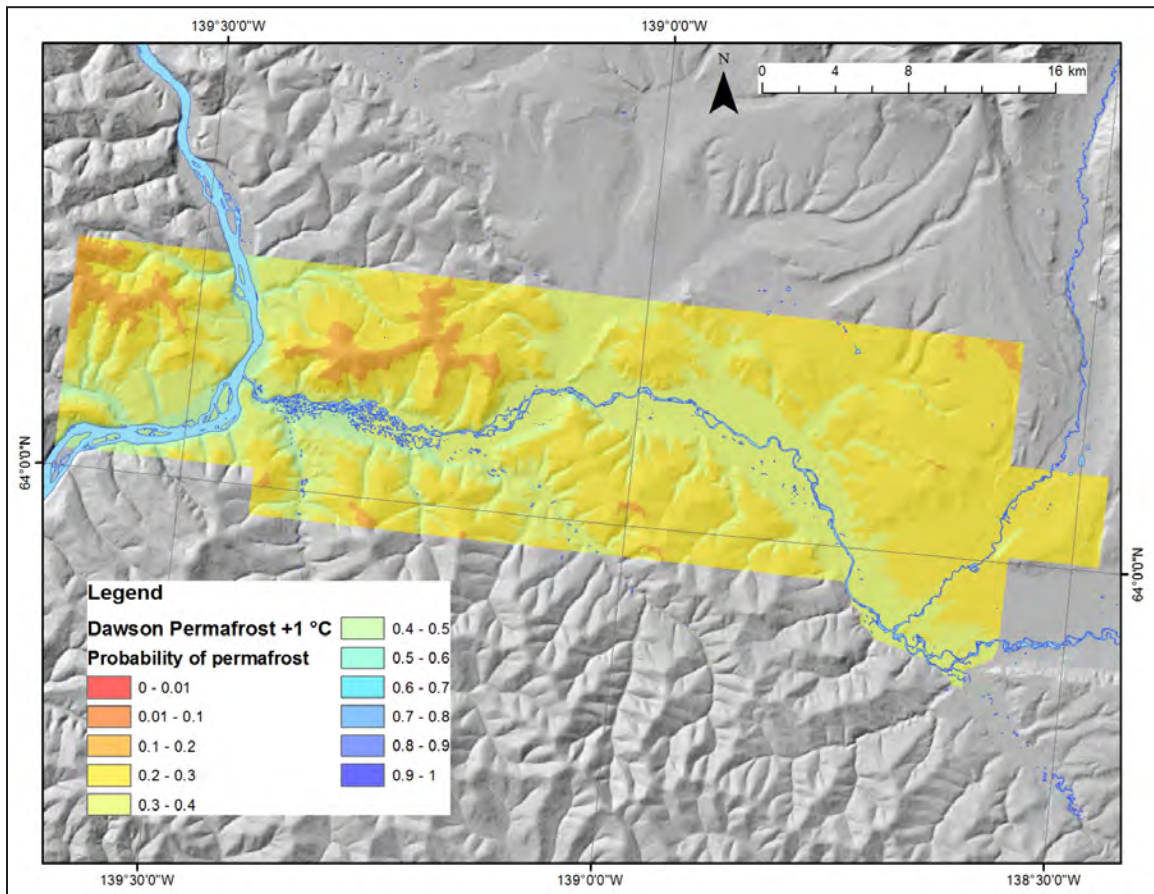
Figure 69. Projected permafrost probability for the Dawson region under an increase in mean annual air temperature of 1°C.
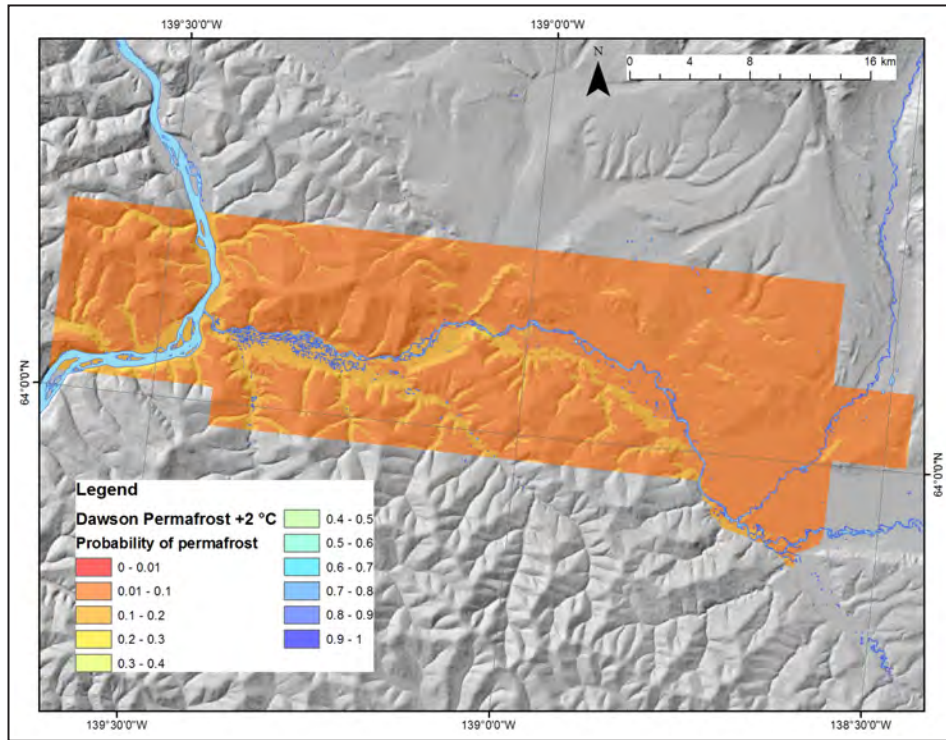
Figure 70. *Projected permafrost probability for the Dawson region under an increase in mean annual air temperature of 2°C.*
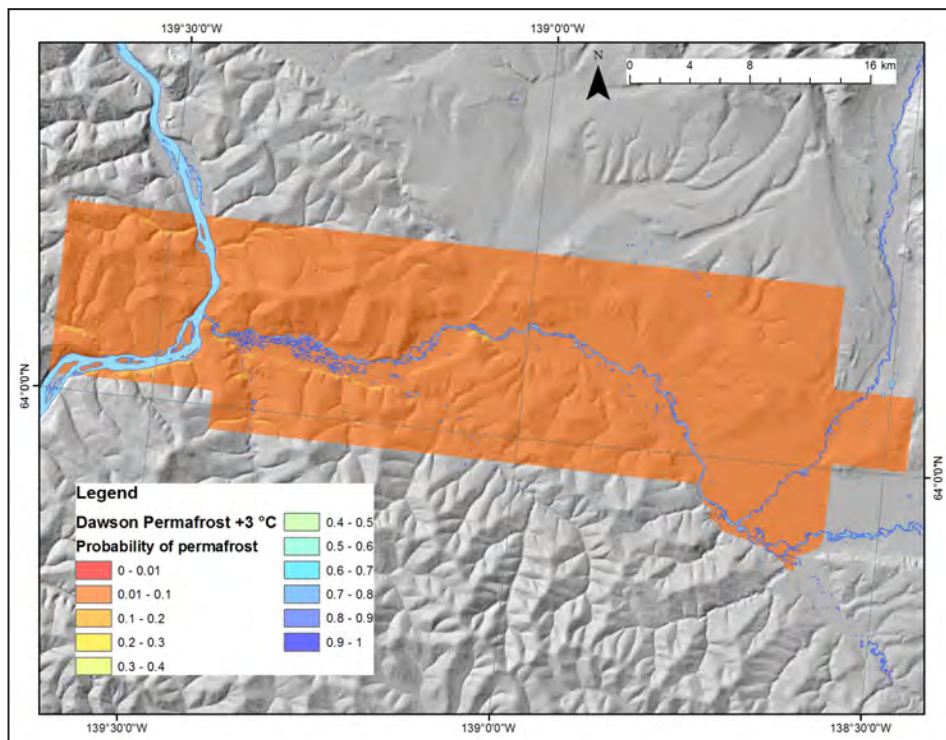
Figure 71. *Projected permafrost probability for the Dawson region under an increase in mean annual air temperature of 3°C.*
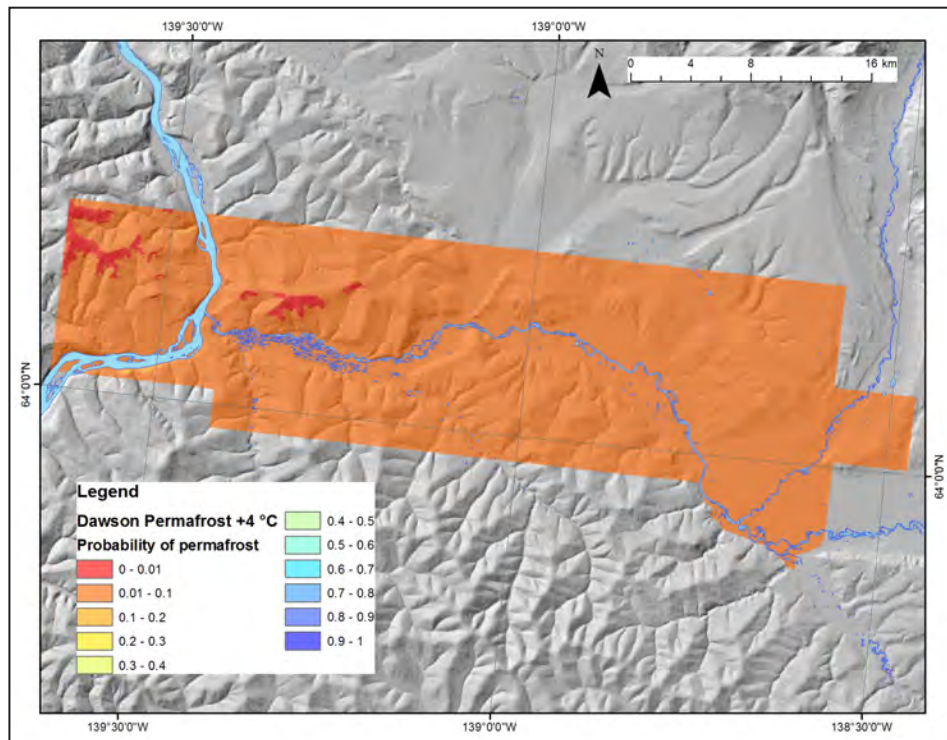
Figure 72. Projected permafrost probability for the Dawson region under an increase in mean annual air temperature of 4°C.
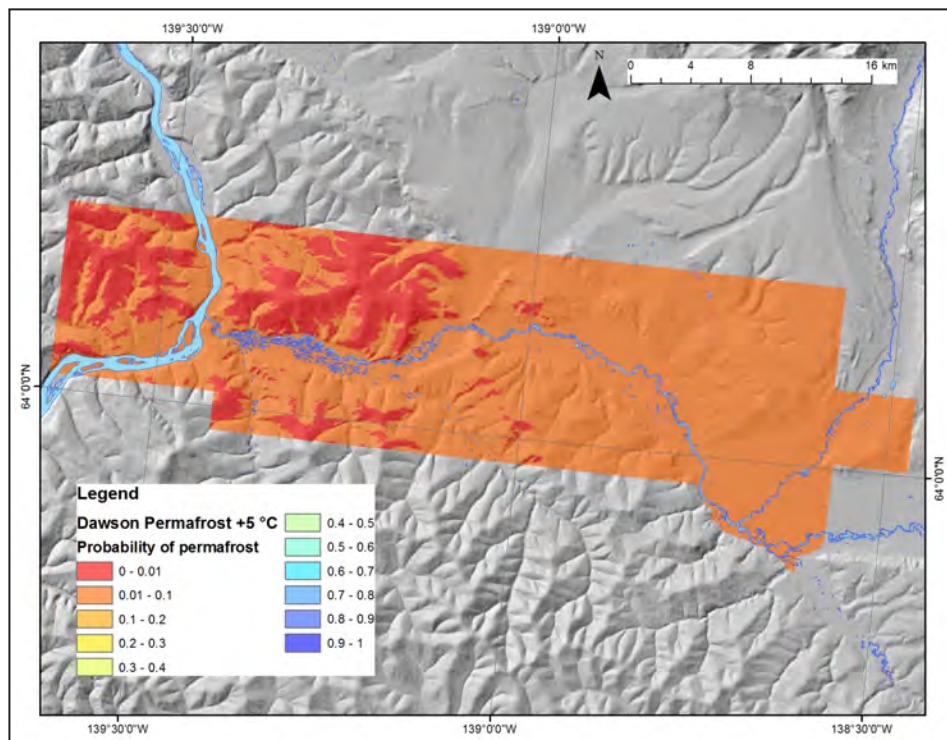
Figure 73. Projected permafrost probability for the Dawson region under an increase in mean annual air temperature of 5°C.

It is important to note that given the very significant thicknesses of permafrost in the study sites (as demonstrated by the ERT profiles), the entire predicted change in permafrost distribution at depth may lag behind the changes in climate by decades or even centuries. However, sites with thinner, warmer permafrost, such as in the Dawson town-site, or sites subject to severe disturbance, can be expected to respond more rapidly. Where permafrost is ice-rich at depth (e.g., where ice wedges or silt with high volumetric ice content are present), thaw settlement can persist for years, particularly where these deposits are thick. Potential declines in permafrost extent under increases in mean annual air temperature, as well as unique patterns of permafrost degradation present in the Dawson region, should be factored into adaptive planning decisions, as permafrost thaw poses a significant hazard risk for infrastructure, which may last for long periods of time.

IMPLICATIONS OF PERMAFROST CHANGE FOR THE DAWSON REGION

Near-surface permafrost degradation in the Dawson region has been occurring since the area was first settled, as a result of development, land clearing and climate change. Continued climate warming, as outlined above, will remain a driver of ongoing permafrost thaw, as will continued development in the region. This will have implications for the stability of surficial materials and local hydrology.

The thawing of ice-rich permafrost has implications for soil moisture – often, soil moisture will increase with permafrost thaw, which can result in decreased terrain stability. Active layer detachment slides, sheetwash and thermokarst erosion may increase as surficial deposits become less stable following the degradation of near-surface permafrost. Most of these processes occur on north-facing slopes, but can also occur on other aspects. (Note that changing hydrological regimes, including streamflow, flooding, groundwater flow, seasonal precipitation patterns and extreme snowmelt and rainfall events, can also affect soil moisture and terrain stability.)

Additionally, permafrost thaw can impact hydrology in the Dawson region. For example, surface and groundwater drainage are affected by changes in permafrost and can cause near-surface sediments to become either wetter or drier depending on site conditions. In ice-rich permafrost, active layer thickening may increase soil moisture and decrease slope stability, whereas in ice-poor permafrost, deepening of the active layer may improve local drainage capacity and increase surface slope stability. Increases in the movement of water in response to permafrost thaw could raise stream levels which, in turn, may enhance incision or aggradation rates, and erosion on stream banks. Alternatively, a deeper active layer may have more storage capacity, buffering runoff times to receiving streams and moderating runoff peaks.

On the floodplains of the Yukon and Klondike rivers, where much of the development in Dawson is concentrated, common material types were noted that are also sensitive to the effects of permafrost thaw. These floodplains are typically composed of layers of organic material overlying layers of silt, sand and gravel. Depending on the location of paleochannels and past flood history, the layers of silt and sand making up these deposits are often interbedded with organic layers. The superposition of different sediment layers can change the behaviour of a given deposit (e.g., its frost susceptibility, hydraulic response, etc.) in response to permafrost thaw.

Typical materials encountered in valley bottom deposits in the Dawson region include silt on sand, sand on gravel, and peat and organic silt on sand. Silt is a frost-susceptible, thaw-sensitive material that should be avoided for land-use planning involving buildings and transportation infrastructure. The impact of a layer of silt over a layer of sand depends on the thickness of the silt layer. When the active layer is entirely composed of silt, significant frost heave and thaw settlement of the surface will occur, especially if the area is poorly drained. When the bottom of the active layer is

composed of sand and the silt layer is drained when freezing occurs, the material can be expected to remain stable. An active layer without coarser material (i.e., sand and/or gravel) does not create significant thaw settlement. In floodplain deposits made up of sand on gravel, the deposits are usually well drained, not frost-susceptible, and mechanically stable upon thawing. In contrast, where peat and organic silt overlie sand, the stratigraphy implies a layer of highly frost-susceptible material (peat and organic silt) over a layer of (typically) non frost-susceptible sand. The impact of this stratigraphy on the stability of the ground upon thawing depends on the thickness of the organic layer. If the active layer is above the boundary between the organic and the mineral soil layers, a change in the thermal regime of the ground will lead to notable settlement due to melting of excess ice and the consolidation of the organic layer, especially if the area is poorly drained. However, a deepening of the active layer in sand will not create significant thaw settlement, and the material can be expected to remain stable.

INTEGRATING RISK IN A LANDSCAPE HAZARDS MAP FOR THE DAWSON REGION

To develop a landscape hazards map for the Dawson region that integrates current and future hazard risks in a changing climate, results from study region characterization, case study site investigations, laboratory analyses, climate projections, and contemporary and future permafrost probability modelling were integrated. Layers of input data related to slope angle, slope aspect, surface materials and permafrost probability were gridded into a raster made up of 30 m^2 pixels, and each pixel in each layer was assigned a hazard risk ranking based on parameters described below. Layers were then fed into a Geographic Information System (GIS) model that generated a cumulative risk ranking for each pixel in the study area by combining weighted risk rankings for each input layer.

Attributes of the individual input layers were classified on a hazard risk scale of 0-9, where zero represents a low hazard risk and nine represents a high hazard risk. Input data and associated hazard risk rankings are described below.

INPUT DATA

Slope angle

Hazard risk rankings associated with different slope angles are summarized in Table 6, which is based on the values recommended by the British Columbia Terrain Classification System (Howes and Kenk, 1997). Steep slopes were ranked with the highest value possible (9), followed by moderately steep slopes (7), moderate slopes (5), gentle slopes (2), and flat to gentle slopes (0). Slope angles were computed and assigned rankings using a digital elevation model with a pixel resolution of 30 m^2 (30 m DEM). Figure 74 depicts ranked risks associated with slope angle for the study area.

Table 6. Hazard risk rankings associated with different slope angles for the Dawson region.

Type of Slope	Slope Percentage (%)	Slope Degree (°)	Hazard Risk Ranking
flat to gentle slope	0-5	0-3	0
gentle slope	6-27	4-15	2
moderate slope	28-49	16-26	5
moderately steep slope	50-70	27-35	7
steep slope	>70	>35	9
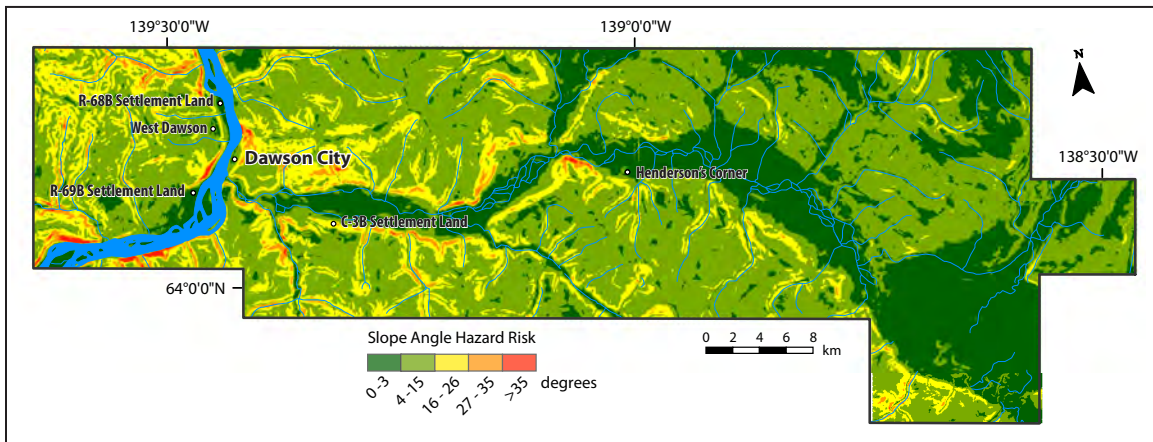
Figure 74. Hazard risk associated with slope angle in the Dawson region.

Slope aspect

Hazard risk rankings associated with different slope aspects were based on soil cryoturbation properties outlined by Bond and Sanborn (2006) and Smith et al. (2009) and are summarized in Table 7. Northeast-facing slopes are most likely to be affected by permafrost processes, while flat and south-facing slopes are at a low risk for ice-rich permafrost and cryoturbation. Figure 75 depicts ranked risks associated with slope aspect for the study area.

Table 7. Hazard risk rankings associated with different slope aspects for the Dawson region.

Slope Direction	Slope Orientation (°)	Hazard Risk Ranking
flat, south	0, 160-205	0
west	250-295	1
southwest	205-250	2
southeast, northwest	115-160, 295-340	4
east	70-115	7
north	340-25	8
northeast	25-70	9
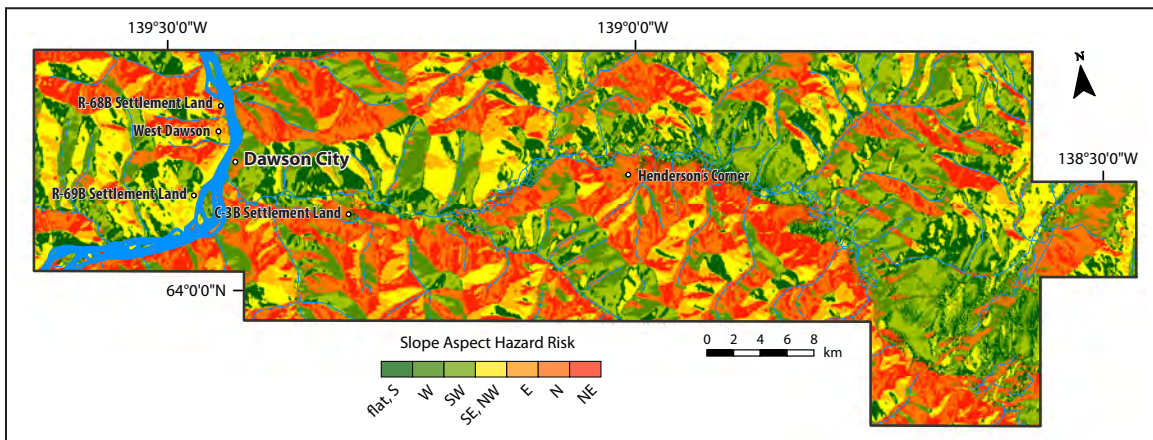
Figure 75. Hazard risk associated with slope aspect in the Dawson region.

PERMAFROST

Because case study sites in Dawson have demonstrated that permafrost thaw can impact surface stability, drainage patterns and subsequent hazard potential, it is important to integrate permafrost distribution into the risk ranking model. The permafrost probability model developed by Bonnaventure et al. (2012) and presented in Figure 39 (p. 44) was added directly to the hazard risk model. As described, this model reflects the spatial distribution of permafrost in Dawson and incorporates inversions and variability in air temperature and solar radiation locally. Hazard risk rankings associated with different permafrost probabilities are summarized in Table 8, and Figure 76 depicts ranked risks associated with permafrost for the study area.

Table 8. Hazard risk rankings associated with modelled permafrost probability for the Dawson region.

Permafrost Probability	Hazard Risk Ranking
0-0.1	0
0.1-0.2	1
0.2-0.3	2
0.3-0.4	3
0.4-0.5	4
0.5-0.6	5
0.6-0.7	6
0.7-0.8	7
0.8-0.9	8
0.9-1.0	9
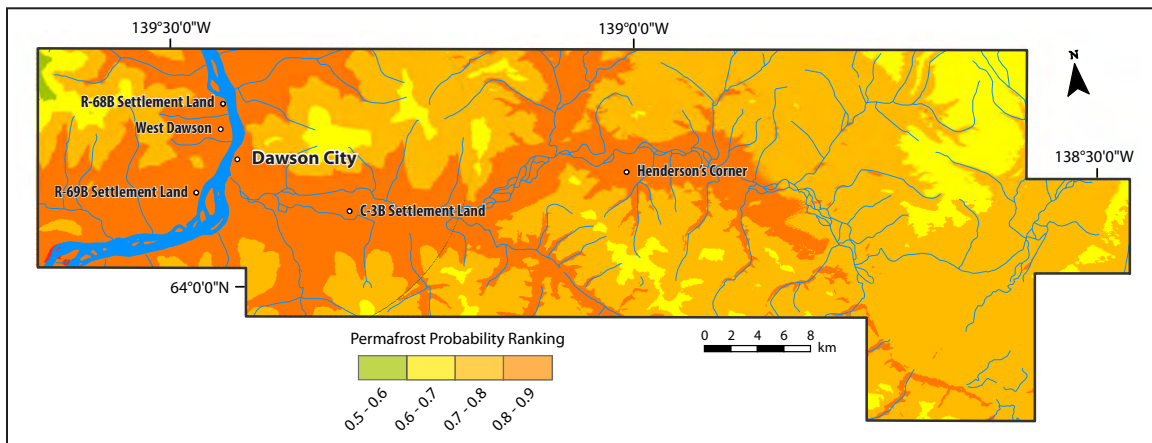
Figure 76. Hazard risk associated with permafrost probability in the Dawson region. Permafrost probabilities of 0.5-0.6 (equivalent to 50-60% likelihood of permafrost occurrence) are associated with lowest risk (green) while probabilities of 0.8-0.9 (equivalent to 80-90% likelihood of permafrost occurrence) are associated with highest risk (red).

SURFICIAL MATERIALS

Hazard risk rankings associated with surficial materials were determined based on a combination of material textures (fine or coarse-grained), material composition, landform shape (potential for drainage), landform location (slope aspect), and geological processes acting on the materials (i.e., permafrost, seasonal or regular inundation by water, and mass movement processes). In general, any geological units that were modified by landslides, thermokarst, ice-wedge polygons, or flooding were given the highest hazard risk ranking (9). Poorly-drained, fine-grained materials in valley-bottom positions were also given high risk rankings (6-9), while most hillslope and colluvial materials were given intermediate risk rankings (3-6). Geological units with the lowest risk ranking include fluvial and glaciofluvial landforms above the floodplain, and weathered bedrock and coarse-grained (rubble) colluvium overlying bedrock (0-2). Figure 77 depicts ranked risks associated with surficial materials for the study area.
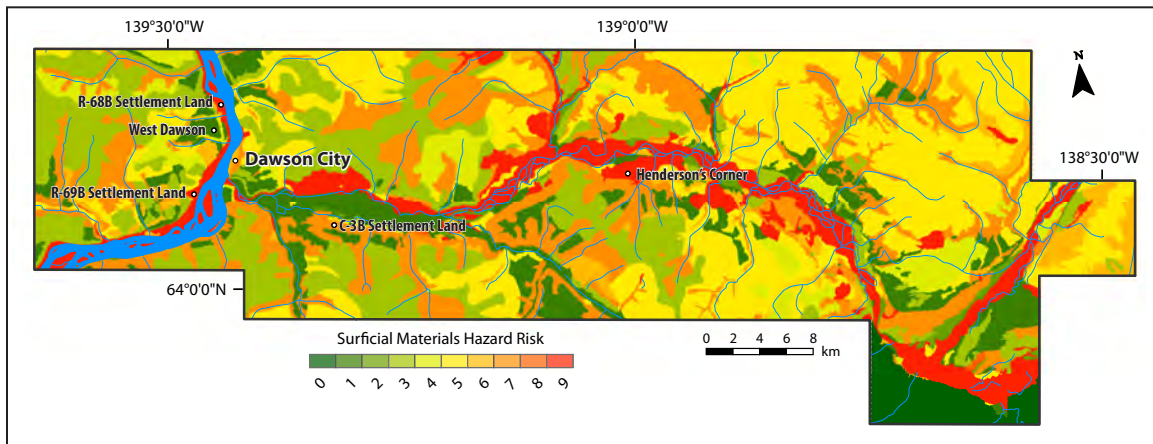
Figure 77. *Hazard risk associated with surficial materials in the Dawson region. Stable geological units (e.g., fluvial and glaciofluvial landforms above floodplains, weathered bedrock, coarse-grained colluvium overlying bedrock) are classified as lowest risk (dark green) while geological units affected by landslides, thermokarst, ice-wedge polygons or flooding are classified as highest risk (dark red).*

MODELLING

The model process employed to generate cumulative hazard risk rankings for the study area is depicted in Figure 78. Each of the input datasets described above and employed by the model was assigned a unique weighting to describe the degree to which they control cumulative hazard risk at a landscape scale. Slope angle (the steepness of the landscape) was given a weighting of 10%. Slope aspect (the degree to which the landscape is exposed to sunlight) was also given a weighting of 10%. Surficial materials (which also integrate flood risk) have a significant impact on landscape stability, and this input dataset was given a weighting of 50%. The likelihood of permafrost occurring on the landscape was given a relative weighting of 30% in the model, as aspects of permafrost distribution are also captured by the surficial materials input layer, and to some degree by the slope aspect input layer.

To calculate cumulative hazard risk for the study area, the weightings for each input layer were combined as follows:

Cumulative risk ranking = 0.1(slope angle risk) + 0.1(slope aspect risk) + 0.5(surficial materials risk) + 0.3(probability of permafrost)

Results of the cumulative risk ranking give a cumulative hazard risk ranking for each 30 m² pixel in the study area on a scale of 0 (low hazard risk) to 9 (high hazard risk). The cumulative hazard risk rankings were reclassified into four categories (low, moderate, moderately high, and high) that represent potential hazards due to permafrost, slope stability, surficial geology, and flooding in the map area (Table 9).
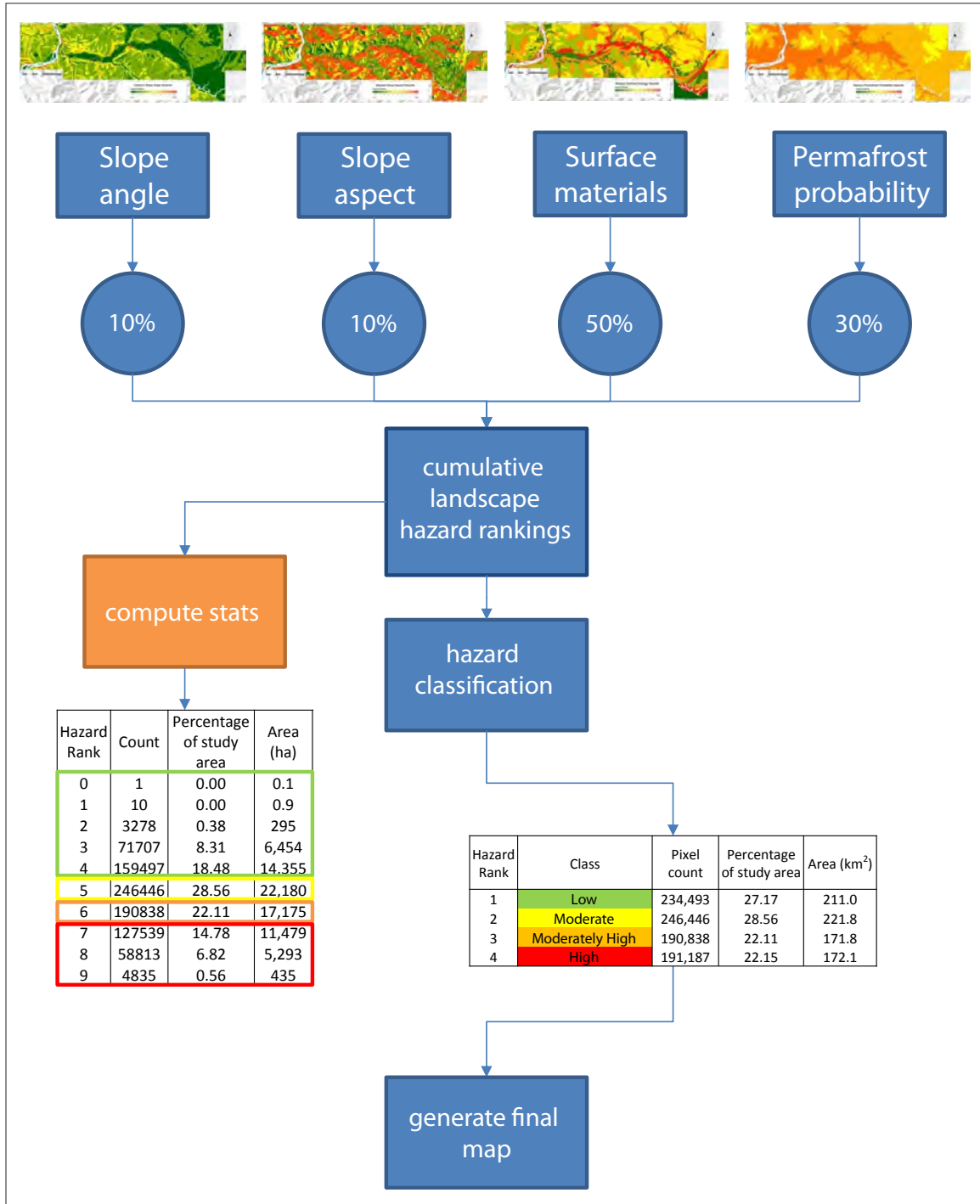
Figure 78. *Flowchart illustrating the process used to create the cumulative hazard risk map out of model input parameters for the Dawson region.*

Table 9. Hazard risk categories assigned to cumulative hazard risk rankings for the Dawson region. Cumulative hazard risk rankings refer to the combined risks of slope aspect, slope angle, permafrost probability, and surficial material risk.

Hazard Risk	Cumulative Hazard Risk Ranking
low	0, 1, 2, 3, 4
moderate	5
moderately high	6
high	7, 8, 9

HAZARD RISK RANKINGS FOR THE DAWSON REGION

Based on the modelling exercise described above, the study region was classified into four colour-coded categories representing hazard risk. These categories are characterized as follows:

Green: Low risk. Characterized by flat to gently sloped terrain, with south and west-facing slopes. Low-risk terrain is found above modern floodplains, and is often comprised of well-drained gravel or weathered bedrock surface materials. Low-risk terrain may contain permafrost, but it is less likely to be ice rich compared with more hazardous terrain.

Yellow: Moderate risk. Characterized by gentle to moderate slopes, and occurs more commonly on west and south-facing slopes. Moderate-risk terrain is found on the steep edges and cold aspects of low-risk landforms (i.e., fluvial terraces and north-facing, high-elevation slopes). Moderate-risk terrain also occurs in coarse-grained (gravel) surficial materials that may be affected by ice-rich permafrost (e.g., downtown Dawson).

Orange: Moderately high risk. Characterized by moderate to steep slopes, and east to north-facing slopes. Moderately high-risk terrain is found on all aspects in the study area and is common in narrow, steep-sided valleys and on more gentle slopes where permafrost is more likely to be present. The difference between moderate and moderately high-risk terrain in the study area is often based on changes in slope angle and slope aspect.

Red: High risk. Characterized by moderate to steep slopes and coldest east and north-facing slopes. Much of the high-risk terrain in the study area is defined by geological boundaries containing high-hazard processes such as landslides, thermokarst, and active floodplains that may be subject to flooding. High-risk terrain in the study area occurs in valley bottoms (flood risk and high permafrost probabilities), on steep north-facing valley slopes and at the base of these slopes, and where landslide processes have affected large areas of the landscape (i.e., bedrock slide on the north side of the Klondike Valley).

Based on the classifications described above, the hazard map for the Dawson study area is comprised of 862,964 individually classified 30 m^2 pixels in a map area measuring 776.7 km^2 (Figure 79, p. 89). Of these, 27% (211 km^2) are classified as low-risk terrain, 29% (221 km^2) are classified as moderate-risk terrain, 22% (172 km^2) are classified as moderately high-risk terrain, and 22% (172 km^2) are classified as high-risk terrain.

Hazard risk associated with each case study site aligns with site-specific findings. The West Dawson case study site is ranked as having low cumulative hazard risk. Based on GIS model inputs, risks

associated with slope angle and surficial geology are low. Case study findings confirm the presence of coarse-grained material (sand and gravel) in the area. Risks associated with slope aspect are moderately high, but because this parameter has a low contribution to cumulative hazard risk (10% weighting), its influence is not significant. There is a high probability of permafrost at the site, and permafrost presence was confirmed during case study investigations – frozen silty sand was found at the site, but it was only ~10 cm thick and therefore its effect on the stability of the ground upon thawing is likely to be minimal. (This is reflected in the low-risk ranking associated with surficial materials.) Although the West Dawson case study site has a low cumulative hazard risk, the presence of permafrost necessitates that the thickness of the silty sand layer overlying the gravel be evaluated on a case by case basis prior to development, and that appropriate mitigation techniques be employed if the silty sand layer is thicker than the active layer. Deep permafrost may or may not contain large amounts of ground ice, which would require deep drilling and coring to confirm.

The case study site located on the C-3B Settlement Land is largely classified as having high cumulative hazard risk, although areas along the north side of the site (generally in the forested area) have low cumulative hazard risk. Input layers to the cumulative hazard risk ranking indicate that risks associated with slope angle are moderate, but risks associated with slope aspect and surficial geology are moderate or high. Permafrost probability modelling indicates there is a high probability of permafrost at this site. Indeed, case study investigations found evidence of permafrost in undisturbed areas of the site (below the forest), and a supra-permafrost talik (an area of permanently unfrozen ground overlying existing permafrost, but underlying the active layer) in disturbed areas. Results align with a high cumulative hazard risk, as findings indicate that disturbance in the area leads to rapid permafrost degradation and notable settlement of the ground, which is likely followed by a period of slower permafrost degradation with less noticeable settlement effects. Poor drainage may be problematic during permafrost degradation, but eventually, thaw rates will likely decline and the ground will become relatively stable (with potential improvements in drainage), albeit with a new thermal regime. For other high-risk areas with surficial material, permafrost and hydrological conditions comparable to the C-3B Settlement Lands, notable permafrost degradation is to be expected following land disturbance and/or clearing, and it is recommended that mitigation techniques that can accommodate ground settlement be employed before construction of building infrastructure. Additionally, development should integrate appropriate drainage techniques to reduce flood-related hazards.

The case study site located on the R-68B Settlement Land is largely classified as having high cumulative hazard risk. The site is located on the floodplain of the Yukon River and is at risk of flooding, which contributes to its high-risk ranking. The risk of hazards associated with slope angle is low, but moderate to high risk is associated with aspect in this area. Permafrost probability modelling indicates a high likelihood of permafrost presence (which was confirmed by field observations that found near-surface permafrost throughout the area, with the exception of some small water channels). Although thaw settlement associated with permafrost at the site is low to moderate, development at this site and in comparable areas would require mitigation techniques to accommodate permafrost thaw, and must integrate flooding as the major hazard in the area. It is likely that site conditions pre-settlement of the Dawson townsite were comparable to those at the R-68B Settlement Lands.

The case study at the R-69B Settlement Land is mainly classified as high risk. This is a result of moderate to high risk associated with most input parameters – there is a moderate to high risk associated with surficial material characteristics, a high probability of permafrost presence, and some high-risk areas associated with slope angle adjacent to the site. Slope aspect is ranked as having a low to moderate risk at this site. The high cumulative hazard risk ranking for this area is

consistent with the position of this site on the floodplain of the Yukon River, and with the presence of permafrost, which was confirmed through field observations. As with the C-3B Settlement Lands, this site exhibits the effects of land clearing and disturbance on permafrost degradation, whereby areas that were cleared in the past exhibit supra-permafrost taliks, or a deep active layer. Field investigations confirmed moderate thaw settlement potential and poor drainage associated with local depressions. At this site, and areas with comparable features, it is recommended that development in undisturbed zones be avoided due to the presence of near-surface, ice-rich permafrost and poor drainage. If vegetation cover is removed or the ground surface is otherwise disturbed, permafrost thaw will occur quickly, although it may eventually stabilize. However, drainage will continue to pose a risk at this site, and mitigation techniques associated with proper drainage and permafrost thaw and settlement will be required should development take place here or at a comparable site.

The cumulative hazard risk ranking for downtown Dawson ranges from moderate to high. High risk areas are concentrated along the base of the steep slopes along the eastern and northern edges of the community. Aspect also plays a role in establishing hazard risk for this area. In terms of surficial material and permafrost risk, moderate and moderately high-risk areas are associated with floodplain materials that are ice-rich. Field investigations and observations of affected infrastructure confirm the presence of moderately ice-rich permafrost underlying Dawson City. Although situated on the floodplain of the Yukon River and subject to major floods in the past, the dike protecting the community reduces the risk of flood-related hazards.

The Henderson's Corner area, which hosts a polygonal network of ice wedges, is also largely ranked as high risk, although there are some low-risk areas close to the junction of the access road and the Klondike Highway. There is a high risk of permafrost probability at this site, exhibited by the ice wedge polygons that have developed, and a high risk of hazards associated with surficial materials. As with other sites in the Dawson region, land clearing has affected the stability of permafrost, and it is recommended that forest cover be preserved wherever possible. Additionally, mitigation techniques associated with reducing permafrost thaw impacts on infrastructure, as well as mitigation techniques suitable for sites with poor drainage should be employed, if additional development takes place at this or comparable sites.

LIMITATIONS

The Dawson hazards map is meant to be used as a preliminary assessment of potential ground conditions in the study area, and does not replace detailed on-site investigations. Cumulative hazard rankings are highly dependent on rankings assigned to surficial material deposits, and both the boundaries of the units and the materials assigned to those units are highly subjective and based on limited field checking conducted during surficial geological mapping studies.

Additionally, flood hazard mapping does not yet exist for the study area and flood potential is based on geological units mapped as active floodplains or as being subject to periodic inundation. These units likely represent areas that are subject to regular annual or decadal flooding, but are unlikely to represent the highest and most catastrophic floods with lower recurrence intervals.

Finally, the resolution of this map is limited by the 30 m^2 pixel size used to calculate slope, aspect, and permafrost probability, and the 1:25 000-scale mapping used to identify surficial materials and landforms. Local variations in all model inputs should be expected, and will be more pronounced for surface materials and permafrost probability.

It is important to note that cumulative hazard rankings are based on general observations of surficial materials, drainage, slope angle, vegetation and the presence of permafrost landforms, as well as subsurface information provided by ERT and GPR profiles, drilling and probing of

permafrost, and textural analyses of surface material and borehole samples. This has resulted in a projected risk ranking that will require geotechnical and/or engineering analyses to quantify. The higher the hazard-risk ranking, the more notable and potentially problematic the hazard risk at a given location is likely to be. Nonetheless, a moderate, moderately high or high-hazard risk ranking does not preclude the possibility of development, should suitable engineering and mitigation techniques be employed. Appendix E describes of types of foundation techniques that may be suitable for buildings in permafrost environments similar to those found in the Dawson region, and may assist in mitigating permafrost thaw.

GENERATING ACTION FROM SCIENCE

The knowledge and data generated by the Dawson hazards mapping project can be used to inform planning and policy development and establish a baseline from which future science can be generated. It is the hope of the authors that the information contained herein informs planning and decision-making processes in the Dawson area.

This project has contributed to the assessment of vulnerability for the Dawson area. In particular, this project has characterized the local landscape and assessed local hazards, while advancing our understanding of potential climate change impacts in the region. This information may serve as a basis for evaluating how community infrastructure, security and well-being may be influenced by climate variability, and how the community might take action to respond. By integrating variability into decision-making through multiple scenarios, robust and responsive adaptation strategies can be developed. In this way, the science of hazards assessment is an important foundation from which to build action.
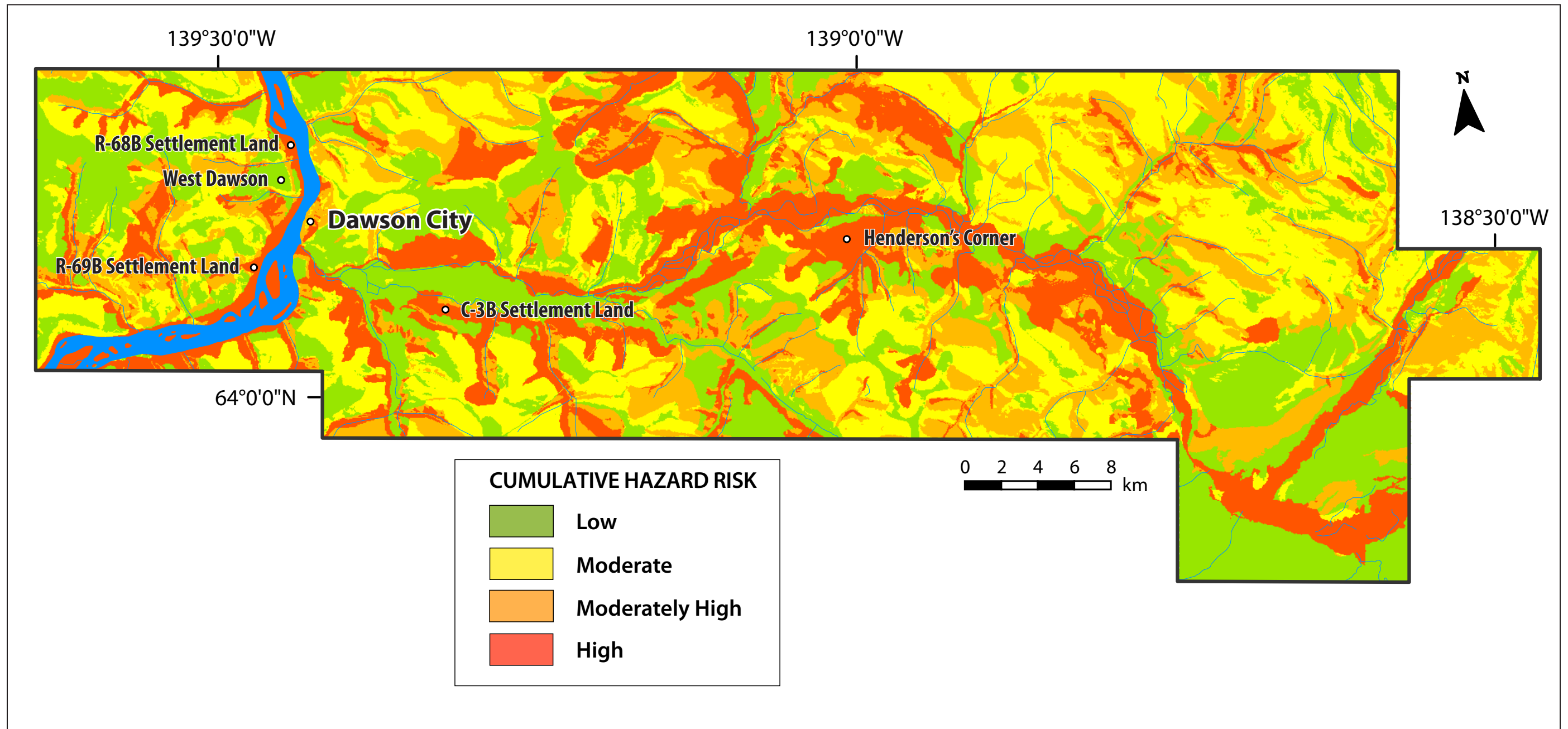
Figure 79. *Map depicting hazard risk ranking for the Dawson area (see Figure 1 for location of the map boundary). A larger fold-out version of this map is included in the map pocket in the back of this report.*

REFERENCES

Balco, G. and Rovey, C., 2010. Absolute chronology for major Pleistocene advances of the Laurentide Ice Sheet. Geology, vol. 38, p. 795.

Barendregt, R.W., Enkin, R.J., Duk-Rodkin, A. and Baker, J., 2010. Paleomagnetic evidence for multiple late Cenozoic glaciations in the Tintina Trench, west-central Yukon, Canada. Canadian Journal of Earth Science, vol. 47, p. 987-1002.

Beasley, E., 2010. Community Flood Planning: An assessment of hazard and response in the Dawson City region, Yukon, Canada, 62 p.

Bond, J.D., 1997. Late Cenozoic history of McQuesten map area, Yukon Territory, with applications to placer gold research. MSc Thesis, University of Alberta, Edmonton, AB, 173 p.

Bond, J.D. and Sanborn, P.T., 2006. Morphology and geochemistry of soils formed on colluviated weathered bedrock: Case studies from unglaciated upland slopes in west-central Yukon. Yukon Geological Survey, Open File 2006-19.

Bonnaventure, P.P. and Lewkowicz, A.G., 2013. Impacts of mean annual air temperature change on a regional permafrost probability model for the southern Yukon and northern British Columbia, Canada. The Cryosphere, vol. 7, p. 935-946, doi:10.5194/tc-7-935-2013.

Bonnaventure, P.P., Lewkowicz, A.G., Kremer, M. and Sawada, M., 2012. A regional permafrost probability model for the southern Yukon and northern British Columbia, Canada. Permafrost and Periglacial Processes, vol. 23, p. 52-68, doi:10.1002/ppp.1733.

Brideau, M.-A., Stead, D., Stevens, V., Roots, C., Lipovsky, P. and Von Gaza, P., 2007. The Dawson City landslide (Dawson map area NTS 116B/3), central Yukon. *In:* Yukon Exploration and Geology 2006, D.S. Emond, L.L. Lewis and L.H. Weston (eds.), Yukon Geological Survey, p. 123-137.

Brideau, M.-A., Stead, D., Roots, C. and Lipovsky, P.S., 2012. Ongoing displacement monitoring at the Dawson City landslide (Dawson map area NTS 116B/3). *In:* Yukon Exploration and Geology 2011, K.E. MacFarlane and P.J. Sack, (eds.), Yukon Geological Survey, p. 17-26.

Brown, R.J.E., 1963. Influence of vegetation on permafrost. First International Conference on Permafrost, Lafayette, PA, November 1963.

Brown, R.J.E. and Péwé, T.L., 1973. Distribution of permafrost in North America and its relationship to the environment: A review, 1963-1973. Second International Conference on Permafrost, Yakutsk, USSR, July 1973.

Brown, J., Ferrians, Jr., O.J., Heginbottom, J.A. and Melnikov, E.S. (eds.), 1997. Circum-Arctic map of permafrost and ground-ice conditions. Washington, DC: U.S. Geological Survey in Cooperation with the Circum-Pacific Council for Energy and Mineral Resources. Circum-Pacific Map Series CP-45, scale 1:10,000,000, 1 sheet.

Burn, C.R., 1994. Permafrost, tectonics, and past and future regional climate change, Yukon and adjacent Northwest Territories. Canadian Journal of Earth Sciences, vol. 31, p. 182-191.

Calmels, F.C., Froese, D.G. and Clavano, W.R., 2012. Cryostratigraphic record of permafrost degradation and recovery following historic (1898-1992) surface disturbances in the Klondike region, central Yukon Territory. Canadian Journal of Earth Sciences, vol. 49, p. 938-952.

Coates, J., 2008. The Impact of Forest Fire on Permafrost Slopes, Klondike Area, Yukon Territory. Unpublished MSc Thesis, Univeristy of Ottawa, Ottawa, ON, 208 p.

Colpron, M. (compiler), 2014. Update of the Yukon bedrock geology map. Yukon Geological Survey, http://www.geology.gov.yk.ca/update_yukon_bedrock_geology_map.html.

Consortium for Climate Risk in the Urban Northeast (CCRUN), 2011. What methods do scientists use to make projections about future climate change and its impacts? CCRUN, Fact Sheet #4, Columbia University, New York, NY, 3 p. [http://ccrun.org/ccrun_files/attached_files/FactSheet4.pdf]. Accessed September, 2014.

Darrow, M.M., Huang, S.L., Shur, Y. and Akagawa, S., 2008. Improvements in frost heave laboratory testing of fine-grained soils. Journal of Cold Regions Engineering, vol. 22, p. 65-78.

De Grandpré, I., Fortier, D. and Stephani, E., 2012. Degradation of permafrost beneath a road embankment enhanced by heat advected in groundwater. Canadian Journal of Earth Sciences, vol. 49, p. 953-962, doi: 10.1139/e2012-018.

Dufresne, M.B., Morison, S.R. and Nesbitt, B.E., 1986. Evidence of hydrothermal alteration in White Channel sediments and bedrock of the Klondike area, west-central Yukon. Indian and Northern Affairs, Exploration and Geological Services Division, Yukon Geology, vol. 1, p. 44-49.

Duk-Rodkin, A., 1996. Surficial Geology NTS 116B&C, Dawson, Yukon Territory. Geological Survey of Canada, Open File 3288, 1:250 000 scale.

Duk-Rodkin, A., Barendregt, R.W., White, J.M. and Singhroy, V.H., 2001. Geological evolution of the Yukon River: Implications for placer gold. Quaternary International, vol. 82, p. 5-31.

Duk-Rodkin, A., Barendregt, R.W. and White, J.M., 2010. An extensive late Cenozoic terrestrial record of multiple glaciations preserved in the Tintina Trench of west-central Yukon: Stratigraphy, paleomagnetism, paleosols, and pollen. Canadian Journal of Earth Science, vol. 47, p. 1003-1028.

Environment Canada, 2014a. Historical Climate Data. Environment Canada, Ottawa, Ontario. [http://climate.weather.gc.ca/index_e.html]. Accessed January, 2015.

Environment Canada, 2014b. Climate Trends and Variations. Environment Canada, Ottawa, Ontario. [http://ec.gc.ca/adsc-cmda/default.asp?lang=En&n=F3D25729-1]. Accessed January, 2015.

Fortier, D. and Allard, M., 2004. Late Holocene syngenetic ice-wedge polygons development, Bylot Island, Canadian Arctic Archipelago. Canadian Journal of Earth Sciences, vol. 41, p. 997-1012.

Fraser, T., 1995. On the nature and origin of muck deposits, Klondike District, Yukon Territory. Unpublished MSc thesis, Carleton University, Ottawa, Canada, 203 p.

Fraser, T.A. and Burn, C.R., 1997. On the nature and origin of "muck" deposits in the Klondike area, Yukon Territory. Canadian Journal of Earth Sciences, vol. 34, p. 1333-1344.

French, H.M., 1983. The Periglacial Environment. Longman Group Limited, London, 309 p.

French, H., 2007. The Periglacial Environment, 3rd edition. John Wiley and Sons, West Sussex, England, 478 p.

French, H. and Shur, Y., 2010. The principles of cryostratigraphy. Earth Science Reviews, vol. 101, p. 190-206.

Froese, D.G. and Hein, F.J., 1996. Sedimentology of a high level terrace placer gold deposit. *In:* Yukon Quaternary Geology, Volume 1. W.P. Lebarge (ed.), Indian and Northern Affairs Canada, Exploration and Geological Services Division, p. 13-26.

Froese, D.G. and Schweger, C.E., 1999. Upper Yukon basin loess: Reconstructing the timing and nature of glacial-interglacial transitions in the western Yukon. *In:* CANQUA meeting, August 23-27, 1999. Canadian Quaternary Association, Program and Abstracts, p. 24.

Froese, D.G. and Westgate, J.A., 2001. Klondike Goldfields Stratigraphy. *In:* D.G. Froese, A. Duk-Rodkin and J.D. Bond (eds.), CANQUA 2001 Field Guide to Quaternary Research in Central and Western Yukon Territory; Occasional Papers in Earth Sciences No. 2, Heritage Branch, Government of Yukon, p. 44-47.

Froese, D.G., Barendegt, R.W., Enkin, R.J. and Baker, J., 2000. Paleomagnetic evidence for multiple late Pliocene-early Pleistocene glaciations in the Klondike area, Yukon Territory. Canadian Journal of Earth Sciences, vol. 37, p. 863-867.

Froese, D.G., Westgate, J.A., Reyes, A.V., Enkin, R.J. and Preece, S.J., 2008. Ancient permafrost and a future, warmer Arctic. Science, vol. 321, p. 1648.

Froese, D.G., Zazula, G.D., Westgate, J.A., Preece, S.J., Sanborn, P.T., Reyes, A.V. and Pearce, N.J.G., 2009. The Klondike goldfields and Pleistocene environments of Beringia. GSA Today, vol. 19, p. 4-10.

Gartner Lee Limited, 2003. Yukon Groundwater and Ground Source Heat Potential Inventory. Prepared for Energy Solutions Centre Inc., Report #GLL 22-680, 258 p.

Global Terrestrial Network for Permafrost, 2013. [http://www.gtnp.org/]. Accessed January, 2015.

Gordey, S.P. and Ryan, J.J., 2005. Geology, Stewart River Area (115O and part of 115J), Yukon Territory. Geological Survey of Canada, Open File 4970, scale 1:250 000.

Hauck, C., Isaksen, K., Vonder Mühll, D. and Sollid, J.L., 2004. Geophysical surveys designed to delineate the altitudinal limit of mountain permafrost: An example from Jotunheimen, Norway. Permafrost and Periglacial Processes, vol. 15, p. 191-205, doi:10.1002/ppp.493.

Haug, G.H., Ganopolski, A., Sigman, D.M., Rosell-Mele, A., Swann, G.E.A., Tiedemann, R., Jaccard, S.L., Bollmann, J., Maslin, M.A. and Leng, M.J., 2005. North Pacific seasonality and the glaciation of North America 2.7 million years ago. Nature, vol. 433, p. 821-825.

Heginbottom, J.A., Dubreuil, M.A. and Harker, P.T., 1995. Permafrost Map of Canada. *In:* The National Atlas of Canada, 5th Edition, (1978-1995), published by Natural Resources Canada, sheet MRC 4177, 1: 7 500 000 scale.

Hidy, A.J., Gosse, J.C., Froese, D.G., Bond, J.D. and Rood, D.H., 2013. A latest Pliocene age for the earliest and most extensive Cordilleran Ice Sheet in northwestern Canada. Quaternary Science Reviews, vol. 61, p. 77-84.

Hilbich, C., Hauck, C., Hoelzle, M., Scherler, M., Schudel, L., Voelksch, I., Vonder Muehll, D. and Maüsbacher, R., 2008. Monitoring mountain permafrost evolution using electrical resistivity tomography: a 7-year study of seasonal, annual, and long-term variations at Schilthorn, Swiss Alps. Journal of Geophysical Research-Earth Surface, vol. 113, F01S90, doi:10.1029/2007JF000799.

Hilbich, C., Marescot, L., Hauck, C., Loke, M.H. and Maüsbacher, R., 2009. Applicability of electrical resistivity tomography monitoring to coarse blocky and ice-rich permafrost landforms. Permafrost and Periglacial Processes, vol. 20, p. 269-284, doi:10.1002/ppp.652.

Howes, D.E. and Kenk, E., 1997. Terrain Classification System for British Columbia (Version 2). Recreational Fisheries Branch, Ministry of Environment and Surveys and Resource Mapping Branch, Ministry of Crown Lands, Province of British Columbia, Victoria, BC, 102 p.

Hughes, O.L., Rampton, V.A., Rutter, N.W., 1972. Quaternary geology and geomorphology, southern and central Yukon. *In:* Guidebook for field excursion A11, XXIV International Geological Congress, Montreal, QC, p. 30-36.

Huntington, H. and Weller, G., 2005. Chapter 1: An Introduction to the Arctic Climate Impact Assessment. *In:* Arctic Climate Impact Assessment Scientific Report, C. Symo, L. Arris and B. Heal (eds.), Cambridge University Press, p. 1-20.

Instanes, A., 2003. Climate change and possible impacts on Arctic infrastructure. Proceedings of the Eighth International Conference on Permafrost, Zurich, Switzerland, June 2003, p. 461-466.

Intera Environmental Consultants Ltd. (Intera), 1975. Groundwater Management Study of the Yukon Territory. Prepared for Department of Indian Affairs and Northern Development, Controller of Water Rights, Whitehorse, YT.

Intergovernmental Panel on Climate Change (IPCC), 2015. Fifth Assessment Report. IPCC, Geneva, Switzerland. [https://www.ipcc.ch/index.htm]. Accessed January, 2015.

Inukshuk Planning and Development, 2000. Tr'ondëk Hwëch'in Dawson Subdivisions Feasibility Study. Prepared for the Tr'ondëk Hwëchin First Nation.

Jackson, L.E., Jr., Froese, D.G., Huscroft, C.A., Nelson, F.E., Westgate, J.A., Telka, A.M., Shimamura, K. and Rotheisler, P.N., 2009. Surficial Geology and Late Cenozoic History of the Stewart River and Northern Stevenson Ridge Map Areas, West Central Yukon Territory. Geological Survey of Canada Open File 6059, 83 p.

Janke, J.R., 2005. Modelling past and future alpine permafrost distribution in the Colorado Front Range. Earth Surface Processes and Landforms, vol. 30, p. 1495-1508, doi: 10.1002/esp.1205.

Janowicz, R., 2002. Tr'ondëk Heritage Site Hydrological Study and Floodplain Analysis. Prepared for Tr'ondëk Heritage Site Steering Committee, 40 p.

Janowicz, R., 2008. Apparent recent trends in hydrologic response in permafrost regions of northwest Canada. Hydrology Research, vol. 39, p. 267-275.

Jorgenson, M.T. and Osterkamp, T.E., 2005. Response of boreal ecosystems to varying modes of permafrost degradation. Canadian Journal of Forest Research, vol. 35, p. 2100-2111.

Kanevskiy, M.Z., Shur, Y., Fortier, D., Jorgenson, M.T. and Stephani, E., 2011. Cryostratigraphy of late Pleistocene syngenetic permafrost (yedoma) in northern Alaska, Itkillik exposure. Quaternary Research, vol. 75, p. 584-596, doi: 10.1016/j.yqres.2010.12.003.

Kneisel, C., Hauck, C. and Vonder Mühll, D., 2000. Permafrost below the timberline confirmed and characterized by geoelectrical resistivity measurements, Bever Valley, eastern Swiss Alps. Permafrost and Periglacial Processes, vol. 11, p. 295-304, doi:10.1002/1099-1530(200012)11:4<295::AID-PPP353>3.0.CO;2-L.

Kneisel, C., Hauck, C., Fortier, R. and Moorman, B., 2008. Advances in geophysical methods for permafrost investigations. Permafrost and Periglacial Processes, vol. 19, p. 157-178.

Kotler, E. and Burn, C.R., 2000. Cryostratigraphy of the Klondike "muck" deposits, west-central Yukon Territory. Canadian Journal of Earth Sciences, vol. 37, p. 849-861.

Kudryavtsev, V.A., 1979. Method of permafrost survey. Moscow State University Publication, Moscow, Russia.

Lewkowicz, A.G., 1992. Factors influencing the distribution and initiation of active-layer detachment slides on Ellesmere Island, Arctic Canada. Periglacial Geomorphology, John Wiley and Sons (eds.), p. 223-250.

Lewkowicz, A.G. and Bonnaventure, P.P., 2011. Equivalent elevation: a method to incorporate variable lapse rates into mountain permafrost modeling. Permafrost and Periglacial Processes, vol. 22, p. 153-162, doi: 10.1002/ppp.720, 2011.

Lewkowicz, A.G. and Ednie, M., 2004. Probability mapping of mountain permafrost using the BTS method, Wolf Creek, Yukon Territory, Canada. Permafrost and Periglacial Processes, vol. 15, p. 67-80.

Lewkowicz, A.G. and Harris, C., 2005. Frequency and magnitude of active-layer detachment failures in discontinuous and continuous permafrost, northern Canada. Permafrost and Periglacial Processes, vol. 16, p. 115-130.

Lewkowicz, A.G., Etzelmüller, B.E. and Smith, S.L., 2011. Characteristics of discontinuous permafrost from ground temperature measurements and electrical resistivity tomography, southern Yukon, Canada. Permafrost and Periglacial Processes, vol. 22, p. 320-342.

Lipovsky, P.S., Coates, J., Lewkowicz, A.G. and Trochim, E., 2006. Active layer detachments following the summer 2004 forest fires near Dawson City, Yukon. *In:* Yukon Exploration Geology 2005, D.S. Emond, G.D. Bradshaw, L.L. Lewis and L.H. Weston (eds.), Yukon Geological Survey, p. 175-194.

Livingstone, J.M., Smith, D.G., Froese, D.G. and Hugenholtz, C.H., 2009. Floodplain stratigraphy of the ice jam dominated middle Yukon River: A new approach to long term flood frequency. Hydrological Processes, vol. 23, p. 357-371.

Lowey, G.W., 2004. Placer geology of the Stewart River (115N&O) and part of the Dawson (116B&C) map areas, west-central Yukon, Canada. Yukon Geological Survey, Bulletin 14, 275 p.

Lunardini, V.J., 1994. Heterogenetic and syngenetic growth of permafrost. Ground Freezing '94, Proceedings of the Seventh International Symposium on Ground Freezing, Nancy, France, p. 361-373.

McConnell, R.G., 1900. Preliminary Report on the Klondike Gold Fields, Yukon District, Canada. Geological Survey of Canada, Publication No. 687, 44 p., 1 map.

McConnell, R.G., 1905. Report on Klondike gold fields. *In:* Annual Report for 1901, Vol. XIV, Part B, Geological Survey of Canada, Publication No. 884, p. 1-71.

McKenna, K., 2013. Air photo analysis of Sunnydale (Dawson, Yukon) agriculture development and permafrost history. Agriculture Branch, Department of Energy Mines and Resources, Government of Yukon, 6 p.

McKenna, K. and Lipovsky, P., 2014. Surficial geology, Dawson region, Yukon (parts of NTS 1150/14 and 15 and 116B/1, 2, 3 and 4. Yukon Geological Survey, Open File 2014-12.

McKillop, R., Turner, D., Johnston, K. and Bond, J., 2013. Property-scale classification of surficial geology for soil geochemical sampling in the unglaciated Klondike Plateau, west-central Yukon. Yukon Geological Survey, Energy, Mines and Resources, Government of Yukon, Open File 2013-15, 85 p.

Milner, M.W., 1977. Geomorphology of the Klondike placer goldfields, Yukon Territory. Department of Indian Affairs and Northern Development, Exploration and Geological Services Division, Yukon, 157 p.

Morison, S.R., 1985. Sedimentology of the White Channel placer deposits, Klondike area, west-central Yukon. MSc thesis, University of Alberta, Edmonton, AB, 298 p.

Morison, S.R. and Hein, F.J., 1987. Sedimentology of the White Channel Gravels, Klondike area, Yukon Territory: Fluvial deposits in a confined valley. *In:* Recent developments in fluvial sedimentology, F.G. Ethridge, R.M. Flores and M.D. Harvey (eds.), Society of Economic Paleontologists and Mineralogists, Special publication 39, p. 205-215.

Muhs, D.R. and Budahn, J.R., 2006. Geochemical evidence for the origin of late Quaternary loess in central Alaska. Canadian Journal of Earth Science, vol. 43, p. 323-337.

Muhs, D.R., Ager, T.A., Bettis, E.A., III, McGeehin, J., Been, J.M., Begét, J.E., Pavich, M.J., Stafford, T.W., Jr. and Stevens, D.A.S.P., 2003. Stratigraphy and paleoclimatic significance of late Quaternary loess-paleosol sequences of the last interglacial-glacial cycle in central Alaska. Quaternary Science Reviews, vol. 22, p. 1947-1986.

Murton, J.B. and French, H.M., 1994. Cryostructures in permafrost, Tuktoyaktuk coastlands, western arctic Canada. Canadian Journal of Earth Sciences, vol. 31, no. 4, p. 737-747.

Naeser, N.D., Westgate, J.A., Hughes, O.L. and Péwé, T.L., 1982. Fission-track ages of late Cenozoic distal tephra beds in the Yukon and Alaska. Canadian Journal of Earth Sciences, vol. 19, p. 2167-2178.

Natural Resources Canada, 2013. Earthquake Resources. [http://www.seismescanada.rncan. gc.ca/resources-eng.php]. Accessed December, 2014.

Nebojša, N., Davidson, O., Davis, G., Grübler, A., Kram, T., La Rovere, E.L., Metz, B., Morita, T., Pepper, W., Pitcher, H., Sankovski, A., Shukla, P., Swart, R., Watson, R. and Dadi, Z., 2000. Emissions Scenarios: A Special Report of Working Group III of Intergovernmental Panel on Climate Change. Intergovernmental Panel on Climate Change, Geneva, Switzerland, 27 p.

Nelson, F.E., Anisimov, O.A. and Shiklomanov, N.I., 2002. Climate change and hazard zonation in the circum-Arctic permafrost regions. Natural Hazards, vol. 26, p. 203-225.

Northern Climate ExChange (NCE), 2011. Dawson City Climate Change Adaptation Plan. Yukon Research Centre, Yukon College, Whitehorse, YT, 64 p.

Noson, L., 2002. Hazard Mapping and Risk Assessment. *In:* Regional Workshop on Best Practices in Disaster Mitigation, Bali, Indonesia, September 24-26, 2002; Asian Disaster Preparedness Center (ADPAC), p. 69-94.

O'Donnell, J.A., Jorgenson, M.T., Harden, J.W., McGuire, A.D., Kanevskiy, M.Z. and Wickland, K.P., 2012. The effects of permafrost thaw on soil hydrologic, thermal and carbon dynamics in an Alaskan peatland. Ecosystems, vol. 15, p. 213-229.

Page, A., 2009. A topographic and photogrammetric study of rock glaciers in the southern Yukon Territory. Unpublished MSc thesis, Department of Geography, University of Ottawa, 160 p.

Pecsi, M., 1990. Loess is not just the accumulation of dust. Quaternary International, vol. 7-8, p. 1-21.

Preece, S.J., Westgate, J.A., Alloway, B.V. and Milner, M.W., 2000. Characterization, identity and distribution and source of late Cenozoic tephra beds in the Klondike district, Yukon. Canadian Journal of Earth Sciences, vol. 37, p. 983-996.

Preece, S.J., Westgate, J.A., Froese, D.G., Pearce, N.J.G. and Perkins, W.T., 2011. A catalogue of late Cenozoic tephra beds in the Klondike goldfields and adjacent areas, Yukon Territory. Canadian Journal of Earth Sciences, vol. 48, p. 1386-1418.

Purves, M., 2010. Climate Change in the Yukon, Updated Observations. Yukon Weather Centre Internal Report YWC-10-110, 81 p. Private correspondence from the author January 24, 2011.

Schweger, C.E., White, J.M. and Froese, D.G., 1999. Preglacial, and interglacial pollen records from central and northern Yukon: 3 Ma of forest history. *In:* CANQUA meeting, August 23-27, 1999. Canadian Quaternary Association, Program and Abstracts, p. 67.

Shur, Y.L. and Jorgenson, M.T., 2007. Patterns of permafrost formation and degradation in relation to climate and ecosystems. Permafrost and Periglacial Processes, vol. 18, doi:lO.l002!ppp. 582.

Smith, M.W. and Riseborough, D.W., 2002. Climate and the limits of permafrost: a zonal analysis. Permafrost and Periglacial Processes, vol. 13, p. 1-15.

Smith, C.A.S., Meikle, J.C. and Roots, C.F. (eds.), 2004. Ecoregions of the Yukon Territory: Biophysical Properties of Yukon Landscapes. PARC Technical Bulletin 04-01, Summerland, British Columbia, Agriculture and Agri-Food Canada, 313 p.

Smith, C.A.S., Sanborn, P.T., Bond, J.D. and Frank, G., 2009. Genesis of turbic cryosols on north-facing slopes in a dissected, unglaciated landscape, west-central Yukon Territory. Canadian Journal of Soil Science, vol. 89, p. 611-622.

Scenarios Network for Alaska and Arctic Planning (SNAP), 2013. [http://www.snap.uaf.edu/about.php]. Accessed September, 2014.

Stephani, E., Fortier, D. and Shur, Y., 2010. Applications of cryofacies approach to frozen ground engineering – Case study of a road test site along the Alaska Highway (Beaver Creek, Yukon, Canada). GEO2010: 63rd Canadian Geotechnical Conference and 6th Canadian Permafrost Conference, Calgary, Canada.

Stephani, E., Fortier, D., Shur, Y., Fortier, R., Doré, G. and Walsh, R., 2014. A geosystems approach to permafrost investigations for engineering applications, an example from a road stabilization experiment, Beaver Creek, Yukon, Canada. Cold Region Science and Technology, vol. 100, p. 20-35.

Tarnocai, C., Smith, C.A.S. and Hughes, O.L., 1985. Soil development on Quaternary deposits of various ages in central Yukon Territory. *In:* Current Research, part A. Geological Survey of Canada, Paper 85-1A, p. 229-238.

Tempelman-Kluit, D., 1980. Evolution of physiography and drainage in southern Yukon. Canadian Journal of Earth Sciences, vol. 17, p. 1189-1203.

Tempelman-Kluit, D.J., 1982. White Channel Gravel of the Klondike. *In:* Yukon Exploration and Geology 1979-1980. Indian Affairs and Northern Development, Exploration and Geologic Services Division, Yukon, p. 7-31.

Tr'ondëk Hwëch'in, 2014. About Us. [http://www.trondek.ca/aboutus.php]. Accessed December, 2014.

Wahl, H.E., Fraser, D.B., Harvey, R.C. and Maxwell, J.B., 1987. Climate of Yukon. Climatological Studies Number 40, Ottawa, Ontario, Atmospheric Environment Service, Environment Canada, 233 p.

Warren, F.J. and Lemmen, D.S. (eds.), 2014. Canada in a Changing Climate: Sector Perspectives on Impacts and Adaptation. Government of Canada, Ottawa, ON, 286 p.

Water Survey of Canada, 2015. National Water Quantity Survey Program. Environment Canada, https://wateroffice.ec.gc.ca.

Westgate, J.A., Stemper, B.A. and Péwé, T.L., 1990. A 3 m.y. record of Pliocene-Pleistocene loess in interior Alaska. Geology, vol. 18, p. 858-861.

Westgate, J.A., Sandhu, A.S., Preece, S.J. and Froese, D.G., 2003. Age of the gold-bearing White Channel Gravel, Klondike district, Yukon. *In:* Yukon Exploration and Geology 2002, D.S. Emond and L.L. Lewis (eds.), Exploration and Geological Services Division, Yukon Region, Indian and Northern Affairs Canada, p. 241-258.

Whitehorse Daily Star, 1979. Disaster! Dawson City Flood. Published May 2, 1979. [http://www. whitehorsestar.com/History/disaster-dawson-city-flood1]. Accessed January, 2015.

Willis, B., 1997. The environmental effects of the Yukon Gold Rush 1896-1906: Alterations to land, destruction of wildlife, and disease. National Library of Canada, 136 p.

Wright, J.S., 2001. "Desert" loess versus "glacial" loess: Quartz silt formation, source areas and sediment pathways in the formation of loess deposits. Geomorphology, vol. 36, p. 231-256.

Yoshikawa, K., Bolton, W.R., Romanovsky, V.E., Fukuda, M. and Hinzman, L.D., 2003. Impacts of wildfire on the permafrost in the boreal forests of Interior Alaska. Journal of Geophysics, vol. 108, doi:10.1029.2001JD000438.

Yukon Bureau of Statistics (YBS), 2014. Government of Yukon Socio-Economic and Web Portal – Dawson City: Housing Tenure, Condition, Period of Construction and Structural Type National Household Survey 2011. [http://www.sewp.gov.yk.ca/data?regionId=YK. DW&subjectId=POPCOM&groupId=POPCOM.DWELL&dataId=NHS_2011_HOUSING_ TENURE&tab=region]. Accessed December, 2014.

Yukon Community Profiles, 2014. Dawson City. [http://yukoncommunities.yk.ca/dawson-city/ population-labour-force]. Accessed December, 2014.

Van Loon, S. and Bond, J.D. (compilers), 2014. Yukon Placer Mining Industry 2010 to 2014. Yukon Geological Survey, Energy, Mines and Resources, Government of Yukon, 230 p.

Zazula, G.D., Froese, D.G., Elias, S.A., Kuzmina, S., La Farge, C., Reyes, A.V., Sanborn, P.T., Schweger, C.E., Smith, C.A.S. and Mathewes, R.W., 2006. Vegetation buried under Dawson Tephra (25,300 ^{14}C years BP) and locally diverse late Pleistocene paleoenvironments of Goldbottom Creek, Yukon, Canada. Palaeogeography, Palaeoclimatology, Palaeoecology, vol. 242, p. 253-286.

APPENDIX A - APPROACH AND METHODS

SURFICIAL GEOLOGY

Surficial geology is the study of unconsolidated material (i.e., the surficial material that overlies bedrock) on the Earth's surface, including all sediments and soils. These sediments may be deposited through a variety of different processes including glacial (deposited directly out of glacial ice); glaciofluvial (formed by glacial rivers and streams); colluvial (deposited on or at the base of hillslopes by gravity); fluvial (river and stream deposits); lacustrine (lake deposits); eolian (wind deposits); and organic (accumulation of vegetative matter). Additionally, organic deposits can accumulate over bedrock or unconsolidated material, particularly in depressions.

Surficial geology mapping involves a combination of aerial photograph interpretation and field work. The maps provide information on the physical properties and characteristics (e.g., texture or grain size) of the surface sediments, the morphology (shape) of the landforms produced, and the genesis or origin of the landforms (the past climate and environment in which the landform was produced), and identifies any geomorphological processes that may have significantly modified those materials (e.g., landslides, gullying, or permafrost). In the process of mapping the surficial geology, the distribution of permafrost is also captured, making these maps an essential part of the hazards assessment process.

Surficial geological field mapping was completed for the study area at a scale of 1:25 000 during the summer of 2013 and a map was produced in 2014 (Open File 2014-12; McKenna and Lipovsky, 2014). Previous mapping of surficial geology within the study area includes 1:250 000-scale regional mapping (Duk-Rodkin, 1996), as well as a number of larger-scale maps for various parts of the study area (Froese, 2005; Froese and Jackson, 2005; Ricker, 1977; Rostad et al., 1977; Thomas and Rampton, 1982). Many of the new surficial geological units created for the 2014 map were based on an existing 1:20 000-scale soil map for the Klondike River Valley produced by a group of soil scientists and surficial geologists in 1987 (Westland Resource Group, 1987). Significant overlap between soil parent material descriptions and surficial geology descriptions made this map a key resource. The focus of new mapping was to provide broader geologic descriptions of surface units and processes, as well as to extend previous mapping to include hillslope and high-elevation surfaces adjacent to the Klondike River Valley.

The Klondike Valley Soil maps (Westland Resource Group, 1987) were digitized by the Yukon Geological Survey with the cooperation of the Yukon Agriculture Branch. The map polygons were then rubber sheeted to the current Canvec base and the soil polygon designators were converted to the Yukon terrain classification system standards (Yukon Digital Surficial Geology Compilation, Digital Release 1, April 8, 2014. Yukon Geological Survey, Page 5: http://data.geology.gov.yk.ca/Compilation/DownloadProduct/39355). Remote predictive mapping was completed using 1:25 000-scale 1995 digital monochrome aerial photographs with PurView/ArcGIS softcopy viewing software. Field checking of units was completed by documenting anthropogenic and natural exposures of surficial materials, and by digging soil pits (up to ~1 m deep) in a broad range of surface sediments and landforms. Previously mapped soil polygons were adopted, modified or merged based on the interpretation and correlation with other mapping and field observations. The map boundary was extended to include uplands north and south of the Klondike Valley and west of the Yukon River. Other new data incorporated includes geophysical profiles of the subsurface (using ground-penetrating radar (GPR) and direct current electrical resistivity (ERT)), and new shallow boreholes. Previously acquired subsurface geological data was made available from borehole, test pits, and water well logs provided by EBA Engineering Consultants Ltd. (R. Trimble, Tetra Tech EBA, pers. comm., 2010).

PERMAFROST

GROUND-PENETRATING RADAR

Ground-penetrating radar (GPR) is a non-invasive method used to identify subsurface features such as stratigraphic boundaries, permafrost, and other anomalies using electromagnetic fields. For this project, GPR was used to gain a two dimensional image below the ground surface. Two GPR systems were used for field investigations. A TerraSIRch Subsurface Interface Radar (SIR) System 3000® with a shielded 200-MHz antenna (Geophysical Survey Systems, Inc. (GSSI)) was employed for shallow profiles (maximum 3 m penetration depth). The collection parameters for the SIR-3000 control unit were set to record at 64 scans per second, with a dielectric constant set at 13, which corresponds to a penetration speed of 0.0914 m/ns to 0.1 m/ns, depending on the ground type. The GPR antenna was hand-towed along the survey line. For deeper profiles (maximum 8 m penetration depth) and for sites located in rough terrain, a Pulse Ekko Pro system with 50 MHz antennas was used. The antennas were moved manually with a separation of 2 m and a step size of 0.5 m. The penetration speed used for this system was between 0.1 and 0.11 m/ns, depending on the ground type.

Where possible, the GPR transects were situated adjacent to sections of the electrical resistivity tomographic profiles and boreholes; site conditions were described in detail. This enabled a comparison of the results from the three techniques and to verify the findings.

Post collection data processing was conducted using RADAN™ (Version 7, GSSI) and Ekko_Project 2 software and applied to all of the profiles. Processing of the GPR data included the following: the correction of the initial pulse to time-zero to ensure that the first reflection is from the ground surface and the subsequent reflections are from deeper below the ground surface; correction of the penetration depth with a common midpoint method or with borehole information; topographic correction where required; the application of a FIR boxcar filter to remove background horizontal noise where required; and the use of range gain adjustments to recover lower-amplitude waves from reflections deeper in the ground (Conyers, 2004). Overall, the processing procedures were employed to reduce signal attenuation with depth, as well as improve the continuity of stratigraphic reflections and the signal-to-noise ratio.

ELECTRICAL RESISTIVITY

Electrical Resistivity Tomography (ERT) profiling is a geophysical technique that measures variations in the ability of the ground to conduct electricity along a transect, producing a two-dimensional image of changes in electrical conductance. In permafrost areas, variations in conductance relate mainly to the changes in frozen versus thawed ground, because water and ice serve as good and poor conductors of electricity, respectively.

ERT profiling has been used extensively to investigate mountain permafrost in Europe (e.g., Kneisel et al., 2000, 2008; Hauck et al., 2004; Hilbich et al., 2008, 2009) and is growing in importance in North America as a technique for permafrost investigations in both mountains and lowlands (e.g., Lewkowicz et al., 2011; Miceli, 2012). ERT is regarded as one of the best methods to examine changes in frozen ground conditions over short distances, such as in areas underlain by discontinuous permafrost.

Many ERT profiles show very clear distinctions relating to frozen ground conditions which can be correlated to surface changes in drainage, vegetation cover, or land use (Lewkowicz et al., 2011). However, like all geophysical techniques, confidence in the interpretation increases where complementary information is available; this may include data from borehole logs, observations

of natural exposures, ground temperature measurements, probing of the active layer, or other geophysical techniques such as ground penetrating radar.

There is a major difference in the resistivity of water and ice, but there is not always a sharp line between the phase of water in soil pores (frozen or unfrozen) at temperatures above and below 0°C. Instead, percentages of unfrozen moisture gradually increase in the pores of frozen soils (especially in fine-grained soils such as silts and clays) as their temperatures approach 0°C. Consequently, the difference in the electrical resistivity of frozen and unfrozen soils can be gradational rather than sharp (Lewkowicz et al., 2011). In addition, because there can be differences in the porewater salinity and in the conductance of the soil minerals, it is not possible to identify a single universal threshold resistivity value below which soils are definitely unfrozen and above which soils are definitely frozen. However, given the scale of the case study sites examined in this project, a threshold value unique to each case study site was determined based on site characteristics and other ground-truthing approaches (e.g., permafrost drilling). This value is typically between 300 and 800 ohm m in the southern Yukon (Lewkowicz et al., 2011), but it depends on the local ground temperatures and stratigraphy. The value used for most of the ERT profiles in this report is 400 ohm m which generally coincided with a gradient in resistivity indicative of phase change. For the Moosehide Slide, a value of 1000 ohm m was considered to be appropriate based on the dry, coarse surface materials present. A uniform shading scale has been used for all the resistivity profiles presented so that visual comparisons can be made among the figures. Blue represents high resistivities (generally indicative of frozen materials or soils) and red represents low resistivities (ice-poor or unfrozen materials or soils).

The ERT profiling included in this report was undertaken in September 2013 and 2014, when the active layer (i.e., depth from ground surface to the top of permafrost) was at its thickest. The equipment used was an ABEM Terrameter LS profiling system with the electrode array (stainless steel pins) inserted into the ground in a Wenner configuration. The electricity entering the ground builds up an image of its resistivity along a profile whose depth depends on the spread of the array of electrodes (25 m for an array 160 m in length, and 8 m for a 40-m array). The penetration depth remains at 25 m, even if surveys longer than 160 m are created using a roll-along technique. Eight ERT profiles were completed.

Each ERT site was described in terms of vegetation and other salient features. UTM co-ordinates (relative to the WGS 84 datum) were taken using a hand-held Garmin Etrex Vista GPS. Relative variations in elevation along the individual profiles were measured in the field using an abney level and are expected to have accuracies of ±1 m.

Resistivity profiles were topographically corrected using the abney level surveys. The actual elevations shown on the surveys are approximate. Measured resistivity data were processed with RES2DINV software (Loke and Barker, 1996) using a robust inversion that can respond to the rapid transitions and high contrasts in resistivity (Loke et al., 2003) that occur between frozen and unfrozen ground. A reversed colour scheme was used to portray the profiles so that blue represents high resistivities (generally indicative of frozen soils) and red represents low resistivities (ice-poor or unfrozen soils). All the resistivity profiles use the same scale to allow for inter-site comparison.

There is no single model that fits the observed resistivities. Instead the modelled results converge by iteration with the measured values. The choice of when to stop iteration in the RES2DINV software is made by the operator. Too few iterations leads to large Root Mean Square (RMS) errors (i.e., the model does not fit the measurements). Too many iterations can result in model 'over-fit' in which the broad patterns are lost. Analyses for this study were stopped after the 4th iteration as RMS errors were all very low (less than 5%) by that point. The profiles are presented with a linear depth scale and no vertical exaggeration. ERT profiles were interpreted in conjunction

with the results of frost probing along the profiles, GPR surveys, field descriptions of vegetation cover at the site, borehole and laboratory analyses undertaken by the research team, and surficial mapping.

DRILLING AND SAMPLE COLLECTION

The drilling program was carried out in September 2013 and August 2014. The objective was to core and collect permafrost samples from predetermined study sites. These sites were selected in advance through a desktop interpretation based on available maps, aerial photos, satellite images and consultation with community members. The drilling and coring operations required the use of four different drills to account for changes in subsurface conditions: two core-drills (a custom GÖLZ™ portable core-drill system and a modified Winkie core-drill system), one auger drill, and one hand auger.

The GÖLZ™ portable core-drill system (Figure A1) is a light hand drill with a high rotation speed (600 rpm) that can be controlled by two people, and is therefore used with minimal impact on the environment. Stainless steel rods measuring 1 m in length and 4.5 cm in diameter, and a core barrel 40 cm long and 10 cm in diameter were used, making it possible to drill up to 5 m into unconsolidated, fine to medium grained material (sand to clay). A core catcher was used to extract the frozen core out of the borehole, which allows for continuous undisturbed permafrost sampling.

Figure A1. *Photograph of the GÖLZ™ portable Earth-drill system used for permafrost coring.*

The Winkie drill is a gas-powered core-drill with a two-speed transmission made for bedrock drilling; this drill has been modified for permafrost drilling in unconsolidated material using a gearbox that lowers the speed to approximately 1200 rpm. Although it is not as mobile as the GÖLZ™ portable core-drill system, it is one of the lightest shift drills on the market (Figure A2) and has the potential to go down to 30 m in ice-rich, fine-grained material. The Winkie core-drill was used with aluminum rods (0.9 and 1.5 m long; Figure A3) and core barrels 10.8 cm in diameter.

Figure A2. Photograph of the Winkie drill, used for permafrost coring.

Figure A3. Photograph of aluminum rods used for the Winkie drill for permafrost coring.

The auger drill is equipped with a Honda GVX160 (144 rpm) motor and flight auger extensions with diameters of 5-46 cm (Figure A4). This drill is destructive and is used to pass through unfrozen sediments of the active layer allowing for bulk 'grab' samples. This type of auger is also useful in retrieving deposits of gravel containing clasts that are cobble to boulder sized at the bottom of a borehole.

The hand auger is used to sample the thawed active layer; it has a 10.2-cm diameter sampling core barrel, and three 1 m-long extension rods (Figure A5). It is ideal for sampling near-surface, fine-grained, unfrozen soil (e.g., clay, silt, sand and fine gravel containing pebbles with a maximum diameter of 25 mm).

Figure A4. Photograph of the Honda drill, used for permafrost coring.

Figure A5. Photograph of the hand auger, used for permafrost coring.

Using a combination of these drills, boreholes were drilled along ERT and GPR profiles in representative areas (e.g., forested areas, open fields) or in an area belonging to a particular surficial geology unit. For each borehole, the same sampling and drilling procedures were followed. The site was first described (e.g., hydrology, vegetation type and density, and topography), photos were taken, and locations were recorded using a handheld GPS. The boreholes were initiated using a hand auger if the ground was soft or an auger drill if the ground was gravelly or compacted. As soon as the permafrost table was reached, the GÖLZ™ portable core-drill system was used. For specific locations where maximum depth was desired, the Winkie core-drill was used.

A sample of every unfrozen layer was collected from each borehole. Each sample was photographed and described in situ (e.g., soil type, soil moisture, presence or absence of organic matter, any particularities). The sample was identified with the borehole name and depth and put in doubled hermetic Ziploc bags for laboratory analyses. Frozen samples were also collected and described on site (Figure A6). Each core was cleaned to remove the drilling mud and photographed.

Figure A6. Photograph of the setup used for in-field core descriptions.

GEOTECHNICAL ANALYSIS OF PERMAFROST

Laboratory analyses were carried out to measure geotechnical properties of active layer and permafrost samples, and additional tests were conducted to evaluate the mechanical behavior of the permafrost upon thawing. Both soil grain characteristics and ice characteristics were evaluated. To evaluate soil grain characteristics, a grain-size analysis was performed on every sample. Additionally, plasticity index, remolded bulk density, porosity, specific gravity and thaw settlement potential were calculated for representative samples. To evaluate ice characteristics in permafrost samples, the cryostructure, volumetric ice content, gravimetric ice content and settlement potential were quantified. These methods are described below.

Grain-Size Analysis

Sieve and hydrometer analysis of grain size were performed following a specifically modified American Standard and Testing Method protocol (ASTM D422-63, 2000). The sieves typically used were 4, 2, 1, 0.5, 0.25, 0.125 and 0.063 mm. A hydrometer test was performed on samples with enough fine-grained material, or on specific samples. A 40-g subsample was passed through 0.25 mm openings, and after sedimentation started, readings were taken after 0.25, 0.50, 0,75, 1, 1.5, 2, 5, 15, 30, 60, 120, 180, 300 and 1440 minutes. A total of 56 analyses were completed.

SPECIFIC GRAVITY

Specific gravity (the ratio of a solid's grain density to the density of water) was systematically measured for every sample collected, and followed the American Standard and Testing Method (ASTM D854-10, 2000). The results were used to compute the porosity of the soil (see below) for 6 types of soils.

CRYOSTRUCTURE

Cryostructure (the geometry of the ice in the permafrost) depends on water availability, as well as the soil's ice-segregation potential and the time of freezing, resulting in the development of ice structures in the soil matrix. Information such as soil genesis, climate conditions at the time of freezing, permafrost development history, and ground vulnerability when permafrost degrades can be interpreted from cryostructure, cryofacies analysis, and general cryostratigraphy.

Because field descriptions are based only on a visual interpretation of the core, the samples were re-examined in the laboratory using a standard terminology that would provide a more detailed description (Stephani et al., 2010; Murton and French, 1994). Frozen core samples were warmed to near 0°C and any refrozen mud was scrapped off prior to the description.

CONSOLIDATION TESTING

Compaction and consolidation testing were carried out at Laval University. They were measured by thawing a soil sample and measuring the associated total settlement. A load was then applied vertically (stress) on a confined and drained sample to simulate the influence of weight from an embankment or a building on consolidation. The total settlement was the sum of two distinct processes: 1) the compaction associated with the water phase change, resulting in a significant decrease in volume, especially when excess ice is present; and 2) the consolidation of the soil under the applied stress following the expulsion of water out of the pore structure and the rearrangement of soil particles. In general, compaction is more prevalent for samples with excess ice (e.g., segregated ice lenses), whereas consolidation is common in samples with interstitial ice (e.g., unsaturated to saturated soils).

During testing, an initial vertical stress of 25 kPa (corresponding to the approximate weight of a thawed active layer) was applied to frozen samples. Using two thermal baths to control the upper and lower temperatures, the permafrost samples were thawed from above by applying heat with a temperature of 2°C ± 1°C. Ultimately, the temperature of both thermal baths was increased to ensure complete thawing of the sample. After complete thawing, when there was no more vertical deformation, the stress was increased to 150 kPa for a minimum period of 24 hours in order to simulate the weight of an embankment or a medium-sized building. By proceeding in near oedometric conditions, it was possible to estimate the index of final voids (e_t) when thawing and consolidation of the grains were completed (at a given applied force). By also determining the index of initial voids in the frozen state (e_f – calculated using the frozen density and water content), it was possible to obtain a total settlement value under different forces for the same sample.

To assess the total settlement (s), the sum of the thaw settlement (s_t) and the subsequent consolidation of the soil (s_c) were calculated by using:

$$s = s_t + s_c \hspace{4cm} [1]$$

When the thickness of the original frozen soil layer (H_f) is subject to effective stress (σ'), the components of the total settlement are expressed using:

$$s_t = A_0 H_f \qquad [2]$$

$$s_c = m_v\, \sigma' H_f \qquad [3]$$

The thawing compaction parameter (A_0) is expressed as a percentage and represents the relationship between void ratio in frozen (e_f) and thawed (e_t) states which is summarized by using:

$$A_0 = \frac{e_f - e_t}{1 + e_f} \qquad [4]$$

The volume change coefficient (m_v) is defined as a volume changing unit added by an effective stress unit. When the effective stress increases from $\sigma\rangle$ to σ_0' and the void ratio decreases from e_t to e, this coefficient is expressed using:

$$m_v = \frac{1}{1 + e_t} \cdot \left(\frac{e_t - e}{\sigma' - \sigma_0'} \right) \qquad [5]$$

In order to determine the total settlement following the thawing of permafrost under loads imposed by buildings or transportation infrastructure, A_0 and m_v values must be determined from consolidation tests on representative soil samples. Once these values are determined, the total compaction of partially or completely thawed frozen soil layers is determined by using:

$$s = \sum_{i=1}^{n} A_{0,i}\, H_i + \sum_{i=1}^{n} m_{v,i}\, H_i\, \sigma_i' \qquad [6]$$

BULK DENSITY

Bulk density and voids in aggregate (ρ_b; the ratio of a dried soil's mass, including its porosity, to its volume (g/cm³)) were calculated following American Standard and Testing Method protocol (ASTM C29 – 09, 2000). Values were generated by weighing a 45-cm³ beaker filled with compacted sediment and subtracting the empty beaker weight. The sediment weight was then divided by the beaker's volume using:

$$\rho_s = \frac{(M_{S+B} - M_B)}{V_B} \qquad [7]$$

where M_{S+B} is the weight of the beaker full of compacted sediment, M_B is the weight of the empty beaker, and V_B is the beaker's internal volume.

GRAVIMETRIC ICE CONTENT

Ice content was calculated using:

$$u_I = \frac{(M_I)}{(M_S)}$$ [8]

where M_I is the ice weight (measured as weight loss after drying (g)) and M_S is dry soil weight (g). Results are expressed as percentages (dimensionless).

VOLUMETRIC ICE CONTENT

Ice volume was measured using a water displacement method. The frozen sample was weighed and lowered into a four-inch diameter PVC tube filled with 1.5 L of water. Water was then extracted from the tube until the initial water level (1.5 L) was achieved. The amount of water displaced was measured using a 250 mL graduated cylinder with a precision of ±2 mL. The sample was then removed from the tube, placed in a clean tin tray, and dried completely in a drying oven at 60°C. The dry sample was then weighed, crushed using a mortar and pestle, vacuum sealed in a clear plastic bag, and labelled according to the borehole and sample increment. The volumes of the vacuum-sealed dry samples were measured using the same methods as the frozen cores, and the volume of the vacuum bags was subtracted from the measurement to obtain a dry sample volume. Assuming the density of ice to be 1.09 cm³/g, the volumetric ice content was calculated using:

$$IVC_{(\%)} = \left(\frac{Wc \times 1.09}{Vtot} \right) \times 100$$ [9]

where W_c is the water mass content and V_{tot} is the total (frozen) core volume. Results are expressed as percentages.

VOLUMETRIC EXCESS ICE CONTENT

The volume of excess ice content was calculated using:

$$V_{tot} - V_{sed} = V_{ice}$$ [10]

where V_{tot} is the total frozen core volume and V_{sed} is the dry soil volume. The volumetric excess ice content (V_{ice}) is then divided by the total frozen core volume (V_{tot}) and expressed as a percentage (fundamentally meaning cm³/cm³). This method is valid for mineral soils only.

PLASTICITY INDEX

The plasticity index (*PI;* the range of water content where the soil has a plastic behaviour) was measured according to the American Standard and Testing method (ASTM D4318-00, 2000) using:

$$PI = LL - PL$$ [11]

where LL is the liquid limit and PL is the plastic limit.

The LL was calculated using the multipoint liquid limit (ASTM method A; ASTM D4318-00, 2000) which requires one of the trials to be between 25 to 35 blows, one closure between 20 and 30 blows, and one trial with a closure requiring 15 to 25 blows. The *PL* was calculated using the *Hand Method* which consists of rolling the mass between the palm or fingers and the ground-glass plate with sufficient pressure to roll the mass into a thread of uniform diameter throughout its length. The thread is further deformed on each stroke so that its diameter reaches 3.2 mm (1⁄8 in).

Borehole Logs

A log for each permafrost borehole was created using the *Rockware Log Plot* software. Borehole logs include GPS coordinates; a description of the surrounding environment; the stratigraphy of the sediment; the depth to the water table, to the frozen table in the active layer, and to the permafrost table; the ice structure (cryostructure); the grain size ratio; the specific gravity; the bulk density; the porosity; the volumetric ice content; and the thaw-settlement potential (see Appendix B for all borehole log descriptions and data).

REFERENCES

ASTM Standard C29 – 09, 2000. Standard Test Method Bulk Density ("Unit Weight") and Voids in Aggregate. West Conshohocken, PA, ASTM International.

ASTM Standard D422 – 63, 2000. Standard Test Method for Particle-Size Analysis of Soils. West Conshohocken, PA, ASTM International.

ASTM Standard D854 – 10, 2000. Standard Test Methods for Specific Gravity of Soil Solids by Water Pycnometer. West Conshohocken, PA, ASTM International.

ASTM Standard D4318 – 00, 2000. Standard Test Methods for Liquid Limit, Plastic Limit, and Plasticity Index of Soils. West Conshohocken, PA, ASTM International.

Conyers, L., 2004. Ground-penetrating radar for Archaeology. AltaMira Press, Walnut Creek, California. 209 p.

Duk-Rodkin, A., 1996. Surficial Geology NTS 116B&C, Dawson, Yukon Territory. Geologic Survey of Canada, Open File 3288, 1:250 000 scale.

Froese, D.G., 2005. Surficial geology, Flat Creek, Yukon Territory NTS 115O/15. GSC Open File 4592, 1:50 000 scale.

Froese, D.G. and Jackson, L.E., Jr, 2005. Surficial geology, Grand Forks, Yukon Territory NTS 115O/14. GSC Open File 4591, 1:50 000 scale.

Hauck, C., Isaksen, K., Vonder Mühll, D. and Sollid, J.L., 2004. Geophysical surveys designed to delineate the altitudinal limit of mountain permafrost: An example from Jotunheimen, Norway. Permafrost and Periglacial Processes, vol. 15, p. 191-205, doi:10.1002/ppp.493.

Hilbich, C., Hauck, C., Hoelzle, M., Scherler, M., Schudel, L., Voelksch, I., Vonder Muehll, D. and Maüsbacher, R., 2008. Monitoring mountain permafrost evolution using electrical resistivity tomography: A 7-year study of seasonal, annual, and long-term variations at Schilthorn, Swiss Alps. Journal of Geophysical Research-Earth Surface, vol. 113, doi:10.1029/2007JF000799.

Hilbich, C., Marescot, L., Hauck, C., Loke, M.H. and Maüsbacher, R., 2009. Applicability of electrical resistivity tomography monitoring to coarse blocky and ice-rich permafrost landforms. Permafrost and Periglacial Processes, vol. 20, p. 269-284, doi:10.1002/ppp.652.

Kneisel, C., Hauck, C. and Vonder Mühll, D., 2000. Permafrost below the timberline confirmed and characterized by geoelectrical resistivity measurements, Bever Valley, eastern Swiss Alps. Permafrost and Periglacial Processes, vol. 11, p. 295-304, doi:10.1002/1099-1530(200012)11:4<295::AID-PPP353>3.0.CO;2-L.

Kneisel, C., Hauck, C., Fortier, R. and Moorman, B., 2008. Advances in geophysical methods for permafrost investigations. Permafrost and Periglacial Processes, vol. 19, p. 157-178.

Lewkowicz, A. G., Etzelmüller, B.E. and Smith, S.L., 2011. Characteristics of discontinuous permafrost from ground temperature measurements and electrical resistivity tomography, southern Yukon, Canada. Permafrost and Periglacial Processes, vol. 22, p. 320-342.

Loke, M.H. and Barker, R.D., 1996. Rapid leastsquares inversion of apparent resistivity pseudosections using a quasi-Newton method. Geophysical Prospecting, vol. 44. p. 131-152, doi:10.1111/j.1365-2478.1996.tb00142.x

Loke, M.H., Acworth, I. and Dahlin, T., 2003. A comparison of smooth and blocky inversion methods in 2D electrical imaging surveys. Exploration Geophysics, vol. 34, p. 182-187.

McKenna, K.M and Lipovsky, P.S., 2014. Surficial geology, Dawson region, Yukon; parts of NTS 115O/14 & 15 and 116B/1, 2, 3 & 4. Yukon Geological Survey, Energy, Mines and Resources, Government of Yukon, Open File 2014-12, 1:25 000 scale.

Miceli, C., 2012. Seasonal cycling in electrical resistivities at ten thin permafrost sites, southern Yukon and northern British Columbia. Unpublished MSc thesis, Department of Geography, University of Ottawa, ON, 201 p.

Murton, J.B. and French, H.M., 1994. Cryostructures in permafrost, Tuktoyaktuk coastlands, western arctic Canada. Canadian Journal of Earth Sciences, vol. 31, no. 4, p. 737-747.

Ricker, K.E., 1977. Quaternary geology of the North Klondike and Upper Blackstone River Systems, Southern Ogilvie Ranges, Yukon Territory, Canada. Geological Survey of Canada, Open File 478, 1:50 000 scale.

Rostad, H.P.W., Kozak, L.M. and Acton, D.F., 1977. Soil survey and land evaluation Yukon Territory. Saskatchewan Institute of Pedology, Publication S174, 495 p. and maps.

Stephani, E., Fortier, D. and Shur, Y., 2010. Applications of cryofacies approach to frozen ground engineering – Case study of a road test site along the Alaska Highway (Beaver Creek, Yukon, Canada). GEO2010: 63rd Canadian Geotechnical Conference and 6th Canadian Permafrost Conference, Calgary, Canada.

Thomas, R.D. and Rampton, V.N., 1982. Surficial Geology and Geomorphology, Upper Blackstone River, Yukon Territory. GSC Preliminary Map 7-1982, 1:100 000 scale.

Westland Resource Group, 1987. Soil Survey of the Klondike River Valley, Yukon Territory. Prepared by Mark Walmsley, Denny Maynard and Karen McKenna for Lands Branch, Government of Yukon and Northern Land Use Planning, Indian and Northern Affairs Canada.

APPENDIX B - BOREHOLE LOGS

Figure B1. *Borehole log for borehole DC_BH01, from the West Dawson case study site (see Figure 50 in the main body of this report for location).*

Figure B2. Borehole log for borehole DC_BH02, from the C-3B case study site (see Figure 54 in the main body of this report for location).

BOREHOLE DC_BH03

Location: Dawson City
Site name: R-68 Settlement
Coordinates: 7W N575905 E7107253

Legend: Water table; Permafrost table; Thawed; G Gravel; S Sand; M Mud (silt and clay)

Depth (cm)	Description	G	S	M	Loss of ignition (%)	Grav. water content (%)	Frozen bulk density	Vol. ice content (%)	Vol. excess ice (%)	25 KPa	75 KPa	125 KPa
0–20	Fibric organic matter	---	---	---	---	---	---	---	---	---	---	---
20	Decomposed organic matter	---	---	---	---	---	---	---	---	---	---	---
40	Fibric organic matter with some silty sand lenses. Porous visible cryostructure	0	69	31	---	130	1.42	88	--	---	---	---
60	Silty sand. Porous invisible cryostructure				4							
80–100	Sandy organic silt with rootlets. Porous visible and microlenticular cryostructures with few ice lenses / Microlenticular and lenticular cryostructures	0	53	47	38	167	1.14	73	---	44	52	58
120–220	Silty sand with wood pieces, rootlets and organic matter lenses. Porous invisible and visible cryostructures; Lenticular and ice veins; Microlenticular, lenticular and crustal cryostructures	0	67	33	5	144	1.29	71	15	12	15	17
240–260	Sand with lenses of organic matter. Porous invisible cryostructure	0	92	8	2	52	1.53	57	7	---	---	---
280–300	Silty sand with lenses of organic matter, roots and wood pieces. Porous invisible cryostructure	0	52	48	2	47	1.57	55	0	---	---	---
320	Sand with lenses of organic matter. Porous invisible cryostructure	0	91	9	2	33	1.7	46	11	---	---	---
340–400	Silty sand with lenses of organic matter. Porous invisible cryostructure	0	67	33	3	45	1.55	45	5	---	---	---

Figure B3. Borehole log for borehole DC_BH03, from the R-68B case study site (see Figure 56 in the main body of this report for location).

BOREHOLE DC_BH04

Location — Dawson City
Site name — R-69B Settlement
Coordinates — 07W E574138 N7102904

Legend
Water table
Permafrost table
Thawed
G — Gravel
S — Sand
M — Mud (silt and clay)

Depth (cm)	Lithology	Cryostructure	Description	Grain size (%)			Loss of ignition (%)	Grav. water content (%)	Frozen bulk density	Vol. ice content (%)	Vol. excess ice (%)	Settlement potential (%)		
				G	S	M						25 KPa	75 KPa	125 KPa
0–20			Peat	---	---	---	---	---	---	---	---	---	---	---
20			Sandy organic silt	---	---	---	---	---	---	---	---	---	---	---
40			Sandy silt	---	---	---	---	---	---	---	---	---	---	---
60			Sandy silt. Microlenticular cryostructure	0	31	69	---	78	1.3	62	31	---	---	---
80–100			Sandy silt with layers of organic matter. Lenticular to microlenticular cryostructures	0	33	67	---	87	1.19	61	37	20	22	24
120–140			Sandy silt with layers of sandy organic silt. Porous invisible, visible and lenticular cryostructures	0	29	70	---	81	1.26	60	---	---	---	---
160–180			Sandy silt. Porous invisible and microlenticular cryostructures	0	49	51	---	97	1.5	80	---	---	---	---
200–220			Sandy silt with layers of organic matter and wood pieces. Porous invisible and microlenticular cryostructures	0	22	78	---	202	1.15	84	---	---	---	---
								61	1.36	57	---	---	---	---
240–280			Sandy silt with lenses of organic matter. Porous invisible cryostructure	0	16	79	---	52	1.4	50	14	10	15	20
300–340			Sandy silt with organic matter fragments. Porous invisible to microlenticular cryostructures	1	17	82	---	110	1.23	70	32	---	---	---
360–380			Decomposed organic matter with roots and wood fragments. Porous invisible cryostructure	0	24	76	---	364	0.84	72	---	---	---	---
								31	1.61	41	13	---	---	---
400–420			Sandy silt. Porous invisible and microlenticular cryostructures	0	13	87	---	50	1.7	62	6	---	---	---

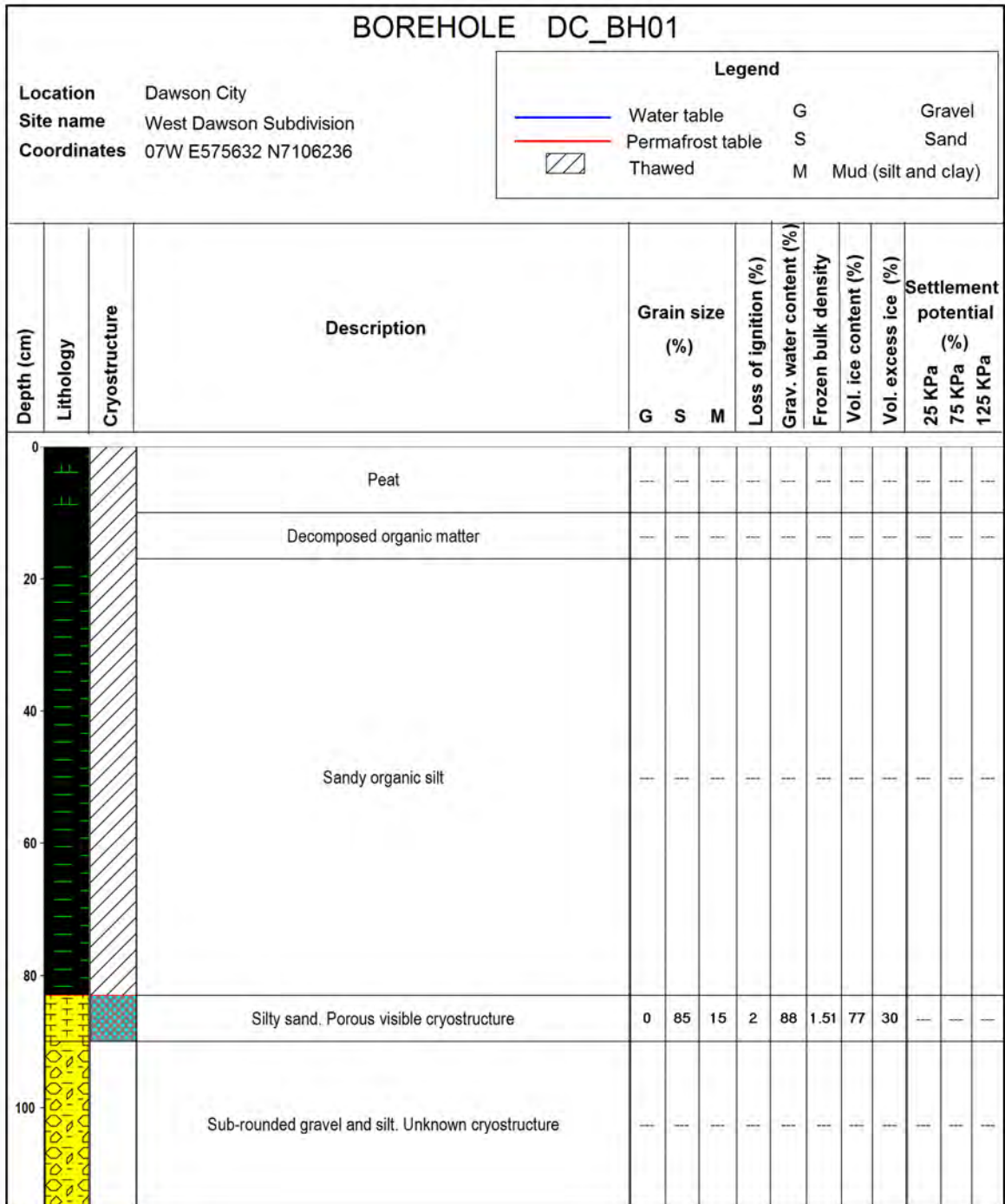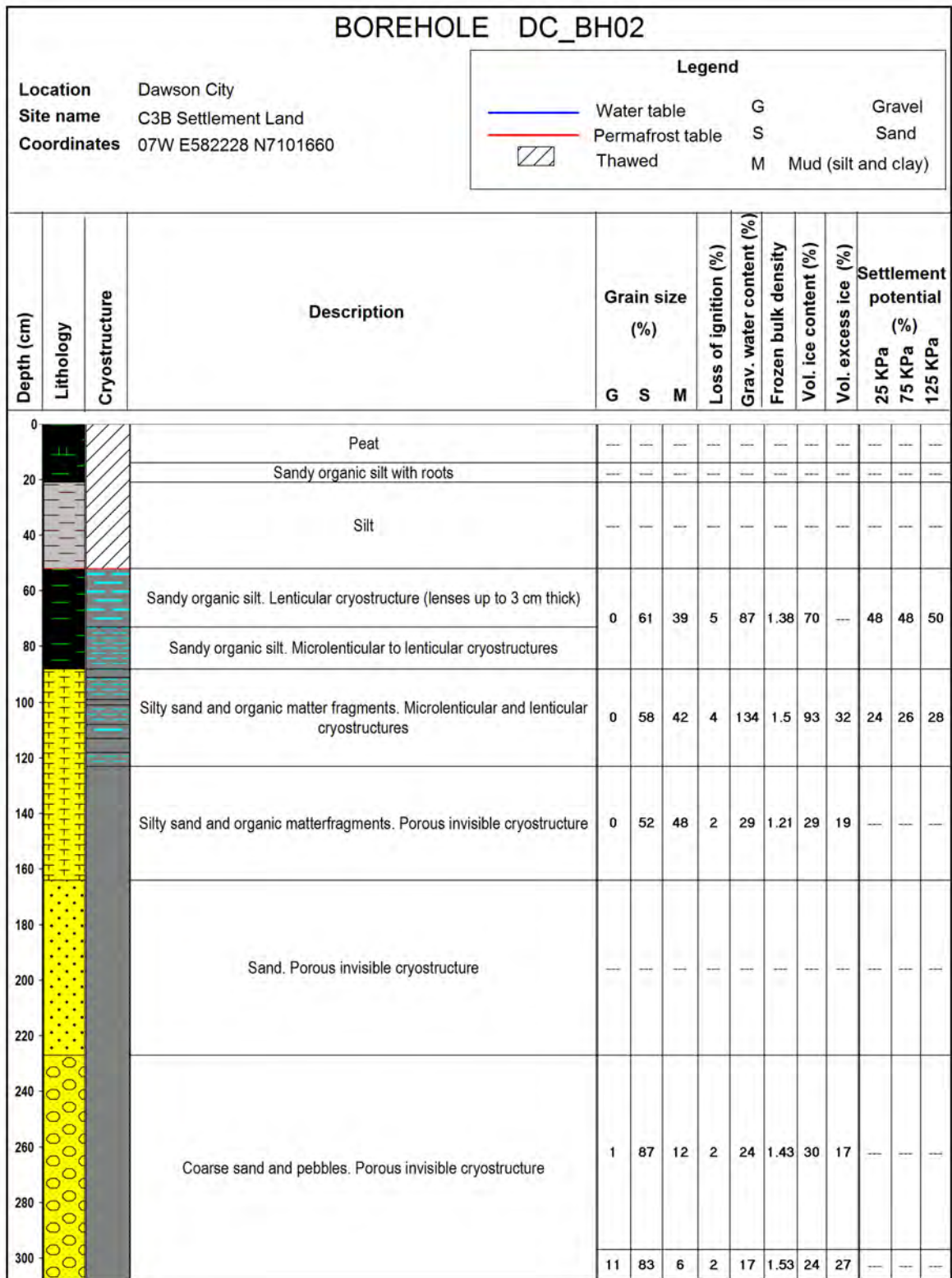**Figure B4.** Borehole log for borehole DC_BH04, from the R-69B case study site (see Figure 60 in the main body of this report for location).

BOREHOLE DC_BH05

Location	Dawson City
Site name	R-69B Settlement
Coordinates	07W E574139 N7102915

Legend

- Water table
- Permafrost table
- Thawed
- G — Gravel
- S — Sand
- M — Mud (silt and clay)

Depth (cm)	Lithology	Cryostructure	Description	Grain size (%) G	Grain size (%) S	Grain size (%) M	Loss of ignition (%)	Grav. water content (%)	Frozen bulk density	Vol. ice content (%)	Vol. excess ice (%)	Settlement potential (%) 25 KPa	75 KPa	125 KPa
0			Peat and wood chips	---	---	---	---	---	---	---	---	---	---	---
20			Peat with coarse grained material (orange and gray)	---	---	---	---	---	---	---		---	---	---
40			Well decomposed organic matter											
60–80			Sandy organic silt with roots and rootlets. Porous visible cryostructure	1	49	50	19	145	1.15	73	---	---	---	---
100–120			Sandy silt mixed with layers of sandy organic silt. Porous visible to microlenticular cryostructures											
140–160			Sandy silt with lenses of organic matter. Porous invisible and visible cryostructures	0	36	64	7	117	1.31	77	46	---	---	---
180–200			Sandy silt with lenses of organic matter. Reticulate cryostructure											
220			Coarse sand and small pebbles. Porous invisible cryostructure	9	48	43	3	35	1.18	34	46	---	---	---
			Sandy silt. Reticulate cryostructure											
240			Gap (gaz pocket)											
260			Sandy silt with lenses of organic matter and rootlets. Porous visible to microlenticular cryostructures	---	---	---	---	---	---	---	---	---	---	---
280			Sandy silt. Suspended cryostructure											
300			Sandy silt mixed with layers of sandy organic silt and rootlets. Porous invisible and visible cryostructures	0	47	53	23	136	1.07	67	---	---	---	---
320			Sandy silt with lenses of organic matter and rootlets. Porous visible cryostructure											
			Sandy silt. Lenticular cryostructure (ice-rich)											
340–380			Sandy silt with lenses of organic matter and rootlets. Porous visible and crustal (around the roots) cryostructures	0	23	77	5	65	1.48	59	22	---	---	---
400			Decomposed organic matter with roots. Porous visible cryostructure											
			Sandy silt with lenses of organic matter. Porous visible cryostructure											
420			Silty sand with few gravel. Microlenticular cryostructure	1	58	41	4	38	1.58	48	27	---	---	---
440			Silty sand with few gravel. Porous invisible cryostructure											

Figure B5. Borehole log for borehole DC_BH05, from the R-69B case study site (see Figure 60 in the main body of this report for location).

Figure B6. *Borehole log for borehole DC_BH06, from the R-69B case study site (see Figure 60 in the main body of this report for location).*

Figure B7. Borehole log for borehole DC_BH07, from the R-69B case study site (see Figure 60 in the main body of this report for location).
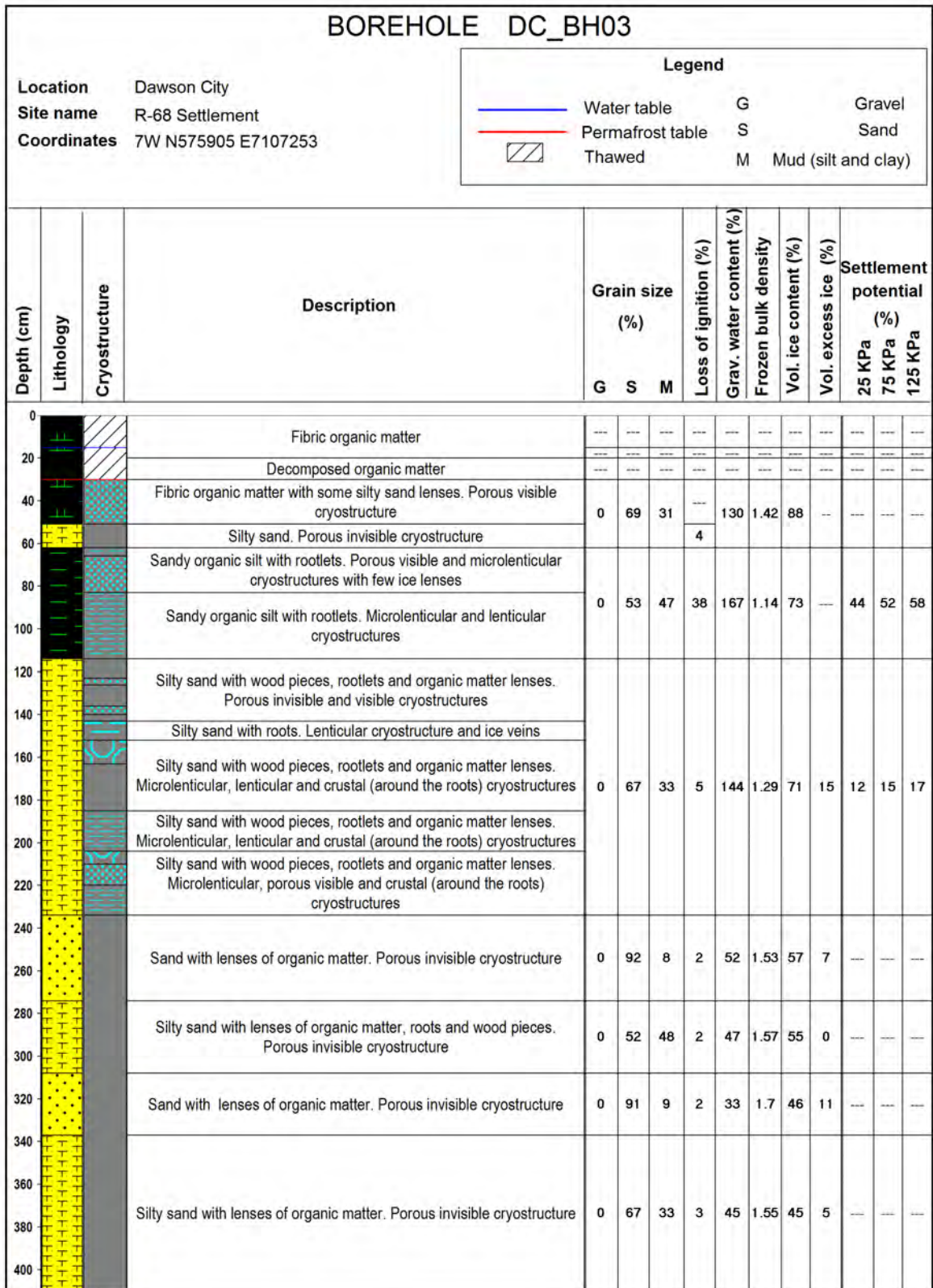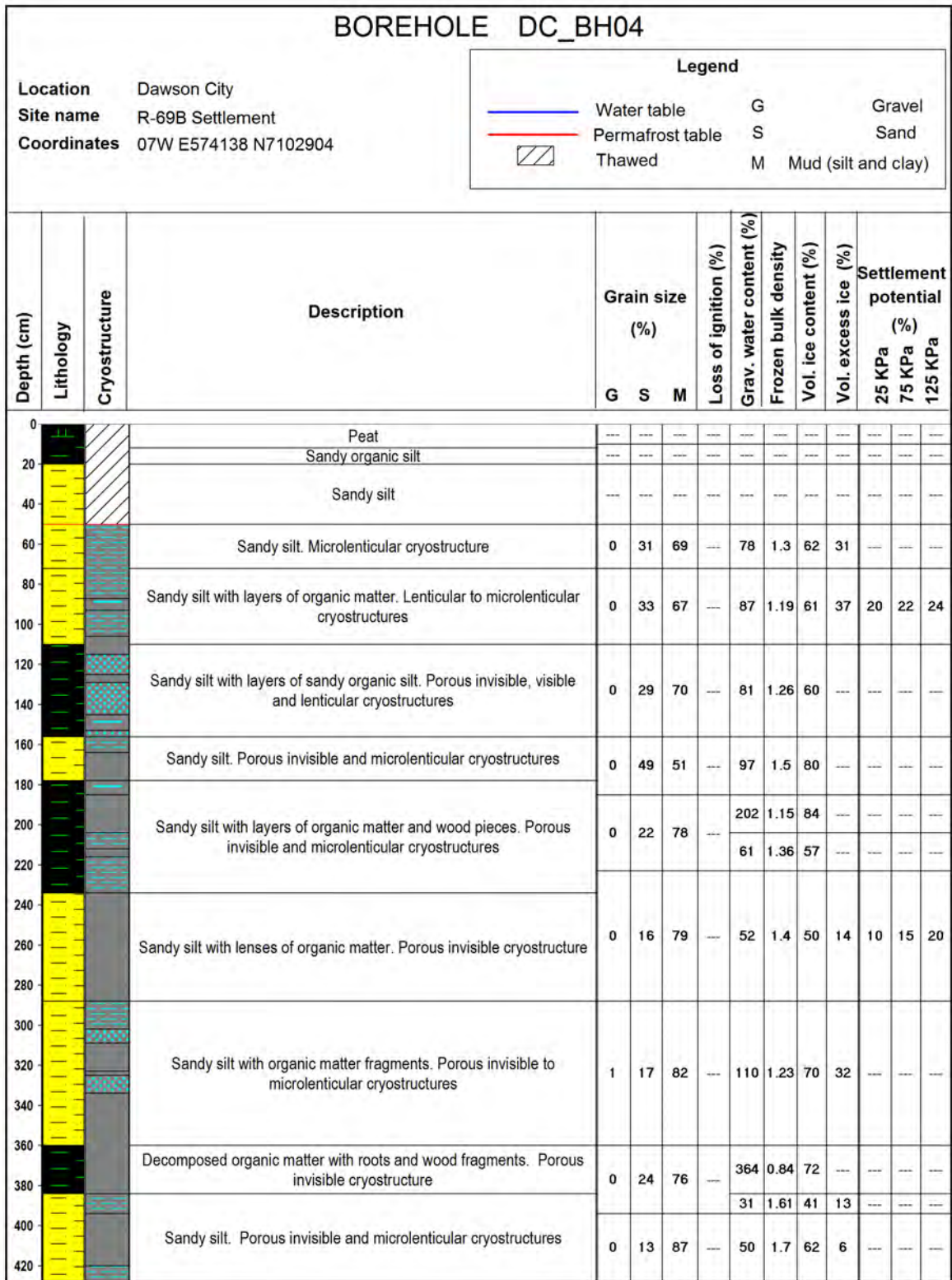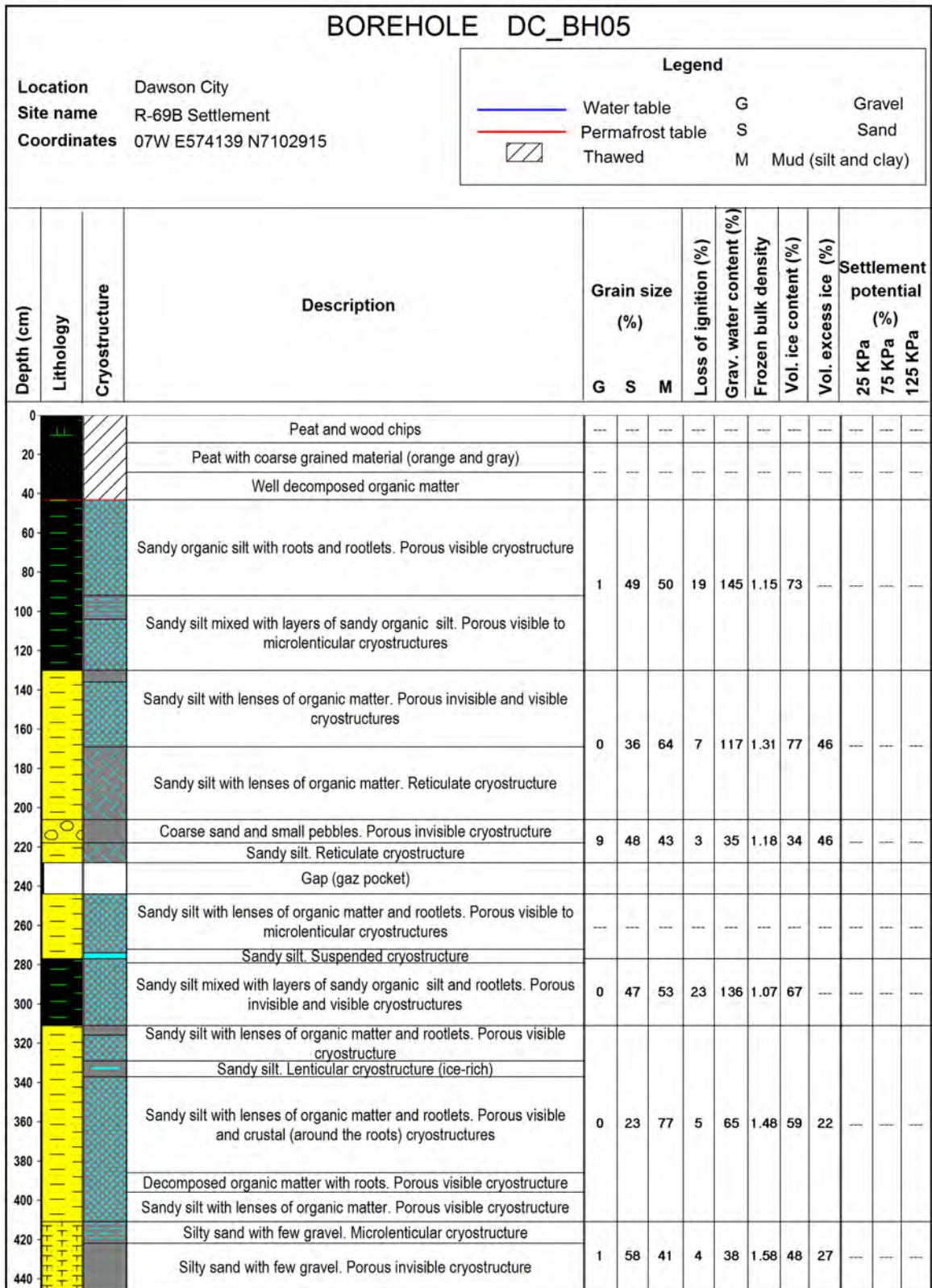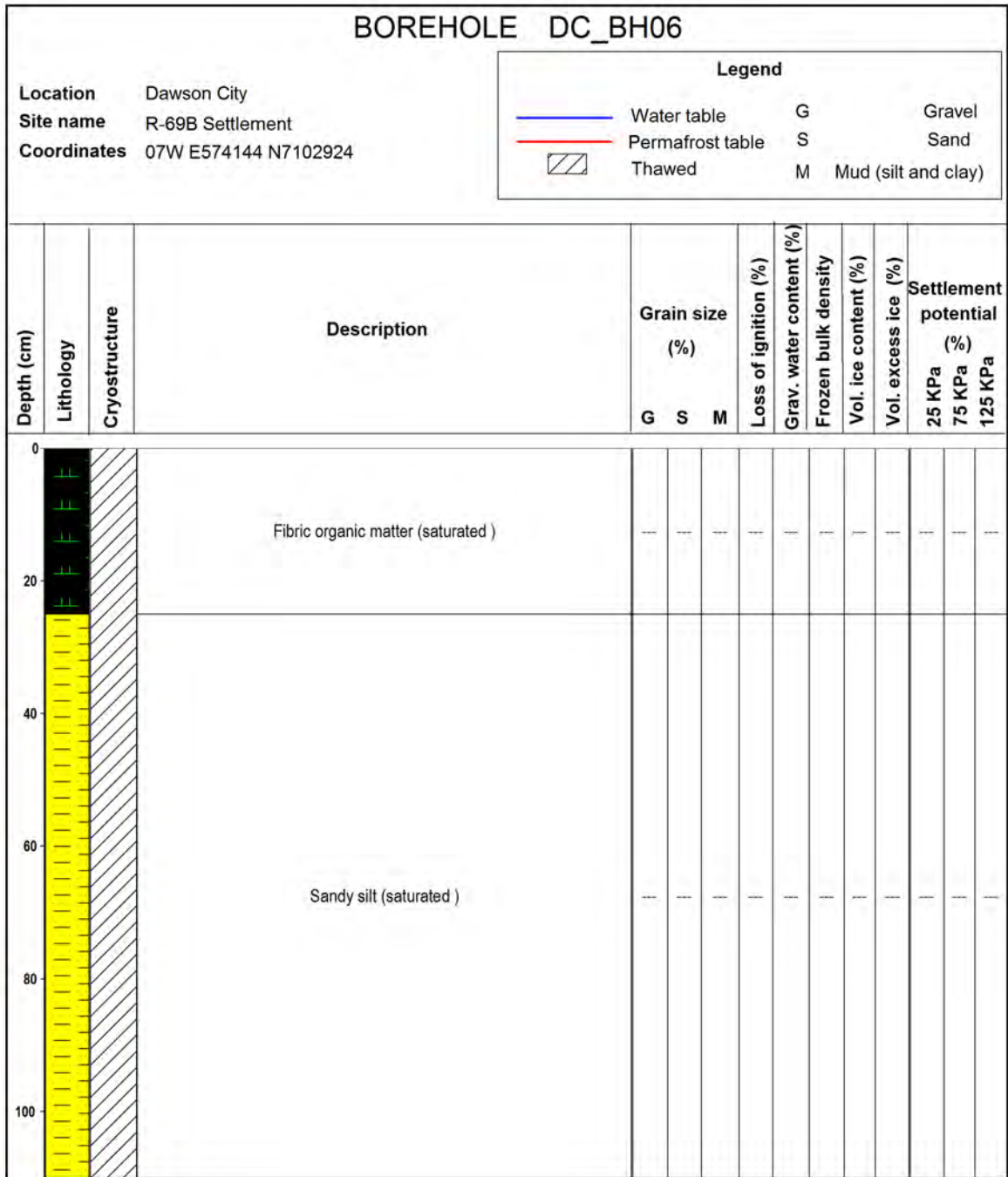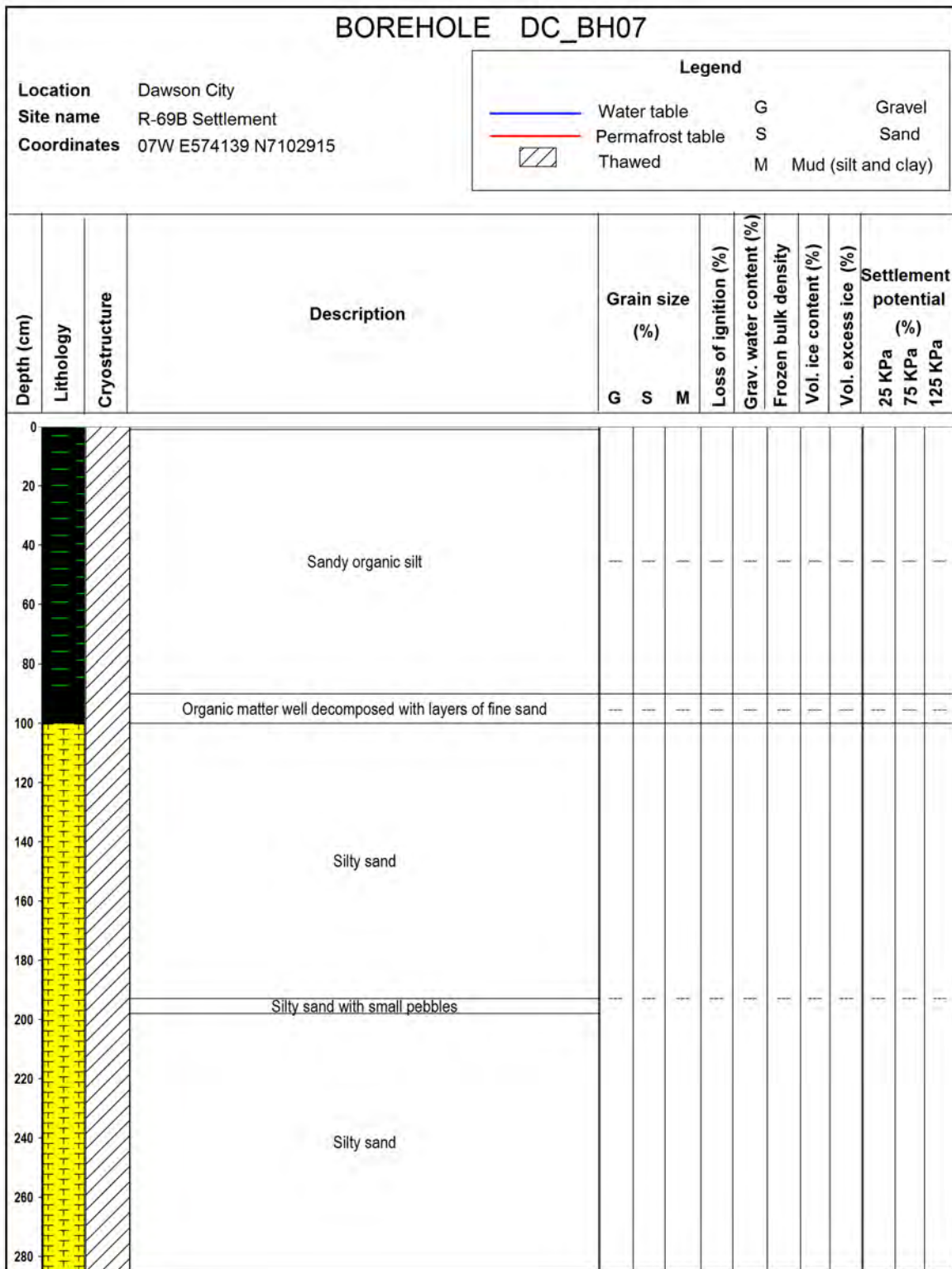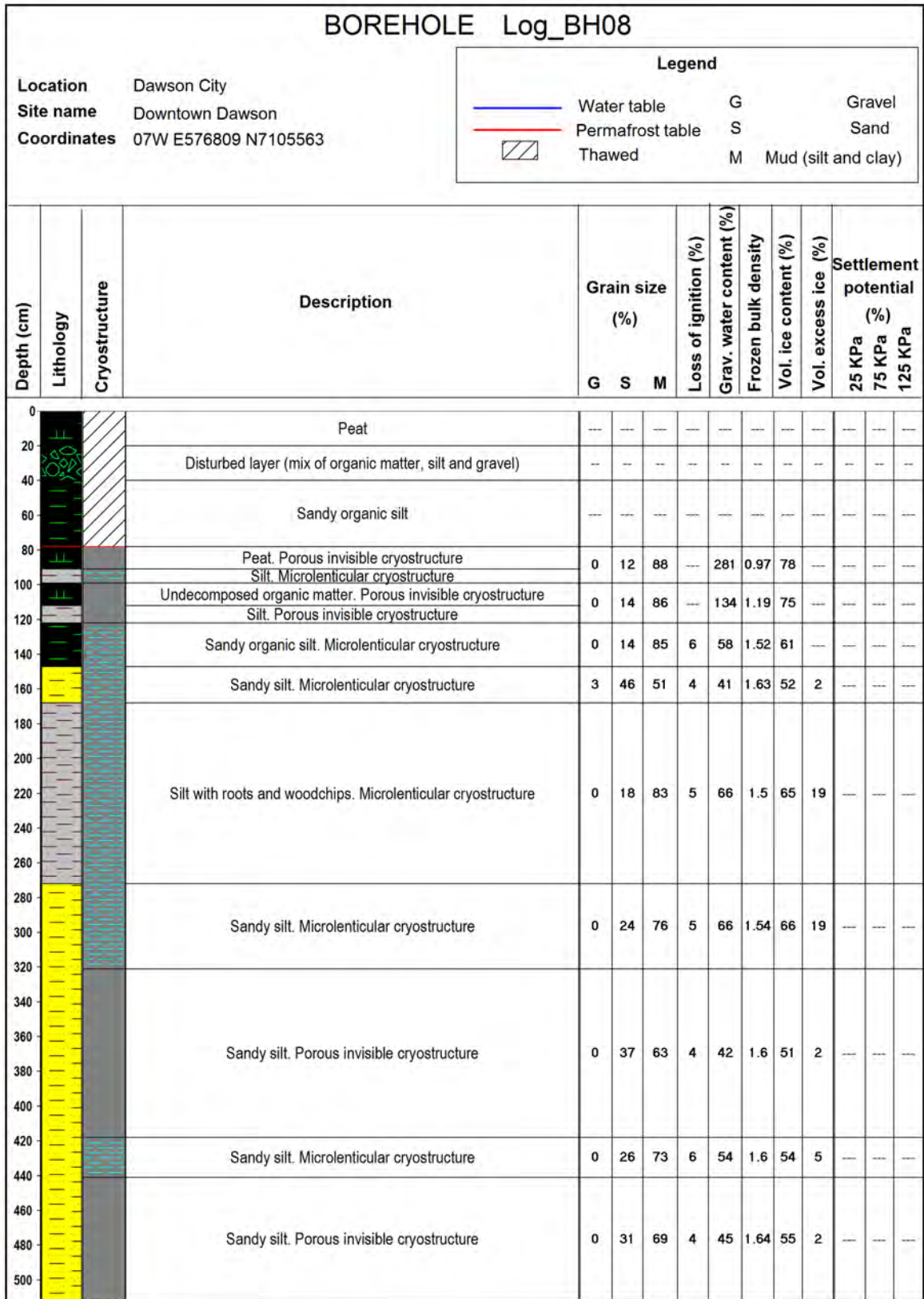
Figure B8. *Borehole log for borehole DC_BH08, from the downtown Dawson case study site (see Figure 66 in the main body of this report for location).*
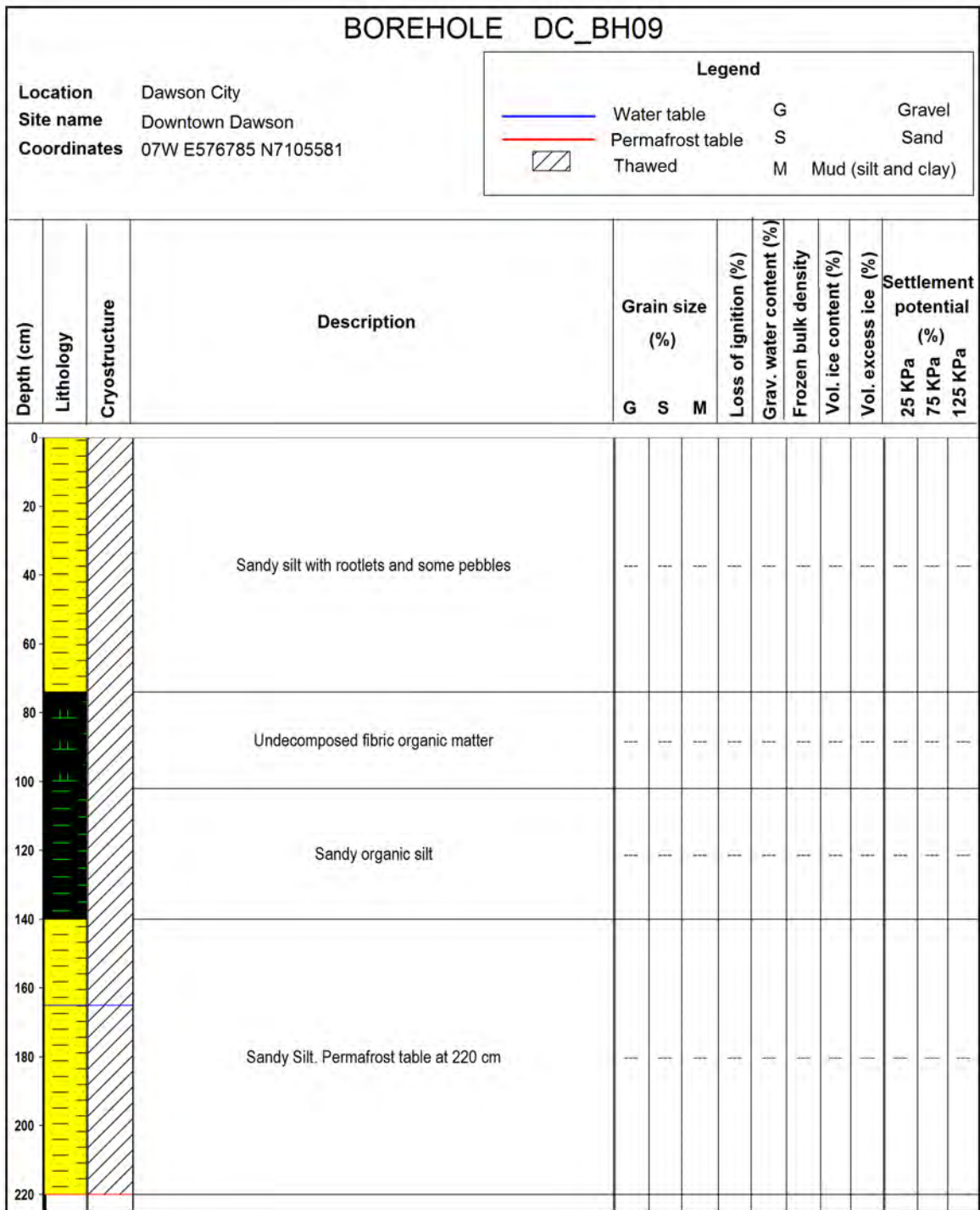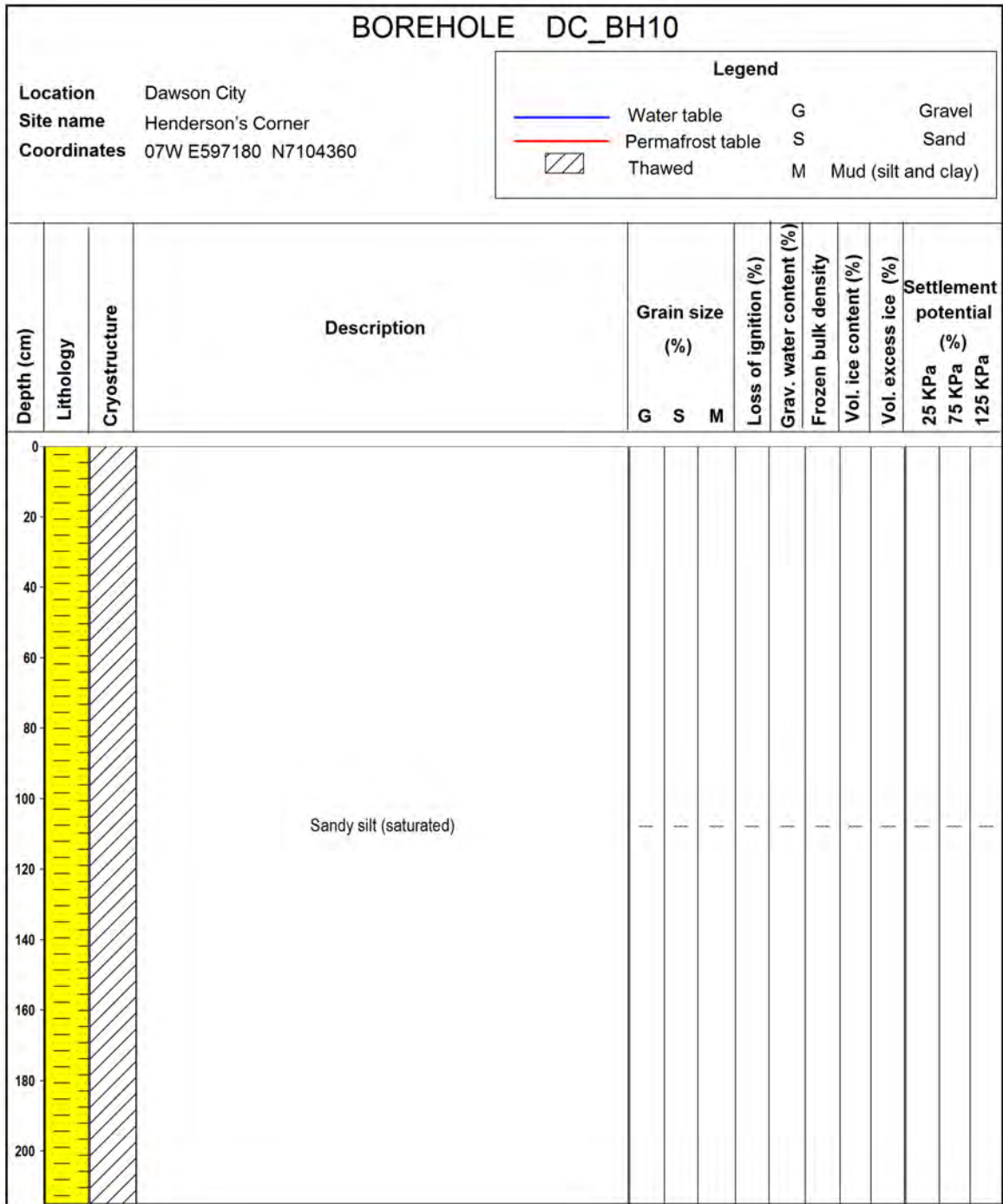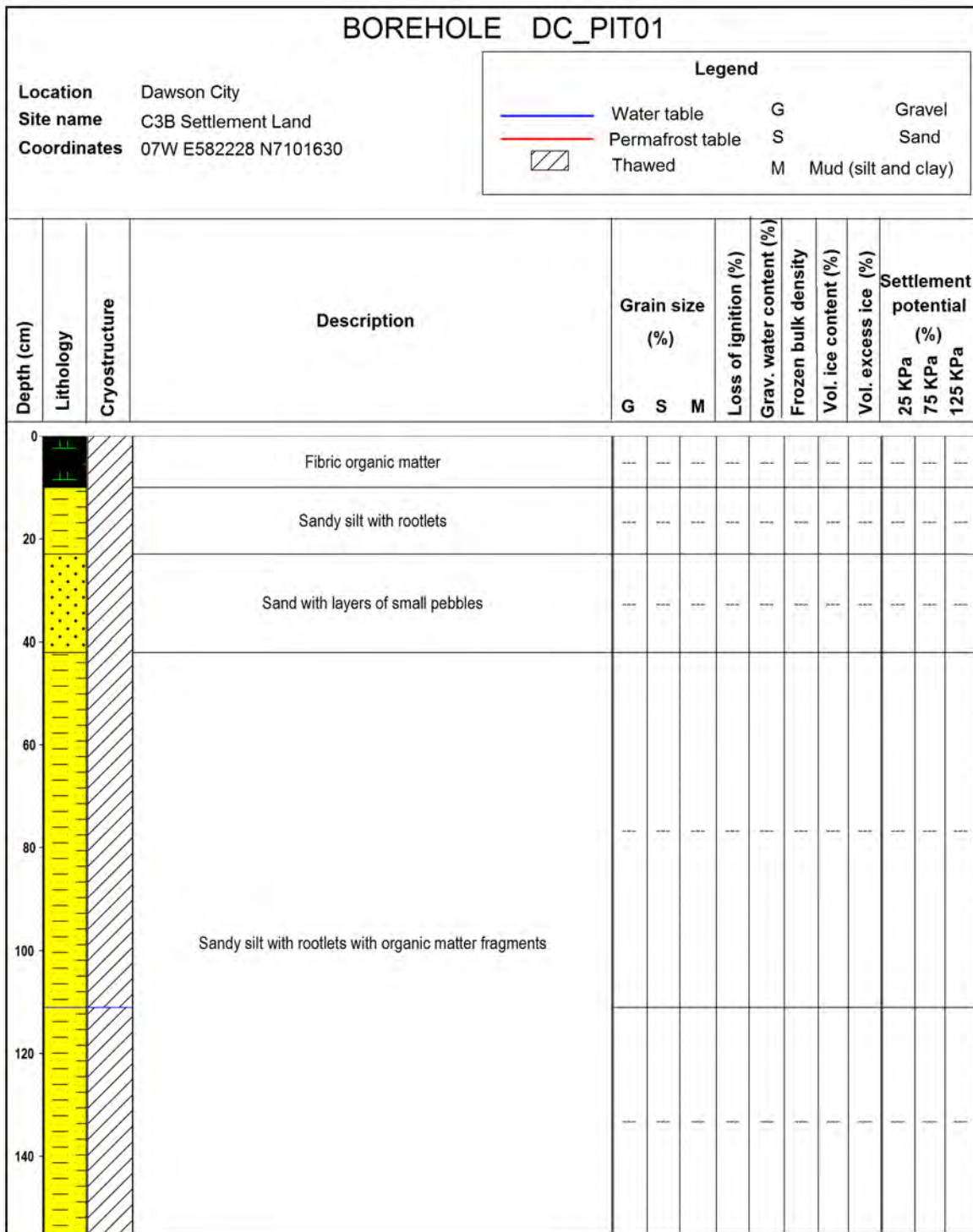
Figure B9. Borehole log for borehole DC_BH09, from the downtown Dawson case study site (see Figure 66 in the main body of this report for location).

Figure B10. *Borehole log for borehole DC_BH10, from the Henderson's Corner case study site (see Figure 68 in the main body of this report for location).*

Figure B11. Log for soil pit DC_PIT01, from the C-3B case study site (see Figure 54 in the main body of this report for location).
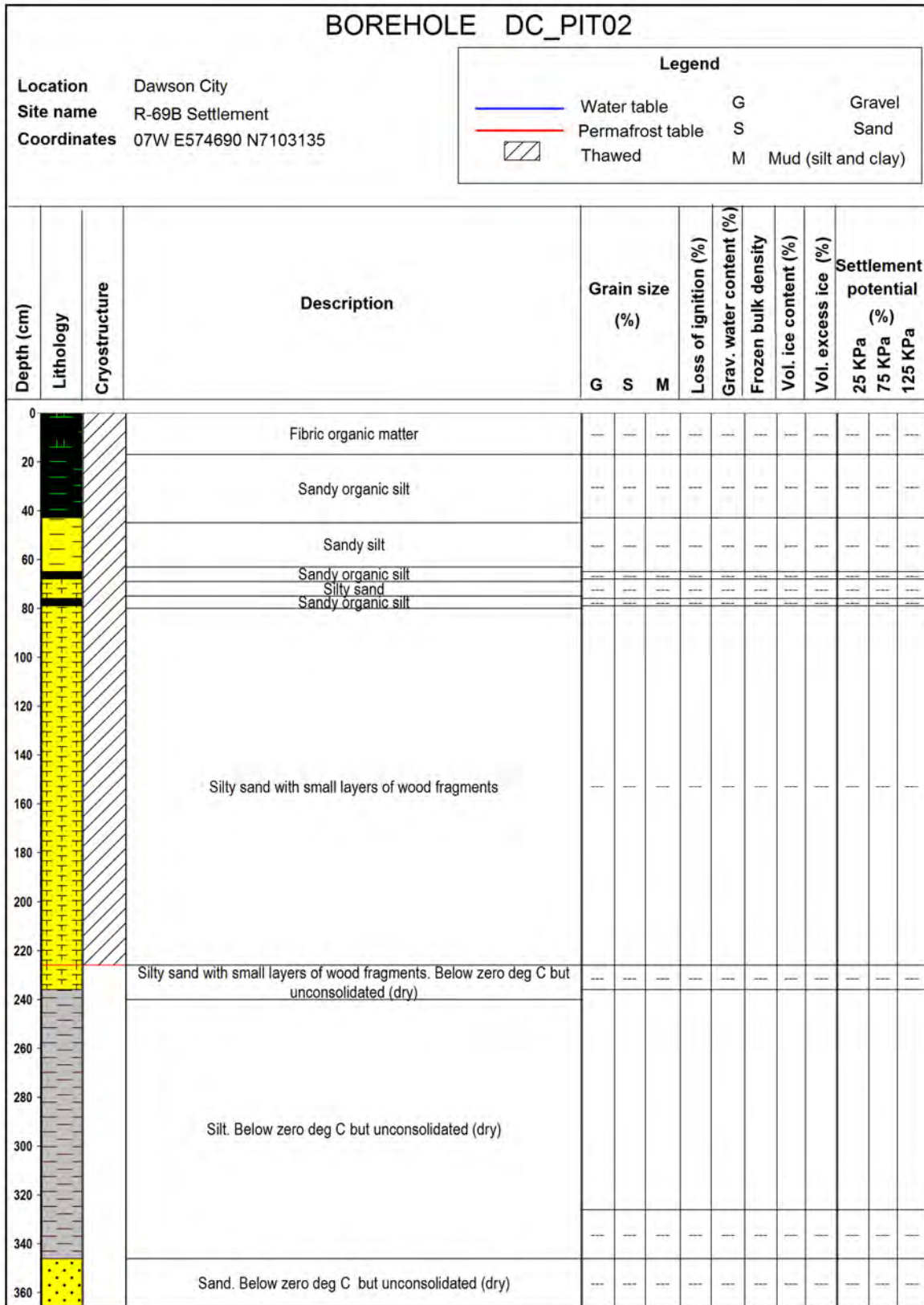
Figure B12. *Log for soil pit DC_PIT02, from the R-69B case study site (see Figure 60 in the main body of this report for location).*

APPENDIX C - GRAIN SIZE ANALYSIS

Table C1. Grain size analysis results for samples collected from boreholes drilled at case study sites in the Dawson area. See Figures 49, 50, 54, 58, 60, 66 and 68 in the main body of this report for location of case study sites and boreholes, and Appendix A for methodology.

Sample Name:	DC_BH1_90	DC_BH02 _88	DC_BH02 _123
Analyst and Date	LPR, 1/13/2015	LPR, 1/13/2015	LPR, 1/13/2015
Sieving Error	0%	0%	0%
Sample Type	Trimodal, Poorly Sorted	Polymodal, Very Poorly Sorted	Trimodal, Poorly Sorted
Textural Group	Slightly Gravelly Muddy Sand	Slightly Gravelly Muddy Sand	Slightly Gravelly Muddy Sand
Sediment Name	Slightly Very Fine Gravelly Very Coarse Silty Fine Sand	Slightly Very Fine Gravelly Very Coarse Silty Fine Sand	Slightly Very Fine Gravelly Very Coarse Silty Fine Sand
% Gravel	0.0	0.4	0.2
% Sand	84.7	60.6	59.4
% Silt & Clay	15.3	39.0	40.4
% Very Coarse Gravel	0.0	0.0	0.0
% Coarse Gravel	0.0	0.0	0.0
% Medium Gravel	0.0	0.0	0.0
% Fine Gravel	0.0	0.0	0.0
% Very Fine Gravel	0.0	0.4	0.1
% Very Coarse Sand	0.0	0.0	0.0
% Coarse Sand	0.2	10.6	3.7
% Medium Sand	6.1	10.9	5.8
% Fine Sand	63.1	26.1	31.6
% Very Fine Sand	15.3	13.0	18.4
% Very Coarse Silt	7.4	15.7	19.6
% Coarse Silt	1.8	11.0	10.3
% Medium Silt	0.5	6.2	3.0
% Fine Silt	0.9	1.2	2.4
% Very Fine Silt	0.9	1.2	2.3
% Clay	3.8	3.7	2.7

Table C2. Grain size analysis results for samples collected from boreholes drilled at case study sites in the Dawson area. See Figures 49, 50, 54, 58, 60, 66 and 68 in the main body of this report for location of case study sites and boreholes, and Appendix A for methodology.

Sample Name:	DC_BH02 _123 (1)	DC_BH02 _156	DC_BH02 _250
Analyst and Date	LPR, 1/13/2015	LPR, 1/13/2015	LPR, 1/13/2015
Sieving Error	0%	0%	0%
Sample Type	Polymodal, Poorly Sorted	Bimodal, Poorly Sorted	Trimodal, Poorly Sorted
Textural Group	Slightly Gravelly Muddy Sand	Slightly Gravelly Muddy Sand	Slightly Gravelly Muddy Sand
Sediment Name	Slightly Very Fine Gravelly Very Coarse Silty Fine Sand	Slightly Fine Gravelly Very Coarse Silty Very Fine Sand	Slightly Very Fine Gravelly Very Coarse Silty Fine Sand
% Gravel	0.2	0.0	0.2
% Sand	55.8	52.1	80.6
% Silt & Clay	44.1	47.9	19.2
% Very Coarse Gravel	0.0	0.0	0.0
% Coarse Gravel	0.0	0.0	0.0
% Medium Gravel	0.0	0.0	0.0
% Fine Gravel	0.0	0.0	0.1
% Very Fine Gravel	0.1	0.0	0.1
% Very Coarse Sand	0.0	0.0	0.0
% Coarse Sand	3.7	0.1	1.3
% Medium Sand	5.8	0.3	5.0
% Fine Sand	31.6	21.0	60.6
% Very Fine Sand	14.7	30.7	13.7
% Very Coarse Silt	27.4	25.2	7.4
% Coarse Silt	8.8	11.3	4.8
% Medium Silt	3.9	0.8	2.4
% Fine Silt	0.6	1.5	0.5
% Very Fine Silt	0.6	1.5	0.5
% Clay	2.7	7.6	3.6

Table C3. Grain size analysis results for samples collected from boreholes drilled at case study sites in the Dawson area. See Figures 49, 50, 54, 58, 60, 66 and 68 in the main body of this report for location of case study sites and boreholes, and Appendix A for methodology.

Sample Name:	DC_BH02 _276	DC_BH02 _297	DC_BH04 _72
Analyst and Date	LPR, 1/13/2015	LPR, 1/13/2015	LPR, 1/13/2015
Sieving Error	0%	0%	-0%
Sample Type	Bimodal, Moderately Sorted	Polymodal, Poorly Sorted	Bimodal, Moderately Sorted
Textural Group	Slightly Gravelly Sand	Gravelly Sand	Slightly Gravelly Sandy Mud
Sediment Name	Slightly Very Fine Gravelly Fine Sand	Fine Gravelly Fine Sand	Slightly Fine Gravelly Very Fine Sandy Very Coarse Silt
% Gravel	1.9	11.0	0.1
% Sand	92.6	82.8	30.6
% Silt & Clay	5.4	6.2	69.4
% Very Coarse Gravel	0.0	0.0	0.0
% Coarse Gravel	0.0	0.0	0.0
% Medium Gravel	0.0	0.0	0.0
% Fine Gravel	0.6	6.2	0.0
% Very Fine Gravel	1.4	4.8	0.0
% Very Coarse Sand	0.0	0.0	0.0
% Coarse Sand	2.2	9.4	3.1
% Medium Sand	7.5	15.7	6.1
% Fine Sand	61.1	49.5	7.5
% Very Fine Sand	21.8	8.2	13.8
% Very Coarse Silt	1.7	1.3	66.8
% Coarse Silt	1.1	0.9	0.0
% Medium Silt	1.0	1.0	0.0
% Fine Silt	0.7	0.7	0.0
% Very Fine Silt	0.7	0.7	0.0
% Clay	0.3	1.6	2.6

Table C4. Grain size analysis results for samples collected from boreholes drilled at case study sites in the Dawson area. See Figures 49, 50, 54, 58, 60, 66 and 68 in the main body of this report for location of case study sites and boreholes, and Appendix A for methodology.

Sample Name:	DC_BH04 _110	DC_BH04 _138	DC_BH04 _156
Analyst and Date	LPR, 1/13/2015	LPR, 1/13/2015	LPR, 1/13/2015
Sieving Error	0%	-0%	-0%
Sample Type	Bimodal, Poorly Sorted	Bimodal, Poorly Sorted	Bimodal, Very Poorly Sorted
Textural Group	Slightly Gravelly Sandy Mud	Slightly Gravelly Sandy Mud	Slightly Gravelly Sandy Mud
Sediment Name	Slightly Very Fine Gravelly Very Fine Sandy Very Coarse Silt	Slightly Very Fine Gravelly Very Fine Sandy Very Coarse Silt	Slightly Very Fine Gravelly Very Fine Sandy Very Coarse Silt
% Gravel	0.0	0.0	0.3
% Sand	33.2	23.9	34.8
% Silt & Clay	66.8	76.1	64.9
% Very Coarse Gravel	0.0	0.0	0.0
% Coarse Gravel	0.0	0.0	0.0
% Medium Gravel	0.0	0.0	0.0
% Fine Gravel	0.0	0.0	0.0
% Very Fine Gravel	0.0	0.0	0.3
% Very Coarse Sand	0.0	0.0	0.0
% Coarse Sand	2.4	1.3	4.6
% Medium Sand	4.4	3.2	7.0
% Fine Sand	9.1	5.6	9.7
% Very Fine Sand	17.2	13.8	13.4
% Very Coarse Silt	59.4	69.0	53.3
% Coarse Silt	0.0	0.0	0.0
% Medium Silt	0.0	0.0	0.0
% Fine Silt	0.0	0.0	0.0
% Very Fine Silt	0.1	0.1	0.1
% Clay	7.4	7.0	11.4

Table C5. Grain size analysis results for samples collected from boreholes drilled at case study sites in the Dawson area. See Figures 49, 50, 54, 58, 60, 66 and 68 in the main body of this report for location of case study sites and boreholes, and Appendix A for methodology.

Sample Name:	DC_BH04 _185	DC_BH04 _223	DC_BH04 _255
Analyst and Date	LPR, 1/13/2015	LPR, 1/13/2015	LPR, 1/14/2015
Sieving Error	-0%	-0%	1%
Sample Type	Bimodal, Poorly Sorted	Bimodal, Poorly Sorted	Bimodal, Moderately Well Sorted
Textural Group	Slightly Gravelly Sandy Mud	Slightly Gravelly Sandy Mud	Slightly Gravelly Sandy Mud
Sediment Name	Slightly Very Fine Gravelly Very Fine Sandy Very Coarse Silt	Slightly Very Fine Gravelly Very Fine Sandy Very Coarse Silt	Slightly Very Fine Gravelly Very Fine Sandy Very Coarse Silt
% Gravel	0.1	0.2	0.2
% Sand	49.4	21.5	21.0
% Silt & Clay	50.5	78.3	78.8
% Very Coarse Gravel	0.0	0.0	0.0
% Coarse Gravel	0.0	0.0	0.0
% Medium Gravel	0.0	0.0	0.0
% Fine Gravel	0.0	0.0	0.0
% Very Fine Gravel	0.0	0.2	0.2
% Very Coarse Sand	0.0	0.0	0.0
% Coarse Sand	3.6	3.5	3.0
% Medium Sand	3.5	4.8	1.9
% Fine Sand	6.2	5.1	2.5
% Very Fine Sand	36.1	8.1	13.6
% Very Coarse Silt	43.6	71.0	78.8
% Coarse Silt	0.0	0.0	0.0
% Medium Silt	0.0	0.0	0.0
% Fine Silt	0.0	0.0	0.0
% Very Fine Silt	0.1	0.1	0.0
% Clay	6.8	7.3	0.0

Table C6. Grain size analysis results for samples collected from boreholes drilled at case study sites in the Dawson area. See Figures 49, 50, 54, 58, 60, 66 and 68 in the main body of this report for location of case study sites and boreholes, and Appendix A for methodology.

Sample Name:	DC_BH04 _288	DC_BH04 _325	DC_BH04 _360
Analyst and Date	LPR, 1/13/2015	LPR, 1/13/2015	LPR, 1/13/2015
Sieving Error	0%	0%	0%
Sample Type	Bimodal, Moderately Well Sorted	Bimodal, Moderately Well Sorted	Bimodal, Poorly Sorted
Textural Group	Slightly Gravelly Sandy Mud	Slightly Gravelly Sandy Mud	Slightly Gravelly Sandy Mud
Sediment Name	Slightly Very Fine Gravelly Very Fine Sandy Very Coarse Silt	Slightly Very Fine Gravelly Very Fine Sandy Very Coarse Silt	Slightly Very Fine Gravelly Very Fine Sandy Very Coarse Silt
% Gravel	0.1	0.1	1.5
% Sand	16.4	18.5	30.6
% Silt & Clay	83.5	81.4	68.0
% Very Coarse Gravel	0.0	0.0	0.0
% Coarse Gravel	0.0	0.0	0.0
% Medium Gravel	0.0	0.0	0.0
% Fine Gravel	0.0	0.0	0.3
% Very Fine Gravel	0.0	0.1	1.2
% Very Coarse Sand	0.0	0.0	0.0
% Coarse Sand	2.2	2.2	5.0
% Medium Sand	2.6	2.9	3.7
% Fine Sand	3.7	4.7	4.8
% Very Fine Sand	8.0	8.8	17.0
% Very Coarse Silt	81.6	81.4	57.2
% Coarse Silt	0.0	0.0	0.0
% Medium Silt	0.0	0.0	0.0
% Fine Silt	0.0	0.0	0.0
% Very Fine Silt	0.0	0.0	0.1
% Clay	2.0	0.0	10.7

Table C7. Grain size analysis results for samples collected from boreholes drilled at case study sites in the Dawson area. See Figures 49, 50, 54, 58, 60, 66 and 68 in the main body of this report for location of case study sites and boreholes, and Appendix A for methodology.

Sample Name:	DC_BH04 _394 (2)	DC_BH04 _428	DC_BH03 _62
Analyst and Date	LPR, 1/13/2015	LPR, 1/14/2015	LPR, 1/13/2015
Sieving Error	0%	0%	-0%
Sample Type	Bimodal, Very Well Sorted	Bimodal, Very Well Sorted	Trimodal, Poorly Sorted
Textural Group	Slightly Gravelly Sandy Mud	Slightly Gravelly Sandy Mud	Slightly Gravelly Muddy Sand
Sediment Name	Slightly Very Fine Gravelly Very Fine Sandy Very Coarse Silt	Slightly Very Fine Gravelly Very Fine Sandy Very Coarse Silt	Slightly Very Fine Gravelly Very Coarse Silty Fine Sand
% Gravel	0.0	0.0	0.1
% Sand	24.5	13.5	69.0
% Silt & Clay	75.5	86.5	30.9
% Very Coarse Gravel	0.0	0.0	0.0
% Coarse Gravel	0.0	0.0	0.0
% Medium Gravel	0.0	0.0	0.0
% Fine Gravel	0.0	0.0	0.0
% Very Fine Gravel	0.0	0.0	0.1
% Very Coarse Sand	0.0	0.0	0.0
% Coarse Sand	1.4	0.5	1.7
% Medium Sand	1.0	0.7	1.9
% Fine Sand	1.9	1.6	45.3
% Very Fine Sand	20.2	10.7	20.1
% Very Coarse Silt	73.5	86.5	18.9
% Coarse Silt	0.0	0.0	7.5
% Medium Silt	0.0	0.0	1.5
% Fine Silt	0.0	0.0	1.1
% Very Fine Silt	0.0	0.0	1.1
% Clay	2.0	0.0	0.9

Table C8. Grain size analysis results for samples collected from boreholes drilled at case study sites in the Dawson area. See Figures 49, 50, 54, 58, 60, 66 and 68 in the main body of this report for location of case study sites and boreholes, and Appendix A for methodology.

Sample Name:	DC_BH03 _83	DC_BH03 _114	DC_BH03 _140
Analyst and Date	LPR, 1/13/2015	LPR, 1/13/2015	LPR, 1/13/2015
Sieving Error	0%	0%	0%
Sample Type	Trimodal, Poorly Sorted	Trimodal, Very Poorly Sorted	Trimodal, Poorly Sorted
Textural Group	Slightly Gravelly Muddy Sand	Slightly Gravelly Muddy Sand	Slightly Gravelly Muddy Sand
Sediment Name	Slightly Very Fine Gravelly Very Coarse Silty Very Fine Sand	Slightly Very Fine Gravelly Very Coarse Silty Very Fine Sand	Slightly Very Fine Gravelly Very Coarse Silty Fine Sand
% Gravel	0.4	0.0	0.0
% Sand	53.4	53.3	76.0
% Silt & Clay	46.2	46.7	23.9
% Very Coarse Gravel	0.0	0.0	0.0
% Coarse Gravel	0.0	0.0	0.0
% Medium Gravel	0.0	0.0	0.0
% Fine Gravel	0.0	0.0	0.0
% Very Fine Gravel	0.4	0.0	0.0
% Very Coarse Sand	0.0	0.0	0.0
% Coarse Sand	3.4	10.7	5.6
% Medium Sand	3.5	11.7	6.6
% Fine Sand	22.8	15.3	44.0
% Very Fine Sand	23.8	15.6	19.7
% Very Coarse Silt	26.2	32.5	11.0
% Coarse Silt	11.2	5.1	4.7
% Medium Silt	2.8	1.9	2.7
% Fine Silt	0.9	1.2	0.8
% Very Fine Silt	0.9	1.2	0.8
% Clay	4.1	4.6	3.9

Table C9. Grain size analysis results for samples collected from boreholes drilled at case study sites in the Dawson area. See Figures 49, 50, 54, 58, 60, 66 and 68 in the main body of this report for location of case study sites and boreholes, and Appendix A for methodology.

Sample Name:	DC_BH03 _177	DC_BH03 _204	DC_BH03 _234 (2)
Analyst and Date	LPR, 1/13/2015	LPR, 1/13/2015	LPR, 1/13/2015
Sieving Error	-0%	0%	0%
Sample Type	Trimodal, Poorly Sorted	Trimodal, Poorly Sorted	Polymodal, Poorly Sorted
Textural Group	Muddy Sand	Slightly Gravelly Muddy Sand	Slightly Gravelly Muddy Sand
Sediment Name	Very Coarse Silty Fine Sand	Slightly Very Fine Gravelly Very Coarse Silty Fine Sand	Slightly Very Fine Gravelly Very Coarse Silty Fine Sand
% Gravel	0.0	0.0	0.1
% Sand	64.8	67.2	59.5
% Silt & Clay	35.2	32.7	40.4
% Very Coarse Gravel	0.0	0.0	0.0
% Coarse Gravel	0.0	0.0	0.0
% Medium Gravel	0.0	0.0	0.0
% Fine Gravel	0.0	0.0	0.0
% Very Fine Gravel	0.0	0.0	0.0
% Very Coarse Sand	0.0	0.0	0.0
% Coarse Sand	1.0	1.2	1.4
% Medium Sand	1.4	1.7	1.6
% Fine Sand	34.9	41.0	31.6
% Very Fine Sand	27.4	23.4	24.9
% Very Coarse Silt	22.2	18.4	20.4
% Coarse Silt	5.2	5.3	12.5
% Medium Silt	0.8	1.9	2.2
% Fine Silt	1.6	0.5	1.1
% Very Fine Silt	1.5	0.5	1.1
% Clay	3.9	6.2	3.1

Table C10. Grain size analysis results for samples collected from boreholes drilled at case study sites in the Dawson area. See Figures 49, 50, 54, 58, 60, 66 and 68 in the main body of this report for location of case study sites and boreholes, and Appendix A for methodology.

Sample Name:	DC_BH03 274	DC_BH03 _308	DC_BH03 _337
Analyst and Date	LPR, 1/13/2015	LPR, 1/13/2015	LPR, 1/13/2015
Sieving Error	0%	0%	0%
Sample Type	Unimodal, Moderately Sorted	Trimodal, Poorly Sorted	Bimodal, Moderately Sorted
Textural Group	Sand	Slightly Gravelly Muddy Sand	Slightly Gravelly Sand
Sediment Name	Moderately Sorted Fine Sand	Slightly Very Fine Gravelly Very Coarse Silty Fine Sand	Slightly Very Fine Gravelly Fine Sand
% Gravel	0.0	0.0	0.0
% Sand	92.3	52.4	90.7
% Silt & Clay	7.7	47.5	9.3
% Very Coarse Gravel	0.0	0.0	0.0
% Coarse Gravel	0.0	0.0	0.0
% Medium Gravel	0.0	0.0	0.0
% Fine Gravel	0.0	0.0	0.0
% Very Fine Gravel	0.0	0.0	0.0
% Very Coarse Sand	0.0	0.0	0.0
% Coarse Sand	2.2	0.6	1.4
% Medium Sand	1.7	0.7	2.2
% Fine Sand	80.7	25.8	71.6
% Very Fine Sand	7.7	25.4	15.5
% Very Coarse Silt	1.0	31.2	2.9
% Coarse Silt	1.2	7.2	3.6
% Medium Silt	0.6	1.9	1.6
% Fine Silt	0.9	0.5	0.5
% Very Fine Silt	0.9	0.5	0.5
% Clay	3.1	6.3	0.3

Table C11. Grain size analysis results for samples collected from boreholes drilled at case study sites in the Dawson area. See Figures 49, 50, 54, 58, 60, 66 and 68 in the main body of this report for location of case study sites and boreholes, and Appendix A for methodology.

Sample Name:	DC_BH03 _375	DC_BH03 _410	DC_BH08 _99
Analyst and Date	LPR, 1/13/2015	LPR, 1/13/2015	LPR, 1/13/2015
Sieving Error	0%	0%	0%
Sample Type	Trimodal, Poorly Sorted	Trimodal, Poorly Sorted	Unimodal, Very Well Sorted
Textural Group	Slightly Gravelly Muddy Sand	Slightly Gravelly Muddy Sand	Slightly Gravelly Sandy Mud
Sediment Name	Slightly Very Fine Gravelly Very Coarse Silty Fine Sand	Slightly Very Fine Gravelly Very Coarse Silty Fine Sand	Slightly Very Fine Gravelly Very Fine Sandy Very Coarse Silt
% Gravel	0.1	0.0	0.0
% Sand	66.9	67.0	12.0
% Silt & Clay	33.0	33.0	87.9
% Very Coarse Gravel	0.0	0.0	0.0
% Coarse Gravel	0.0	0.0	0.0
% Medium Gravel	0.0	0.0	0.0
% Fine Gravel	0.0	0.0	0.0
% Very Fine Gravel	0.1	0.0	0.0
% Very Coarse Sand	0.0	0.0	0.0
% Coarse Sand	1.0	1.1	0.0
% Medium Sand	1.0	1.0	1.4
% Fine Sand	42.9	42.9	3.4
% Very Fine Sand	22.0	22.0	7.2
% Very Coarse Silt	19.2	18.5	87.9
% Coarse Silt	6.7	5.2	0.0
% Medium Silt	1.6	1.2	0.0
% Fine Silt	1.2	0.9	0.0
% Very Fine Silt	1.2	1.0	0.0
% Clay	3.1	6.2	0.0

Table C12. Grain size analysis results for samples collected from boreholes drilled at case study sites in the Dawson area. See Figures 49, 50, 54, 58, 60, 66 and 68 in the main body of this report for location of case study sites and boreholes, and Appendix A for methodology.

Sample Name:	DC_BH08 _122	DC_BH08 _147	DC_BH08_168
Analyst and Date	LPR, 1/13/2015	LPR, 1/13/2015	LPR, 1/13/2015
Sieving Error	0%	0%	0%
Sample Type	Bimodal, Well Sorted	Bimodal, Well Sorted	Bimodal, Moderately Well Sorted
Textural Group	Slightly Gravelly Sandy Mud	Slightly Gravelly Sandy Mud	Slightly Gravelly Sandy Mud
Sediment Name	Slightly Very Fine Gravelly Very Fine Sandy Very Coarse Silt	Slightly Very Fine Gravelly Very Fine Sandy Very Coarse Silt	Slightly Fine Gravelly Very Fine Sandy Very Coarse Silt
% Gravel	0.2	0.7	2.6
% Sand	13.7	14.1	46.3
% Silt & Clay	86.1	85.2	51.1
% Very Coarse Gravel	0.0	0.0	0.0
% Coarse Gravel	0.0	0.0	0.0
% Medium Gravel	0.0	0.0	0.0
% Fine Gravel	0.0	0.1	1.6
% Very Fine Gravel	0.2	0.6	1.0
% Very Coarse Sand	0.6	0.9	0.8
% Coarse Sand	1.0	1.0	1.1
% Medium Sand	1.6	1.6	2.0
% Fine Sand	3.2	2.9	7.4
% Very Fine Sand	7.4	7.7	35.1
% Very Coarse Silt	86.1	85.2	51.1
% Coarse Silt	0.0	0.0	0.0
% Medium Silt	0.0	0.0	0.0
% Fine Silt	0.0	0.0	0.0
% Very Fine Silt	0.0	0.0	0.0
% Clay	0.0	0.0	0.0

Table C13. Grain size analysis results for samples collected from boreholes drilled at case study sites in the Dawson area. See Figures 49, 50, 54, 58, 60, 66 and 68 in the main body of this report for location of case study sites and boreholes, and Appendix A for methodology.

Sample Name:	DC_BH08 _272	DC_BH08 _294	DC_BH08 _321
Analyst and Date	LPR, 1/13/2015	LPR, 1/13/2015	LPR, 1/13/2015
Sieving Error	0%	0%	0%
Sample Type	Bimodal, Very Well Sorted	Bimodal, Well Sorted	Bimodal, Moderately Well Sorted
Textural Group	Sandy Mud	Slightly Gravelly Sandy Mud	Slightly Gravelly Sandy Mud
Sediment Name	Very Fine Sandy Very Coarse Silt	Slightly Very Fine Gravelly Very Fine Sandy Very Coarse Silt	Slightly Fine Gravelly Very Fine Sandy Very Coarse Silt
% Gravel	0.0	0.1	0.3
% Sand	17.5	21.4	25.7
% Silt & Clay	82.5	78.5	73.9
% Very Coarse Gravel	0.0	0.0	0.0
% Coarse Gravel	0.0	0.0	0.0
% Medium Gravel	0.0	0.0	0.0
% Fine Gravel	0.0	0.0	0.2
% Very Fine Gravel	0.0	0.1	0.1
% Very Coarse Sand	0.0	0.2	0.4
% Coarse Sand	0.0	0.4	0.8
% Medium Sand	0.0	0.8	2.0
% Fine Sand	0.0	3.8	5.3
% Very Fine Sand	17.5	16.3	17.2
% Very Coarse Silt	82.5	78.5	73.9
% Coarse Silt	0.0	0.0	0.0
% Medium Silt	0.0	0.0	0.0
% Fine Silt	0.0	0.0	0.0
% Very Fine Silt	0.0	0.0	0.0
% Clay	0.0	0.0	0.0

Table C14. Grain size analysis results for samples collected from boreholes drilled at case study sites in the Dawson area. See Figures 49, 50, 54, 58, 60, 66 and 68 in the main body of this report for location of case study sites and boreholes, and Appendix A for methodology.

Sample Name:	DC_BH08 _353	DC_BH08 _372	DC_BH08 _397
Analyst and Date	LPR, 1/13/2015	LPR, 1/13/2015	LPR, 1/13/2015
Sieving Error	0%	0%	0%
Sample Type	Bimodal, Moderately Well Sorted	Bimodal, Well Sorted	Bimodal, Moderately Well Sorted
Textural Group	Sandy Mud	Slightly Gravelly Sandy Mud	Sandy Mud
Sediment Name	Very Fine Sandy Very Coarse Silt	Slightly Very Fine Gravelly Very Fine Sandy Very Coarse Silt	Very Fine Sandy Very Coarse Silt
% Gravel	0.0	0.0	0.0
% Sand	34.2	41.3	43.2
% Silt & Clay	65.8	58.6	56.8
% Very Coarse Gravel	0.0	0.0	0.0
% Coarse Gravel	0.0	0.0	0.0
% Medium Gravel	0.0	0.0	0.0
% Fine Gravel	0.0	0.0	0.0
% Very Fine Gravel	0.0	0.0	0.0
% Very Coarse Sand	0.9	0.2	0.2
% Coarse Sand	0.7	0.3	0.4
% Medium Sand	1.5	0.7	1.6
% Fine Sand	4.7	4.5	8.0
% Very Fine Sand	26.4	35.7	33.0
% Very Coarse Silt	65.8	58.6	56.8
% Coarse Silt	0.0	0.0	0.0
% Medium Silt	0.0	0.0	0.0
% Fine Silt	0.0	0.0	0.0
% Very Fine Silt	0.0	0.0	0.0
% Clay	0.0	0.0	0.0

Table C15. Grain size analysis results for samples collected from boreholes drilled at case study sites in the Dawson area. See Figures 49, 50, 54, 58, 60, 66 and 68 in the main body of this report for location of case study sites and boreholes, and Appendix A for methodology.

Sample Name:	DC_BH08 _418	DC_BH08 _441	DC_BH08 _462
Analyst and Date	LPR, 1/13/2015	LPR, 1/13/2015	LPR, 1/13/2015
Sieving Error	0%	0%	0%
Sample Type	Bimodal, Moderately Well Sorted	Bimodal, Moderately Well Sorted	Bimodal, Well Sorted
Textural Group	Slightly Gravelly Sandy Mud	Slightly Gravelly Sandy Mud	Slightly Gravelly Sandy Mud
Sediment Name	Slightly Very Fine Gravelly Very Fine Sandy Very Coarse Silt	Slightly Very Fine Gravelly Very Fine Sandy Very Coarse Silt	Slightly Very Fine Gravelly Very Fine Sandy Very Coarse Silt
% Gravel	0.6	0.6	0.1
% Sand	27.6	26.1	32.7
% Silt & Clay	71.8	73.4	67.2
% Very Coarse Gravel	0.0	0.0	0.0
% Coarse Gravel	0.0	0.0	0.0
% Medium Gravel	0.0	0.0	0.0
% Fine Gravel	0.0	0.2	0.0
% Very Fine Gravel	0.5	0.4	0.1
% Very Coarse Sand	0.9	0.4	0.3
% Coarse Sand	0.9	0.5	0.3
% Medium Sand	1.5	1.6	1.0
% Fine Sand	4.9	5.1	5.8
% Very Fine Sand	19.5	18.5	25.3
% Very Coarse Silt	71.8	73.4	67.2
% Coarse Silt	0.0	0.0	0.0
% Medium Silt	0.0	0.0	0.0
% Fine Silt	0.0	0.0	0.0
% Very Fine Silt	0.0	0.0	0.0
% Clay	0.0	0.0	0.0

Table C16. Grain size analysis results for samples collected from boreholes drilled at case study sites in the Dawson area. See Figures 49, 50, 54, 58, 60, 66 and 68 in the main body of this report for location of case study sites and boreholes, and Appendix A for methodology.

Sample Name:	DC_BH08 _512	DC_BH05 _75	DC_BH05 _104
Analyst and Date	LPR, 1/13/2015	LPR, 1/13/2015	LPR, 1/13/2015
Sieving Error	0%	0%	0%
Sample Type	Bimodal, Well Sorted	Bimodal, Poorly Sorted	Bimodal, Moderately Well Sorted
Textural Group	Sandy Mud	Slightly Gravelly Sandy Mud	Slightly Gravelly Muddy Sand
Sediment Name	Very Fine Sandy Very Coarse Silt	Slightly Very Fine Gravelly Very Fine Sandy Very Coarse Silt	Slightly Very Fine Gravelly Very Coarse Silty Very Fine Sand
% Gravel	0.0	1.6	0.8
% Sand	29.0	45.0	62.7
% Silt & Clay	71.0	53.4	36.5
% Very Coarse Gravel	0.0	0.0	0.0
% Coarse Gravel	0.0	0.0	0.0
% Medium Gravel	0.0	0.0	0.0
% Fine Gravel	0.0	0.3	0.2
% Very Fine Gravel	0.0	1.3	0.7
% Very Coarse Sand	0.3	2.7	1.1
% Coarse Sand	0.3	4.3	1.9
% Medium Sand	1.0	7.0	3.9
% Fine Sand	4.9	12.1	8.2
% Very Fine Sand	22.5	18.9	47.6
% Very Coarse Silt	71.0	53.4	36.5
% Coarse Silt	0.0	0.0	0.0
% Medium Silt	0.0	0.0	0.0
% Fine Silt	0.0	0.0	0.0
% Very Fine Silt	0.0	0.0	0.0
% Clay	0.0	0.0	0.0

Table C17. Grain size analysis results for samples collected from boreholes drilled at case study sites in the Dawson area. See Figures 49, 50, 54, 58, 60, 66 and 68 in the main body of this report for location of case study sites and boreholes, and Appendix A for methodology.

Sample Name:	DC_BH05 _134	DC_BH05 _160	DC_BH05 _206
Analyst and Date	LPR, 1/13/2015	LPR, 1/13/2015	LPR, 1/13/2015
Sieving Error	0%	0%	0%
Sample Type	Bimodal, Moderately Well Sorted	Bimodal, Moderately Well Sorted	Bimodal, Moderately Sorted
Textural Group	Sandy Mud	Slightly Gravelly Sandy Mud	Slightly Gravelly Sandy Mud
Sediment Name	Very Fine Sandy Very Coarse Silt	Slightly Very Fine Gravelly Very Fine Sandy Very Coarse Silt	Slightly Very Fine Gravelly Very Fine Sandy Very Coarse Silt
% Gravel	0.0	0.1	0.1
% Sand	38.4	36.4	35.1
% Silt & Clay	61.6	63.5	64.8
% Very Coarse Gravel	0.0	0.0	0.0
% Coarse Gravel	0.0	0.0	0.0
% Medium Gravel	0.0	0.0	0.0
% Fine Gravel	0.0	0.0	0.0
% Very Fine Gravel	0.0	0.1	0.1
% Very Coarse Sand	0.0	0.6	0.5
% Coarse Sand	0.0	1.6	2.0
% Medium Sand	0.0	4.1	5.1
% Fine Sand	12.8	8.9	9.4
% Very Fine Sand	25.6	21.3	18.1
% Very Coarse Silt	61.6	63.5	64.8
% Coarse Silt	0.0	0.0	0.0
% Medium Silt	0.0	0.0	0.0
% Fine Silt	0.0	0.0	0.0
% Very Fine Silt	0.0	0.0	0.0
% Clay	0.0	0.0	0.0

Table C18. Grain size analysis results for samples collected from boreholes drilled at case study sites in the Dawson area. See Figures 49, 50, 54, 58, 60, 66 and 68 in the main body of this report for location of case study sites and boreholes, and Appendix A for methodology.

Sample Name:	DC_BH05 _228	DC_BH05 _311	DC_BH05 _329
Analyst and Date	LPR, 1/13/2015	LPR, 1/13/2015	LPR, 1/13/2015
Sieving Error	0%	0%	0%
Sample Type	Trimodal, Very Poorly Sorted	Bimodal, Poorly Sorted	Bimodal, Very Well Sorted
Textural Group	Gravelly Muddy Sand	Sandy Mud	Sandy Mud
Sediment Name	Very Fine Gravelly Very Coarse Silty Very Fine Sand	Very Fine Sandy Very Coarse Silt	Very Fine Sandy Very Coarse Silt
% Gravel	9.4	0.0	0.0
% Sand	47.8	47.0	28.1
% Silt & Clay	42.8	53.0	71.9
% Very Coarse Gravel	0.0	0.0	0.0
% Coarse Gravel	0.0	0.0	0.0
% Medium Gravel	0.0	0.0	0.0
% Fine Gravel	0.4	0.0	0.0
% Very Fine Gravel	9.0	0.0	0.0
% Very Coarse Sand	11.9	0.0	0.0
% Coarse Sand	5.8	0.0	0.0
% Medium Sand	5.9	13.1	0.0
% Fine Sand	7.7	16.4	0.0
% Very Fine Sand	16.4	17.5	28.1
% Very Coarse Silt	42.8	53.0	71.9
% Coarse Silt	0.0	0.0	0.0
% Medium Silt	0.0	0.0	0.0
% Fine Silt	0.0	0.0	0.0
% Very Fine Silt	0.0	0.0	0.0
% Clay	0.0	0.0	0.0

Table C19. Grain size analysis results for samples collected from boreholes drilled at case study sites in the Dawson area. See Figures 49, 50, 54, 58, 60, 66 and 68 in the main body of this report for location of case study sites and boreholes, and Appendix A for methodology.

Sample Name:	DC_BH05 _359	DC_BH05 _386	DC_BH05 _414	DC_BH05 _446
Analyst and Date	LPR, 1/13/2015	LPR, 1/13/2015	LPR, 1/13/2015	LPR, 1/13/2015
Sieving Error	0%	0%	0%	0%
Sample Type	Bimodal, Very Well Sorted	Bimodal, Very Well Sorted	Bimodal, Moderately Well Sorted	Trimodal, Poorly Sorted
Textural Group	Sandy Mud	Sandy Mud	Slightly Gravelly Sandy Mud	Slightly Gravelly Muddy Sand
Sediment Name	Very Fine Sandy Very Coarse Silt	Very Fine Sandy Very Coarse Silt	Slightly Very Fine Gravelly Very Fine Sandy Very Coarse Silt	Slightly Very Fine Gravelly Very Coarse Silty Very Fine Sand
% Gravel	0.0	0.0	0.5	1.0
% Sand	29.0	12.3	24.2	57.9
% Silt & Clay	71.0	87.7	75.3	41.1
% Very Coarse Gravel	0.0	0.0	0.0	0.0
% Coarse Gravel	0.0	0.0	0.0	0.0
% Medium Gravel	0.0	0.0	0.0	0.0
% Fine Gravel	0.0	0.0	0.2	0.1
% Very Fine Gravel	0.0	0.0	0.4	0.9
% Very Coarse Sand	0.0	0.0	0.4	2.1
% Coarse Sand	0.0	0.0	0.8	4.7
% Medium Sand	0.0	0.0	3.6	9.6
% Fine Sand	0.0	0.0	6.5	16.4
% Very Fine Sand	29.0	12.3	12.8	25.2
% Very Coarse Silt	71.0	87.7	75.3	41.1
% Coarse Silt	0.0	0.0	0.0	0.0
% Medium Silt	0.0	0.0	0.0	0.0
% Fine Silt	0.0	0.0	0.0	0.0
% Very Fine Silt	0.0	0.0	0.0	0.0
% Clay	0.0	0.0	0.0	0.0

APPENDIX D - CLIMATE PROJECTIONS

Projections of changes in mean annual air temperature (MAAT) were prepared for this report based on annual air temperature modelling, and were enhanced to reflect heterogeneity in the local landscape (specifically, mountainous terrain). This represents a significant increase in the understanding of MAAT. This approach incorporated specific topographical features in the study region (e.g., mountains) and knowledge about related area-specific surface lapse rates (SLRs) at fine resolution (30 x 30 m). To develop these enhanced air temperature models and predictions, current MAAT modeling was conducted. Work drew on data from clusters of previously established air temperature monitoring stations in Yukon. Each monitoring station consisted of a radiation shield mounted at 1.5-1.6 m on a metal pole. An Onset Hobo Pro data-logger (accuracy ±0.2°C), equipped with an external thermistor, was used to monitor air temperature inside the screen. In order to predict MAAT across the region, a 3rd order polynomial trend surface of annual SLR values below treeline was generated (Lewkowicz and Bonnaventure, 2011). This surface was then combined with a 4th order polynomial trend surface of treeline elevations, which was separately developed from sampling topographic maps and Google Earth images to limit the application of the SLR values to terrain below treeline. Above this level, it was assumed that standard environmental lapse rates of -6.5°C/km prevail. In addition, a 3rd order polynomial trend surface of projected sea level temperature was generated from the long-term records of 18 climate stations in the region (Environment Canada, 2013), which had been reduced to sea level (e.g., Etzelmuller et al., 2007) by applying the projected SLR value for each station based on its continentality (Lewkowicz and Bonnaventure, 2011). The projected sea level temperature surface was then readjusted using a digital elevation model at 30 x 30 m resolution, the SLR grid for elevations up to treeline, and the standard environmental lapse rate from treeline upwards. The result was a gridded model of MAAT for the region based on elevation with the measured variability in SLR taken into account but not including aspect or localized topographic effects on cold-air pooling.

The basis for developing projections of MAAT incorporating the SLRs (also called perturbed MAAT models) involved using statistically downscaled GCM data obtained from the Scenarios Network for Arctic and Alaska Planning at the University of Alaska Fairbanks (SNAP, 2012; www.snap.uaf.edu). The SNAP dataset contains multiple GCM scenarios for mean annual air temperatures, as well as modelled average temperature surfaces for past climate normals (e.g., 1980-2009). The data used to obtain the perturbed MAAT models included the 2 km-resolution projection surfaces provided by SNAP for the IPCC scenarios of A1B, A2 and B1. These particular scenarios were chosen for this application because they represent the most commonly used scenarios in GCM modelling and represent a broad range of potential climate conditions. To develop each scenario, SNAP drew on data from five separate models, thereby ensuring the greatest range of predictions within each scenario. Perturbed MAAT models were developed by examining the difference (and thus change) between what the SNAP model predicted for the current climate (i.e., the 1980-2009 climate normal) and each of the three scenarios for the years 2020, 2050 and 2080. In addition, a backcasted model was also produced which examined the difference between current climate (1980-2009) and the climate normal from 1950-1979. Hence, modelling efforts examined the predicted difference between each time slice for each scenario and adjusted the previously created MAAT model accordingly. In order to incorporate the data from the 2 x 2 km grid cells for each SNAP model, the cell size was resampled to 30 x 30 m. This effectively provided a broad geographic basis for sample change at a territorial scale (macroclimate), which could then be topographically corrected to site specific SLRs in the Dawson study area. The differences between the predicted SNAP models were then added (forecasting) or subtracted (backcasting) to the current MAAT model using raster calculator in ArcGIS$^©$ 10.1 (ESRI, USA). The results of

these models provide significantly more information about the variable nature of spatial climate in geographically mountainous areas than the raw GCM data itself, which typically displays high levels of inaccuracies in the mountainous regions of Yukon.

Results are presented in Figures D1 to D10, below. Current (i.e., 1980-2009) MAAT results in the area of Dawson City fall within the range of -3.2 to -4.0°C, and temperatures were found to be colder in the backcasted (1950-1979) model for the area by about 1.5°C. A summary of temperature results for each model for the study region are presented below in Table D1.

Note that additional climate projections, based on data provided by SNAP (2012), are available by contacting the Northern Climate ExChange (Yukon Research Centre, Yukon College). Projections are available for mean annual and seasonal temperature and precipitation, as well as freeze and thaw dates and growing degree days, for the A1B and B1 scenarios, for the 2020s and 2050s, as well as the 1960-1990 time period.

Table D1. Statistics generated for the B1, A1B and A2 climate scenarios, showing mean, minimum and maximum air temperature in the 2020s, 2050s and 2080s.

Projection	Air Temperature (°C)		
	Mean	Minimum	Maximum
Current MAAT	-3.6	-4.0	-3.2
1950 - 1979	-5.0	-5.5	-4.7
B1 2020s	-3.6	-4.0	-3.2
B1 2050s	-3.0	-3.4	-2.6
B1 2080s	-1.9	-2.3	-1.5
A1B 2020s	-3.6	-4.0	-3.2
A1B 2050s	-2.3	-2.7	-1.9
A1B 2080s	-0.8	-1.3	-0.4
A2 2020s	-3.6	-4.0	-3.2
A2 2050s	-2.7	-3.1	-2.3
A2 2080s	-0.6	-1.0	-0.2

REFERENCES

Environment Canada, 2013. Canadian Climate Normals 1971-2000. Ottawa, Ontario: Environment Canada. [http://www.climate.weatheroffice.gc.ca/climate_normals/index_e.html]. Accessed January 2013.

Etzelmüller, B., Farbrot, H., Guomundsson, A. and Humlum, O., 2007. The regional distribution of mountain permafrost in Iceland. Permafrost and Periglacial Processes, vol. 18, p. 185-199.

Lewkowicz, A.G. and Bonnaventure, P.P., 2011. Equivalent elevation: A method to incorporate variable lapse rates into mountain permafrost modeling. Permafrost and Periglacial Processes, vol. 22, p. 153-162.

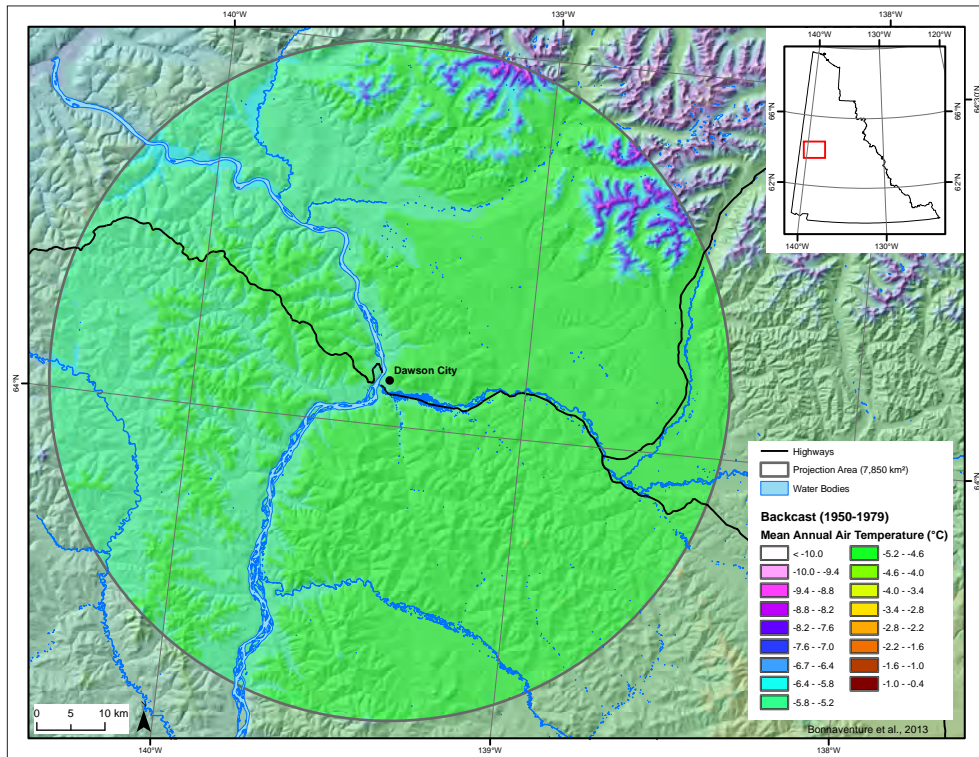SNAP (Scenarios Network for Alaska and Arctic Planning), 2012. www.snap.uaf.edu.

Figure D1. *Mean annual air temperature for the Dawson area, backcasted for the 1950-1979 period.*
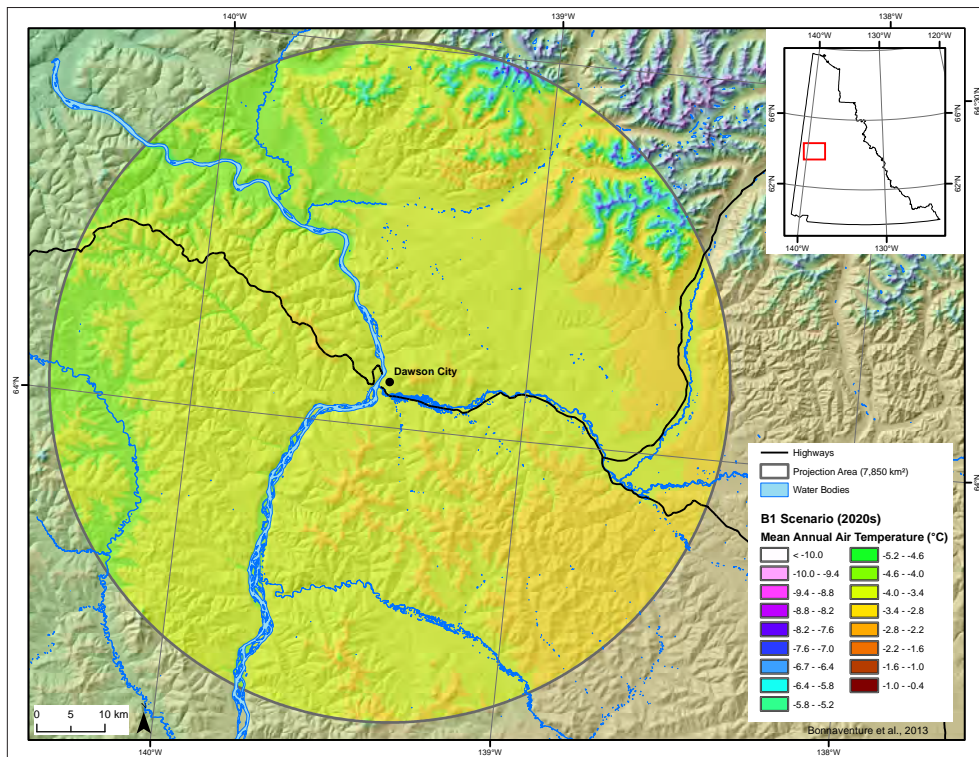

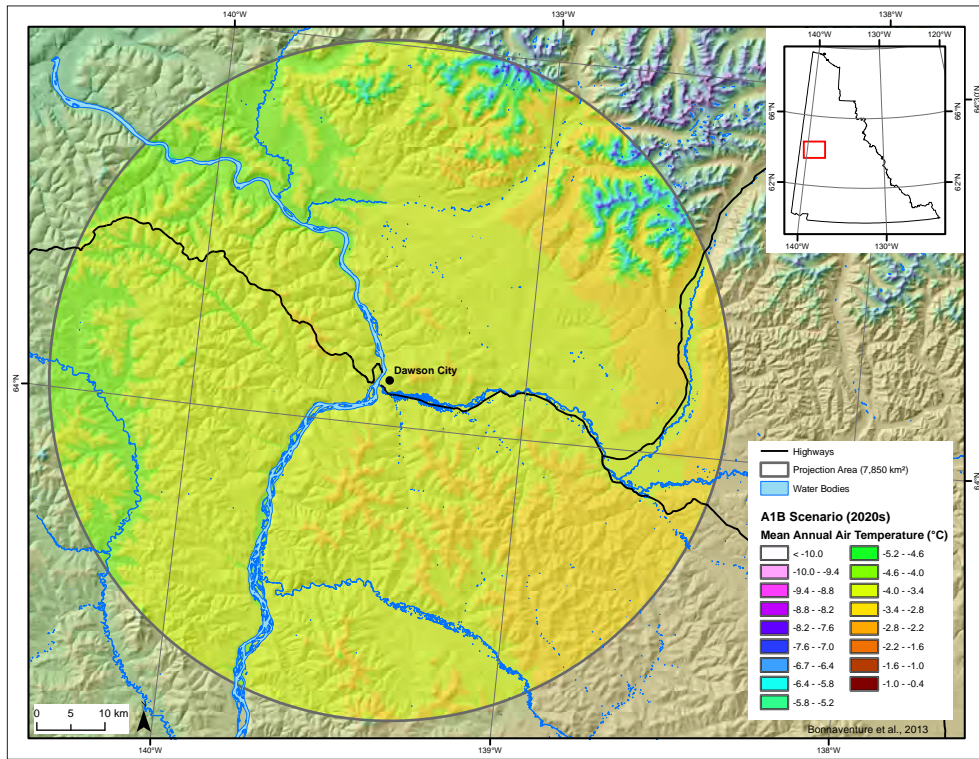**Figure D2.** *Mean annual air temperature for the Dawson area for 2020, projected using the B1 scenario.*

Figure D3. *Mean annual air temperature for the Dawson area for 2020, projected using the A1B scenario.*
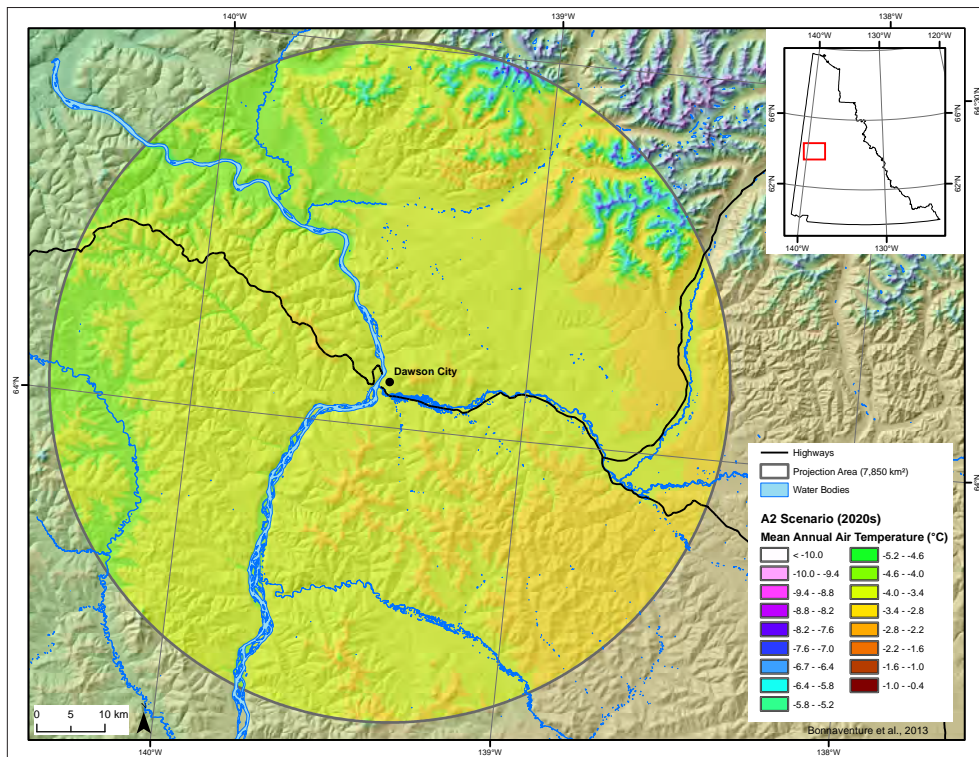

Figure D4. *Mean annual air temperature for the Dawson area for 2020, projected using the A2 scenario.*
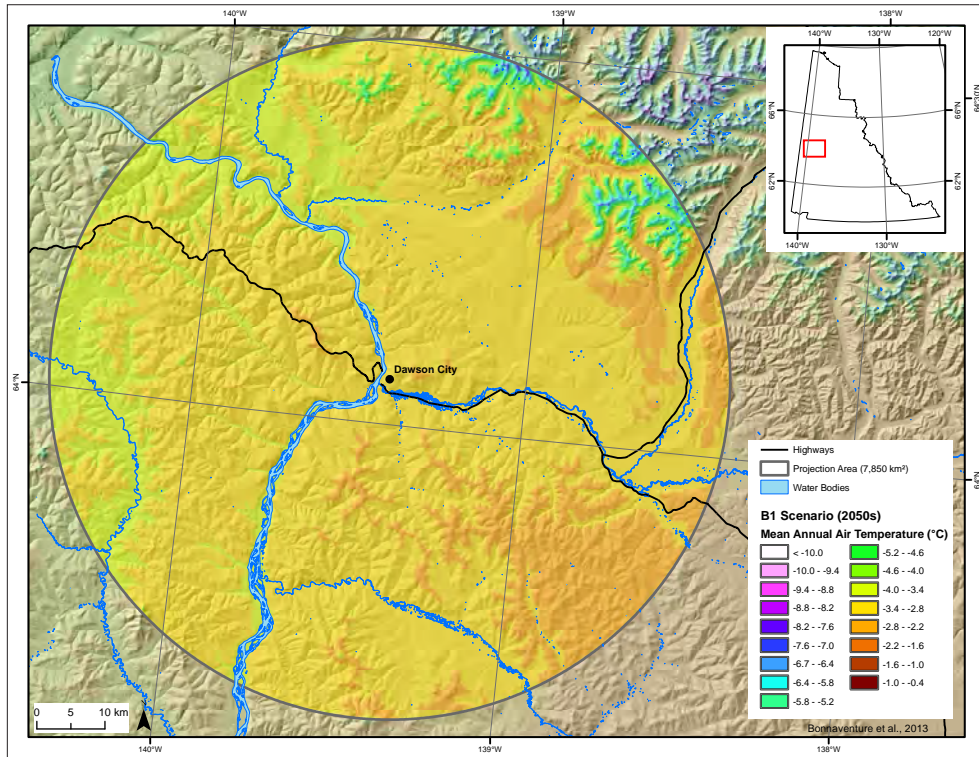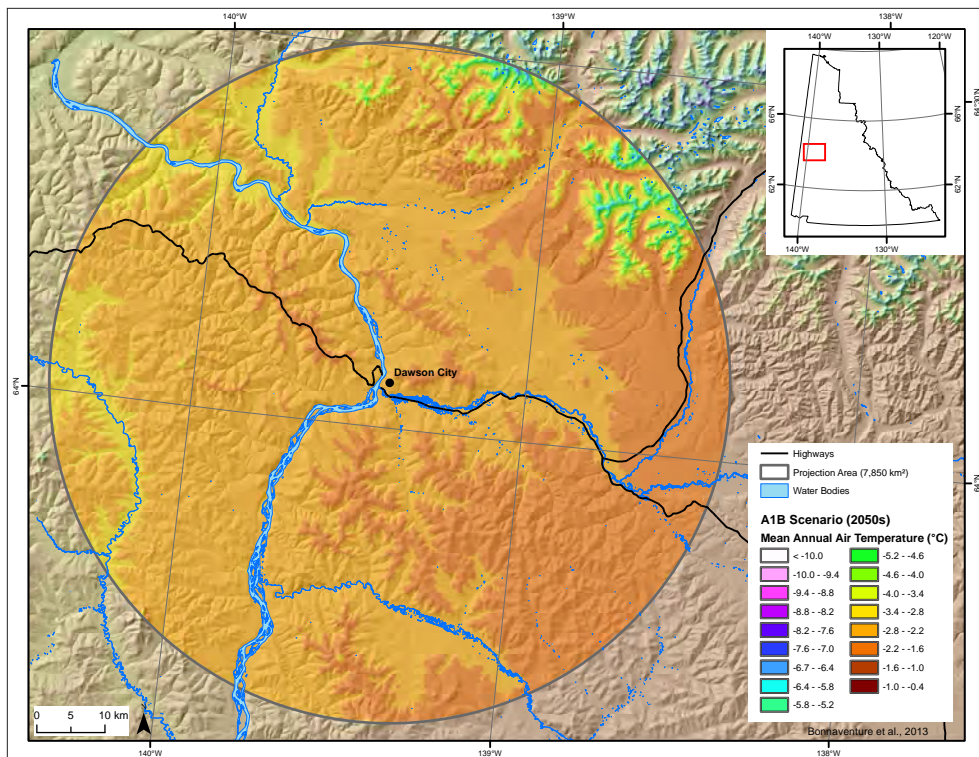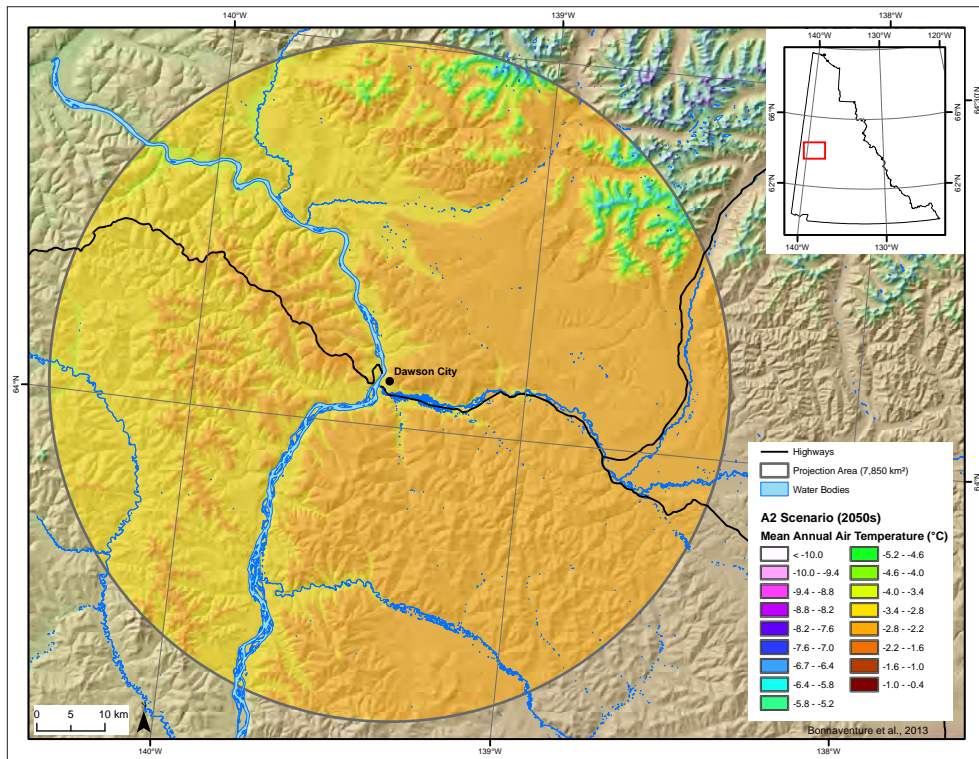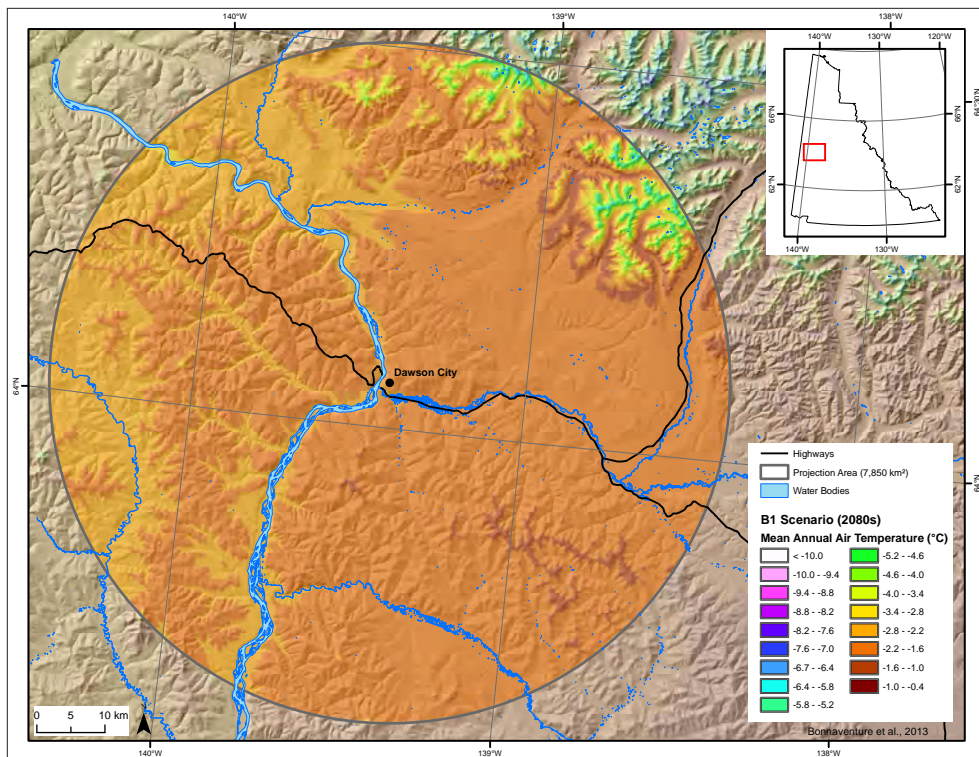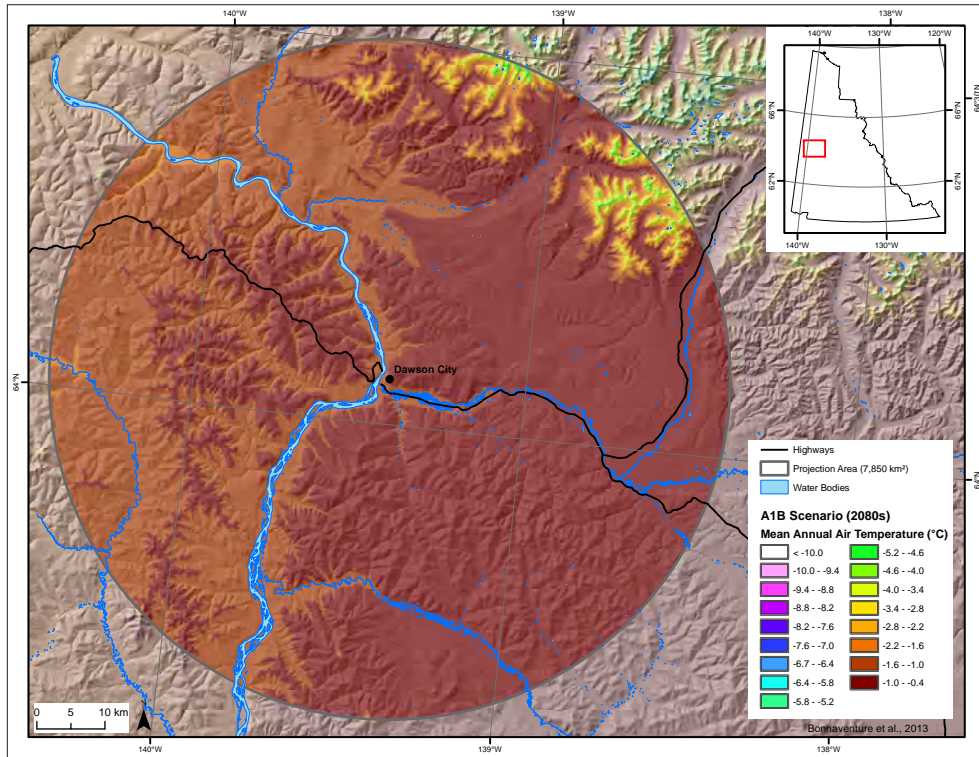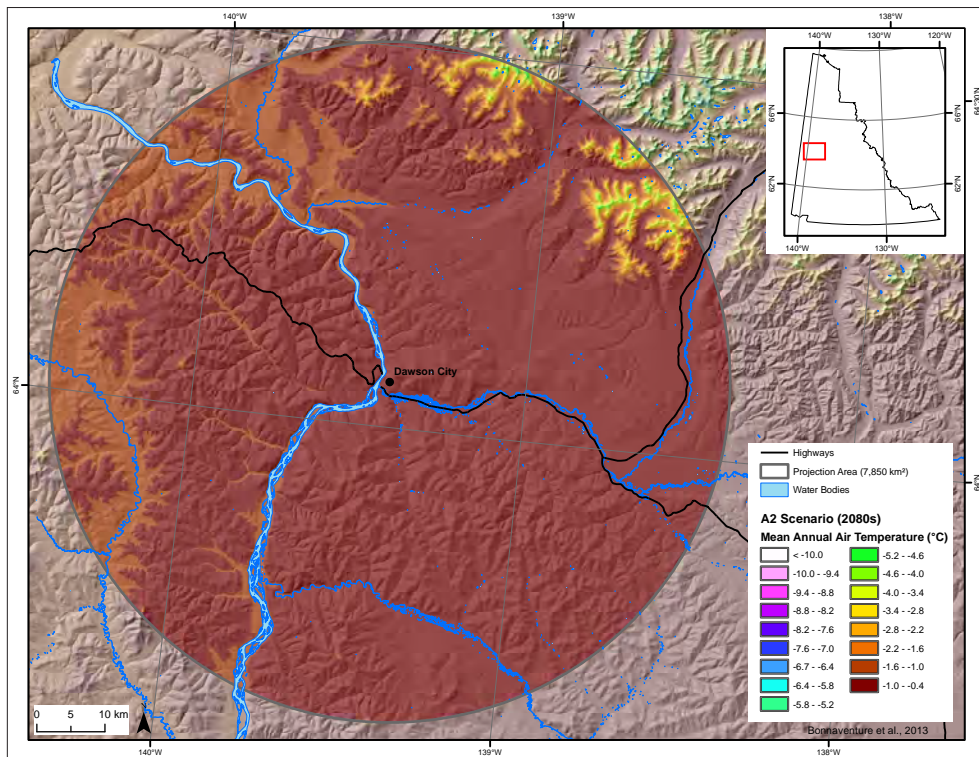
143

Figure D5. Mean annual air temperature for the Dawson area for 2050, projected using the B1 scenario.

Figure D6. Mean annual air temperature for the Dawson area for 2050, projected using the A1B scenario.

Figure D7. *Mean annual air temperature for the Dawson area for 2050, projected using the A2 scenario.*

Figure D8. *Mean annual air temperature for the Dawson area for 2080, projected using the B1 scenario.*

145

Figure D9. Mean annual air temperature for the Dawson area for 2080, projected using the A1B scenario.

Figure D10. Mean annual air temperature for the Dawson area for 2080, projected using the A2 scenario.

APPENDIX E - SAFE HOME CONSTRUCTION ON PERMAFROST

Prepared by

Julie Malenfant-Lepage (M.A., Eng.) and Benoit Loranger (Jr. Eng.)

Northern Climate ExChange, Yukon Research Centre, Yukon College

TABLE OF CONTENTS

INTRODUCTION

Construction in permafrost environments requires a good understanding of the nature of permafrost as well as the surficial geology. There are several principles and techniques for building on permafrost that have been proven efficient in various parts of northern Canada and Alaska. This report aims to briefly present the different approaches applied in construction of new buildings. In some ways, it can be considered as an introductory guide for basic principles, design and construction on permafrost. It is important to note, however, that this report is not prepared as an engineering design text and should not be used as such.

This report on safe home construction in permafrost environments will provide an overview of building construction on permafrost including issues related to house construction on permafrost, types of surface materials and thawing processes, preliminary investigation procedures, construction data requirements, types of foundations built in northern regions, basic principles to maintain permafrost under existent structures, and finally, recommendations that should be followed throughout the construction process.

CONSTRUCTION ON PERMAFROST

The best advice that could be given to an individual or to a contractor is to avoid building on permafrost terrain. If possible, it is always better to find a new site than to face the extra expense and maintenance involved in construction on permafrost. However, in many regions where permafrost is extensive (e.g., in northern Canada, including the Yukon) or where other factors preclude construction on non-permafrost terrain, this advice is sometimes impossible to follow. Building directly on bedrock is a good practice and should be done whenever possible (Figure F1).

Figure F1. Houses in Ilulissat, western Greenland, built directly on bedrock.

In areas underlain by continuous permafrost, permafrost is one of the major controlling factors in design parameters. As a result, it is important to design and build in a way that will preserve the underlying permafrost. Stability and lifetime of the infrastructure depend directly on the success of this endeavour.

Areas that are underlain by discontinuous permafrost offer the greatest engineering challenge since it is very difficult to determine exactly where there is underlying permafrost as it may change on a very local scale. Despite the high costs associated with the analysis of a potential construction site by drilling, these analyses will never confidently ensure the presence or absence of permafrost. If the site is located in a thaw-stable area, more conventional and less expensive construction techniques can be used without risk of destabilizing the ground. However, if the site is located in an area of ice-rich soil, which is considered thaw-unstable, standard structural foundations may thaw the underlying permafrost and potentially lead to an eventual failure of the structure. It is sometimes possible to remove or thaw permafrost on a site before starting construction, but this is a process that is rarely performed. The choice of a good structural foundation design and good mitigation techniques will help preserve permafrost, as well as respect a budget, which is the main challenge in regions underlain by discontinuous permafrost (Permafrost Technology Foundation, 2000).

PROBLEMS RELATED TO HOUSE CONSTRUCTION ON PERMAFROST

The most significant impact to permafrost usually occurs immediately beneath the house as heat is conducted downwards into the soil foundation. If a heated building is directly placed on permafrost, it will warm the ground throughout the entire year (Figure F2). However, if the building is not in contact with the ground surface, as is commonly found in northern communities, thawing is still possible due to the following: obstructed water drainage, insulation of ground by snow piling, and wind obstruction beneath the house. Furthermore, impacts from site preparation and infrastructure construction such as vegetation clearance, surface grading, and removal or compression of the organic layer, can increase heat intake by the ground surface. These ground disturbances usually result in an increase of ground temperatures, deepening of the thaw depth, and subsequent thaw settlement. In most cases, it will take several years for permafrost temperatures to reach a new equilibrium following construction.
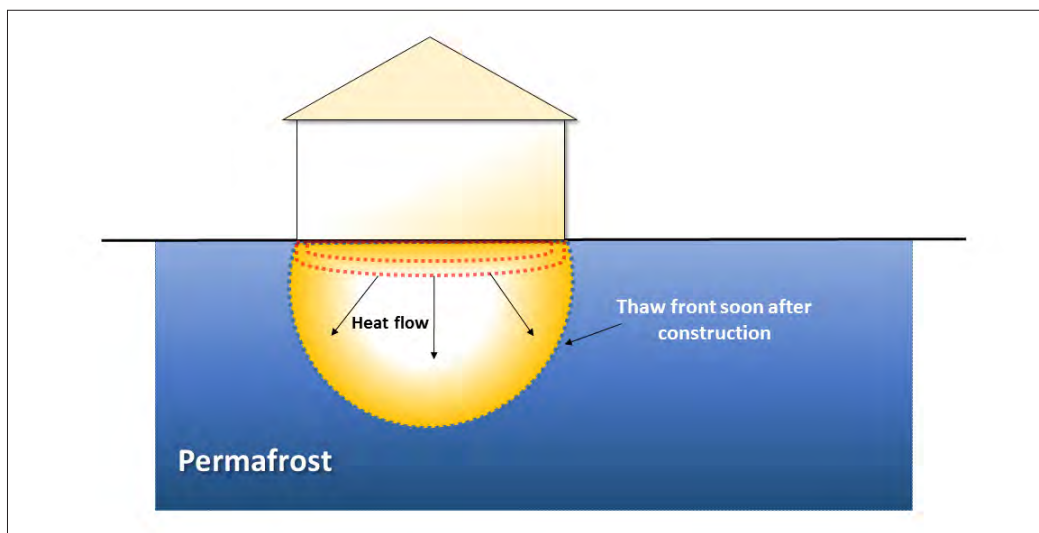

Figure F2. Cross section displaying the evolution of permafrost degradation under house construction. Based on Barriault (2012).

Foundation failure does not normally occur in a short period of time. Sudden collapse is extremely rare in the context of permafrost and is more likely associated with thermal erosion by water. The

time it takes for heat generated by a building to diffuse into the underlying permafrost depends on permafrost type, as well as factors such as the thickness of the active layer (i.e., layer of soil that thaws and freezes annually), the soil type, the temperature of the permafrost, the presence of water in the soil, and the amplitude of temperature change at the surface. However, once the process of warming is initiated, thawing of the soil is irreversible.

If buildings are left unattended, soil degradation can end up affecting the structure and will lead to the formation of cracks and bindings on doors, walls and ceilings (Figure F3). Tilted floors can also be associated with permafrost-related problems. Eventually, a building can become non-functional and even condemned. Damage associated with permafrost degradation should therefore be monitored and repaired as soon as possible to ensure viability of the structure. Monitoring can also be used to collect relevant data that would be useful in assessing permafrost-related damage. It is by far more cost effective to initiate repairs at the first signs of permafrost-related failures.

Figure F3. Examples of unmaintained buildings in Pyramiden, Svalbard, displaying cracks and uneven settlement in response to permafrost thaw.

TYPES OF SURFACE MATERIALS AND THE THAWING PROCESSES

In permafrost regions, coarse, granular surface material (sand and gravel) and rocks without ice inclusions are typically the best material on which to construct a foundation. Upon thawing, these materials are stable and have good bearing capacity. Bearing capacity refers to the load a surface material can safely withstand, without significant compaction or settlement. Foundation design in such materials should follow the current practice of moderate temperature regions.

Conversely, fine-grained surface materials, which are often ice-rich, have low permeability and tend to be oversaturated after thawing. Pore-pressure generated during thawing may result in a significant loss of stiffness (bearing capacity) and volume (Figure F4). For fine-grained deposits, foundation design in permafrost poses several challenges when attempting to control differential settlement of the materials that leads to the deformation of structures. The bearing capacity of fine-grained materials is largely a function of the amount and temperature of ground ice present.
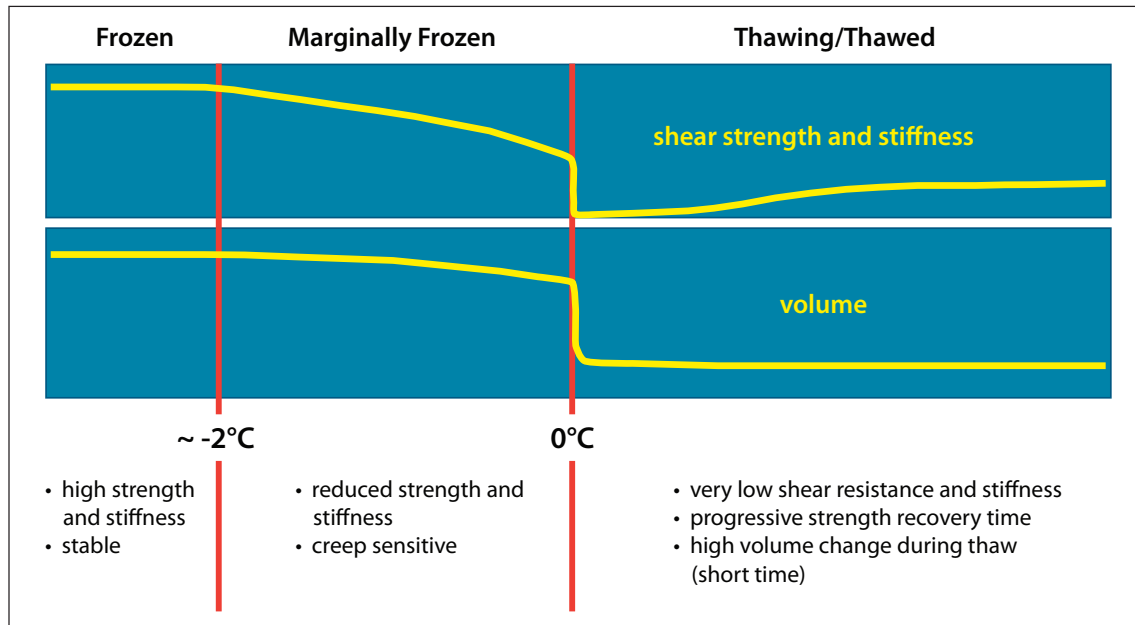
Figure F4. *Mechanical properties of frozen ground undergoing thaw (Doré, 2011).*

As the amount of ground ice commonly varies across a construction site in zones of discontinuous permafrost, bearing capacity may differ within a foundation, causing different portions of the structure to experience settlement at different rates. Furthermore, since ice-rich deposits consolidate and discharge excess water as they thaw, variably distributed ground ice can result in the settlement of specific areas of the ground, causing distortion in the structure above. Therefore, these types of surface materials do not offer good support for construction of buildings (Canadian Standard Association (CSA), 2010).

It is also important to note that permafrost with a temperature between -2°C and 0°C is marginally frozen (i.e., considered to be 'warm permafrost') and may not appear to be warming rapidly. At this temperature, a significant amount of heat transfer is mainly used to melt ground ice instead of warming the surface materials. Consequently, the strength of permafrost under the structure will be reduced significantly as the ground ice melts even if the temperature of the sediments remains below 0°C (see Figure F4). Moreover, several problems of creeping related to thick gravel pads and heavy structures are commonly associated with warm permafrost. Creep is related to slow ice deformation within the ground under a constant load. Ice then reacts as a malleable material and tends to flow laterally, away from the load source.

In summary, fine deposits of silt and clay are more likely to be problematic because of their frost susceptibility. Well-drained materials such as sand and gravel will be more stable; however, it is important to note that many sandy and gravelly deposits may contain a significant amount of fines that could pose a threat to the integrity of a structure. Frost susceptibility appears when approximately 10% of the mass of the surface deposit is composed of material with a fine grain size, i.e., 80 μm. If in doubt, it is best to seek advice from a geotechnical engineer.

SITE INVESTIGATION

The objectives of the site investigation are to identify terrain units, determine relevant surface material properties, and identify areas of thaw-sensitive or unstable deposits. The type of building

and its lifespan define the quantity and complexity of information necessary. The following section provides the current practices used during the site investigation.

PRELIMINARY OBSERVATIONS

The first step is an attentive observation of all permafrost-related features that could be present at the site. Features such as frost mounds, cracks, depressions and uneven terrain are typical characteristics of a permafrost landscape. Therefore, it is important to pay close attention to terrain morphology and topography since these are indicators of underlying permafrost conditions.

FROST PROBING

When the top of the permafrost is shallow and the active layer is relatively soft, frost probing is an effective method for locating depth to permafrost (Figure F5). This technique uses a steel rod with a handle, which is pushed into the ground manually until the top of the permafrost is reached. With this method, shallow permafrost can easily be detected, and its depth measured. Frost probing is inexpensive, fast and very useful for preliminary site investigations.

Figure F5. *Frost-probing to determine depth to permafrost.*

Figure F6. *Example of ice-rich permafrost core from the Beaver Creek area, Yukon.*

DRILLING

The most effective way to determine ground ice conditions at a potential site is to drill boreholes and collect samples of permafrost for geotechnical analysis (Figure F6). This provides specific information about soil characteristics and conditions at the subsurface at a particular location. A good borehole log will provide information at varying depths, including the thickness of the active layer, the soil or rock types, the ice content, the depth and characteristics of permafrost, the presence of massive ice bodies, and in some cases, the depth to bedrock.

The information derived from multiple boreholes in a given area can be extrapolated to obtain a spatial representation of subsurface conditions. It is very important to drill deep enough to obtain the appropriate information for each project. Generally speaking, the larger the building, the deeper the drilling must be. Permafrost drilling requires trained personnel with proper equipment adapted to site conditions.

GEOPHYSICS

If a larger area is being surveyed, complementary geophysical approaches like electrical resistivity tomography (ERT) and ground penetrating radar (GPR) surveys should be considered. Both applications work by sending signals into the ground and measuring the rate or strength of their return, and using those results to map subsurface conditions.

Geophysical surveys can be applied to help extrapolate information between boreholes. It is particularly useful for determining the thickness and extent of permafrost bodies, and zones of unfrozen ground within permafrost (Figure F7 a,b). ERT and GPR are applied for different detection purposes and professional geophysicists will select the most appropriate technique for the site. Geophysical surveys have the advantage of covering a relatively large area in a short period of time. Furthermore, ERT and/or GPR surveys are a cost-effective way to minimize the number of boreholes that need to be completed at any given site. The results obtained by drilling, coupled with geophysical surveys allow for a more comprehensive analysis of the subsurface conditions of the entire site.
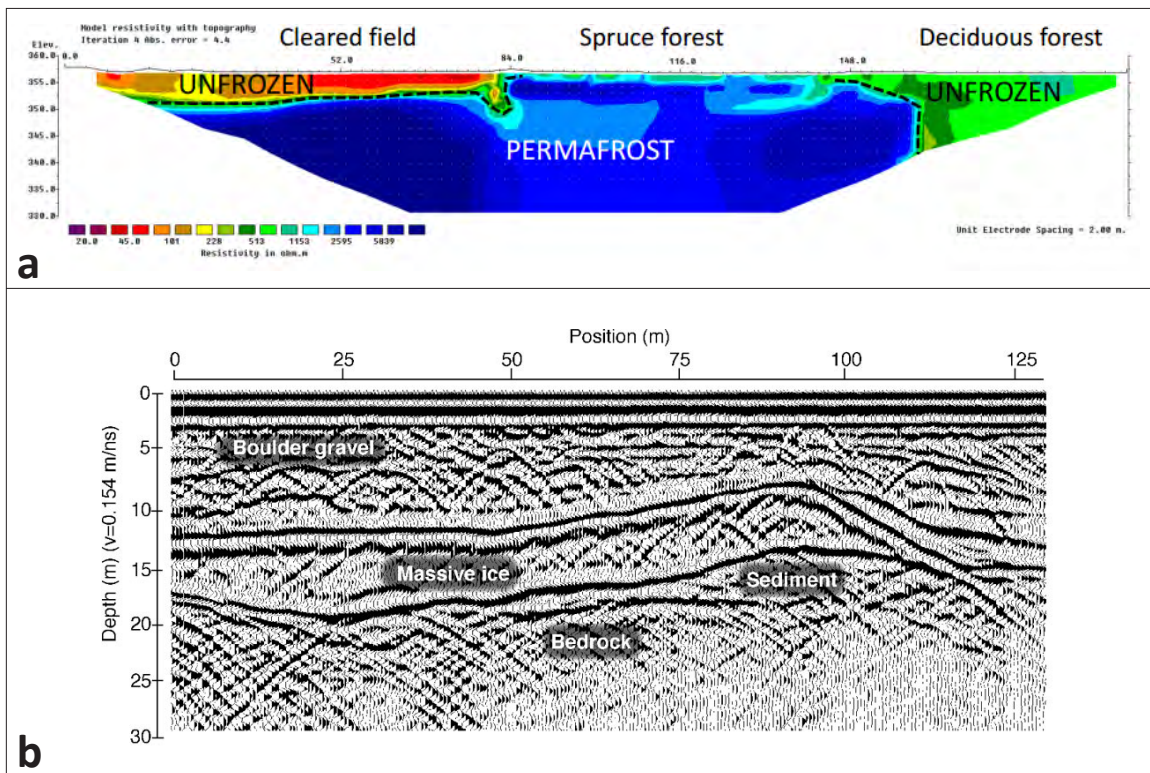

Figure F7. (a) *ERT profile from the Klondike Valley, Yukon (Lewkowicz et al., 2014).* *(b)* *GPR profile along an ice-cored esker near Carat Lake, Northwest Territories (Moorman et al., 2007).*

FOUNDATIONS IN PERMAFROST

Robust foundations for infrastructure in permafrost areas are critical for long-term building stability. General data requirements and the most common types of foundations are presented below.

CONSTRUCTION DATA REQUIREMENTS

The following list indicates principal information requirements related to construction and foundation design (Andersland and Ladanyi, 2004). This list is for large-scale projects and only needs to be fully applied in those cases. However, some elements are essential in the selection of the right type of foundation, such as the amount and temperature of ground ice, as well as the active layer thickness. It is good practice to gather as much information as possible about a site prior to construction.

1. Site data:
    a. location
    b. climate
    c. physiography and geology
    d. subsurface materials and their characteristics
    e. thermal regime
    f. hydrology and drainage
    g. materials and construction
    h. transportation facilities and access
    i. construction cost factors
    j. Availability of :
        i. labor, skills, and knowledge
        ii. construction equipment
        iii. support facilities and equipment
2. Design policies, general criteria, and cost limitations
3. Technology (state of the art)
4. Facility technical data
    a. size and design life (e.g., permanent versus temporary)
    b. foundation loading
    c. thermal conditions
    d. movement and distortion

FOUNDATION TYPES

Good foundation construction in the North is essential to assure a full service life of a structure. Proper foundation design will be the difference between a safe, stable structure with relatively low maintenance costs, and one with constant stability problems leading to a shorter lifespan. The selection of a foundation type will generally depend on the soil behaviour upon thawing. Foundations built on permafrost can be divided into three main categories: 1) surface pads; 2) deep foundations, and; 3) foundations with heat exchangers.

Surface gravel pads

Construction on a surface pad to preserve the temperature of the underlying permafrost is common in northern Canada. According to Allard et al. (2010), houses built on properly designed, compacted, granular foundations should not undergo significant thaw settlement because the adjustment of the thermal profile to the new geometry leads to a rise of the permafrost into the gravel pad (Figure F8 a,b). The active layer then becomes limited to the non-frost sensitive foundation, which ensures stability over cycles of freezing and thawing. Gravel pads are frequently used with insulant panels and techniques that allow airflow beneath the building.
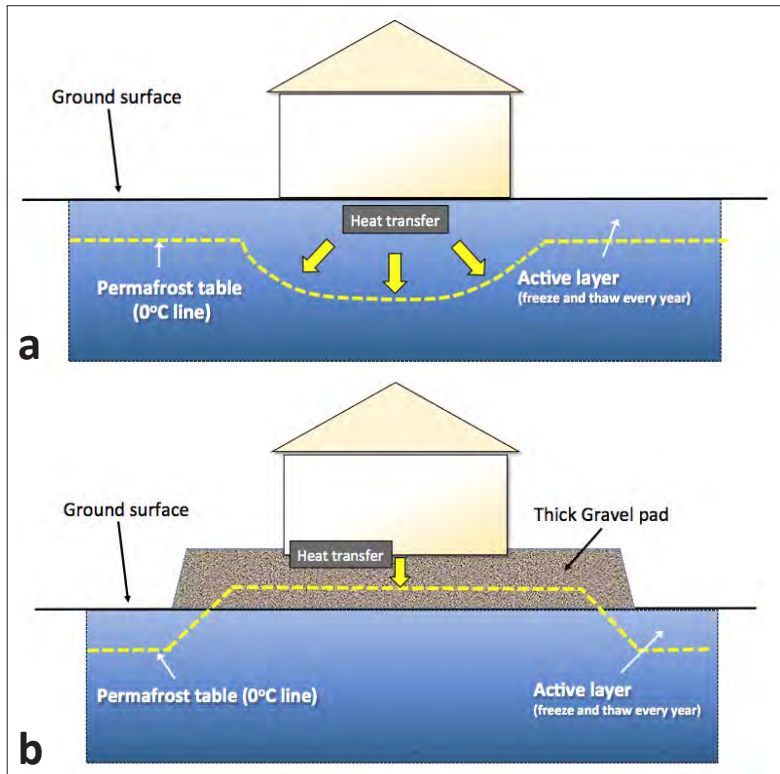
Figure F8. *Schematics demonstrating the theoretical position of the permafrost table underneath **(a)** a building built directly on the ground, and **(b)** a building built on a gravel pad.*

INSULATION

Structures may be built directly on insulating material (Figure F9). Insulation will slow the rate at which heat enters the ground, but it does not eliminate heat exchange. It is possible to add enough layers of insulation to establish a new thermal balance between heat input from the area around the building and winter cooling, but this procedure is almost never performed due to the high cost. Insulation is commonly applied along with a gravel pad.
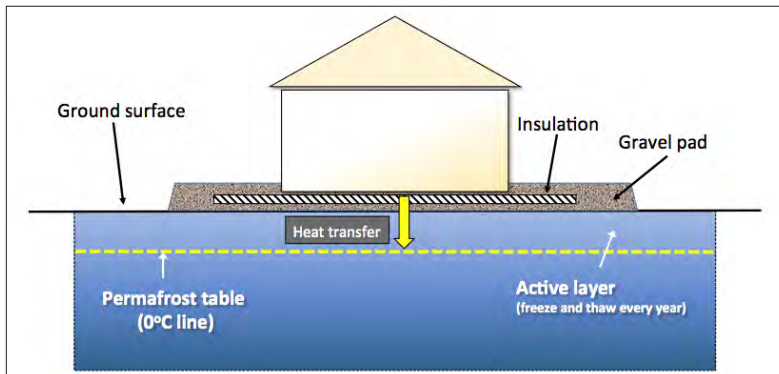

Figure F9. *Basic insulation-pad foundation design (modified from CSA, 2010).*

Several types of insulation can be considered in the construction of an unheated foundation. An insulated layer that is intended to be in contact with the soil must be able to withstand deterioration of its thermal properties and physical shape in the presence of soil moisture, soil chemicals, physical loading and other outside forces (Permafrost Technology Foundation, 2000).

SCREW-JACK FOUNDATIONS

In the 1980s, the Société d'Habitation du Québec developed a concept for house foundations to preserve permafrost. It involved buildings that are constructed on adjustable metal jacks over a compacted granular foundation (Figure F10). The granular foundation is laid directly on the ground surface without the removal of the vegetation cover. To date, this construction technique has been proven very effective for preserving permafrost (Gravel, 2012). The foundation must raise the building high enough to promote uninhibited air circulation beneath the building. It allows the wind to flow freely under the building, mainly to avoid snow accumulation that could increase the soil temperature (by insulation) under the foundation. Under these conditions, a snow bank will form approximately six metres away from the dwelling's foundation. It is important that nothing be stored in the space between the floor and the ground surface so as to not interfere with the free air circulation during the winter months. The winter airflow allows for the extraction of heat from the ground beneath the building, and helps preserve permafrost. Sufficient insulation should be placed under the floor of the structure so the energy loss from the bottom of the building is minimized and the floor inside the building is comfortable for residents.
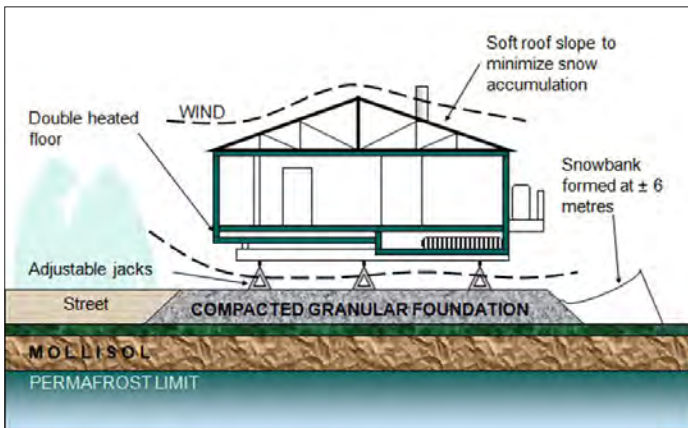

Figure F10. Conceptual design of a screw-jack foundation on a compact granular foundation (Gravel, 2012).

Once or twice a year, maintenance of a building on jacks needs to be performed in order to preserve the building's stability. During the maintenance process, screws in the middle of the jacks are used to raise or lower the height of the building (Figure F11). For a small, single-family house, it is common to use about nine adjustable jacks which can withstand nearly 35 000 kg each (Gravel, 2012). It is important to ensure that the slope of the terrain around the building allows for adequate drainage of surface water away from the structure.

Figure F11. Examples of adjustable-jack foundations from Gravel (2012) and CSA (2010).

Timber-block foundations

Timber-block foundations (Figure F12) work on the same principle as the screw-jack technique. However, screw jacks are not always easily obtainable and it can be more convenient to use timber blocks. Timber blocks are normally screwed together to ensure lateral stability. Timber blocks are commonly sited directly on natural ground (without a gravel pad).

Maintenance operations are almost the same as for screw-jack foundations, described above; however, the operator must use a hydraulic jack to lift the load of the building before shimming the timber blocks. Maintenance for this style of foundation is therefore more labour intensive than for screw-jack foundations.

Figure F12. *Example of a timber-block foundation used in Nunavut (Government of Nunavut, 2013).*

Space-frame foundations

Another surface foundation that has proven successful in permafrost regions is the rigid, three-dimensional, truss-type foundation (Figure F13). This is a commercially available, pre-manufactured foundation that consists of metal tube members flattened on each end and connected by metal node pieces at the top and bottom to form approximately one metre-square cells. It is custom-made to fit the building, and is assembled directly on-site on a compacted, granular foundation.

A screw at each structural node is used to level the building in the event of permafrost thaw underneath the building. These types of foundations are quite expensive, and are used mainly for service buildings and large, public infrastructure.

Figure F13. *Examples of space-frame foundations in Nunavut (Barriault, 2012).*

Pile foundations

In the far North, the majority of public and private dwellings, as well as commercial buildings, are built on steel piles. Piles are long steel pipes driven into the ground to stabilize buildings into the permafrost or bedrock (Figure F14). This type of foundation requires little to no gravel,

which can be a very expensive resource to procure and transport to northern communities. The use of steel piles also allows for construction on harsher and steeper terrain compared with conventional foundations. The steel piles are also more resilient to climate change compared to other foundation types when they are placed directly on bedrock.

Figure F14. *Example a steel-pile foundation in Nunavik (Gravel, 2012).*

There are two principal pile types currently in use in the Canadian North: 1) adfreeze piles (driven and slurry), and 2) rock-socketed piles. Their design and applications are fundamentally different. Adfreeze piles are commonly installed where permafrost extends to substantial depths without encountering bedrock. These piles rely on the bond with the surrounding ground for their load-bearing capacity. They can be driven directly into the ground, or a drill hole can be fixed to accommodate the pile. Slurry is then used to fill the empty space between the soil and the pile. For this application, the ground can be ice-rich, but should be below -3°C, or colder if the soil is saline (CSA, 2010).

Rock-socketed piles are used where bedrock occurs within a practical depth below the surface. These piles are designed to transfer the full load of a structure to the underlying bedrock. In Nunavut, rock-socketed piles are commonly used. Adfreeze piles have been either discontinued or are being driven deeper due to a deepening of the active layer (Barriault, 2012).

In response to ground warming, if the active layer deepens, foundation systems that rely on piles may experience increased frost heaving (Figure F15 a,b,c). This frost heaving occurs when a small part of each pile's surface is frozen to the surrounding soil year-round, while a larger part of the pile's surface is exposed to the lifting force exerted through soil expansion when the water in the active layer re-freezes in the autumn and winter (CSA, 2010). If piles are used in a frost-sensitive soil and cannot be placed directly on bedrock, the piles must be equipped with anti-lift shafts to prevent the exertion of a vertical force by seasonal frost, which can distort the building's structure. Various methods can prevent frost heaving when using pile jacking and a competent engineer should be consulted if this method is being considered.
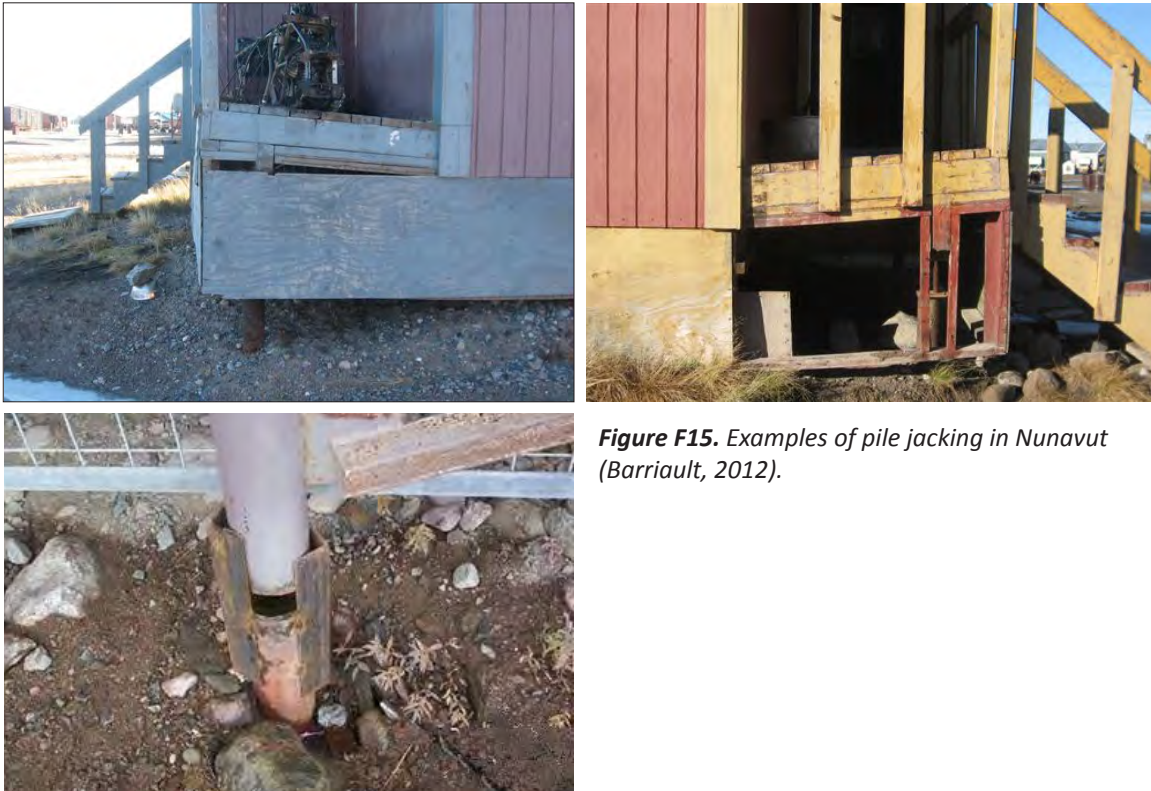
Figure F15. *Examples of pile jacking in Nunavut (Barriault, 2012).*

Figure F16. *Example of thermosyphons, a foundation system that requires a significant amount of expertise to design, install, maintain and monitor (CSA, 2014).*

FOUNDATIONS WITH HEAT EXCHANGERS

Foundations enhanced with heat exchangers are now widespread in Canada's North. They are generally used where heated crawl spaces and warm first floors at finished grade are required. For such structures, systems are built to intercept heat that would otherwise flow into the ground and affect the underlying permafrost. Thermosyphons are the most widely used heat exchangers (Figure F16). Two-phase thermosyphons work passively during the winter to extract heat from the ground and preserve permafrost (Figure F17 a,b,c). When designs using thermosyphons are being considered, detailed geothermal analyses are required. The inclusion of climate warming in the design process requires careful consideration of the conditions of the site chosen for the design, particularly in winter when low temperatures drive heat removal (CSA, 2010). Due to their high cost, thermosyphons are mainly placed in strategic locations next to high-risk service buildings, bridges or pipelines.
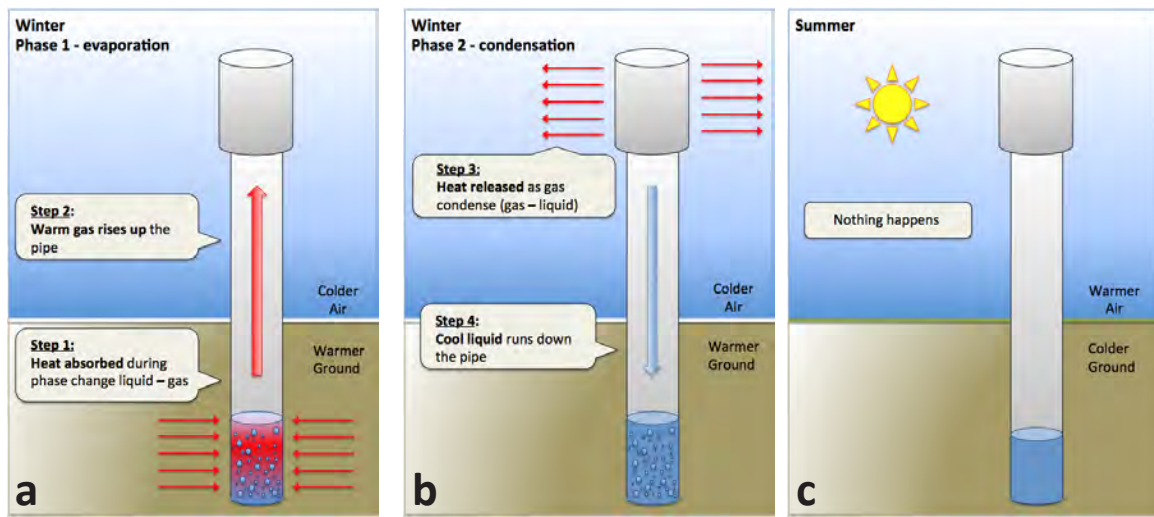
Figure F17. Schematic demonstrating (a) and (b) a winter two-phase thermosyphon cycle, as well as (c) the non-operative state during summer.

BASIC PRINCIPLES TO MAINTAIN PERMAFROST

Once construction of a building is finished, it is essential to maintain the permafrost beneath and around it. Basic elements to consider are outlined below. For more detail, please refer to the Canadian Standards Council (CSA, 2014 and 2013).

DRAINAGE

Because water transfers heat to the ground and can negatively impact permafrost, ditches should not be excavated in permafrost. Proper surface drainage to avoid water ponding beneath or next to the building is very important (Figure F18), especially with regards to spring meltwater (which can result in a high volume of flow during a short period of time). Slopes of approximately 4% are considered sufficient to drain any water at least 4 m (and preferably 6 m) from a building. Any terrain modification that could alter water paths should be carefully considered.

Figure F18. Example of water ponding around a foundation built on permafrost (Government of Nunavut, 2013). Water ponding can have a negative impact on permafrost thermal regimes.

VENTILATION

Winter airflow under buildings extracts considerable heat from the ground and thereby keeps the ground frozen. Air space should be at minimum 0.5-1 m to allow free circulation. Nothing should be stored beneath the building, in order to avoid restricting ventilation. Furthermore, snow should be managed such that it does not reduce ventilation and insulate the ground near the building. Frequent snow clearing may be required.

SHADING

In some cases, vegetation cover or a sun shade may be put in place to shade the ground surface. As mentioned above, it is important to not interfere with airflow or to enhance snow accumulation near the building. Natural vegetation and trees that exist prior to construction should not be disturbed in order to promote shading.

HEAT EXTRACTION

Active heat extraction systems like thermosyphons may be installed if required. These are described in more detail above.

MONITORING

The effectiveness of measures used to preserve permafrost should be monitored to ensure performance is maintained. Ground temperature should also be monitored to detect changes to the ground thermal regime that may affect permafrost – the temperature regime can be a powerful forecasting tool. For example, thermistor cables may be inserted along a pile if drilling is used during the construction phase.

CONCLUSIONS AND RECCOMMENDATIONS

Construction in regions underlain by permafrost is a process that requires many steps, including preliminary site investigation, drilling, data analysis, as well as the appropriate choice of foundation design, construction and maintenance. In summary, several recommendations related to building on permafrost can be made:

- Foundations need to be adapted to local permafrost and landscape conditions.

- The organic layer should not be removed before construction.

- The best available geotechnical measures and techniques should be applied for all construction.

- A geotechnical investigation should be completed before construction.

- Compacted granular foundations should be built at least two years in advance of construction to allow the rise of the permafrost table and the stabilization of the soil (Allard et al., 2010).

The permafrost thermal regime should be considered in the design-phase of construction while at the same time integrating the anticipated effects of climate warming in northern Canada.

It may also be appropriate, in some areas, to develop a municipal program with appropriate regulations to ensure yearly maintenance of houses and infrastructure (Allard et al., 2010).

It must be reiterated that this guide does not replace the necessary engineering design needed for building on permafrost. It is important to consult permafrost experts in order to get appropriate advice at the preliminary investigation stages, as well as through the construction and maintenance phases. Additionally, for detailed guidance with respect to roads and permafrost, the *"Guidelines for Development and Management of Transportation Infrastructure in Permafrost Regions"* should be consulted (McGregor et al., 2010).

REFERENCES

Allard, M., L'Hérault, E., Gybérien, T. and Barrette, C., 2010. Impact des changements climatiques sur la problématique de la fonte du pergélisol au village de Salluit (Nunavik). Rapport final, Centre for Northern Studies, Université Laval, Quebec City, QC, 69 p.

Andersland, O.B. and Ladanyi, B., 2004. Frozen Ground Engineering, 2nd Edition. Wiley, Hoboken, NJ, 384 p.

Barriault, A., 2012. Climatic Adaptations to Construction in Nunavut. Nunavut Housing Corporation, Northern Forum, April 18 2012, Quebec City, QC.

Canadian Standards Association (CSA), 2014. Standards Council of Canada Approves New National Standard to Help Address the Effect of Climate Change on Canada's North. [https://www.scc.ca/en/news-events/news/2014/standards-council-canada-approves-new-national-standard-help-address-effects-climate-change-canadas]. Accessed February, 2015.

Canadian Standards Association (CSA), 2010. Technical guide: Infrastructure in permafrost: A guideline for climate change adaptation, 1st edition. Canadian Standards Association Publication, 112 p.

Canadian Standards Association (CSA), 2013. Moderating the Effects of Permafrost Degradation on Building Foundations. Document S501 Draft Standard No. 3, 42 p.

Doré, G. 2011, Advanced Seminar on Permafrost Engineering Applied to Transportation Infrastructure, lecture notes, Yukon College, Whitehorse.

Government of Nunavut, 2013. A Homeowner's Guide to Permafrost in Nunavut: Keep Your House on Solid Ground. Government of Nunavut, 28 p.

Gravel, J.-F., 2012. Impact of climate change on habitat development in Nunavik (Société d'habitation du Québec). Northern Forum, Quebec City, QC.

Lewkowicz, A., Miceli, M., Duguay, M., Bevington, A., 2014. Electrical Resistivity Tomography (ERT) as an Essential Tool to Investigate Sites in Discontinuous Permafrost. University of Ottawa. EUCOP, June 18-21 2014.

Moorman, B.J., Robinson, S.D. and Burgess, M.M., 2007. Imaging Periglacial Conditions with Ground-Penetrating Radar. University of Calgary, Alberta, Canada. 17 p.

Permafrost Technology Foundation, 2000. Design Manual for New Foundations on Permafrost. Permafrost Technology Foundation publications, 94 p.

McGregor, R., Hayley, D., Wilkins, D., Hoeve, E., Grozic, E., Roujanski, V., Jansen, A. and Doré, G., 2010. Guidelines for Development and Management of Transportation Infrastructure in Permafrost Regions. Transportation Association of Canada, Ottawa, ON, 177 p.